Dendrimers for the Targeted Delivery of Chemotherapeutic Agents in Cancer

THESIS

Submitted in partial fulfilment
of the requirements for the degree of
DOCTOR OF PHILOSOPHY

by

BHATT HIMANSHU NARENDRAKUMAR

ID. No. 2015PHXF0013H

Under the Supervision of

Prof. Swati Biswas

&

Under the co-supervision of

Dr. Balaram Ghosh

BITS Pilani
Pilani | Dubai | Goa | Hyderabad

BIRLA INSTITUTE OF TECHNOLOGY AND SCIENCE
PILANI (RAJASTHAN) INDIA
2020

BIRLA INSTITUTE OF TECHNOLOGY AND SCIENCE, PILANI

CERTIFICATE

This is to certify that the thesis titled **"Dendrimers for the Targeted Delivery of Chemotherapeutic Agents in Cancer"** submitted by **BHATT HIMANSHU NARENDRAKUMAR,** ID No**. 2015PHXF0013H** for award of Ph.D. of the Institute embodies original work done by him/her under my supervision.

Signature of the Supervisor:

Name in capital letters: **SWATI BISWAS**

Designation: **Associate Professor**

Date: 10/10/2020

Signature of the Co-supervisor:

Name in capital letters: **BALARAM GHOSH**

Designation: **Assistant Professor**

Date: 10/10/2020

Acknowledgement

This research work is a synergistic product of many persons. It is not a chronology of events, but a collection of ideas at work. This thesis had its own set of challenges; therefore, this is the time to say sincere thanks to all those who have, in some way or the other helped me to sail through. It is my great pleasure to acknowledge all those who have contributed towards the conception, origin and nurturing of this project.

I would like to express my gratitude to my esteemed guide, Prof. Swati Biswas for taking me under her tutelage and giving me the opportunity to pursue Ph.D. degree under her guidance. Respected Madam, it was pleasure knowing you and learning from you many things, both said and unsaid, which I will cherish throughout my life time. Thank you for your guidance, encouragement and support throughout the course of my study. Respected Madam, I am privileged to complete my Ph.D. under your guidance. Your endless optimism, enthusiasm and infectious energy towards breakthrough research will always be a source of inspiration for me.

I feel very fortunate to have the opportunity to work with my co-supervisor Dr. Balaram Ghosh who introduced me in the lab for pursuing my Ph.D. Dear Sir, it was very nice journey by sharing your vast experience and technical knowledge with me in the need of hour. You are a positive motivational force, who is always helpful in troubleshooting of the critical and trivial issues. You have always created a friendly conducive environment in laboratory and made my time memorable in BITS. Your infinite patience, stimulating discussion and friendly critics have been most invaluable to the accomplishment of this thesis.

I am whole heartedly thankful to Prof. V. V. Vamsi Krishna, Department of Pharmacy, BITS Pilani Hyderabad who acted as Doctoral Advisory Committee (DAC) members for his detailed constructive comments and support throughout this work.

I wish to express my warm and sincere thanks to Prof. Onkar Kulkarni, Department of Pharmacy, BITS Pilani Hyderabad who acted as a Doctoral Advisory Committee (DAC) member for his suggestions and invaluable time to review my dissertation report.

I wish to express my gratitude to Prof. D. Sriram, Prof. P. Yogeeswari, Prof. Punna Rao Ravi, Prof. Arti Dhar, Dr. Nirmal Jain and Dr. Akash Chaurasiya for giving me unrestricted access to use instruments and facilities in laboratories.

I also expressed my profound gratitude to Prof. Sajeli Begum, Professor and Head, Department of Pharmacy, for her support and extending the facilities to work at the institute.

It is my duty to express my sincere thanks to the Chancellor, BITS Pilani for providing necessary infrastructural support to carry out my research work. I am sincerely thankful to Prof. G. Sundar, Director; Prof. Souvik Bhattacharyya, Vice Chancellor; Mr. Ernest Samuel Ratnakumar J, Registrar; Prof. Venkata Vamsi Krishna Venuganti, Dean, Academic - Graduate Studies and Research; and Prof. Niranjan Swain, Dean, General Administration for facilitating my research work at the institute.

I would like to thank central analytical laboratory of BITS, Pilani-Hyderabad Campus for providing me a scientific platform to excel in my career.

I am fortunate to have met nice colleagues and lab mates in BITS where I got an opportunity to work with them during various occasions. I am grateful to Rimpy, Suresh, Nikhila, Kalyani, Kavita, Ekta, Teja, Avantika, Yamini, Ganesh, Milan,

Soniya, Sanjay, Sravani, Tarun, Asif and Ashutosh. Thanks, all of you for remembrance and being a source of happiness.

Words cannot express my gratitude to seniors Omkar, Preeti, Prakruti, Shailender, Anup, Suman who were very supportive, their attention and timely concern for my Ph.D. gave me lot of enthusiasm.

I am thankful to Mrs. Sarita, Mrs. Rekha, Mrs. Sunita and Mr. Rajesh for their kind co-operation during the lab in the entire tenure of my PhD.

I am indebted to CSIR, Daewoong Pharmaceuticals and BITS, Pilani-Hyderabad Campus for providing me scholarship and necessary financial support to pursue my Ph.D. work without any hindrance.

My deepest thanks to my friends Dr. Brijesh Shah and Mr. Dignesh Khunt, who have been a pillar of strength always supporting and standing beside me, irrespective of situations.

Praise God for leading me to everything I have achieved. I would express humble gratitude to that positive energy from God, which was my driving force during the entire duration of my PhD, its support and motivation made me to choose right direction in my career. I could never repay to God for help and timely motivation which played a key role in giving the right direction to my work.

My deepest gratitude goes to my family for their unflagging love and support throughout my life; this dissertation is simply impossible without them. I am indebted to my father Mr. Narendrakumar for his care and love. I have no suitable words that can fully describe his everlasting love to me. I cannot ask for more from my sweet mother as she is simply perfect. Their blessings always inspire me to work hard and to overcome all the difficulties throughout my life.

I would like to thank everybody who was important for the successful completion of this research work that I may have inadvertently failed to mention.

Himanshu Bhatt

Abstract

Dendrimers have gained much attention in the recent years for their unique architecture and feasibility of surface modification to cater various functions in drug delivery. They have been successfully explored for delivery of poorly soluble anti-cancer molecules to different types of cancers. The purpose of the present research is to study the delivery potential of dendrimers in targeting anti-cancer agents specifically to tumors by utilizing various benefits they offer in improving the biopharmaceutical properties of the drugs. The current thesis focuses on the delivery of paclitaxel (PTX), a poorly soluble chemotherapeutic agent to cancer cells utilizing Generation 4 (G4) poly(amidoamine) (PAMAM) dendrimers as delivery system.

First, α-tocopheryl succinate (α-TOS) was conjugated to the surface amino groups of generation 4.0 PAMAM dendrimer via acid/amine coupling reaction to yield G4-TOS. Polyethylene glycol was conjugated to the terminated amines of the G4-TOS conjugate to improve the long circulation in the body and reduce the toxicity of positively charged dendrimers. Another conjugate G4-poly (ethylene glycol)PEG was also prepared to assess the therapeutic potential of PTX. PTX was loaded physically into both the synthesized dendrimer conjugates α-TOS anchored PEGylated G4 PAMAM dendrimer (G4-TOS-PEG) and PEGylated G4 PAMAM dendrimer (G4-PEG) to yield PTX loaded α-TOS anchored PEGylated G4 PAMAM dendrimer (G4-TOS-PEG-PTX) and PTX loaded PEGylated G4 PAMAM dendrimer (G4-PEG-PTX) respectively. The newly synthesized dendrimers nano-conjugates were characterized by proton nuclear magnetic resonance (NMR), gel permeation chromatography (GPC), dynamic light scattering and in-vitro release measurements to confirm the construction of conjugates. From the GPC results, it was observed that there were 3.47 molecules of TOS and 8.044

molecules of PEG that were attached on each PAMAM dendrimer molecule. The hemolytic assay of the developed conjugates revealed that the PEGylated dendrimers were non-toxic to the cells and α-TOS attachment did not cause any toxicity. The synthesized nano-conjugates were assessed in murine melanoma cancer cells (B16F10) and human breast adenocarcinoma cells (MDA MB231) in cell monolayers and 3D multicellular spheroids well. The α-TOS anchored nano-conjugate G4-TOS-PEG was internalized significantly into the cancer cells as evaluated by microscopy and flow cytometry experiments. The anti-cancer activity of PTX was significantly enhanced when loaded into the G4-TOS-PEG compared to free PTX. Attachment of α-TOS further improved the delivery of PTX to cancer cells due to solubilization of PTX into dendrimer cavity and anticancer activity of α-TOS. The studies in multi-layered 3D spheroids clearly showed the benefit of attaching α-TOS to the surface of dendrimers which improved the penetration into 3D spheroids thereby accumulating the more amount of drug into cancer cells. Further, the in vivo efficacy study using B16F10 xenografted C57Bl6/J mice indicated that the G4-TOS-PEG localized in tumor sections. G4-TOS-PEG-PTX reduced the tumor growth significantly compared to free PTX and G4-PEG-PTX. G4-TOS-PEG-PTX had more apoptotic potential in tumor sections as analyzed by terminal deoxynucleotidyl transferase dUTP nick end labelling (TUNEL) assay.

In the next study, active targeting strategy was employed to deliver the drug into the cancer cells only. Transferrin (Tf), a human serum glycoprotein of molecular weight 80 KDa serves as a cargo for iron and receptor of which are overexpressed in cancer cells was conjugated over the surface of synthesized dendrimer nano-conjugate to yield Tf conjugated α-TOS anchored PEGylated G4 PAMAM dendrimer (G4-TOS-PEG-Tf). The PTX was loaded physically into the synthesized dendrimer conjugate G4-TOS-

PEG-Tf to yield PTX loaded Tf conjugated α-TOS anchored PEGylated G4 PAMAM dendrimer (G4-TOS-PEG-Tf-PTX). The transferrin targeted and non-targeted conjugates were evaluated in vitro in human cervical cancer cells (HeLa) which overexpress transferrin receptors abundantly. The size exclusion chromatography (SEC) results showed that 3.67 molecules of TOS, 7.27 molecules of maleimide PEG and 4.19 molecules of Tf were conjugated to each G4 PAMAM dendrimer. Transferrin saturation studies in HeLa cell lines were carried out to evaluate the uptake pathway of transferrin anchored dendrimer nano-conjugate into cells. It was observed that the Transferrin anchored dendrimer conjugate was found to internalize actively via the transferrin receptors. The G4-TOS-PEG-Tf-PTX revealed the highest cytotoxicity and penetration in cell monolayers as well as 3D spheroids in comparison to G4-TOS-PEG-PTX and free drug.

Third, Vitamin-E-succinate (VES) was conjugated to the surface amino groups of generation 4.0 PAMAM dendrimer (D) via acid/amine coupling reaction to yield VES anchored G4 PAMAM dendrimer (VES-D). Further, the Polyethylene glycol (P) was conjugated to the terminated amines of the VES-D conjugate to improve the long circulation in the body and reduce the toxicity of positively charged dendrimers. The VES anchored PEGylated G4 PAMAM dendrimer (VES-PD) conjugate was anchored with a cell penetrating peptide octa-arginine (R) to yield (RVES-PD) to improve the penetration of conjugate (VES-PD) into the cancer cells. The PTX was loaded physically into the synthesized dendrimer conjugate RVES-PD to yield RVES-PD-PTX.

The newly synthesized dendrimers nano-conjugates were characterized by proton NMR, gel permeation chromatography (GPC), dynamic light scattering and in-vitro release measurements to confirm the construction of conjugates. From the GPC results,

it was found that 3.41 molecules of VES, 8.07 molecules of PEG and 2.40 molecules of octa-arginine were conjugated on each dendrimer molecule. The synthesized nano-conjugates were assessed in murine melanoma cancer cells (B16F10) and human lung carcinoma cells (A549) in cell monolayers and 3D multicellular spheroids well. The octa-arginine anchored nano-conjugate RVES-PD was internalized significantly into the cancer cells as evaluated by microscopy and flow cytometry experiments. The anti-cancer activity of PTX was significantly enhanced when loaded into the RVES-PD compared to free PTX. Attachment of VES and octa-arginine further improved the delivery of PTX to cancer cells due to solubilization of PTX into dendrimer cavity and anticancer activity of VES as well as attachment of cell penetrating peptide octa-arginine. The studies in multi-layered 3D spheroids clearly showed the benefit of attaching VES and octa-arginine to the surface of dendrimers which improved the penetration into 3D spheroids thereby accumulating the more amount of drug into cancer cells. Further, the in vivo efficacy study using B16F10 xenografted C57Bl6/J mice indicated that the RVES-PD localized in tumor sections. RVES-PD-PTX reduced the tumor growth significantly compared to free PTX and VES-PD-PTX. RVES-PD-PTX had more apoptotic potential in tumor sections as analyzed by TUNEL assay.

Altogether, these studies concluded the ability of multifunctional PAMAM dendrimer system in efficiently delivering PTX to cancer cells thereby improving the cytotoxic potential. Therefore, the newly developed PAMAM dendrimer-based drug delivery system is promising approach to deliver chemotherapeutics to cancer clinically.

Table of Contents	Page No.
Certificate	i
Acknowledgments	ii-v
Abstract	vi-ix
Table of Contents	x-xi
List of Tables	xii
List of Figures	xiii-xvii
List of Abbreviations	xviii-xx
Chapter 1 Introduction 1.1 Cancer 1.2 Cell biology of cancer disease 1.3 Biological hallmarks for cancer and their targeting 1.4 Cancer treatments 1.5 Nanoparticulate drug delivery system 1.6 Targeted drug delivery systems 1.7 Intracellular targeting 1.8 Dendrimers 1.9 Paclitaxel 1.10 Objectives	1-43
Chapter 2 α-Tocopherol Succinate-Anchored PEGylated Poly (amidoamine) Dendrimer for the Delivery of Paclitaxel: Assessment of in Vitro and in Vivo Therapeutic Efficacy 2.1 Abstract 2.2 Introduction 2.3 Materials and methods 2.4 Results and discussion 2.5 Conclusion	44-81
Chapter 3 Transferrin/α-tocopherol modified PAMAM Dendrimers for improved tumor targeting and anticancer activity of Paclitaxel 3.1 Abstract 3.2 Introduction 3.3 Materials and methods 3.4 Results and discussion 3.5 Conclusion	82-117
Chapter 4 Cell Penetrating Peptide and α-Tocopherol Conjugated Poly(amidoamine) Dendrimers for Improved Delivery and Anticancer Activity of Loaded Paclitaxel 4.1 Abstract 4.2 Introduction 4.3 Materials and methods 4.4 Results and discussion 4.5 Conclusion	118-160

Chapter 5	**Comparison of Paclitaxel loaded dendrimers** 5.1 Introduction 5.2 Comparison of particle size, zeta potential, EE%, DL% and *in-vitro* release 5.3 Comparison of cell uptake, cytotoxicity, apoptosis and growth inhibition of spheroids 5.4 Comparison of tumor volume reduction in B16F10 tumor-bearing C57Bl/6 mice 5.5 Conclusion	161-166
Chapter 6	**Conclusion**	167-170
Future scope of work		171-172
Appendix		173-175
List of publications and presentations		
Biography of candidate		A
Biography of supervisor		B
Biography of co-supervisor		C

List of Tables

Table No.	Title	Page No.
Table 1.1	Currently FDA and EMA approved nano-systems	14
Table 1.2	Approximate diameters (Generations = 0-7) of PAMAM dendrimers	25
Table 2.1	Molecular weight and approximate number of TOS and PEG attached to each PAMAM dendrimer assessed by GPC analysis	59
Table 2.2	Size, PDI, zeta potential, %EE and %DL values of PTX loaded dendrimer formulations and plain G4 dendrimer (Mean±SD, n=3)	61
Table 3.1	Molecular weight of each conjugates and estimated number of TOS, PEG and Tf attached to each PAMAM dendrimer obtained by SEC analysis	97
Table 3.2	Size, PDI, zeta potential, %EE and %DL values of PTX loaded dendrimer formulations and plain G4 dendrimer (Mean±SD, n=3)	99
Table 4.1	Relative molecular weight of each conjugate and estimation of the number of VES, PEG and octa-arginine attached to each PAMAM dendrimer obtained by SEC analysis	135
Table 4.2	Size, polydispersity index, zeta potential, % encapsulation efficiency and % drug loading values of various dendrimer nano-constructs (Mean ± standard deviation, n=3)	136
Table 5.1	Physical characteristics of PTX loaded dendrimer conjugates	162

List of Figures

Figure No.	Title	Page No.
Figure 1.1	Global burden of cancer	1
Figure 1.2	Estimated global burden of cancer in male in 2018	2
Figure 1.3	Estimated global burden of cancer in female in 2018	2
Figure 1.4	Cancer statistics in India according to WHO cancer country profiles 2020	3
Figure 1.5	The biological hallmarks of cancer	6
Figure 1.6	Therapeutic targeting of the hallmarks of cancer	6
Figure 1.7	Most commonly used nanoparticles for drug delivery	13
Figure 1.8	Schematic representation of the passively targeting DDS and the influence of nanoparticles for EPR	15
Figure 1.9	Schematic representation of the actively targeting DDS.	17
Figure 1.10	Synthesis of dendrimers by the divergent growth method	22
Figure 1.11	Synthesis of dendrimers by the convergent growth method	23
Figure. 1.12	Synthesis of dendrimers by the double exponential growth technique	23
Figure 1.13	Chemical structure of Paclitaxel	30
Figure 2.1	Schematic representation for α-TOS and PEG conjugation onto the G4 PAMAM dendrimer.	49
Figure 2.2	Proton NMR spectrum of G4-TOS-PEG in D2O at 300 MHz.	59
Figure 2.3	GPC chromatograms. (A) G4-TOS. (B) G4-TOS-PEG	60
Figure 2.4	In vitro release study (pH 7.4) (each data point is expressed as mean ± SD; n = 3).	62
Figure 2.5	(A) Percent hemolysis analyzed by the interaction between dendrimer conjugates and the RBCs. Data are represented as mean ± SD, n=3. The statistical significance of difference was assessed by ANOVA, and *p < 0.05. (B) Images of tubes containing centrifuged blood following treatment with formulations.	63
Figure 2.6	Cellular uptake of F-G4-PEG and F-G4-TOS-PEG in B16F10 (A) and MDA MB231 cells (B) measured by a flow cytometer at 1 and 4 h. The mean fluorescence data were plotted as bar graphs. The data were represented as mean ± SD, n = 3. The statistical significance of difference was evaluated by one-way ANOVA, and *p < 0.05 and **p < 0.01	64

Figure 2.7	Confocal microscopic images of (A) B16F10 and (B) MDA MB231 cells following treatment with FITC-labeled G4-PEG and G4-TOS-PEG for 1−4 h to assess the cellular internalization potential of the nanocarriers.	65
Figure 2.8	Percent cell viability of B16F10 and MDA MB231 cells treated with free PTX, Blank G4-PEG, Blank G4-TOS-PEG and PTX-loaded nanocarriers (at PTX concentrations at 0-50 μg/mL) and blank nanocarriers (without PTX loading) for 24 and 48 h (mean ± SD; n = 3). The significance of difference was calculated by one-way ANOVA. ** and * indicate $p < 0.01$ and 0.05, respectively.	66
Figure 2.9	Quantitative assessment of apoptosis in MDA-MB231 cells induced by free PTX, G4-PEG-PTX, and G4-TOS-PEG-PTX as studied by the AnnexinV assay (Q1, necrotic cells; Q2, late apoptosis; Q3, live cells; and Q4, early apoptotic cells)	67
Figure 2.10	Penetration efficiency of fluorescent-labeled G4-PEG and G4-TOS-PEG in MDA MB231 3D spheroids at various depths (Z-stacks) observed using a confocal microscope following 1 and 4 h of incubation	68
Figure 2.11	Quantitative evaluation of MDA MB231 3D spheroidal uptake of F-G4-PEG and F-G4-TOS-PEG by flow cytometry (data represented as mean ± SD; n = 3). The mean fluorescence data were plotted as bar graphs. The statistical significance of the difference between groups was assessed by ANOVA, and ***$p < 0.001$ and **$p < 0.01$.	69
Figure 2.12	(A) Bright field microscopic images of MDA MB231 spheroids after treatment with free PTX, G4-PEG-PTX, and G4-TOS-PEG-PTX captured at day 0, 3, 6, and 9 at 10× magnification. (B) MDA MB231 spheroid growth inhibition was shown in a bar graph (mean of diameter in μm with standard deviation; n = 3). The statistical significance of the difference between the groups was assessed by one-way ANOVA. ** indicates $p < 0.01$	70
Figure 2.13	Fluorescence microscopic images of the B16F10 tumor sections showing the localization of fluorescently labeled G4-PEG and G4-TOS-PEG after the intraperitoneal administration at 10 mg/kg. Objective, 20X	72
Figure 2.14	(A) Graph representing the tumor volume reduction over time. (B) Graphical representation of the body weight over time. (C) A Bar graph representing tumor weight of individual groups after study. (D) Images of tumors collected randomly from mice that received treatment as mentioned. The statistical significance of the difference between the groups was assessed by one-way ANOVA, and **$p < 0.01$ and *$p < 0.05$.	73
Figure 2.15	Detection of apoptosis by TUNEL assay in tumor cryosections treated with PTX formulations and free PTX as visualized by a fluorescence microscope. Magnification, 20X	74

Figure 3.1	Schematic representation of the synthesis of α-tocopheryl succinate, poly (ethylene glycol) and G4-TOS-PEG-Tf.	87
Figure 3.2	^{1}H NMR spectra of G4-TOS-PEG in D2O at 300 MHz	96
Figure 3.3	SEC chromatograms of synthesized dendrimer conjugates. (A) G4, (B) G4-TOS, (C) G4-TOS-PEG, (D) G4-TOS-PEG-Tf.	97
Figure 3.4	Free PTX and G4-TOS-PEG-PTX. (A) FTIR; (B) XRD; (C) TEM	100
Figure 3.5	*In vitro* PTX release study in PBS (pH 7.4) (Mean ± SD; n = 3)	101
Figure 3.6	(A) Cellular uptake study of FITC-labelled non-targeted G4-TOS-PEG and targeted G4-TOS-PEG-Tf in HeLa cells as assessed by flow cytometry instrument after 1 and 4 h (Mean ± standard deviation, triplicates). The bar graph represented the mean fluorescence observed. The statistical significance was assessed by applying one-way ANOVA, ***p<0.001. (B) assessment of cell internalization mechanism of fluorescently tagged non-targeted G4-TOS-PEG and targeted G4-TOS-PEG-Tf in HeLa cells assessed by flow cytometry instrument after 1 h and 4 h (Mean ± standard deviation, triplicates).	102
Figure 3.7	Cellular uptake and assessment of internalization mechanism of non-targeted G4-TOS-PEG and targeted G4-TOS-PEG-Tf in HeLa cells using confocal microscope	103
Figure 3.8	% cell viability of HeLa cells treated with free drug and drug loaded dendrimer conjugates (Mean with standard deviation; triplicates). The statistical significance was analyzed by applying one-way ANOVA test, ** and * represented p < 0.01 and 0.05, respectively.	105
Figure 3.9	Quantitative assessment of apoptosis. (a) control, (b) free paclitaxel, (c) PTX loaded non-targeted G4-TOS-PEG, (d) paclitaxel loaded targeted G4-TOS-PEG-Tf assessed by AnnexinV reagent. (Q1 denotes necrotic cells population, Q2 denotes late apoptotic population, Q3 denotes live cells population, Q4 denotes early apoptotitc population)	106
Figure 3.10	Penetration efficiency of fluorescently tagged G4-TOS-PEG as well as G4-TOS-PEG-Tf in HeLa spheroids at different depths visualized under confocal laser scanning microscope after 1 h and 4 h time points	107
Figure 3.11	Quantitative evaluation of uptake in HeLa spheroid treated with non-targeted F-G4-TOS-PEG and targeted F-G4-TOS-PEG-Tf as analyzed by flow cytometer (Mean and standard deviation; n = 3). The bar graph represented the mean fluorescence observed. The statistical significance between all the groups was carried out by applying one-way ANOVA test, ***p < 0.001	108
Figure 3.12	(A) Brightfield images of HeLa spheroids after treatment with free drug and drug loaded dendrimer conjugates. The images were captured at 0th Day, 2nd day, 4th day and 6th day at 10X magnification. (B) Representation of growth inhibition of HeLa	109

	spheroids as bar graph. The statistical significance between all the groups was assessed by applying one-way ANOVA test, ***p < 0.001 and **p<0.01.	
Figure 3.13	LIVE/DEAD cell assay of HeLa cells treated with free drug and drug loaded dendrimer conjugates	110
Figure 4.1	Scheme for the synthesis of RVES-PD	124
Figure 4.2	Proton nuclear magnetic resonance spectrum of RVES-PD in $CDCl_3$ at 300 MHz	133
Figure 4.3	SEC chromatograms of synthesized dendrimer conjugates. (A) G4 PAMAM dendrimer, (B) VES-D, (C) VES-PD, (D) RVES-PD	134
Figure 4.4	*In vitro* drug release study. Release of PTX from RVES-PD and VES-PD at pH 7.4 (Mean ± SD; n = 3)	137
Figure 4.5	(A) Flow cytometry analysis of cellular uptake of FITC-labelled RVES-PD and VES-PD in A549 cells. (B) Uptake of FITC-RVES-PD and VES-PD in A549 spheroids analyzed by flow cytometry. Data in graph is represented as mean ± standard deviation performed in triplicates. The bar graph represented the mean fluorescence observed. The significance was assessed by applying one-way analysis of variance, ***p<0.001	138
Figure 4.6	Cellular uptake and assessment of internalization mechanism of VES-PD and RVES-PD in A549 cells using confocal microscope.	140
Figure 4.7	Determination of cell viability by MTT assay performed using B16F10 and A549 cells. Percent cell viability of A549 and B16F10 cells incubated with free PTX, VES-PD-PTX and RVES-PD-PTX was determined at 24 and 48 h post incubation (n=3, mean with standard deviation). The statistical significance was analyzed by applying one-way analysis of variance test, ** and * represented p < 0.01 and 0.05, respectively	141
Figure 4.8	Annexin V assay. Quantitative assessment of apoptosis in A549 cells induced by RVES-PD-PTX, VES-PD-PTX and free PTX. R5-R2 denote necrotic, late apoptotic, early apoptotic, and live cells population, respectively	142
Figure 4.9	Penetration efficiency of fluorescently tagged RVES-PD and VES-PD in A549 spheroids at different depths visualized under confocal laser scanning microscope following 1 h and 4 h incubation	143
Figure 4.10	(A) Bright field images of A549 spheroids after treatment with free PTX, VES-PD-PTX and RVES-PD-PTX. The images were captured at 0, 2, 4 and 6 th day at 10X magnification. (B) Graphical representation of the growth inhibition of A549 spheroids. The significance between all the groups was assessed by one-way analysis of variance test, ***p < 0.001 and **p<0.01	144
Figure 4.11	(A) Fluorescence microscopic images of tumor, heart and kidney sections isolated from the mice treated with FITC-labeled VES-PD and RVES-PD for 4, 8 and 24 h. (B) Fluorescence microscopic images of liver, spleen and lungs sections isolated	146

	from the mice treated with FITC-labeled VES-PD and RVES-PD for 4, 8 and 24 h. Tumor sections are visualized at 20 X objective.	
Figure 4.12	Assessment of therapeutic efficacy of RVES-PD-PTX, VES-PD-PTX and free PTX in B16F10 tumor bearing C57Bl/6 mice. Graphical representation of (A) tumor volume vs. days during treatment, (B) Measurement of body weight during treatment, and (C) The average weight of tumors isolated from various treatment groups. (D) Representative tumors isolated from animals' post treatment, (E) Measurement of caspase 3/7 levels in tumor homogenates. The significance between the groups was evaluated by one-way analysis of variance, where ***$p < 0.001$, **$p < 0.01$ and *$p < 0.05$	147
Figure 4.13	Determination of apoptosis by TUNEL assay. The treated tumor sections are visualized under fluorescence microscope with 20X magnification	149
Figure 5.1	Graph representing the tumor volume reduction of different dendrimer based formulations over time	165

List of Abbreviations and Symbols	
1H NMR	Proton nuclear magnetic resonance
A549	lung carcinoma cells
B16F10	Murine melanoma cancer cells
CPZ	Chlorpromazine
D_2O	Deuterium oxide
DAPI	4',6-diamidino-2-phenylindole
DIPEA	N-ethyl-di-isopropylamine
DL	Drug loading
DMEM	Dulbecco's modified Eagle's media
EDC.HCl	1-ethyl-3-(3-dimethylaminopropyl) carbodiimide hydrochloride
EE	Encapsulation efficiency
F	Fluorescein
FBS	Fetal bovine serum
FITC	Fluorescein isothiocyanate
FTIR	Fourier-transform infrared spectroscopy
G4	Generation 4.0
G4 PAMAM or D	Generation 4 Poly(amidoamine)
G4-PEG	PEGylated G4 PAMAM dendrimer
G4-PEG-PTX	Paclitaxel loaded PEGylated G4 PAMAM dendrimer
G4-TOS-PEG	α-tocopheryl succinate conjugated PEGylated G4 PAMAM dendrimer
G4-TOS-PEG-PTX	Paclitaxel loaded α-tocopheryl succinate conjugated PEGylated G4 PAMAM dendrimer
G4-TOS-PEG-Tf	Transferrin conjugated α-tocopheryl succinate conjugated PEGylated G4 PAMAM dendrimer
G4-TOS-PEG-Tf-PTX	Paclitaxel loaded transferrin conjugated α-tocopheryl succinate conjugated PEGylated G4 PAMAM dendrimer
GPC	Gel permeation chromatography
GPC	Gel Permeation Chromatography
HeLa	Human cervical carcinoma cells
HPLC	High-performance liquid chromatography

mal-PEG-NHS ester	Maleimide-polyethyleneglycol-N-hydroxysuccinimidyl ester
MDA MB231	Breast adenocarcinoma cells
MDR	Multiple drug resistance
mg	Milligram
min	Minute
mL	Millilitre
mM	Millimolar
mm	Millimetre
mol	Moles
MTT	3-(4,5-dimethylthiazol-2-yl)-2,5-diphenyltetrazolium bromide
mV	Millivolts
MWCO	Molecular weight cut-off
NHS	N-hydroxysuccinimide
nm	Nanometer
NMR	Nuclear magnetic resonance
PBS	Phosphate buffer saline
PDI	Polydispersity index
PEG or P	Polyethylene glycol
PI	Propidium iodide
PTX	Paclitaxel
R8 or R	octa-arginine; A549, lung carcinoma cells
RVES-PD	Octaarginine anchored Vitamin-E succinate conjugated PEGylated G4 PAMAM dendrimer
RVES-PD-PTX	PTX loaded Octaarginine anchored Vitamin-E succinate conjugated PEGylated G4 PAMAM dendrimer
SD	Standard deviation
SEC	Size exclusion chromatography
Tf	Transferrin
UV	Ultraviolet
VES	Vitamin-E succinate
VES-D	Vitamin-E succinate conjugated G4 PAMAM dendrimer

VES-PD	Vitamin-E succinate conjugated PEGylated G4 PAMAM dendrimer
VES-PD-PTX	Paclitaxel loaded Vitamin-E succinate conjugated PEGylated G4 PAMAM dendrimer
WHO	World health organization
XRD	x-ray powder diffraction
α-TOS	α-tocopheryl succinate
λmax	Wavelength maxima for UV-absorbance
μg	Microgram
μL	Microlitre
μM	Micromolar

Chapter 1

Introduction

1.1 Cancer

Cancer is the malignant and autonomous progress of cells which is induced by epigenetic and genetic mutations thereby escaping normal cell cycle (Rubin, Strayer, and Rubin 2008). The millions of people are killed every year due to cancer disease irrespective of age, gender and origin. The normal cells are transformed to cancer cells due to external stimulus by damaging DNA in the normal cells e.g. certain carcinogens like ultraviolet light, cigarette, tobacco, food contaminants, water pollutants, certain viral/bacterial infections, or genetic mutations (Rubin, Strayer, and Rubin 2008, Nair, Varghese, and Swaminathan 2005). Lifestyle related factors like excessive alcohol use, unhealthy diet, and physical inactivity also pose considerable risk of developing cancer (Ingole, Kakde, and Bonde 2016).

Cancer is the first or second leading cause of premature death in 134 of 183 countries in the world (Ferlay et al. 2019). In 2018, there were an estimated 18.1 million new cases and 9.6 million deaths from cancer. Cancer will develop in one in five people before they reach the age of 75 (Organization 2020). The cancer statistics in world is reported has been below.

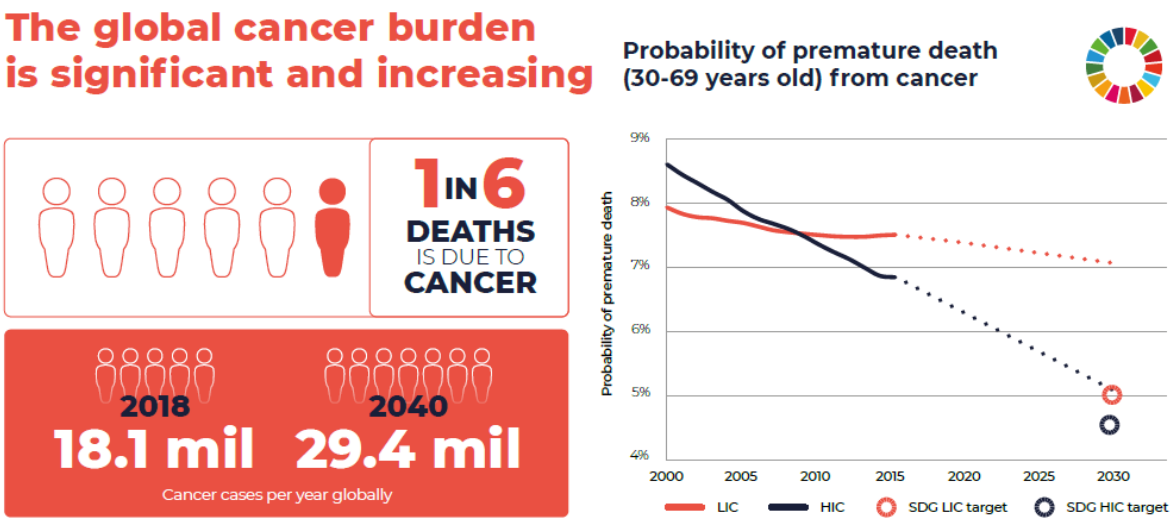

Figure 1.1. Global burden of cancer (Organization 2020)

	Incident cases	
Lung	1 368 524	**14.5%**
Prostate	1 276 106	**13.5%**
Colorectum	1 026 215	**10.9%**
Stomach	683 754	**7.2%**
Liver	596 574	**6.3%**
Bladder	424 082	**4.5%**
Oesophagus	399 699	**4.2%**
Non-Hodgkin lymphoma	284 713	**3%**
Kidney	254 507	**2.7%**
Leukaemia	249 454	**2.6%**
Other cancers	2 892 790	**30.6%**
Total Cases	**9 456 418**	**100%**

Figure 1.2. Estimated global burden of cancer in male in 2018 (Organization 2020).

	Incident cases	
Breast	2 088 849	**24.2%**
Colorectum	823 303	**9.5%**
Lung	725 352	**8.4%**
Cervix uteri	569 847	**6.6%**
Thyroid	436 344	**5.1%**
Corpus uteri	382 069	**4.4%**
Stomach	349 947	**4.1%**
Ovary	295 414	**3.4%**
Liver	244 506	**2.8%**
Non-Hodgkin lymphoma	224 877	**2.6%**
Other cancers	2 482 031	**28.8%**
Total Cases	**8 622 539**	**100%**

Figure 1.3. Estimated global burden of cancer in female in 2018 (Organization 2020).

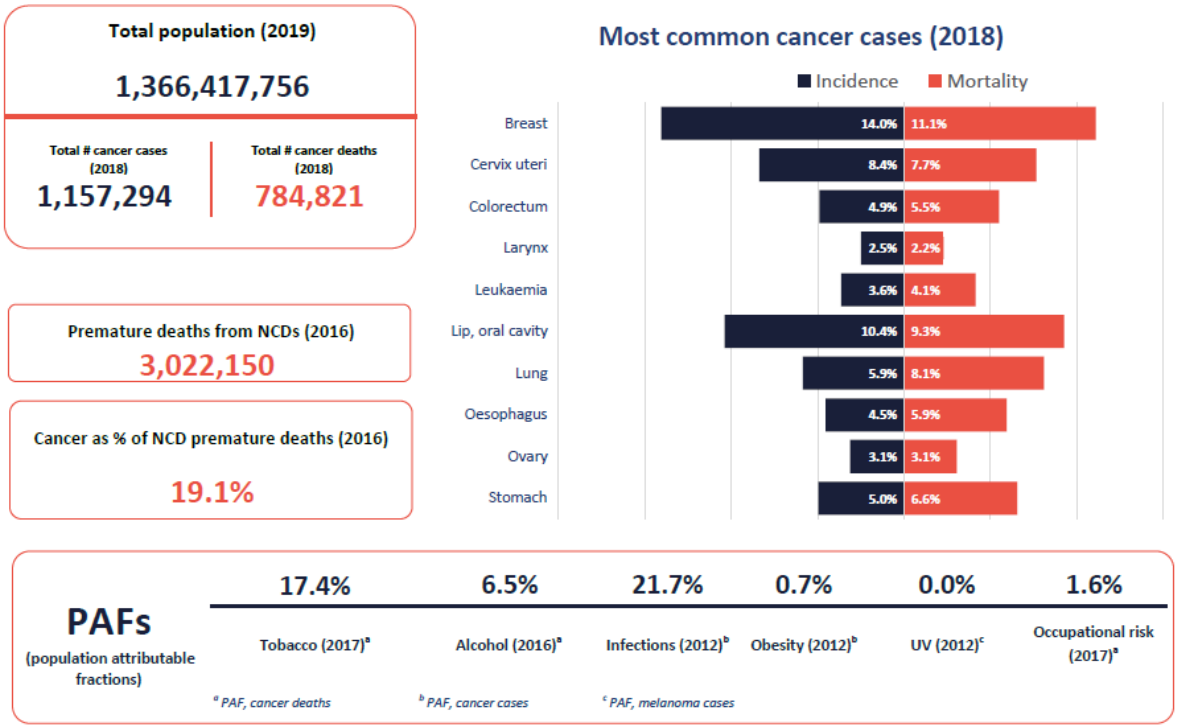

Figure 1.4. Cancer statistics in India according to WHO cancer country profiles 2020 (https://www.who.int/cancer/country-profiles/IND_2020.pdf?ua=1).

The normal cells in the human body are developed and divide to form new cells as per the need of the human body (Sherwood 2015). As time goes, the normal cells die or become damaged, and those old cells are replaced by new cells formed as a general mechanism whenever it is necessary in a healthy human being. Sometimes the normal cells may start growing uncontrollably due to fault in cell to cell communication which leads to irregularities in the cell growth. These abnormalities make the old or damaged cells continue to live which resulted the formation of tumor. They spread in the whole human body to places where they do not belong due to loss of ability to distinguish their own boundaries. The division of the cells is controlled and functioned by the nucleus which contains the genetic material deoxyribonucleic acid (DNA), a blueprint for everything the cell does, depending on the body's need (O'Connor, Adams, and Fairman 2010).

The structural proteins are synthesized by certain genes whereas some other genes direct the cell to form hormones, growth factors or cytokines, which travel outside the cell and start signal transmission with other cells. The regulatory proteins is synthesized by some genes which control the function of proteins or convey other genes when to turn "on" or "off." (Griffiths et al. 2005).

In the mitosis, the cells divide from parent to daughter cells, a event is called cell cycle. The cell cycle consists of mitosis phase (M phase) and a synthetic phase called S Phase. DNA is synthesized during S phase. Between M phase and S phase is G1 phase where RNA, proteins, and enzymes needed for DNA synthesis in S phase are produced. After S phase is the G2 phase which prepares the cell for M phase. G0 phase is the resting phase where the non-dividing cells fall. The normal cells are divided according to this process of cell cycle (Hartwell and Weinert 1989).

1.2 Cell biology of cancer disease

The 90% of all cancers induced due to damage in DNA which causes genetic mutations occur in somatic cells arbitrarily, or by exposure to certain carcinogens such as ultraviolet light, cigarette, tobacco, food contaminants, water pollutants, certain viral/bacterial infections like human papilloma virus (HPV) (Siegel, Naishadham, and Jemal 2012, Curiel and Douglas 2007). The remaining 10% of cancers are induced by heredity from the family history such as breast cancer 1 (BRCA1), breast cancer 2 (BRCA2) (Walsh and King 2007), or adenomatous polyposis coli (APC) for familial adenomatous polyposis colorectal cancers (Curiel and Douglas 2007).

Cancer is induced by the genetic mutations like inactivation tumour suppressor genes or activation of oncogenes (Rubin, Strayer, and Rubin 2008, Walsh and King 2007). The genetic mutations include frameshift mutations (change in reading frame), missense mutations (change in amino acid sequences), or non-sense mutations

(truncated proteins) which affect functions of other proteins responsible for the DNA damage repair, cell functions, cell cycle and apoptosis such as p53 (Walsh and King 2007, Muyrers-Chen and Paro 2001). This irregularities is the major cause for cancer developed due to gene mutations (Rubin, Strayer, and Rubin 2008, Walsh and King 2007, Muyrers-Chen and Paro 2001). Hence, there are some hallmarks of cancer which shows typical characteristics of cancer which are not seen in healthy human beings (Rubin, Strayer, and Rubin 2008, Walsh and King 2007, Verma, Agarwal, and Verma 2014, Hanahan and Weinberg 2011). These are as follows:

- Loss of contact through abnormal cell adhesion.
- Irregularities in cell cycle and apoptosis
- Augmented response to growth inducing agents by altering the transmission of growth regulating signals.
- Weakness in immune defence.
- Irregularities in angiogenesis.

Cancer due to epigenetic inheritance is developed by the non-encoded genes in the primary sequence of the DNA, or changes in histone acetylation, histone methylation and DNA methylation (Muyrers-Chen and Paro 2001, Verma, Agarwal, and Verma 2014, Phillips 2008). Sometimes chronic inflammation (i.e. Crohn's disease, hepatitis, cystitis) also cause cancer (about 15–25%) by providing the right environment to growth factors, DNA-damaging agents like oxidative stress which promote the exaggerated proliferation (Eiró and Vizoso 2012, Kawasaki and Abe 2012).

1.3 Biological hallmarks for cancer and their therapeutic targeting

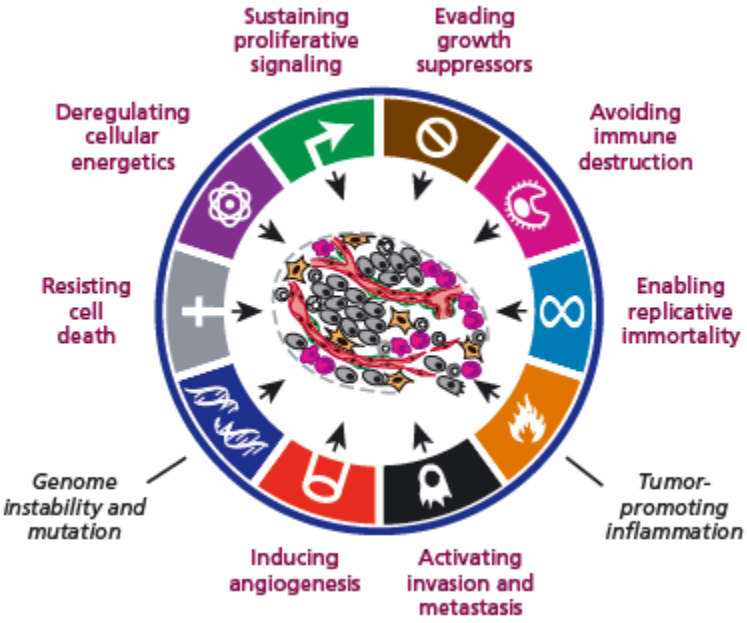

Figure 1.5. The biological hallmarks of cancer (Hanahan and Weinberg 2011).

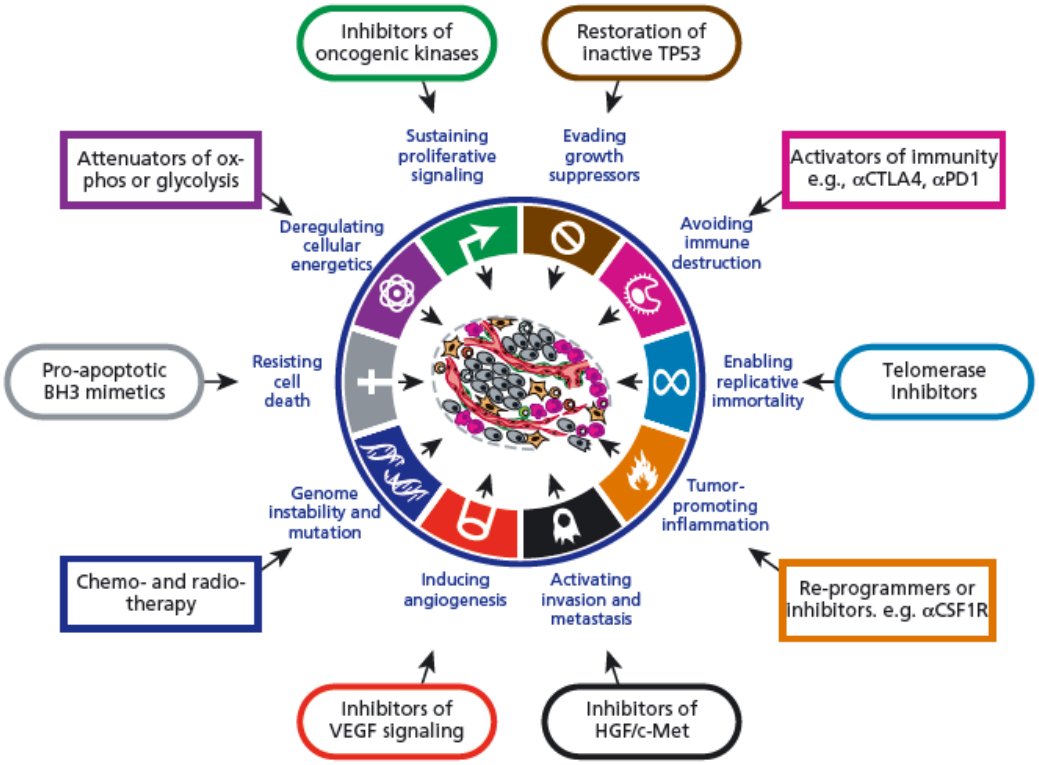

Figure 1.6. Therapeutic targeting of the hallmarks of cancer (Hanahan and Weinberg 2011)

Hanahan et al. has identified the hallmarks acquired at different stages in the cancer which has distinct characteristics for each type of human cancers like carcinoma,

sarcoma, myeloma, leukemia, lymphoma and mixed types (Hanahan and Weinberg 2011). The six hallmarks of cancer are sustaining proliferative signaling, evading growth suppressors, resisting cell death, enabling replicative immortality, inducing angiogenesis, and activating invasion and metastasis.

The anti-cancer drugs targeting hallmarks have been developed which interfere with all six hallmarks, and including genome instability and tumor-promoting inflammatory markers. Some of these chemotherapeutic drugs are in clinic, some are being tested in the clinical trials while others are being tested pre-clinically. Eventually, the development of resistance during cancer treatment with these hallmark targeting drugs is apparent and co-targeting of multiple hallmarks with chemotherapeutics may prevent the emergence of drug resistance clinically and preclinically (Hanahan 2014).

1.4 Cancer treatments

The suitable cancer treatments which include chemotherapy, radiotherapy and surgery, are given to the patients depending on the type and stage of cancer as well as age and gender of the human being. The chemotherapy and radiotherapy are commonly used cancer treatments, often given in combinations followed by surgery (Urruticoechea et al. 2010). But, these commonly used cancer treatments have several drawbacks like poor prognosis and severe side effects. Hence, there is a need to develop better treatments to improve the current outcomes.

1.4.1 Chemotherapy

Chemotherapy is the most commonly used cancer treatment which consists of several hormones, targeted immunotherapy or most commonly used cytotoxic drugs. The cytotoxic drugs categorized based on the mechanism of action are: alkylating agents (cyclophosphamide, ifosfamide, dacarbazine, carmustine, lomustine), antimetabolites (Folate antagonists, purine analogues), natural products and microtubule inhibitors.

Taxanes (paclitaxel, docetaxel, and cabazitaxel), and vinca alkaloids (vincristine, vinblastine, vinorelbine) act on the spindle apparatus during cell division. These drugs can be given before surgery to reduce the tumour size or adjuvantly after surgery to inhibit metastasis, or in the combination with radiotherapy or hormonal therapy (Huitink and Teoh 2013). The cytotoxic drugs act rapidly on dividing cells but they are not able to distinguish between cancer cells and healthy labile cells like bone marrow cells, gastric mucosa lining, and skin cells (Huitink and Teoh 2013, Urruticoechea et al. 2010, Galmarini, Galmarini, and Galmarini 2012). These drugs are given at the maximum tolerated dose (MTD) resulting in dose limiting toxicity in the healthy cell also. Moreover, these drugs cause myelosuppression, nausea, vomiting, mucositis and alopecia (Frishman et al. 1997). Furthermore, these anti-cancer agents such as anthracyclines cause damage to permanent tissues like heart, kidneys and brain. The cyclophosphamide and ifosfamide cause cardiac failure and life-threatening arrhythmias at high doses (Frishman et al. 1997). The doxorubicin and cyclophosphamide cause neurocognitive deficits such as impaired learning, attention, memory and information processing speed in approx. 40% breast cancer treated patients (Monje and Dietrich 2012, Jansen et al. 2008). Consequently, due to these side effects, survival rate of patients falls with the chemotherapy which limits its application in clinic (Galmarini, Galmarini, and Galmarini 2012).

1.4.2 Radiation and surgery

Radiation therapy is rarely given alone, and often is given in combination with chemotherapy to treat approximately 60% of all cancers, or post-surgery to remove any malignant cells post-surgery (Huitink and Teoh 2013, Urruticoechea et al. 2010).

Ionizing radiation is applied to induce DNA damage in malignant cells which cause programmed cell death and reduce tumour size. Though, the patients suffer severe side

effects in normal tissue after radiation therapy resulting in failure to treat the cancer leads to poor prognosis (Mayer et al. 2011).

Surgical treatments are frequently used in the treatment of breast cancer (lumpectomy), ovarian cancer, some intestinal cancers, and lung cancers (pneumonectomy). But these procedures cause other morbidities like psychological problems and deprived quality of life. The pain is induced after mastectomy in 25% of women which cause depression social isolation, anxiety and low self-esteem (Miaskowski et al. 2012, Enache 2012).

1.4.3 Limitations of conventional cancer treatments

The current cancer treatments have some drawbacks although the cytotoxic drugs are being used alone or in combinations.

Poor solubility in water and biological fluid: More than 90% of the anti-cancer agents are poorly water soluble and necessitate some toxic solvents in formulations. These chemotherapeutic agents suffer from low bioavailability problems and needs dosing frequently to achieve minimum effective therapeutic concentrations in blood. Intravenous dosage forms require the active agents in solubilized form in aqueous media to stay in the biological system. For example, Paclitaxel (PTX), a highly potent anti-cancer agent has poor solubility of less than 0.5 mg/L (Kakde et al. 2011). Hence, Taxol ® was developed to solubilize the PTX in Cremophor EL (castor oil derivative) and dehydrated alcohol to be administered intravenously which causes serious toxicities to heart, kidney, brain, hypersensitivity, systemic toxicity, and peripheral neuropathy (Rowinsky et al. 1993). Moreover, when the drug is solubilized in the surfactants in the formulations, it may get precipitated in vivo, due to their high critical micelle concentration in biological fluids.

Non-specific toxic effect: When conventional anticancer agents are administered by intravenous route, they go into the blood circulation and reaches to the cancer cells and

normal cells well. These agents have broad biodistribution profile and show non-specific toxicities resulting in serious side effects such as bone marrow depression, systemic toxicity, alopecia, anaemia, weight loss, nausea, diarrhoea, infertility, cardiovascular toxicity, vomiting etc. Also, the cells develop drug resistance to these single agent therapies over the period of time (Stortecky and Suter 2010). The absence of selective mechanism of action is a noticeable drawback of conventional chemotherapy.

Internalization by reticuloendothelial system (RES): The rapid clearance of hydrophobic drugs from systemic circulation is major drawback due to presence of macrophages and monocytes in the reticular connective tissue (ex: liver, spleen) compose the reticuloendothelial system (Kakde et al. 2011). They eliminate the foreign particles and pathogens from the circulation by phagocytosis mechanism. Most of the anti-cancer agents are lipophilic in nature and they get engulfed by the RES which results in rapid clearance of drug from the systemic circulation. Hence, very high drug concentrations need to be administered to reach the therapeutic concentrations at the target site and elicit the good response. RES uptake is influenced by the lipophilicity of the delivery system, particle size and surface charge.

Drug resistance (MDR): The cancers cells become resistant to the drugs over the period of time and it is the major drawback associated with conventional chemotherapy. The over-expression of P-glycoprotein (P-gp), a the major efflux protein of the family of ATP binding cassette (ABC) transporters, in the resistance cells effluxes the drugs out of the cell obstructing intracellular accumulation of therapeutic agents (Kakde et al. 2011, Chidambaram, Manavalan, and Kathiresan 2011).

Poor vascularization: Tumor environment decreases the drug accumulation to the entire cancer tissue due to poor vascularization leading to low therapeutic efficacy of drugs in

cancer cells. Some of the basic drugs get ionized in the acidic environment of the tumor which prevents their movement across the cell membrane. High interstitial pressure and low microvascular pressure may also holdback the extravasation of drug molecules. Apart from the drug efflux pumps, cancer cells also show drug resistance by decreasing the uptake of drug, increasing the drug metabolism, altering the drug targets, impair apoptotic pathways and cell cycle checkpoints (Bar-Zeev, Livney, and Assaraf 2017).

The ideal cancer chemotherapy involves the delivery of the right amount of drugs in a controlled manner for the suitable time period to the tumor to achieve the desired therapeutic response and cause no damage to the normal cells. To accomplish this objective, the delivery systems should be designed in such a way that it should hold required amount of chemotherapeutic agent and it should eliminate the drawback of poor bioavailability, unfavourable biodistribution, rapid clearance, non-specific toxicities, and drug resistance. Hence, the drug delivery system should be able to remain in the systemic circulation for longer period of time, with tumor specificity, more drug accumulation in tumor, and modified drug release, providing the maximum therapeutic efficacy of the chemotherapeutic agents.

1.5 Nanoparticulate drug delivery system

Pharmaceutical nanotechnology is a developing branch in pharmaceutical and biomedical sciences. It involves the applications of nanotechnology to pharmaceuticals and biopharmaceuticals as nanomaterials for drug delivery, diagnostic, imaging, and biosensors as an alternative to conventional dosage form. Nanoparticulate drug delivery system is powerful tool which provided more fine-tuned diagnosis and focused treatments for various diseases such as cancer, diabetes mellitus, neurodegenerative diseases, detecting the microorganisms and viruses at a molecular level. It is anticipated

that the pharmaceutical market will be flooded with nanotechnology-based medicine called nanomedicine in next 10 years (Rana and Sharma 2019).

The nanocarriers allows the materials to carry, bind, or absorb a variety of drugs, genetic material, peptides and, diagnostic agents with great efficacy due to their nanometer size (1-1000 nm) and high surface to volume ratio which discriminate nanomaterials from other conventional materials. The nanomedicine are capable of improving the solubility of poorly soluble drugs, and improving the bioavailability of poorly absorbed drugs in the human body (Senapati et al. 2018, Chavda 2019).

The nanocarriers discovered in the cancer chemotherapy can be categorized into targeted and non-targeted nanocarriers. Liposomes, polymeric nanoparticles, nanocrystals, dendrimers, polymeric micelles, albumin bound nanoparticles, metal nanoparticles, and polymer-drug conjugates are some of the widely explored nano systems for delivery of chemotherapeutic agents (Peer et al. 2007).

The drug is either covalently conjugated to the system or it can be entrapped physically in the delivery system to provide the drug release in controlled manner. The drug degradation, first pass metabolism and precipitation in the biological system can be prevented by entrapping the drugs inside the nanocarriers leading to improved bioavailability (Bobo et al. 2016).

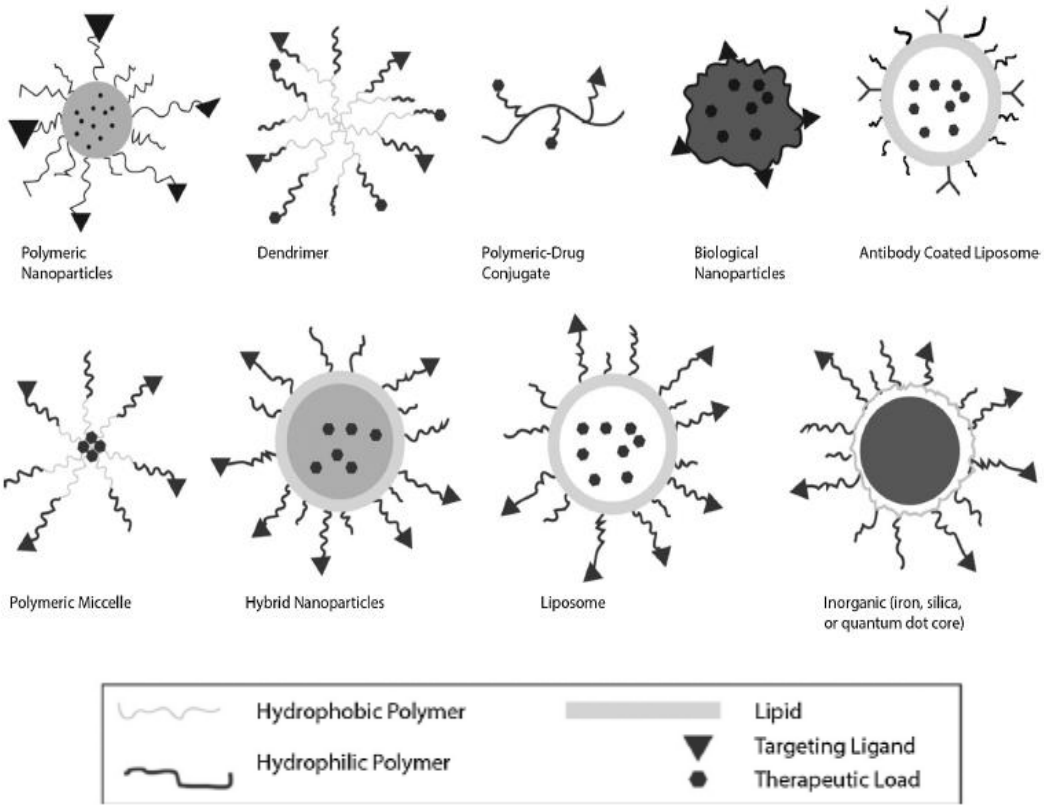

Figure 1.7. Most commonly used nanoparticles for drug delivery (Cerqueira et al. 2015)

In 1960, the liposome was developed as first nanocarriers by encapsulating the chemotherapeutic drug doxorubicin to treat various cancers (Farokhzad and Langer 2009). As research progressed over the period of time, the various nanocarriers have been investigated for the delivery of anti-cancer agents due to their capability of improving the solubility and stability of lipophilic drugs, reducing the non-specific uptake in the body, improving circulation time in blood, reducing undesirable side effects, improving cellular association, and effective targeting to tumors.

Name	Nanosystems	Active component	Target	Company
Myocet™	Liposomal	Doxorubicin	Breast cancer	Elan Pharmaceuticals
Abraxane	Albumin bound	Paclitaxel	Metastatic breast cancer	Abraxis Bioscience
Doxil	PEGylated liposomal	Doxorubicin	Ovarian cancer	Ortho Biotech
Eligard	Biodegradable polymer	Leuprolide acetate	Prostate cancer	Sanofi
Caelyx	PEGylated liposomal	Doxorubicin	Kaposi's sarcoma	Schering Plough
DaunoXome	PEGylated liposomal	Daunorubicin	Kaposi's sarcoma	Diatos
Genexol-PM	Polymeric micelles	Paclitaxel	Breast and lung cancer	Samyang Biopharmaceuticals
Oncaspar	Polymeric micelles	L-asparaginase	Lymphoblastic leukaemia	Sigma-Tau Pharmaceuticals

Table 1.1. Currently FDA and EMA approved nano-systems (Cerqueira et al. 2015).

The nanocarriers offer following advantages:

- Improvement in the therapeutic index of encapsulated drugs encapsulated in compared to their conventional dosage forms.
- Augmenting the drug efficacy by sustaining the steady state therapeutic concentrations over a period of time.
- Capable of escaping the phagocytosis by RES with the help of surface modification with polymers such as polyethylene glycol.
- Potential to conjugate a variety of ligands/drugs which can actively target the receptors overexpressed in the cell.
- Capability of accumulating in the tumor tissue passively by enhanced permeation and retention (EPR) effect due to the nano size.

1.6 Targeted drug delivery systems (TDDS)

Conventional dosage forms for tumor treatment are usually administered through intravenous injection or oral route. Though, the drug molecules will be distributed systemically after entering into the systemic circulation, they are rapidly eliminated from the body leading to poor bioavailability of drugs and unwanted toxic side effects.

Hence, a typical strategy to overcome these issues is the surface functionalization of nanocarriers or drugs by proteins, nucleic acids, enzymes, receptors and other functional biological molecules to effectively reach tumor sites in a highly selective manner. So the design of functional DDSs needs to specifically deliver the drug to target sites (Torchilin 2006, Breunig, Bauer, and Göpferich 2008, Bae and Park 2011). The targeting of drugs can be divided into two major categories in general: passive targeting and active targeting (Koo et al. 2011).

1.6.1 Passive tumor targeting

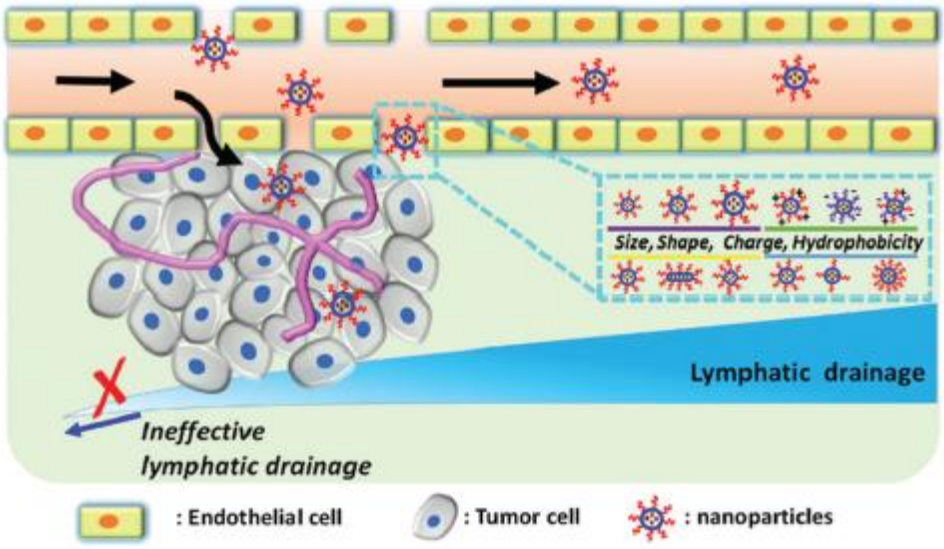

Figure 1.8. Schematic representation of the passively targeting DDS and the influence of nanoparticles for EPR. Nanoparticles passively extravasate though the leaky vasculature and accumulate in tumors due to the damaged lymphatic drainage (Dai et al. 2016).

Most solid tumors have unique pathophysiological characteristics such as augmented angiogenesis, defective vascular architecture, limited lymphatic drainage, and increased production of a number of permeability mediators (Maeda et al. 2000, Petrova et al. 2004). Hence, the passive targeting to the solid tumor majorly depends on the enhanced permeation and retention (EPR) effect that has been unanimously observed in solid tumors (Greish 2012). Matsumara et al. discovered the EPR effect in 1986 and

was considered as ‘‘a crucial step’’ by the researchers (Torchilin 2011). Moreover, the rapid vascularization allows the external nutrients and oxygen which are important for rapid tumor growth. The defects in the tumor blood vessels allow to extravasate the large molecules and nanocarriers and enhances their retention in the tumor.

In addition, high interstitial fluid pressure and impaired lymphatic drainage in the tumor environment governs the passive targeting by the size of nanocarriers/macromolecular drugs preferably with suitable size around 100 nm by accumulating the higher amount of drug in the tumor (Dai et al. 2016). The nanoparticles with size around 100 nm facilitate the leakage from defective tumor vessels, avoid kidney filtration and evade the capture by RES (Qiu et al. 2010, Chithrani, Ghazani, and Chan 2006).

Moreover, the surface charges of the nanocarriers also influence the phagocytic uptake by RES. For example, negatively charged/neutral nanoparticles have arbitrary effect on the systemic clearance (Bertrand et al. 2014) but positively charged nanoparticles are up taken more rapidly compared to other charged particles due to the electrostatic interactions with negatively charged cell membrane (Thorek and Tsourkas 2008, Wang et al. 2010). Hence, the EPR effect offers a great opportunity for targeting of lipid or polymer conjugated anticancer drugs/nanocarriers to the tumor tissues (Figure 8).

1.6.2 Active tumor targeting

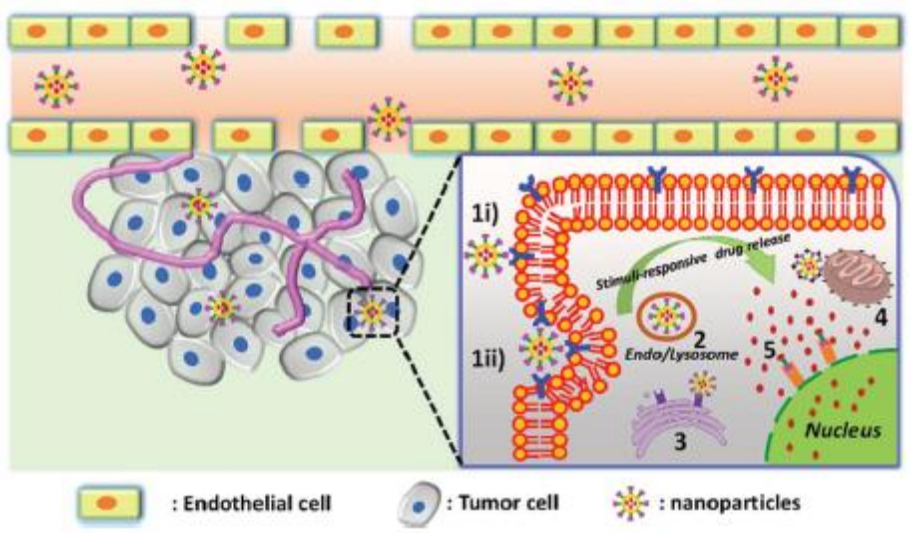

Figure 1.9. Schematic representation of the actively targeting DDS. Targeting ligands grafted on the surface of nanocarriers bind to receptors overexpressed by tumor cells and facilitate internalization via receptormediated endocytosis. Target receptor/sites mainly exist on the tumor (1) cytomembrane, (2) endo/lysosome, (3) endoplasmic reticulum, (4) mitochondria and (5) nucleus. Intracellular drug release is triggered by special stimuli (Dai et al. 2016).

The surface of nanocarriers are capable for modification by attaching specific ligands or antibodies which is called active targeting or ligand-mediated targeting. This targeting approach can enhance the uptake of nanocarriers in tumors and improve the therapeutic efficacy of the anticancer agents in the tumor sites. In addition, it could also reduce the unwanted side effects and toxicities because the ligand mediated nanocarriers bind specifically to the over-expressed receptors in tumors (Figure 9). Some of the widely used ligands for active targeting of nanocarriers include transferrin, folic acid, biotin, hyaluronic acid, lactoferrin, angiopep, cyclic RGD peptide etc.

The antitumor efficacy of cytotoxic drugs could be enhanced by developing the smart nanocarriers which effectively deliver the chemotherapeutic drugs to the cytoplasm in response to various endogenous (pH, redox, etc.) and exogenous (temperature, light, ultrasound, magnetic, etc.) stimuli. Hence, the actively targeted nano systems has gained more attention and they have shown better performance than non-targeted nano

systems in terms of enhanced cytotoxicity to tumor cells and the elimination of side effects.

1.7 Intracellular targeting

The chemotherapeutic agents are localized in the particular targets in the intracellular compartments (cytosol, mitochondria or nuclei) thereby reaching the targets through diffusion which depends on biological forces responsible for the cell penetration. These vectors provide improved delivery of chemotherapeutic drugs to these subcellular compartments thereby leading to enhanced specificity and efficacy, with lesser toxicity (Pandya and Debinski 2012). One such approach of intracellular targeting to specific organelles can be achieved by special class of peptides called cell penetrating peptides.

Some carriers enter into endo/lysosomes and release the drugs or escape into the cytosol and then release the drugs. The released drug molecules have to translocate from the cytosol to the nucleus. This cytosol-targeted drug delivery followed by drug nuclear localization is achieved by increasing cytosolic drug concentration to facilitate the drug nuclear accumulation (Minotti et al. 2004).

Attaching nanocarriers with biorecognized molecules such as ligands whose receptors are overexpressed on tumor cell surface leads to receptor-mediated endocytosis and thus promote their cellular uptake. Such ligands including folic acid (FR), peptides, antibodies, transferrin (Tf), interleukin 13, epidermal growth factor (EGFR) and transforming growth factor-α and some other moieties have been shown to contribute to nuclear delivery of various chemotherapeutic drugs (Zaki and Tirelli 2010, Yoon et al. 2011).

Generally, nanocarriers are internalized by receptor-mediated endocytosis, become entrapped in endosomes, and eventually encounter late endosomes and lysosomes where active degradation of the nanoparticles and drugs takes place. The pH of early

endosomes is typically near 6, the pH of late endosomes is near 5 and that of lysosomes is about 4 to 5. The acid pH and related enzymes in these compartments are extensively used to trigger drug release from the carriers for the drugs to diffuse into the cytosol and nucleus (Ganta et al. 2008, Sahay, Alakhova, and Kabanov 2010, Steinman et al. 1983).

1.7.1 Cell penetrating peptides

Ineffective penetration of chemotherapeutic agents and nanoparticles is a noteworthy concern with chemotherapy (Ruoslahti 2017). The tumor microenvironment contains dense connective tissue which restricts the free movement of drug molecule into the tumor cells (Ruoslahti 2017, Uchida et al. 2011). In addition, the leaky vasculature creates high osmotic pressure zone within the tumor due to which fluid cannot penetrate inside, and hence, the chemotherapeutics cannot enter freely. Eventually, very little drug amount reaches to the core of tumor cells. Hence, the cells in the core of tumor develop resistant over multiple drug administrations (Ruoslahti 2017). This concern can be overcome by using cell penetrating peptides (CPPs).

CPPs are short peptides which consist less than 40 amino acids and are able to deliver the bioactive cargoes intracellularly in energy-dependent or independent manner by means of various endocytosis mechanisms (Langel 2007, Ye et al. 2016). Most of the CPPs are cationic, assume amphipathic structures and are rich in lysine and arginine residues (Hackett 2012).

The mechanism of internalization largely depends on the nature of CPP employed such as its length, charge, amphiphilicity along with the properties of cargo being transported. It further depends on the type of cell target and the CPP to cell ratio employed (Papadopoulou and Tsiftsoglou 2013). The mechanism of cellular uptake mainly is the endocytosis. CPPs enter into the cells via clathrin/caveolin mediated

endocytosis or macropinocytosis. The arginine rich positively charged CPPs were reported to establish electrostatic interactions and hydrogen bonding between the guanidine group of arginine and the negatively charged cell membrane (like heparin sulphate proteoglycans, phosphates or carboxylates) before undergoing endocytosis or macropinocytosis (Papadopoulou and Tsiftsoglou 2013, Shin et al. 2014).

Deshpande et al. has reported that the optimum number of arginine residues needed for maximum activity is around 8 among polyarginines (Deshpande et al. 2018). A reduction in the activity was reported for polyarginines longer or shorter arginine residues than 8. Therefore, the CPP, octa-arginine (R8) can be regarded as a basic or a proto-type of the proteintransduction domains. Khalil et al. Studied that the mechanism of cellular internalization of liposomes modified with a low R8 density shifted from clathrin-mediated endocytosis to macropinocytosis when the density of R8 was increased (Khalil et al. 2006). Further, PEGylation of CPP-conjugated system protects the delivery system from the proteolytic enzymes in blood circulation. This improves the half time of the system by reducing the filtration by kidneys due to increase in size (Koren and Torchilin 2012). R8 was studied for its ability to improve the anticancer drug delivery by various research groups.

El-Sayed et al. investigated the role of nanocarriers whose surface was modified with an octaarginine peptide (R8). It was revealed that R8 on the liposome surface stimulates efficient escape from endocytic vesicles via a fusion mechanism that works at both neutral and acidic pH (El-Sayed et al. 2008).

Zhang and co-workers developed the gold nanocarriers modified with R8 to assess the effectiveness in colorectal cancer cell line LS180. The R8-modified gold nanoparticles were efficiently up taken by LS180 cells (Zhang et al. 2018).

Biswas S. et al. have worked on surface functionalization of doxorubicin loaded liposomes using octa-arginine for enhanced anti-cancer activity. Arg8 was conjugated to PEG-DOPE co-polymer. The modified liposomes significantly improved the intracellular and intratumoral delivery of doxorubicin as studied by flow cytometry and confocal laser scanning microscopy (Biswas, Dodwadkar, et al. 2013).

Deshpande et al. studied R8 and transferrin modified DOX-loaded liposomes to improve targeting of A2780 ovarian carcinoma cells for intracellular DOX delivery. It was concluded that R8 and Tf combination elevated the therapeutic potential of DOX loaded liposome and intracellular delivery via R8 (Deshpande et al. 2018).

1.8 Dendrimers

The remarkable efforts have been done to develop adequate biodegradable polymeric macromolecules in the 20th century. As a result, the dendrimers have been discovered as emerging innovations in the field of polymer chemistry. Tomalia et al. and Buhleier et al. synthesized dendrimers for the first time during 1970-1990 which have indeed controlled architecture with tailor-made surface groups, which could be surface modified (Buhleier 1978, Tomalia et al. 1985).

The term dendrimer is derived from a Greek word dendron indicates tree like typical structure with a number of branching units. They are synthetic macromolecules characterized by high branching units, three-dimensional globular structure, monodisperse and size range in nanometer (1-100 nm) with a large number of surface groups that can be modified to offer a template in the field of drug delivery (Newkome et al. 1985, Tomalia, Naylor, and Goddard III 1990).

Dendrimers are nano-sized macromolecules which constitute three discrete domains: i) a core at the center of dendrimer having an atom or a molecule having at least two identical chemical functions; ii) branches, originating from the central core having

repeated units whose repetition is organized in such a way that results in a series of radially concentric layers called “generations”; and iii) terminal functional groups located at the surface of dendritic molecules which determine the properties of dendritic macromolecules (Fréchet 1994).

Dendrimers are used to deliver vaccines, drugs (small molecules and peptides), and genes effectively. They are being utilized in numerous applications such as drug solubilization, gene therapy, drug delivery, immunoassays, imaging and diagnostics. Dendrimers were found to be well tolerated cutaneously, intravenously, orally, rectally, and vaginally when being employed as nanodrug formulations.

The different strategies have been used to synthesize dendrimers from monomers: (i) divergent synthesis, (ii) convergent synthesis, (iii) double exponential growth technique, (iv) self-assembling synthesis, (v) Lego chemistry, and (vi) Click chemistry (Menjoge, Kannan, and Tomalia 2010).

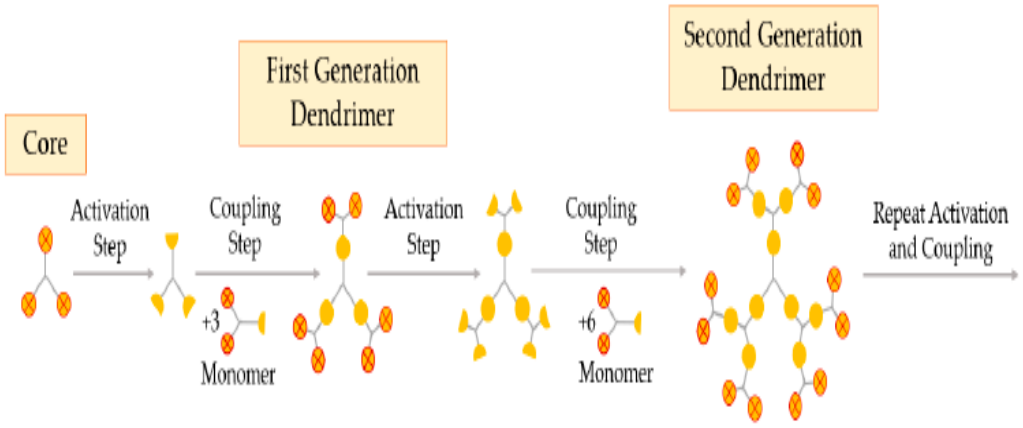

Figure 1.10. Synthesis of dendrimers by the divergent growth method (Santos, Veiga, and Figueiras 2020)

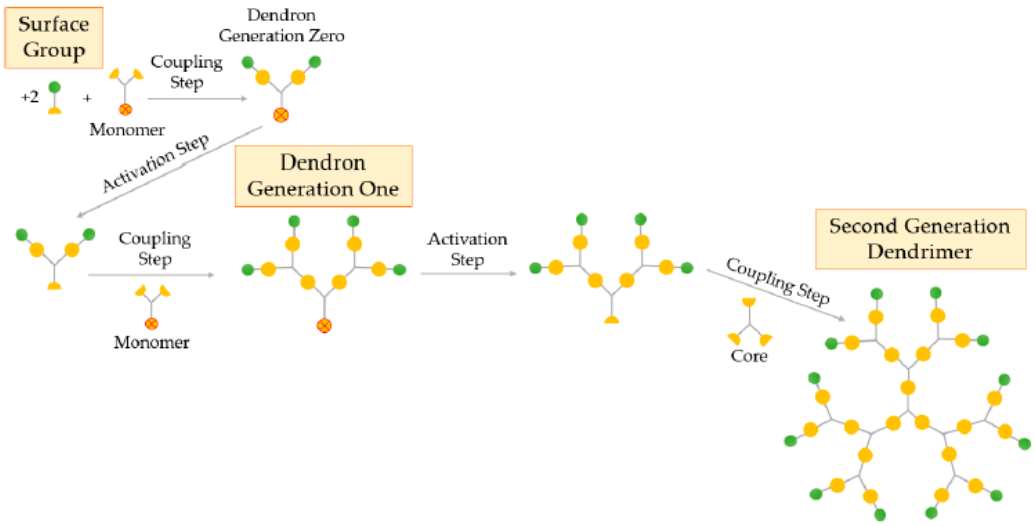

Figure 1.11. Synthesis of dendrimers by the convergent growth method (Santos, Veiga, and Figueiras 2020)

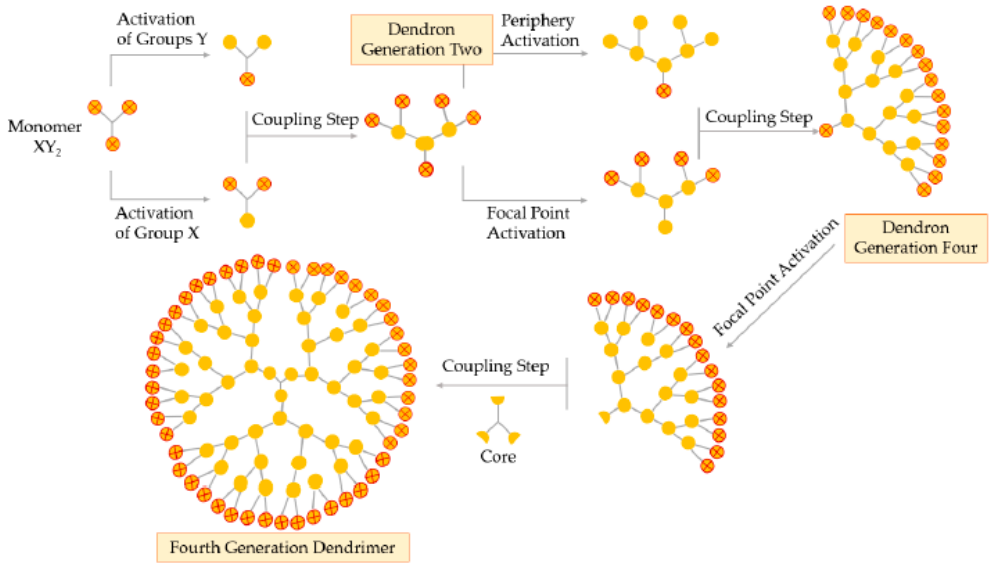

Figure 1.12. Synthesis of dendrimers by the double exponential growth technique (Santos, Veiga, and Figueiras 2020)

1.8.1 Types of dendrimers

The recent advances in synthetic chemistry leaded very fast development of dendritic nanocarriers with defined nanometric size and abundant numbers of functional end groups which can be finely tuned [59]. The types of dendrimers are as follows: Poly(amidoamine) dendrimers (PAMAM), Poly(propylene imine) dendrimers (PPI),

Liquid crystalline dendrimers, Core shell (tecto) dendrimers, Chiral dendrimers, Peptide dendrimers, Glycodendrimers, Hybrid dendrimers, PAMAM-organosilicon (PAMAMOS) dendrimers Poly(ethylene imine) dendrimers (PEI) (Kesharwani, Jain, and Jain 2014, Menjoge, Kannan, and Tomalia 2010).

1.8.2 PAMAM dendrimers

PAMAM dendrimers are now commercially available as ‘‘Starburst dendrimer’’, a sub-class of these hyperbranched polymers on a tris-aminoethylene-imine core. The name itself indicates the star-like pattern observed when the dendrimer structure is viewed in 2D. PAMAM dendrimers commercially available have multiple options for core materials which includes ethylenediamine, diaminobutane, diamonododecane, diaminohexane, and cystamine. The terminal groups on surface can be of hydroxyl, carboxylic acid, or amine functionality. One of the major advantages of PAMAM dendrimers is their spherical, globular structure resembling endogenous proteins (Pourianazar, Mutlu, and Gunduz 2014).

Basically, a PAMAM dendrimers have three distinct architectural components: (i) a core, (ii) interior layers called generations consisting of repeating units which are attached radially to the core, and (iii) end functional groups (Jain et al. 2010). Each branching unit is termed a generation (G). The molecular diameter increases by about 1 nm with each generation and ranges from 1.1 to 12.4 nm as they multiply from generations 1 to 10 in the PAMAM series (Maiti et al. 2004, Pourianazar, Mutlu, and Gunduz 2014). The shape of the dendrimers is changed by the number of generations. For example, lower generations (G0-G4) PAMAM dendrimers are planar and elliptical while higher generations (G5-G10) have spherical/globular with densely packed branches. The molecular weight, size, and the number of surface groups are also

changed from generations to generations in PAMAM dendrimers (Pourianazar, Mutlu, and Gunduz 2014).

Generations	Number of amine groups on the periphery	Molecular formula	Molecular weight (Daltons)	Hydrodynamic diameter (nm)
0	4	$C_{24}H_{52}N_{10}O_1S_2$	609	1.5
1	8	$C_{64}H_{132}N_{26}O_{12}S_2$	1522	2.2
2	16	$C_{144}H_{292}N_{52}O_{22}S_2$	3348	2.9
3	32	$C_{304}H_{612}N_{122}O_{60}S_2$	7001	3.6
4	64	$C_{624}H_{1252}N_{250}O_{124}S_2$	14307	4.5
5	128	$C_{1264}H_{2532}N_{506}O_{252}S_2$	28918	5.4
6	256	$C_{2544}H_{5092}N_{1012}O_{509}S_2$	58140	6.7
7	512	$C_{5104}H_{10212}N_{2042}O_{1020}S_2$	116585	8.1

Table 1.2. Approximate diameters (Generations = 0-7) of PAMAM dendrimers (Pourianazar, Mutlu, and Gunduz 2014)

1.8.3 PEGylated PAMAM dendrimers

The major drawbacks of dendrimers are haemolytic toxicity, immunogenicity, RES uptake, stability, drug leakage etc. which limits their application to the biomedical field. Dendrimers interact with the components of cell such as plasma membranes, cell organelles, and proteins such as enzyme etc. effectively because of their size in nanometre range. The dendrimers which are being used in the drug delivery field have surface cationic charge e.g. PPI, PAMAM and PLL and they show remarkable in vitro cytotoxicity due positive charge (Agashe et al. 2006). These limitations can be overcome by attaching PEG or ligands over the surface of dendrimers (Jain et al. 2012). Additionally, conjugation of PEG or other moieties over the dendrimer surface enhance the solubility of hydrophobic drugs. PEG offers some favourable features such as non-toxicity, non-antigenic, non-immunogenic, high solubility in water and FDA approval. The PEG-drug-dendrimer conjugates decrease degradation of drug by metabolic enzymes and improve the residence time in body (Jain et al. 2012). There are several type of PEG derivatives which are being conjugated to dendrimers e.g. bromo, amino,

carboxymethyl, succinimido succinate,tosylate, mesylate, aldehyde, octadesylamine, monopalmi-tate, and stearyloxy, or methoxy PEG (MPEG) (Harris 1985).

PEGylated PAMAM dendrimers are one of the most efficient nanocarrier to deliver the anti-cancer agents to tumor site by evading the opsonization and RES uptake and improve the biodistribution and pharmacokinetics profile of poorly soluble chemotherapeutic agent (Layek, Lipp, and Singh 2015). Moreover, these PEGylate PAMAM dendrimers offer higher drug loading and controlled drug release property. Further, partial conjugation of PEG on the nanoconjugates imparts optimal cationic charge for cellular association and help in endocytosis of PEG-PAMAM conjugates (Kesharwani, Jain, and Jain 2014).

1.8.4 PAMAM dendrimers in drug delivery

PAMAM dendrimers are hydrophilic molecules capable of entrapping lipophilic molecules which makes them good solubility enhancers. PAMAM dendrimers of generation 3.0 to 5.0 are most widely explored for the delivery of drugs and macromolecules. PAMAM dendrimers offer wide choice of load to be delivered to the target site owing to its versatility in physical holding of drugs or chemical conjugation. Hydrophobic/hydrophilic molecules can be entrapped inside the dendrimers (dendrimer-drug networks) by host guest interactions inside their empty cavities present around core (Jang et al. 2009).

In one study, 5-fluorouracil (5-FU) was loaded into PEGylated pH-responsive dendrimer nanocarrier to tumors for hypoxia treatment. It was revealed that the 5-FU-loaded nanocarrier improved circulation and residence time in the body after intravenous administration in mice and showed tumor targeting efficiently (Jin et al. 2011).

Liu et al. developed PTX loaded hybrid lipid-PAMAM and assessed for in vitro and in vivo cytotoxic activity on ovarian cancer cell line (Liu et al. 2015). It was concluded that this nanocarrier significantly improved the PTX activity by 37-fold compared to free PTX. In addition, this lipid-PAMAM hybrid nanocarriers improved the solubility of PTX approximately 465-fold compared to PAMAM alone (Liu et al. 2015).

Zheng and co-workers developed amine terminated PAMAM dendrimer generation 5 (PAMAM-G5) modified selenium nanoparticles for delivery of small interfering RNA (siRNA) and cisplatin (Zheng et al. 2015). It was revealed that the formulated nanocarriers significantly improved the cytotoxicity through apoptosis. Additionally, in vivo results proved that these nanocarriers improved the antitumor efficacy of drug without causing abnormality in organs.

Biswas S. et al. investigated the use of dendrimer in SiRNA delivery. They have synthesized a conjugate consisting poly(amidoamine) dendrimer (generation 4)-poly (ethylene glycol)-1,2-dioleoyl-sn-glycero-3-phosphoethanolamine (DOPE). This polyplexes were formed to be stable in serum and improved the cellular internalization and transfection efficiency (Biswas, Deshpande, et al. 2013).

Huihui Liao and Hui Liu along with their co-workers encapsulated Doxorubicin in PEGylated G5 PAMAM dendrimer. Methoxy PEG with COOH end group was conjugated to amine terminated G5 PAMAM dendrimer. The conjugate loaded with Doxorubicin was water soluble and stable. Cytotoxicity using MTT assay was performed in HeLa cells which was effective than unconjugated doxorubicin (Liao et al. 2014).

Mekuria et al. developed DOX loaded PAMAM-G4.5 conjugated with IL-6 antibody and a peptide, arginine-glycine-aspartate (RGD) to improve the activity of DOX for treatment of cervical cancer (Mekuria et al. 2016). PAMAM-IL6/DOX showed higher

encapsulation efficiency of 51.3%, higher loading and faster release which corresponded to greater cytotoxicity.

Urbiola et al. conjugated the Tf over the surface of PAMAM dendrimer (P-Tf) with enhanced gene delivery to cancer cells. This new vector showed good transfection efficacy in HeLa, HepG2 and CT26 cell lines (Urbiola et al. 2015).

1.9 Paclitaxel

Paclitaxel is one of the most potent and effective chemotherapeutic drug which is active against a broad range of cancers like lung carcinoma, ovarian, and breast carcinoma (Jordan and Wilson 2004). The PTX promotes and stabilizes microtubules and inhibits late G2 or M phases of cell cycle which results into the cell death (Ma and Mumper 2013). Paclitaxel (PTX), a white crystalline powder, was isolated from the bark of Pacific Yew tree *Taxus brevifolia* by Mrs. Monroe E. Wall and Mansukh C. Wani firstly (Ma and Mumper 2013). The PTX also induces cellular processes which lead to programmed cell death (Poruchynsky et al. 1998). There are many genes e.g. Bcl-2 which are responsible in the regulation of the apoptotic pathways modulated by post-translational phosphorylation thereby targeting the microtubules (Blagosklonny et al. 1997, Markman and Mekhail 2002). Although PTX has massive therapeutic potential, it suffers serious drawbacks of poor aqueous solubility, lack of cancer specificity, and substrate to P-gp efflux proteins (Sarisozen, Abouzeid, and Torchilin 2014). The low solubility problem was overcome by developing the PTX formulations based on Cremophor EL (e.g. Taxol®) and administered via slow intravenous infusion following dilution with normal saline (0.9% NaCl) or dextrose (5%) solutions. Nevertheless, the Taxol® shows serious side effects such as brain toxicity and kidney toxicity because of the excipient Cremophor EL which was used to solubilize PTX (Yuan et al. 2016). Therefore, Cremophor EL-free formulations of PTX have been investigated and

numerous attempts were carried out to enhance its therapeutic potential by incorporating the PTX in different nanocarriers.

The various attempts were reported to enhance the solubility and efficacy of PTX. For example, PTX is encapsulated in PLA-b-mPEG diblock co-polymers (Paxceed®) which forms micelles with water. Presently, Paxceed® is in phase II clinical trials (Ehrlich et al. 2004). In 2005, Albumin-bound PTX-NPs (Abraxane®) was approved by US FDA to treat patients of metastatic breast cancer who fail other chemotherapy or relapse and to treat non-small cell lung cancer approved in October 2012 (Green et al. 2006). Another micellar formulation is based on the co-polymer of PEG and polyaspartate (NK 105) by incorporating the PTX into the core of the micelles via hydrophobic interaction which is in phase III clinical trials (Kazunori et al. 1993). The most promising poly (L-glutamic acid)-PTX conjugate (CT-2103) was developed where PG is conjugated to 2′-OH position of PTX via an ester linker which is in phase III clinical studies currently (Singer 2005). A PTX-Angiopep-2 conjugate (ANG 1005) is a novel drug-peptide conjugate, which consists of three PTX molecules conjugated to one molecule of an Angiopep-2 thereby targeting low-density lipoprotein receptor-related protein 1 (LRP1) receptor to facilitate PTX delivery to across blood brain barrier for the treatment of brain cancer. The ANG 1005 is in phase II clinical trials recently (Regina et al. 2008).

1.9.1 Physicochemical properties of paclitaxel

Paclitaxel (C47H51NO14; molecular weight: 853.9 g/mol), is a cyclodecane derivative isolated from the bark of the Pacific yew tree, *Taxus brevifolia* and other Taxus spp. Sold under the brand name Taxol®, it is a fine, white to off-white crystalline powder which is poorly soluble in water. Paclitaxel is soluble in alcohols (methanol: 50mg/ml;

ethanol: 1.5mg/ml) and DMSO (50mg/ml). Paclitaxel is rapidly degraded in weakly alkaline, aqueous solutions with minimum degradation observed between pH 3–5. Paclitaxel melts at 213°C and has a logP~3, with the UV absorption maxima at 227 nm. The chemical structure of paclitaxel is shown in Figure 1.14. It has 4 hydrogen bond donors and 14 hydrogen bond acceptors ("National Center for Biotechnology Information, PubChem Compound Database; CID=36314").

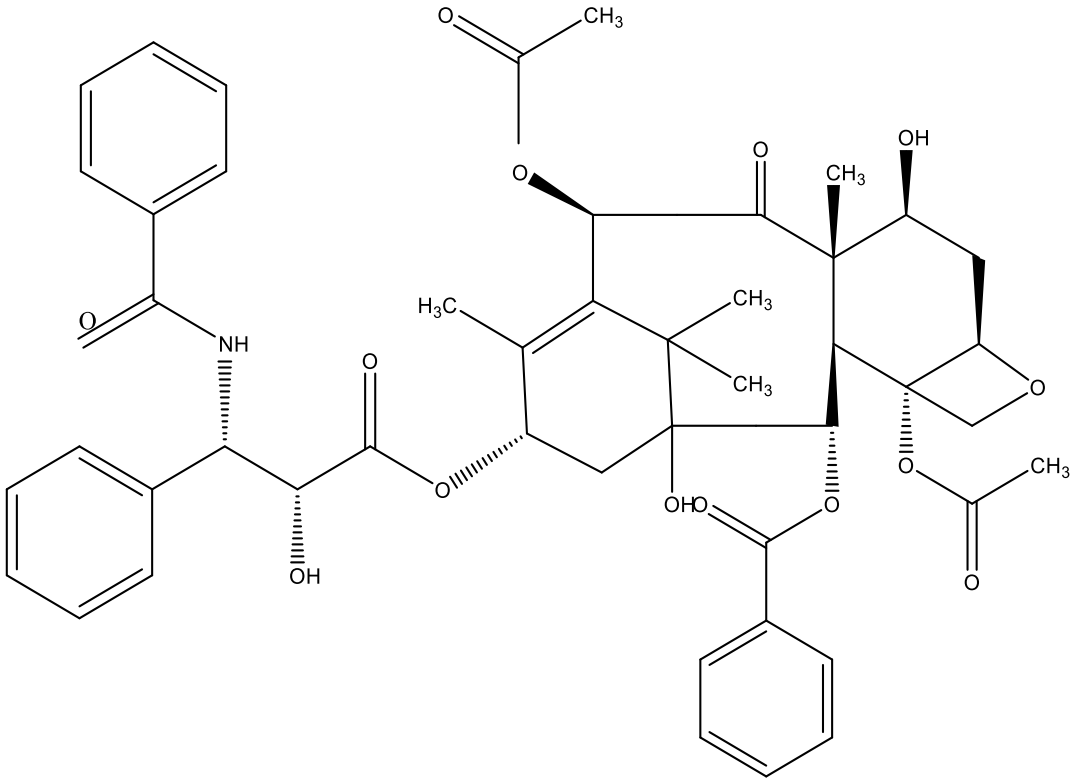

Figure 1.13. Chemical structure of Paclitaxel

IUPAC name: [4,12-diacetyloxy-15- (3-benzamido-2-hydroxy-3 phenylpropanoyl) oxy-1,9 dihydroxy-10,14,17,17-tetramethyl-11-oxo-6 oxatetracyclo [11.3.1.$0^{3,10}$.$0^{4,7}$] heptadec-13-en-2-yl] benzoate

1.10 Objectives

The core objective of the proposed research work was to synthesize and assess the surface modified PAMAM dendrimer nano-conjugates for the delivery of a chemotherapeutic agent, paclitaxel (PTX). The PTX has very limited application in the

clinic due to its poor aqueous solubility, non-specific delivery to other organs, drug efflux by P-glycoprotein transporters and unwanted side effects. The various efforts were performed to overcome the abovementioned challenges by improving the availability of PTX inside the cancer cells. To that end, α-TOS or VES was conjugated to G4 PAMAM dendrimer. The PEGylation strategy was used to make nano-carriers long circulating. The various ligands were attached onto the surface modified PAMAM dendrimer e.g. Transferrin (Tf) or octa-arginine (R) for effective delivery of PTX into the cancer cells. The chief objectives and definite aims of this thesis are:

Objective 1: To synthesize α-TOS anchored PEGylated multifunctional G4 PAMAM dendrimer system to deliver PTX.

Specific aims:

(i) To synthesize α-TOS anchored G4 PAMAM dendrimer conjugate by using EDC/NHS coupling reaction.

(ii) To attach the PEG onto the synthesized G4-TOS which yields G4-TOS-PEG.

(iii) To load the PTX physically inside the synthesized G4-TOS-PEG dendrimer nano-conjugate.

(iv) To perform the physico-chemical characterization of the conjugates using proton NMR, hydrodynamic size, zeta potential, encapsulation efficiency, drug loading and GPC analysis.

(v) To assess the PTX loaded G4-TOS-PEG dendrimer conjugate in vitro in cancer cell monolayers and multi-layered 3D spheroids.

(vi) To evaluate the therapeutic efficacy of the multifunctional dendrimer conjugate in tumor-bearing mice.

Objective 2: To develop Transferrin anchored multifunctional G4 PAMAM dendrimer system to deliver PTX.

Specific aims:

(i) To synthesize α-TOS anchored G4 PAMAM dendrimer conjugate by using EDC/NHS coupling reaction.

(ii) To attach the PEG onto the synthesized G4-TOS which yields G4-TOS-PEG.

(iii) To conjugate the targeting ligand Transferrin onto the G4-TOS-PEG which yield G4-TOS-PEG-Tf.

(iv) To load the PTX physically inside the synthesized G4-TOS-PEG-Tf dendrimer nano-conjugate.

(v) To perform the physico-chemical characterization of the conjugates using proton NMR, hydrodynamic size, zeta potential, encapsulation efficiency, drug loading, FTIR, XRD, TEM and GPC analysis.

(vi) To assess the PTX loaded G4-TOS-PEG dendrimer conjugate in vitro in cancer cell monolayers and multi-layered 3D spheroids.

Objective 3: To synthesize octa-arginine (R) anchored PEGylated multifunctional G4 PAMAM dendrimer system to deliver PTX.

Specific aims:

(i) To synthesize VES anchored G4 PAMAM dendrimer conjugate by using EDC/NHS coupling reaction to yield VES-D.

(ii) To attach the PEG onto the synthesized VES-D which yields VES-PD.

(iii) To conjugate the cell penetrating peptide octa-arginine (R) onto the VES-PD which yield RVES-PD.

(iv) To load the PTX physically inside the synthesized RVES-PD dendrimer nano-conjugate.

(v) To perform the physico-chemical characterization of the conjugates using proton NMR, hydrodynamic size, zeta potential, encapsulation efficiency, drug loading and GPC analysis.

(vi) To assess the PTX loaded RVES-PD dendrimer conjugate in vitro in cancer cell monolayers and multi-layered 3D spheroids.

(vii) To evaluate the therapeutic efficacy of the multifunctional dendrimer conjugate in tumor-bearing mice.

References

Agashe, Hrushikesh B, Tathagata Dutta, Minakshi Garg, and NK Jain. 2006. "Investigations on the toxicological profile of functionalized fifth-generation poly (propylene imine) dendrimer." *Journal of pharmacy and pharmacology* no. 58 (11):1491-1498.

Bae, You Han, and Kinam Park. 2011. "Targeted drug delivery to tumors: myths, reality and possibility." *Journal of controlled release* no. 153 (3):198.

Bar-Zeev, Maya, Yoav D Livney, and Yehuda G Assaraf. 2017. "Targeted nanomedicine for cancer therapeutics: towards precision medicine overcoming drug resistance." *Drug Resistance Updates* no. 31:15-30.

Bertrand, Nicolas, Jun Wu, Xiaoyang Xu, Nazila Kamaly, and Omid C Farokhzad. 2014. "Cancer nanotechnology: the impact of passive and active targeting in the era of modern cancer biology." *Advanced drug delivery reviews* no. 66:2-25.

Biswas, Swati, Pranali P Deshpande, Gemma Navarro, Namita S Dodwadkar, and Vladimir P Torchilin. 2013. "Lipid modified triblock PAMAM-based nanocarriers for siRNA drug co-delivery." *Biomaterials* no. 34 (4):1289-1301.

Biswas, Swati, Namita S Dodwadkar, Pranali P Deshpande, Shruti Parab, and Vladimir P Torchilin. 2013. "Surface functionalization of doxorubicin-loaded liposomes with octa-arginine for enhanced anticancer activity." *European Journal of Pharmaceutics and Biopharmaceutics* no. 84 (3):517-525.

Blagosklonny, Mikhail V, Paraskevi Giannakakou, Wafik S El-Deiry, David GI Kingston, Paul I Higgs, Len Neckers, and Tito Fojo. 1997. "Raf-1/bcl-2 phosphorylation: a step from microtubule damage to cell death." *Cancer research* no. 57 (1):130-135.

Bobo, Daniel, Kye J Robinson, Jiaul Islam, Kristofer J Thurecht, and Simon R Corrie. 2016. "Nanoparticle-based medicines: a review of FDA-approved materials and clinical trials to date." *Pharmaceutical research* no. 33 (10):2373-2387.

Breunig, Miriam, S Bauer, and Achim Göpferich. 2008. "Polymers and nanoparticles: intelligent tools for intracellular targeting?" *European Journal of Pharmaceutics and Biopharmaceutics* no. 68 (1):112-128.

Buhleier, Egon. 1978. "" CASCADE"-AND" NONSKID-CHAIN-LIKE" SYNTHESES OF MOLECULAR CAVITY TOPOLOGIES."

Cerqueira, Brenda Brenner S, Annette Lasham, Andrew N Shelling, and Raida Al-Kassas. 2015. "Nanoparticle therapeutics: Technologies and methods for overcoming cancer." *European Journal of Pharmaceutics and Biopharmaceutics* no. 97:140-151.

Chavda, Vivek P. 2019. "Nanobased Nano Drug Delivery: A Comprehensive Review." In *Applications of Targeted Nano Drugs and Delivery Systems*, 69-92. Elsevier.

Chidambaram, Moorthi, R Manavalan, and K Kathiresan. 2011. "Nanotherapeutics to overcome conventional cancer chemotherapy limitations." *Journal of pharmacy & pharmaceutical sciences* no. 14 (1):67-77.

Chithrani, B Devika, Arezou A Ghazani, and Warren CW Chan. 2006. "Determining the size and shape dependence of gold nanoparticle uptake into mammalian cells." *Nano letters* no. 6 (4):662-668.

Curiel, David T, and Joanne T Douglas. 2007. *Cancer gene therapy*: Springer Science & Business Media.

Dai, Liangliang, Junjie Liu, Zhong Luo, Menghuan Li, and Kaiyong Cai. 2016. "Tumor therapy: targeted drug delivery systems." *Journal of Materials Chemistry B* no. 4 (42):6758-6772.

Deshpande, Pranali, Aditi Jhaveri, Bhushan Pattni, Swati Biswas, and Vladimir Torchilin. 2018. "Transferrin and octaarginine modified dual-functional liposomes with improved cancer cell targeting and enhanced intracellular delivery for the treatment of ovarian cancer." *Drug delivery* no. 25 (1):517-532.

Ehrlich, Alison, Susan Booher, Yvonne Becerra, Debra L Borris, W Douglas Figg, Maria L Turner, and Andrew Blauvelt. 2004. "Micellar paclitaxel improves severe psoriasis in a prospective phase II pilot study." *Journal of the American Academy of Dermatology* no. 50 (4):533-540.

Eiró, Noemí, and Francisco J Vizoso. 2012. "Inflammation and cancer." *World journal of gastrointestinal surgery* no. 4 (3):62.

El-Sayed, Ayman, Ikramy A Khalil, Kentaro Kogure, Shiroh Futaki, and Hideyoshi Harashima. 2008. "Octaarginine-and octalysine-modified nanoparticles have different modes of endosomal escape." *Journal of Biological Chemistry* no. 283 (34):23450-23461.

Enache, Rodica Gabriela. 2012. "The relationship between anxiety, depression and self-esteem in women with breast cancer after surgery." *Procedia-Social and Behavioral Sciences* no. 33:124-127.

Farokhzad, Omid C, and Robert Langer. 2009. "Impact of nanotechnology on drug delivery." *ACS nano* no. 3 (1):16-20.

Ferlay, Jacques, M Ervik, F Lam, M Colombet, L Mery, M Piñeros, A Znaor, I Soerjomataram, and F Bray. 2019. "Global cancer observatory: cancer today." *Lyon, France: International Agency for Research on Cancer*.

Fréchet, Jean M. 1994. "Functional polymers and dendrimers: reactivity, molecular architecture, and interfacial energy." *Science* no. 263 (5154):1710-1715.

Frishman, William H, Henry CM Yee, Deborah Keefe, Helen M Sung, Linda L Liu, Avi I Einzig, and Janice Dutcher. 1997. "Cardiovascular toxicity with cancer chemotherapy." *Current problems in cancer* no. 21 (6):301-360.

Galmarini, Darío, Carlos M Galmarini, and Felipe C Galmarini. 2012. "Cancer chemotherapy: a critical analysis of its 60 years of history." *Critical reviews in oncology/hematology* no. 84 (2):181-199.

Ganta, Srinivas, Harikrishna Devalapally, Aliasgar Shahiwala, and Mansoor Amiji. 2008. "A review of stimuli-responsive nanocarriers for drug and gene delivery." *Journal of controlled release* no. 126 (3):187-204.

Green, MR, GM Manikhas, S Orlov, B Afanasyev, AM Makhson, P Bhar, and MJ Hawkins. 2006. "Abraxane®, a novel Cremophor®-free, albumin-bound particle form of paclitaxel for the treatment of advanced non-small-cell lung cancer." *Annals of Oncology* no. 17 (8):1263-1268.

Greish, Khaled. 2012. "Enhanced permeability and retention effect for selective targeting of anticancer nanomedicine: are we there yet?" *Drug Discovery Today: Technologies* no. 9 (2):e161-e166.

Griffiths, Anthony JF, Susan R Wessler, Richard C Lewontin, William M Gelbart, David T Suzuki, and Jeffrey H Miller. 2005. *An introduction to genetic analysis*: Macmillan.

Hackett, Gavin S. 2012. *Intracellular delivery of therapeutic antibodies*, University of Nottingham.

Hanahan, Douglas. 2014. "Rethinking the war on cancer." *The Lancet* no. 383 (9916):558-563.

Hanahan, Douglas, and Robert A Weinberg. 2011. "Hallmarks of cancer: the next generation." *cell* no. 144 (5):646-674.

Harris, J Milton. 1985. "Laboratory synthesis of polyethylene glycol derivatives." *Journal of Macromolecular Science-Reviews in Macromolecular Chemistry and Physics* no. 25 (3):325-373.

Hartwell, Leland H, and Ted A Weinert. 1989. "Checkpoints: controls that ensure the order of cell cycle events." *Science* no. 246 (4930):629-634.

Huitink, Johannes M, and Wendy HL Teoh. 2013. "Current cancer therapies–a guide for perioperative physicians." *Best Practice & Research Clinical Anaesthesiology* no. 27 (4):481-492.

Ingole, Sangita P, Aruna U Kakde, and Priti B Bonde. 2016. "A review on statistics of cancer in India." *J Environ Sci Toxicol Food Technol* no. 10:107-16.

Jain, Keerti, Prashant Kesharwani, Umesh Gupta, and Narendra K Jain. 2012. "A review of glycosylated carriers for drug delivery." *Biomaterials* no. 33 (16):4166-4186.

Jain, Keerti, Prashant Kesharwani, Umesh Gupta, and NK Jain. 2010. "Dendrimer toxicity: Let's meet the challenge." *International journal of pharmaceutics* no. 394 (1-2):122-142.

Jang, Woo-Dong, KM Kamruzzaman Selim, Chi-Hwa Lee, and Inn-Kyu Kang. 2009. "Bioinspired application of dendrimers: from bio-mimicry to biomedical applications." *Progress in Polymer Science* no. 34 (1):1-23.

Jansen, Catherine E, Marylin J Dodd, Christine A Miaskowski, Glenna A Dowling, and Joel Kramer. 2008. "Preliminary results of a longitudinal study of changes in cognitive function in breast cancer patients undergoing chemotherapy with doxorubicin and cyclophosphamide." *Psycho-Oncology* no. 17 (12):1189-1195.

Jin, Yiguang, Xia Ren, Wei Wang, Lijing Ke, Erjuan Ning, Lina Du, and Jeremy Bradshaw. 2011. "A 5-fluorouracil-loaded pH-responsive dendrimer nanocarrier for tumor targeting." *International journal of pharmaceutics* no. 420 (2):378-384.

Jordan, Mary Ann, and Leslie Wilson. 2004. "Microtubules as a target for anticancer drugs." *Nature Reviews Cancer* no. 4 (4):253-265.

Kakde, Deepak, Deepti Jain, Vivek Shrivastava, Rajendra Kakde, and AT Patil. 2011. "Cancer therapeutics-opportunities, challenges and advances in drug delivery." *Journal of Applied Pharmaceutical Science* no. 1 (9):1-10.

Kawasaki, Hiroaki, and Hiroyuki Abe. 2012. "Epigenetics in cancer and inflammation." *Personalized Medicine Universe* no. 1 (1):7-12.

Kazunori, Kataoka, Yokoyama Masayuki, Okano Teruo, and Sakurai Yasuhisa. 1993. "Block copolymer micelles as vehicles for drug delivery." *Journal of Controlled Release* no. 24 (1-3):119-132.

Kesharwani, Prashant, Keerti Jain, and Narendra Kumar Jain. 2014. "Dendrimer as nanocarrier for drug delivery." *Progress in Polymer Science* no. 39 (2):268-307.

Khalil, Ikramy A, Kentaro Kogure, Shiroh Futaki, and Hideyoshi Harashima. 2006. "High density of octaarginine stimulates macropinocytosis leading to efficient intracellular trafficking for gene expression." *Journal of Biological Chemistry* no. 281 (6):3544-3551.

Koo, Heebeom, Myung Sook Huh, In-Cheol Sun, Soon Hong Yuk, Kuiwon Choi, Kwangmeyung Kim, and Ick Chan Kwon. 2011. "In vivo targeted delivery of nanoparticles for theranosis." *Accounts of chemical research* no. 44 (10):1018-1028.

Koren, Erez, and Vladimir P Torchilin. 2012. "Cell-penetrating peptides: breaking through to the other side." *Trends in molecular medicine* no. 18 (7):385-393.

Langel, Ü. 2007. "Handbook of Cell-Penetrating Peptides:(Eds.: U. Langel) CRC Taylor & Francis." *Boca Raton*.

Layek, Buddhadev, Lindsey Lipp, and Jagdish Singh. 2015. "Cell penetrating peptide conjugated chitosan for enhanced delivery of nucleic acid." *International journal of molecular sciences* no. 16 (12):28912-28930.

Liao, Huihui, Hui Liu, Yulin Li, Mengen Zhang, Helena Tomás, Mingwu Shen, and Xiangyang Shi. 2014. "Antitumor efficacy of doxorubicin encapsulated within PEGylated poly (amidoamine) dendrimers." *Journal of Applied Polymer Science* no. 131 (11).

Liu, Yuanjie, Yiwei Ng, Ming R Toh, and Gigi NC Chiu. 2015. "Lipid-dendrimer hybrid nanosystem as a novel delivery system for paclitaxel to treat ovarian cancer." *Journal of Controlled Release* no. 220:438-446.

Ma, Ping, and Russell J Mumper. 2013. "Paclitaxel nano-delivery systems: a comprehensive review." *Journal of nanomedicine & nanotechnology* no. 4 (2):1000164.

Maeda, Hiroshi, Jun Wu, Tomohiro Sawa, Yasuhiro Matsumura, and Katsuyoshi Hori. 2000. "Tumor vascular permeability and the EPR effect in macromolecular therapeutics: a review." *Journal of controlled release* no. 65 (1-2):271-284.

Maiti, Prabal K, Tahir Çağın, Guofeng Wang, and William A Goddard. 2004. "Structure of PAMAM dendrimers: Generations 1 through 11." *Macromolecules* no. 37 (16):6236-6254.

Markman, Maurie, and Tarek M Mekhail. 2002. "Paclitaxel in cancer therapy." *Expert opinion on pharmacotherapy* no. 3 (6):755-766.

Mayer, Claudia, Odilia Popanda, Burkhard Greve, Eberhard Fritz, Thomas Illig, Friederike Eckardt-Schupp, Maria Gomolka, Axel Benner, and Peter Schmezer. 2011. "A radiation-induced gene expression signature as a tool to predict acute radiotherapy-induced adverse side effects." *Cancer letters* no. 302 (1):20-28.

Mekuria, Shewaye Lakew, Tilahun Ayane Debele, Hsiao-Ying Chou, and Hsieh-Chih Tsai. 2016. "IL-6 antibody and RGD peptide conjugated poly (amidoamine) dendrimer for targeted drug delivery of HeLa cells." *The Journal of Physical Chemistry B* no. 120 (1):123-130.

Menjoge, Anupa R, Rangaramanujam M Kannan, and Donald A Tomalia. 2010. "Dendrimer-based drug and imaging conjugates: design considerations for nanomedical applications." *Drug discovery today* no. 15 (5-6):171-185.

Miaskowski, Christine, Bruce Cooper, Steven M Paul, Claudia West, Dale Langford, Jon D Levine, Gary Abrams, Deborah Hamolsky, Laura Dunn, and Marylin Dodd. 2012. "Identification of patient subgroups and risk factors for persistent breast pain following breast cancer surgery." *The Journal of Pain* no. 13 (12):1172-1187.

Minotti, Giorgio, Pierantonio Menna, Emanuela Salvatorelli, Gaetano Cairo, and Luca Gianni. 2004. "Anthracyclines: molecular advances and pharmacologic developments in antitumor activity and cardiotoxicity." *Pharmacological reviews* no. 56 (2):185-229.

Monje, Michelle, and Jörg Dietrich. 2012. "Cognitive side effects of cancer therapy demonstrate a functional role for adult neurogenesis." *Behavioural brain research* no. 227 (2):376-379.

Muyrers-Chen, Inhua, and Renato Paro. 2001. "Epigenetics: unforeseen regulators in cancer." *Biochimica et Biophysica Acta (BBA)-Reviews on Cancer* no. 1552 (1):15-26.

Nair, M Krishnan, Cherian Varghese, and R Swaminathan. 2005. "Cancer: Current scenario, intervention strategies and projections for 2015." *NCHM Background papers-Burden of Disease in India*:219-25.

Newkome, GR, ZQ Yao, GR Baker, and VK Gupta. 1985. Cascade Molecules-a New Approach to Micelles. Paper read at ABSTRACTS OF PAPERS OF THE AMERICAN CHEMICAL SOCIETY.

O'Connor, Clare M, Jill U Adams, and Jennifer Fairman. 2010. "Essentials of cell biology." *Cambridge, MA: NPG Education* no. 1:54.

Organization, World Health. 2020. "WHO report on cancer: setting priorities, investing wisely and providing care for all."

Pandya, Hetal, and Waldemar Debinski. 2012. "Toward Intracellular Targeted Delivery of Cancer Therapeutics." *BioDrugs* no. 26 (4):235-244.

Papadopoulou, Lefkothea C, and Asterios S Tsiftsoglou. 2013. "The potential role of cell penetrating peptides in the intracellular delivery of proteins for therapy of erythroid related disorders." *Pharmaceuticals* no. 6 (1):32-53.

Peer, Dan, Jeffrey M Karp, Seungpyo Hong, Omid C Farokhzad, Rimona Margalit, and Robert Langer. 2007. "Nanocarriers as an emerging platform for cancer therapy." *Nature nanotechnology* no. 2 (12):751.

Petrova, Tatiana V, Terhi Karpanen, Camilla Norrmén, Russell Mellor, Tomoki Tamakoshi, David Finegold, Robert Ferrell, Dontscho Kerjaschki, Peter Mortimer, and Seppo Ylä-Herttuala. 2004. "Defective valves and abnormal mural cell recruitment underlie lymphatic vascular failure in lymphedema distichiasis." *Nature medicine* no. 10 (9):974-981.

Phillips, Theresa. 2008. "The role of methylation in gene expression." *Nature Education* no. 1 (1):116.

Poruchynsky, Marianne S, Emily E Wang, Charles M Rudin, Mikhail V Blagosklonny, and Tito Fojo. 1998. "Bcl-xL is phosphorylated in malignant cells following microtubule disruption." *Cancer research* no. 58 (15):3331-3338.

Pourianazar, Negar Taghavi, Pelin Mutlu, and Ufuk Gunduz. 2014. "Bioapplications of poly (amidoamine)(PAMAM) dendrimers in nanomedicine." *Journal of Nanoparticle Research* no. 16 (4):2342.

Qiu, Yang, Ying Liu, Liming Wang, Ligeng Xu, Ru Bai, Yinglu Ji, Xiaochun Wu, Yuliang Zhao, Yufeng Li, and Chunying Chen. 2010. "Surface chemistry and aspect ratio mediated cellular uptake of Au nanorods." *Biomaterials* no. 31 (30):7606-7619.

Rana, Vikas, and Radhika Sharma. 2019. "Recent advances in development of nano drug delivery." In *Applications of Targeted Nano Drugs and Delivery Systems*, 93-131. Elsevier.

Regina, A, M Demeule, C Che, I Lavallee, J Poirier, R Gabathuler, R Beliveau, and J-P Castaigne. 2008. "Antitumour activity of ANG1005, a conjugate between paclitaxel and the new brain delivery vector Angiopep-2." *British journal of pharmacology* no. 155 (2):185-197.

Rowinsky, EK, EA Eisenhauer, Vinay Chaudhry, SG Arbuck, and Ross C Donehower. 1993. Clinical toxicities encountered with paclitaxel (Taxol®). Paper read at Seminars in oncology.

Rubin, Raphael, David S Strayer, and Emanuel Rubin. 2008. *Rubin's pathology: clinicopathologic foundations of medicine*: Lippincott Williams & Wilkins.

Ruoslahti, Erkki. 2017. "Tumor penetrating peptides for improved drug delivery." *Advanced drug delivery reviews* no. 110:3-12.

Sahay, Gaurav, Daria Y Alakhova, and Alexander V Kabanov. 2010. "Endocytosis of nanomedicines." *Journal of controlled release* no. 145 (3):182-195.

Santos, Ana, Francisco Veiga, and Ana Figueiras. 2020. "Dendrimers as Pharmaceutical Excipients: Synthesis, Properties, Toxicity and Biomedical Applications." *Materials* no. 13 (1):65.

Sarisozen, Can, Abraham H Abouzeid, and Vladimir P Torchilin. 2014. "The effect of co-delivery of paclitaxel and curcumin by transferrin-targeted PEG-PE-based mixed micelles on resistant ovarian cancer in 3-D spheroids and in vivo tumors." *European Journal of Pharmaceutics and Biopharmaceutics* no. 88 (2):539-550.

Senapati, Sudipta, Arun Kumar Mahanta, Sunil Kumar, and Pralay Maiti. 2018. "Controlled drug delivery vehicles for cancer treatment and their performance." *Signal transduction and targeted therapy* no. 3 (1):1-19.

Sherwood, Lauralee. 2015. *Human physiology: from cells to systems*: Cengage learning.

Shin, Meong Cheol, Jian Zhang, Kyoung Ah Min, Kyuri Lee, Youngro Byun, Allan E David, Huining He, and Victor C Yang. 2014. "Cell-penetrating peptides: Achievements and challenges in application for cancer treatment." *Journal of Biomedical Materials Research Part A: An Official Journal of The Society for*

Biomaterials, The Japanese Society for Biomaterials, and The Australian Society for Biomaterials and the Korean Society for Biomaterials no. 102 (2):575-587.

Siegel, Rebecca, Deepa Naishadham, and Ahmedin Jemal. 2012. "Cancer statistics, 2012." *CA: a cancer journal for clinicians* no. 62 (1):10-29.

Singer, Jack W. 2005. "Paclitaxel poliglumex (XYOTAX™, CT-2103): a macromolecular taxane." *Journal of controlled release* no. 109 (1-3):120-126.

Steinman, Ralph M, Ira S Mellman, William A Muller, and Zanvil A Cohn. 1983. "Endocytosis and the recycling of plasma membrane." *The Journal of cell biology* no. 96 (1):1-27.

Stortecky, Stefan, and Thomas M Suter. 2010. "Insights into cardiovascular side-effects of modern anticancer therapeutics." *Current opinion in Oncology* no. 22 (4):312-317.

Thorek, Daniel LJ, and Andrew Tsourkas. 2008. "Size, charge and concentration dependent uptake of iron oxide particles by non-phagocytic cells." *Biomaterials* no. 29 (26):3583-3590.

Tomalia, Donald A, H Baker, J Dewald, M Hall, G Kallos, S Martin, J Roeck, J Ryder, and P Smith. 1985. "A new class of polymers: starburst-dendritic macromolecules." *Polymer journal* no. 17 (1):117-132.

Tomalia, Donald A, Adel M Naylor, and William A Goddard III. 1990. "Starburst dendrimers: molecular-level control of size, shape, surface chemistry, topology, and flexibility from atoms to macroscopic matter." *Angewandte Chemie International Edition in English* no. 29 (2):138-175.

Torchilin, Vladimir. 2011. "Tumor delivery of macromolecular drugs based on the EPR effect." *Advanced drug delivery reviews* no. 63 (3):131-135.

Torchilin, Vladimir P. 2006. "Recent approaches to intracellular delivery of drugs and DNA and organelle targeting." *Annu. Rev. Biomed. Eng.* no. 8:343-375.

Uchida, Masaki, Hisanori Kosuge, Masahiro Terashima, Deborah A Willits, Lars O Liepold, Mark J Young, Michael V McConnell, and Trevor Douglas. 2011. "Protein cage nanoparticles bearing the LyP-1 peptide for enhanced imaging of macrophage-rich vascular lesions." *ACS nano* no. 5 (4):2493-2502.

Urbiola, Koldo, Laura Blanco-Fernández, Gemma Navarro, Wolfgang Rödl, Ernst Wagner, Manfred Ogris, and Conchita Tros de Ilarduya. 2015. "Evaluation of improved PAMAM-G5 conjugates for gene delivery targeted to the transferrin receptor." *European Journal of Pharmaceutics and Biopharmaceutics* no. 94:116-122.

Urruticoechea, Ander, Ramon Alemany, J Balart, Alberto Villanueva, Francesc Viñals, and Gabriel Capella. 2010. "Recent advances in cancer therapy: an overview." *Current pharmaceutical design* no. 16 (1):3-10.

Verma, Mukesh, Neelesh Agarwal, and Mudit Verma. 2014. "Epigenetics and Animal Models: Applications in Cancer Control and Treatment." In *Animal Biotechnology*, 57-72. Elsevier.

Walsh, Tom, and Mary-Claire King. 2007. "Ten genes for inherited breast cancer." *Cancer cell* no. 11 (2):103-105.

Wang, Jin, Shaomin Tian, Robby A Petros, Mary E Napier, and Joseph M DeSimone. 2010. "The complex role of multivalency in nanoparticles targeting the transferrin receptor for cancer therapies." *Journal of the American Chemical Society* no. 132 (32):11306-11313.

Ye, Junxiao, Ergang Liu, Zhili Yu, Xing Pei, Sunhui Chen, Pengwei Zhang, Meong-Cheol Shin, Junbo Gong, Huining He, and Victor C Yang. 2016. "CPP-assisted intracellular drug delivery, what is next?" *International journal of molecular sciences* no. 17 (11):1892.

Yoon, Dennis J, Christina T Liu, Devin S Quinlan, Parsa M Nafisi, and Daniel T Kamei. 2011. "Intracellular trafficking considerations in the development of natural ligand-drug molecular conjugates for cancer." *Annals of biomedical engineering* no. 39 (4):1235-1251.

Yuan, Xun, Wenxiang Ji, Si Chen, Yuling Bao, Songwei Tan, Shun Lu, Kongming Wu, and Qian Chu. 2016. "a novel paclitaxel-loaded poly (D, L-lactide-co-glycolide)-Tween 80 copolymer nanoparticle overcoming multidrug resistance for lung cancer treatment." *International journal of nanomedicine* no. 11:2119.

Zaki, Noha M, and Nicola Tirelli. 2010. "Gateways for the intracellular access of nanocarriers: a review of receptor-mediated endocytosis mechanisms and of strategies in receptor targeting." *Expert opinion on drug delivery* no. 7 (8):895-913.

Zhang, Xuyang, Hao Wang, Jonathan Andrew Coulter, and Ruijie Yang. 2018. "Octaarginine-modified gold nanoparticles enhance the radiosensitivity of human colorectal cancer cell line LS180 to megavoltage radiation." *International journal of nanomedicine* no. 13:3541.

Zheng, Wenjing, Chengwen Cao, Yanan Liu, Qianqian Yu, Chuping Zheng, Dongdong Sun, Xiaofan Ren, and Jie Liu. 2015. "Multifunctional polyamidoamine-modified

selenium nanoparticles dual-delivering siRNA and cisplatin to A549/DDP cells for reversal multidrug resistance." *Acta biomaterialia* no. 11:368-380.

Chapter 2

α-Tocopherol Succinate-Anchored PEGylated Poly (amidoamine) Dendrimer for the Delivery of Paclitaxel: Assessment of in Vitro and in Vivo Therapeutic Efficacy

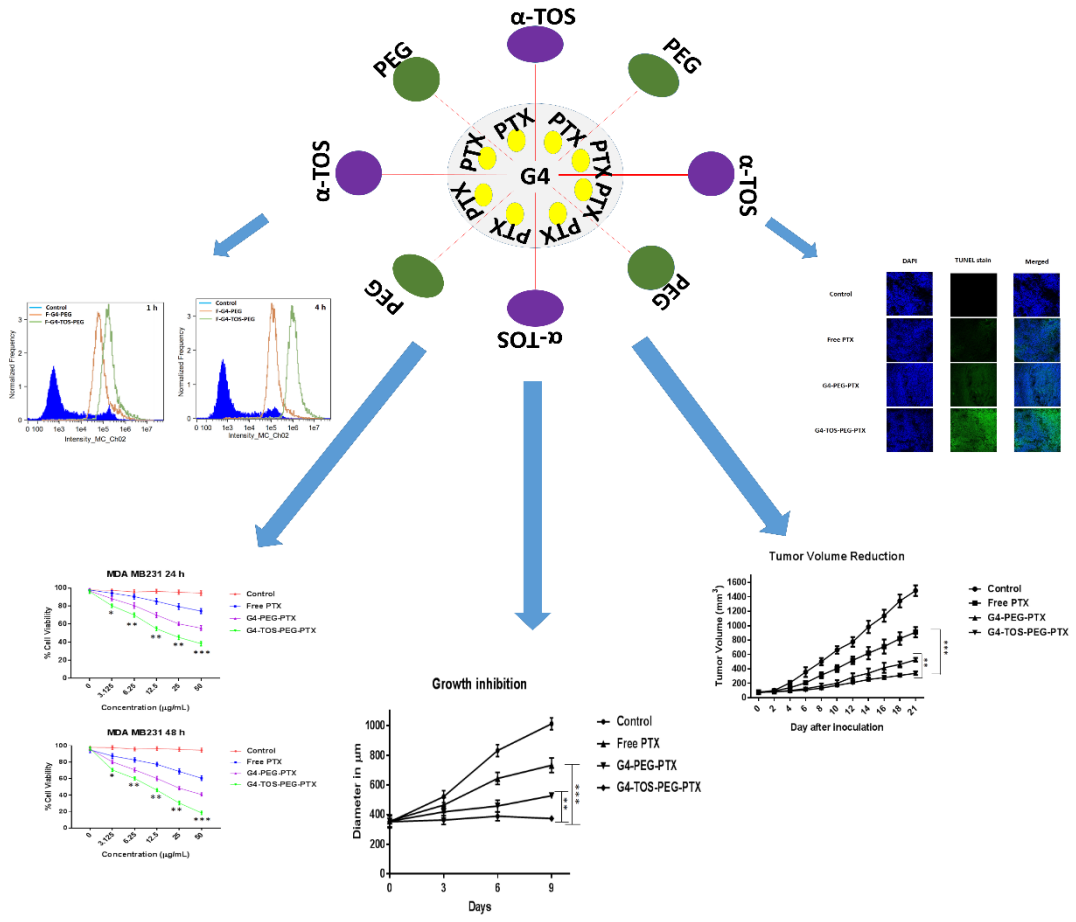

2.1 Abstract

This study involves development of a dendrimer-based nanoconstruct by conjugating α-tocopheryl succinate (α-TOS) and polyethylene glycol (PEG) on a poly (amidoamine) dendrimer (G4 PAMAM) to improve intracellular delivery of a poorly water-soluble chemotherapeutic drug, paclitaxel (PTX). The conjugates were characterized by NMR, and PTX-loaded nanocarriers (G4-TOS-PEG-PTX) were evaluated for hydrodynamic diameter, polydispersity index (PDI), zeta potential, percentage encapsulation efficiency (%EE), and percentage drug loading (%DL). A hemolysis study was performed, which indicated that the synthesized dendrimer conjugates were not toxic to red blood cells; hence, they were biocompatible. A cellular uptake study in (B16F10 and MDA MB231) monolayer cells and 3D spheroids showed that α-TOS conjugation improved the time dependent uptake of nanosized dendrimer conjugates. The cell viability assay revealed that G4-TOS-PEG-PTX enhanced the cytotoxicity of PTX as compared to free PTX and PTX-loaded G4-PEG (G4-PEG-PTX) at tested concentrations. Correspondingly, the α-TOS-anchored dendrimer induced more apoptosis as compared to free PTX and G4-PEG-PTX. Moreover, the fluorescently labeled G4-TOS-PEG penetrated deeper into MDA MB231 3D spheroids as visualized by confocal microscopy. G4-TOS-PEG-PTX showed significant growth inhibition in 3D spheroids as compared to free PTX and G4-PEG-PTX. Further, the in vivo efficacy study using B16F10 xenografted C57Bl6/J mice indicated that the G4-TOS-PEG localized in tumor sections. G4-TOS-PEG-PTX reduced the tumor growth significantly compared to free PTX and G4-PEG-PTX. G4-TOS-PEG-PTX had more apoptotic potential in tumor sections as analyzed by TUNEL assay. Hence, the newly developed dendrimer conjugate, G4-TOS-PEG, has the potential to target loaded drug to the tumor, and G4-TOS-PEG-PTX has the potential to be utilized successfully in cancer treatment.

2.2 Introduction

Nanotechnology plays a vital role in providing new strategies for the development of effective therapeutics for cancer with minimal side effects and improved bioavailability. The chemotherapeutic drugs can be entrapped or conjugated on the nanocarriers, which provide stability, improved pharmacokinetics, longer circulation times, specificity toward cancer cells, and improved therapeutic efficacy. Various types of nanodrug delivery systems include lipid nanocarriers, polymer-drug conjugates, polymeric micelles, inorganic nanoparticles, and dendrimers. Even though the effectiveness of these nanoparticles improved compared to conventional free drug treatment, the toxicity associated with the polymeric systems, premature drug release from the nanocarriers, and overall effectivity in human cancers still poses challenges and necessitates further research in this direction to develop superior treatment strategies for cancer (Biswas et al. 2011).

Dendrimers are hyper-branched synthetic macromolecules having an ordered nanometric architecture. Dendrimers are available in many generations and possess a central core withbranches emanating from it, which makes them modifiable by attaching the desired functional groups at the periphery. For the past decade, poly(amidoamine) dendrimers (PAMAM) gained more attention over the other nanocarriers in the delivery of small molecules, proteins and peptides, and gene-based materials in various diseases (Kesharwani, Jain, and Jain 2014). The toxicity of dendrimers is attributed mainly to the end group present over the periphery (Malik et al. 2000). However, the toxicity can be overcome by modifying their periphery using anionic or neutral groups (e.g., polyethylene glycol, PEG), which also improve the systemic circulation in vivo (Roberts, Bhalgat, and Zera 1996, Fuchs et al. 2004, Kesharwani et al. 2011). These nanocarriers passively enter into the tumor tissue via leaky vasculature by an enhanced permeability

and retention (EPR) effect. Still the internalization of the dendrimeric nanocarriers into the cell membrane is limited and energy dependent, which can be largely modulated by surface modification.

α-Tocopheryl succinate (α-TOS) is a well-known hydrophobic analogue of vitamin E that has been extensively used in preclinical studies by conjugating it to PEG to improve the solubility of poorly soluble drugs, and it was proven to be an efficient penetration enhancer (Gill, Kaddoumi, and Nazzal 2012, Chandrasekharan et al. 2011). Moreover, α-TOS has proven its anticancer activities in a variety of human cancer cell lines (Abu-Fayyad et al. 2015, Emami et al. 2015, Nam et al. 2015, Gruber et al. 2014, Muddineti et al. 2017, Neuzil et al. 2002). α-TOS has apoptosis inducing potential in various cancer cell lines (Neuzil et al. 2002, Kline, Yu, and Sanders , Yu et al. 2001). α-TOS has proven its inhibitory effect on cell proliferation by cell cycle arrest at G0 or G1 cycle block in MDA-MB-435 breast cancer cells (Yu, Sanders, and Kline 2002). α-TOS can reduce the multidrug resistance of various chemotherapeutic drugs (paclitaxel, curcumin, and doxorubicin) by inhibition of Pglycoprotein (P-gp) (Duhem, Danhier, and Préat 2014, Guo et al. 2013).

In the present study, we have conjugated α-TOS with the G4 PAMAM dendrimer, which was further coupled with PEG to explore its potential to deliver the chemotherapeutic agent, paclitaxel (PTX), to the cancer cells as well as to the solid tumor. The PTX-loaded dendrimer conjugates were evaluated in the triple negative breast cancer cell (MDA MB231) in monolayers and 3D spheroids, the murine melanoma cell line (B16F10), and in B16F10-xenografted C57BL/6 mice to assess in vitro and in vivo therapeutic efficacy.

2.3 Materials and methods

2.3.1 Materials

The generation 4 PAMAM (G4 PAMAM) dendrimer was procured from Dendritech (USA). PTX wasgiven as a gift sample from Fresenius Kabi India Pvt., Ltd. (Gurgaon,

India). Methoxy-polyethylene glycol-succinimidyl carboxymethyl ester (mPEG-SCM ester, MW 2000 Da) was purchased from Jenkem Technology (USA). N-Ethyldiisopropylamine (DIPEA) was purchased from Avra Chemicals, India. NHS-Fluorescein was procured from Thermo Scientific (USA). α-TOS was obtained from Sigma-Aldrich Chemicals (Bangalore, India). N-(3-(Dimethylamino)propyl)-N′-ethylcarbodiimide hydrochloride (EDC·HCl, 98%) and N-hydroxysuccinimide (NHS, 98%) were procured from Sigma-Aldrich Chemicals (USA). The regenerated cellulose dialysis membrane (MWCO 2 kDa, 3.5 kDa, and 14 kDa) was purchased from Spectrum Laboratories, Inc. (USA). All other chemicals and solvents used for the study were of analytical grade.

Murine melanoma cancer cells (B16F10) and triple negative breast adenocarcinoma cells (MDA MB231) were procured from the National Center for Cell Sciences (NCCS, Pune, India). Heat-inactivated fetal bovine serum (FBS), leibovitz (L-15) media, Dulbecco's modified Eagle's media (DMEM), and penicillin/streptomycin solution were obtained from Himedia Laboratories (Mumbai, India). B16F10 cell lines were grown in DMEM (10% FBS and 100 IU/mL of penicillin/streptomycin solution) at 37 °C and 5% CO2 atmosphere. MDA MB231 cell lines were grown in L-15 medium (10% FBS and 100 IU/mL of penicillin/streptomycin solution) with the same incubation conditions.

2.3.2 Methods

2.3.2.1 Synthesis of the α-TOS-Conjugated G4 PAMAM Dendrimer (G4-TOS)

The amine terminated G4 PAMAM dendrimer (50 mg, 3.52 μmol) was dissolved in 2 mL of anhydrous dimethylformamide (DMF). α-TOS of about 5 mol equiv (9.341 mg, 17.6 μmol) was dissolved in 1 mL of DMF containing EDC (10.13 mg, 52.8 μmol) and NHS (6.072 mg, 52.8 μmol), and this mixture was stirred for 3 h to activate the carboxylic acid group of α-TOS. Then, the activated α-TOS was dropwise added to the G4 solution

in DMF containing 20 µL of DIPEA under vigorous magnetic stirring. The stirring process was continued overnight to complete the reaction in an inert atmosphere. The DMF was evaporated by rotary evaporator, and the reaction mixture was purified by dialysis and lyophilized to get G4-TOS. The scheme of the synthesis is shown in Figure 2.1.

2.3.2.2 Conjugation of PEG to G4-α-TOS

mPEG-NHS of about 10 mol equiv (67.82 mg, 33.91 µmol) of G4-TOS was dissolved in 1 mL of DMF and was mixed with G4-TOS (50 mg, 3.391 µmol) dissolved in 2 mL of DMF containing 20 µL of DIPEA under vigorous magnetic stirring. The stirring process was continued overnight to complete the reaction in an inert atmosphere. The DMF was evaporated by rotary evaporator, and the reaction mixture was purified by dialysis (MWCO 12-14 kD) and lyophilized to get G4-TOS-PEG.

2.3.2.3 Conjugation of PEG to the G4 PAMAM Dendrimer

mPEG-NHS (10 mol equiv of G4 PAMAM dendrimer, 70.4 mg, 35.2 µmol) was dissolved in 1 mL of DMF and mixed with G4 (50 mg, 3.52 µmol) dissolved in 2 mL of DMF containing20 µL of DIPEA under vigorous magnetic stirring. The stirring process was continued overnight to complete the reaction in an inert atmosphere. The DMF was evaporated by rotary evaporator, and the reaction mixture was purified by dialysis (MWCO 12-14 kD) and lyophilized to get G4-PEG.

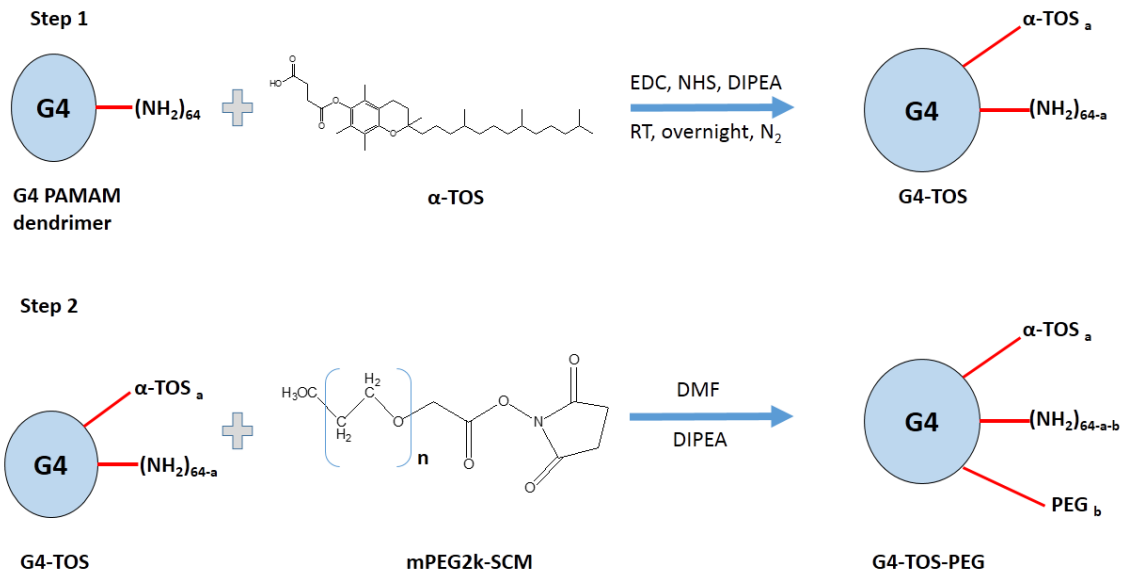

Figure 2.1. Schematic representation for α-TOS and PEG conjugation onto the G4 PAMAM dendrimer.

2.3.3 Characterization of Multifunctional Conjugate

The proton NMR in D2O (300 MHz, Bruker, USA) was done for the synthesized dendrimer conjugates. The hydrodynamic diameter, PDI, and surface potential of the synthesized conjugates were performed using a Malvern Zetasizer (Nano ZS, Malvern Instruments, UK). The dendrimer samples were diluted in deionized water and analyzed by dynamic light scattering using a Malvern zetasizer at 25 °C. The gel permeation chromatography was carried out to determine the molecular weight of the synthesized G4-conjugates. Ultrahydrogel linear (7.8 mm ID × 300 mm × 6 μ) size size exclusion column was used to elute the samples in GPC system (Waters Alliance series). Tris buffer (40 mM) and potassium chloride (80 mM) was used as a mobile phase with flow rate of 1 ml/min. The standard molecular weight compounds were run before analysing the sample to plot the calibration curve. The calibration curve was plotted using different molecular weight pullulan standards of molecular weight range 0.63×10^4, 0.98×10^4, 2.20×10^4, 4.71×10^4, 10.7×10^4, 20.1×10^4, 33.4×10^4, 64.2×10^4 Da.

2.3.4 PTX Loading in the G4-α-TOS-PEG Nanoconjugate

For drug loading, an excess (5 mg) of PTX was added to the G4-PEG (25 mg) and G4-TOS-PEG (25 mg) dendrimer conjugates dissolved in methanol under slow stirring at 50 rpm for 24 h. The methanol was evaporated by rotary evaporator, and PBS was added to the dried mixture. The suspension was centrifuged at 5000 rpm, and the supernatant was taken and estimated by HPLC to determine the amount of drug loaded within the dendrimer.

2.3.5 Percentage Entrapment Efficiency (%EE) and Drug Loading (%DL)

Entrapment and drug loading were carried out for G4-PEG and G4-TOS-PEG by diluting the sample in methanol to release PTX from dendrimer. PTX concentration was determined by using an HPLC LC-20AD system (Shimadzu, Kyoto, Japan), LC-20AD prominence pump, SIL-20ACHT autoinjector, and SPD-20A UV detector. The mobile phase was phosphate buffer saline pH 7.4 and acetonitrile (60:40 v/v) with a flow rate of 1 mL/min at λmax 227 nm. After centrifugation, the supernatant was diluted with mobile phase to determine the amount of PTX. %EE and %DL of PTX-loaded G4-PEG and G4-TOS-PEG were calculated by the following equations:

$$\%EE = \frac{amount\ of\ drug\ in\ supernatant\ of\ dendrimer\ conjugate}{amount\ of\ drug\ added} \times 100$$

$$\%DL = \frac{amount\ of\ drug\ in\ supernatant\ of\ dendrimer\ conjugate}{amount\ of\ drug\ and\ dendrimer\ conjugate} \times 100$$

2.3.6 In Vitro Release Study

A dialysis method was used to determine the PTX release from dendrimer formulations (Kulhari et al. 2016). Two milliliters of G4-PEG-PTX and G4-TOS-PEG-PTX (equivalent to 2 mg of PTX) solution were filled into dialysis bags (MWCO 2000 Da) using PBS (pH 7.4) as a release media (50 mL) and stirred at 100 rpm at 37 °C. At different time points, an 1 mL aliquot was taken out from the media, and the same volume of fresh medium was replaced again to maintain the sink condition. The aliquots were diluted (if necessary) and filtered through a 0.22 μm membrane filter. The amount of

PTX release was analyzed by HPLC. Free PTX was dissolved in the mixture of Tween 80 and ethanol, and it was used as the control. The sink condition was maintained using 20% methanol added to the media. The experiment was done in triplicate. The graph was plotted for the percentage cumulative amount of PTX released versus time (mean ± SD, n = 3).

2.3.7 Hemolytic Toxicity Study

This assay was carried out to evaluate the safety of the newly synthesized α-TOS-anchored dendrimer conjugate in vivo following a previously reported literature (Rompicharla et al. 2018). Briefly, the rat blood (5 mL) was collected in heparinzed tubes. Further, the red blood cells (RBCs) were isolated by centrifugation of blood for 30 min at 3000 rpm at 4°C. The supernatant was discarded, and these cells were resuspended by diluting with PBS after a thorough washing (5% v/v suspension). In the next step, a RBC solution of 5% v/v was incubated with G4-PEG and G4-TOS-PEG (dissolved in PBS at 5 and 10 mg/mL) for 1 h at 37 °C (without PTX). PBS and Triton-X 100 (1% solution) were added in the RBC solution as the negative and positive controls, respectively. After incubation, all the samples were subjected to centrifugation for 20 min at 7000 rpm. The haemoglobin (Hb) present in the supernatant was analyzed by a microplate reader (Spectramax, Molecular Devices, USA) at 576 nm. The degree of hemolysis was derived from the following formula:

$$\%\, Hemolysis = \frac{(A_{\text{sample}} - A_{(-)})}{A_{(-)})/(A_{(+)} - A_{(-)})} \times 100$$

where A_{sample} = the absorbance of the sample, $A_{(-)}$ = the absorbance of sample treated with just PBS, and $A_{(+)}$ = the absorbance of the 100% lysed sample (Triton X-100).

2.3.8 Cellular Uptake by Flow Cytometry

The internalization of the α-TOS-conjugated dendrimer was evaluated by flow cytometry. The B16F10 and MDA MB231 cells were seeded at a cell density of 0.8 × 10^6 cells/well and allowed to attach overnight in 6-well tissue culture plates. On the next day, the cells were treated with fluorescently labeled G4-PEG (F-G4-PEG) and G4-TOS-PEG (F-G4-TOS-PEG) (25 μg/mL) and kept for incubation at 37 °C for 1 and 4 h. After incubation for 1 and 4 h, the cells were washed with sterile PBS and trypsinized. To obtain the cell pellet, the cells were centrifuged for 7 min at 1000 rpm. Next, the cells were suspended again in sterile PBS before analysis using a flow cytometer (Amnis FlowSight, Millipore, USA) with an argon laser of λexc at 488 nm. Cells without any formulation treatment were taken as the control. The data were analyzed by plotting histograms using IDEAS software (version 6.0). The mean fluorescence of samples (n = 3) was plotted as a bar diagram.

2.3.9 Confocal Microscopy

Confocal microscopy was used to visualize the internalization of the α-TOS-conjugated dendrimer. B16F10 and MDA MB231 cells were seeded at a cell density of 50000 cells/well in complete media onto the tissue culture plates (12-well) on top of circular coverslips. On the next day, cells were treated with fluorescently labeled G4-PEG and G4-TOS-PEG (25 μg/mL) for 1 and 4 h at 37 °C. Following incubation, the cells were washed two times with PBS and treated with DAPI (1 μg/mL) for 5 min to stain the nucleus. Further, the cells were washed with PBS and fixed using 4% para-formaldehyde for 15 min. The treated coverslips were mounted upside down on microscopic slides using fluoromount-G mounting medium. These microscopic slides mounted with coverslips were visualized under a confocal microscope (Leica DMi8, Leica Microsystems, Germany) using FITC and DAPI filters, and the images were captured. The images were analyzed by ImageJ software.

2.3.10 Cytotoxicity Study

The MTT assay was carried out to assess the in vitro cytotoxicity of free PTX and PTX-loaded dendrimer formulations in B16F10 and MDA MB231 cells. The cells were seeded at a density of 10,000 cells/well in culture medium in tissue culture plates (96-well). On the next day, the cells were treated with the above formulations (PTX concentration 0−50 μg/mL) and kept for incubation in an incubator (5% CO2) at 37 °C for 24 and 48 h. Free PTX was dissolved in DMSO (not more than 0.5% v/v) and diluted further with culture medium. Following 24 and 48 h of incubation, the growth medium was removed, and the MTT reagent (50 μL, 5 mg/mL) was added to the cells and incubated for 4 h. The MTT reagent was discarded, and the formed formazan crystals were dissolved in dimethyl sulfoxide (DMSO) (150 μL). The optical density was assessed by a microplate reader (Spectramax M4, Molecular Devices, California, USA) at 590 nm by keeping reference λmax at 620 nm. Cells with no treatment were taken as the control. Percentage cell viability was determined by the following equation:

$$Percentage\ cell\ viability = \frac{\text{Abs}_{\text{sample}}}{\text{Abs}_{\text{control}}} \times 100$$

where $\text{Abs}_{\text{sample}}$ = absorbance of the cells treated with free PTX as well as the formulations, while $\text{Abs}_{\text{control}}$ = average absorbance of the untreated living cells. The data were shown as the mean ± SD; n = 3.

2.3.11 Apoptosis Study

MDA MB231 cells at a density of 0.5×10^6/well were seeded in tissue culture plates (6-well) and kept for incubation with free PTX and PTX-loaded dendrimer formulations (PTX concentration 25 μg/mL) for 18 h at 37 °C in a CO2 incubator to assess the apoptosis. The study was carried out as per the manufacturer's instruction. Following 18 h, cells were washed with cold PBS and centrifuged, and the cell pellets were suspended using the AnnexinV binding buffer (100 μL). Then, 5 μL of propidium iodide (PI)

solution and 5 µL of AnnexinV were added to stain the cells and kept for incubation for 15 min. AnnexinV binding buffer (200 µL) was added to each sample and characterized by a flow cytometer (Amnis Flowsight, Millipore, USA). The cells with no treatment were taken as the controls. The 10 000 cells were gated, and the fluorescence of FITC and PI was measured at 535 and 550 nm, respectively. PI versus Annexin V-FITC with quadrant gating was done as a dot plot, which represents live cells (Q3, Annexin V-FITC−PI−), early apoptosis (Q4, Annexin V-FITC+PI−), late apoptosis (Q2, Annexin V-FITC+PI+), and necrotic (Q1, Annexin V-FITC−PI+). To determine the extent of apoptosis, early and late apoptotic events were taken. The apoptosis data of the histogram were plotted by IDEAS software version 6.0.

2.3.12 Evaluation of the α-TOS-Conjugated Dendrimer in 3D Spheroid Model

2.3.12.1 Formation of MDA MB231 Spheroids

The MDA MB231 cancer cell spheroids model was developed by the liquid overlay method as reported previously (Kumari et al. 2018, Rompicharla et al. 2018). Briefly, 1.5% (w/v) agar as a base was prepared in L-15 (serum free) medium and sterilized. To prevent cell adhesion, agar solution (50 µL/well) was added to the 96-well plates to prevent cell adhesion, and the plates were kept for drying (30 min) before use. In 8-well plates, 150 µL of agarose solution was added. MDA MB231 cells (10000 cells/well) were seeded in 96-well plates which were precoated with agar. Further, the plates were centrifuged for 15 min at 1000 rcf. The spheroids were visualized daily by an inverted microscope.

2.3.12.2 Penetration Efficiency in MDA MB231 Spheroids

The MDA MB231 3D spheroids were developed in 8-well tissue culture plates with a cell density of 1 × 104 cells/well. The depth of penetration of fluorescently labeled G4-PEG and G4-TOS-PEG into the spheroids was assessed by confocal microscope (Leica

DMi8, Leica Microsystems, Germany). After incubation for 1−4 h, the spheroids were washed with PBS and then visualized by a confocal microscope at 10× magnification. Z-stack images were captured from the top surface toward the equatorial plane of spheroids at the thickness of 20 μm intervals. Images were assessed by ImageJ software.

2.3.12.3 MDA MB231 3D Spheroids Uptake by Flow Cytometry

Quantitative assessment of cellular internalization of the α-TOS-conjugated dendrimer in MDA MB231 3D spheroids was done by flow cytometry. The 5-day old MDA MB231 spheroids were kept for incubation for 1 and 4 h with NHSfluorescein-labeled G4-PEG and G4-TOS-PEG. Twelve spheroids were collected to achieve sufficient cell count as one replicate at the 1 and 4 h time points. Following being washed with PBS, the 3D spheroids were dissociated by Accutase (200 μL) solution and kept for gentle shaking for 10 min at 37 °C. The cell suspension was transferred to centrifuge tubes, and FBS was added to neutralize the effect of Accutase. After centrifugation, the cells were again suspended in PBS (200 μL) to be analyzed by a flow cytometer (BD FACSCANTO II, BD Biosciences, USA). The intracellular fluorescence exhibited by NHS-fluorescein-labeled G4-PEG and G4-TOS-PEG-treated 3D spheroids was reported as a bar diagram. The data were analyzed by plotting histograms using FCS express software (version 6.0).

2.3.12.4 Growth Inhibition of the MDA MB231 3D Spheroids

The MDA MB231 3D spheroids were grown with density (10,000 cells/well) in tissue culture plates (96-well). When the spheroids attained integrity and uniform size, they were incubated with free PTX and PTX-loaded dendrimer formulations (PTX concentration 25 μg/mL) for 9 days. The growth medium was changed on alternate days. Growth inhibition in MDA MB231 spheroids was visualized under a fluorescence microscope (Leica DMi8, Leica Microsystems) at predetermined intervals (0, 3, 6, and 9

days) at 10X magnification, and the images were captured. The quantitative data are reported as the mean diameter of four spheroids with standard deviation.

2.3.13 Determination of Therapeutic Efficacy in Vivo

The antitumor efficacy of free PTX and various PTX-loaded formulations was evaluated in 6−8 week old female C57BL/6 mice with weights of 18−22 g. The animals were obtained from the Sainath Agency, Hyderabad, India. Mice were kept in in-housed conditions at a controlled temperature of 19−23 °C with 12 h nocturnal−diurnal cycles with a relative humidity of 50−60%, and they were allowed free access to food and water. For 1 week, animals were subjected to adaptation before initiating the experiment. The study was performed following the approval from the Institutional Animal Ethics Committee.

The subcutaneous tumor was developed by injecting B16F10 cells (1 × 106 cells suspended in 100 µL of Hank's balanced salt solution) into the dorsal flank region of mice. The animals were supervised for 10−14 days for the palpable appearance of a solid tumor. The tumor volume ((length × width2)/2) was measured using the vernier caliper every alternate day, and body weight was also measured.

2.3.13.1 Localization of Denrimeric Nanocarriers in Tumor

The animals were considered to be used for the treatment when the average volume of the tumor reached 200 mm3. The animals were divided into two groups (n = 4). Fluorescently labelled G4-PEG and G4-TOS-PEG were injected intraperitoneally into the tumor bearing mice at a dose of 10 mg/kg in PBS. After 8 and 24 h, the tumors were isolated after sacrificing the mice using CO2. The isolated tumors were frozen by immersing them in tissue freezing media after being washed with PBS (pH 7.4) and stored at −80 °C. The frozen tumors were cryosectioned with a thickness of 5 µm by a Cryotome, and they were mounted on glass slides. The sections were treated with DAPI

at 1 μg/mL for 5 min and washed with PBS, and the sections were fixed in 4% paraformaldehyde at 25 °C for 15 min. The stained section was visualized by a fluorescence microscope at 20× magnification.

2.3.13.2 Tumor Inhibition Study

After injecting B16F10 cells (1 × 106 cells), when the tumor volume reached 50−100 mm3, the mice were divided into four different groups (each group having 5 animals). Intratumoral treatment with PBS, free PTX, and PTX-loaded dendrimer formulations was given at PTX doses of 10 mg/kg/day. Free PTX was dissolved in Tween 80 and ethanol (500 μL each), and a further dilution was made by vigorous stirring and dropwise addition of PBS. The animal groups were as follows: (i) PBS (controls), (ii) free PTX, (iii) G4-PEG-PTX, and (iv) G4-TOS-PEG-PTX (n = 5 per group). Intratumoral injections were given near the vicinity of solid tumors on alternate days for up to 10 days. The volume of the tumor and body weight were noted at alternate days for all tumor-bearing mice for 21 days, including the control group. After the end of the study period, mice were sacrificed by cervical dislocation, and the mass of the tumor was collected surgically and weighed.

2.3.13.3 TUNEL Assay in Tumor Cryosections

The tumors were cryosectioned with 5 μm thickness by a cryostat (Leica biosystems, Germany) and fixed with 4% paraformaldehyde. The tumor sections were subjected to treatment with TUNEL reagent (FragEL DNA Fragmentation Detection Kit, Merck, Darmstadt, Germany) as per the manufacturer's instructions to determine the level of apoptosis in tumor sections. The green fluorescence emitted from TUNEL (+) cells was observed in the DAPI and FITC filter using a fluorescence microscope. The images were captured and evaluated by ImageJ software.

2.3.14 Statistical Analysis

Above experiments were carried out in triplicate, and data are represented as mean ± standard deviation (SD). Among all the groups, the significance was assessed by applying one way ANOVA analysis followed by the Bonferroni's post hoc test Graph Pad prism 7 (GraphPad Software, Inc.; CA, USA). A p value < 0.05 in data was considered to be statistically significant. The denotation of *, **, and *** in figures corresponds to p values < 0.05, 0.01, and 0.001, respectively.

2.4 Results and discussion

2.4.1 Synthesis and Characterization of Multifunctional Dendrimer Conjugate

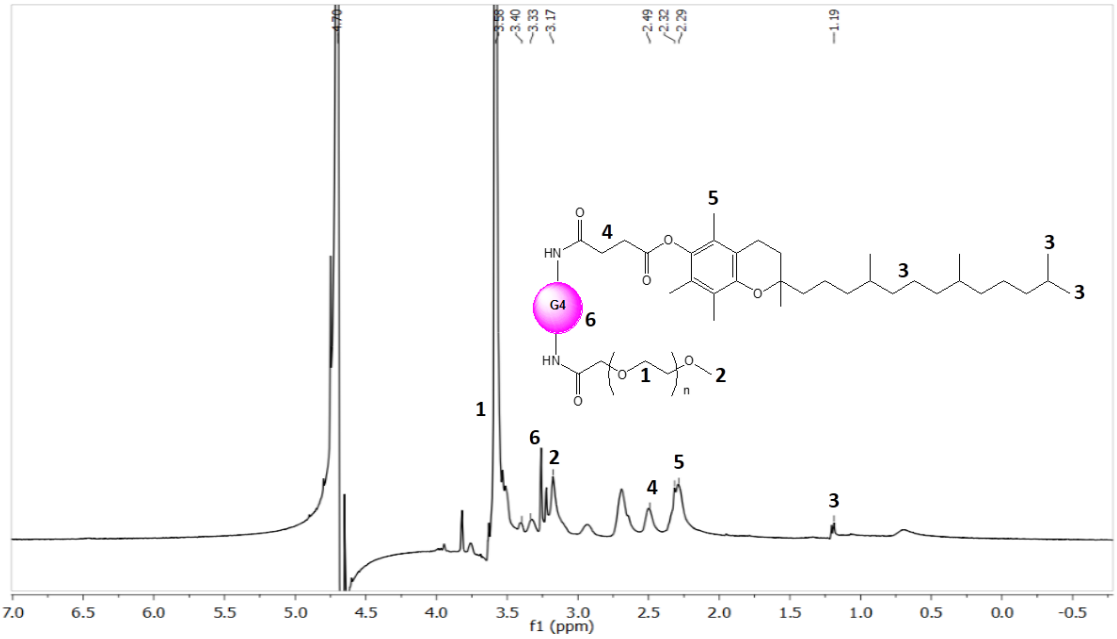

Figure 2.2. Proton NMR spectrum of G4-TOS-PEG in D2O at 300 MHz.

The ^{1}H NMR of the G4-TOS-PEG is shown in Figure 2.2. The NMR spectrum showed the PEG chain protons at a chemical shift of δ (ppm) 3.17-3.7 and the G4 dendrimeric protons at a chemical shift of δ (ppm) 1.20-3.4. The chemical shift of δ (ppm) 1.2−2.6 relates to the α-TOS protons. The NMR spectra confirm the conjugation of TOS and PEG in the dendrimer to form G4-TOS-PEG. The chemical shift of δ (ppm) 4.7 relates to the D2O protons.

Conjugates	Relative Molecular weight (Dalton)	No. of molecules attached approximately to each PAMAM dendrimer
G4	14359	-
G4-TOS	16206	3.47
G4-TOS-PEG	32294	8.044

Table 2.1. Molecular weight and approximate number of TOS and PEG attached to each PAMAM dendrimer assessed by GPC analysis.

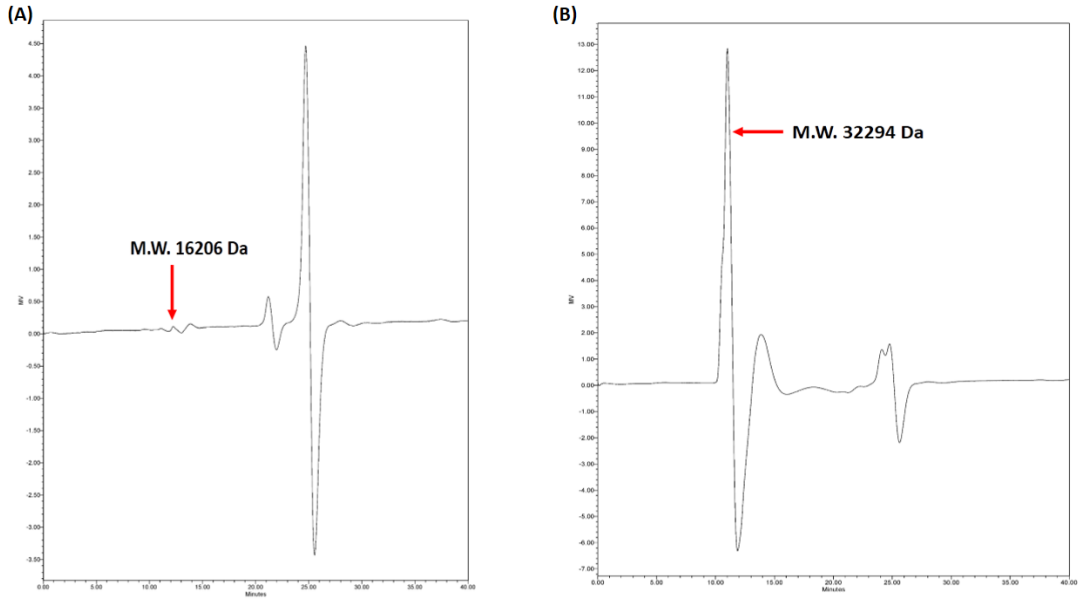

Figure 2.3. GPC chromatograms. (A) G4-TOS. (B) G4-TOS-PEG

The conjugation efficiency of TOS and PEG to the PAMAM dendrimer was calculated by gel permeation chromatography (GPC) analysis. From the GPC results, it was calculated that there were 3.47 molecules of TOS and 8.044 molecules of PEG that were attached on each PAMAM dendrimer (Figures 2.3 and Table 2.1).

From the above Table 2.3, the molecular weight of plain G4 PAMAM dendrimer was found to be 14359 Da. The molecular weight of G4-TOS conjugate was found to be 16206 Da. The molecular weight of each TOS molecule is 530.79 Da. α-TOS of about 5 molar equivalents was taken to conjugate with each PAMAM dendrimer initially as mentioned in the method section. Hence, the TOS molecules got attached to each PAMAM dendrimer was calculated as follows:

$$\text{Number of TOS molecules attached to each PAMAM dendrimer} = \frac{(\text{molecular weight of G4} - \text{TOS conjugate}) - (\text{molecular weight of G4})}{molecular\ weight\ of\ each\ TOS\ molecules}$$

The molecular weight of G4-TOS-PEG conjugate was found to be 32294 Da. The molecular weight of each PEG molecule is 2000 Da. PEG of about 10 molar equivalents was taken to conjugate with each PAMAM dendrimer initially as mentioned in the method section. Hence, the PEG molecules got attached to each PAMAM dendrimer was calculated as follows:

$$\text{Number of PEG molecules attached to each PAMAM dendrimer} = \frac{(\text{molecular weight of G4} - \text{TOS} - \text{PEG conjugate}) - (\text{molecular weight of G4} - \text{TOS})}{\textit{molecular weight of each PEG molecules}}$$

2.4.2 Characterization of Dendrimer Conjugates by Dynamic Light Scattering

Surface conjugation was also further confirmed by measuring the zeta potential of conjugates at each step after synthesis (Table 2.2).

Dendrimer conjugates	Size (nm)	PDI	Zeta potential (mV)	%EE	%DL
G4	13.67 ± 0.06	0.197 ± 0.005	17.6 ± 0.82	-	-
G4-PEG-PTX	15.39 ± 0.06	0.233 ± 0.104	10.4 ± 1.11	65.79 ± 3.11	10.49 ± 1.31
G4-TOS-PEG-PTX	31.19 ± 0.07	0.150 ± 0.092	5.32 ± 0.37	78.33 ± 2.81	14.93 ± 1.64

Table 2.2. Size, PDI, zeta potential, %EE and %DL values of PTX loaded dendrimer formulations and plain G4 dendrimer (Mean±SD, n=3)

The plain G4 dendrimer amine functional groups at the terminal ends. Further, after PTX loading in G4-PEG, the charge was reduced to +10.4 mV due to the nonionic nature of PEG, which also shields the surface charge. After conjugation with α-TOS and loading of PTX in G4-TOS-PEG, the surface potential was decreased to +5.32 mV due to anionic nature of α-TOS. The hydrodynamic diameter of the plain G4 dendrimer, G4-PEG-PTX, and G4-TOS-PEG-PTX was found to be 13.67 ± 0.067, 15.39 ± 0.060, and 31.19 ± 0.073 nm, respectively. %EE and %DL. The PTX loading was found to be 14.93 ± 1.64 and 10.49 ± 1.31% in G4-TOS-PEG and G4-PEG, respectively. The solubility of PTX in G4-

PEG and G4-TOS-PEG was 521.5 ± 3.4 and 742.3 ± 2.8 µg/mL in water, respectively. The increase in %DL in the case of G4-TOS-PEG could be due to the presence of α-TOS on the surface of the dendrimer, which could solubilize PTX and facilitate entrapment in the dendrimer. It has also been proven that α-TOS promotes solubilization of hydrophobic drugs (Duhem, Danhier, and Préat 2014).

2.4.3 In Vitro Release Study from Dendrimers Nanoconjugates

Release of PTX from free PTX solution, G4-PEG, and G4-TOS-PEG in PBS was represented graphically as the % cumulative PTX release over time (Figure 4).

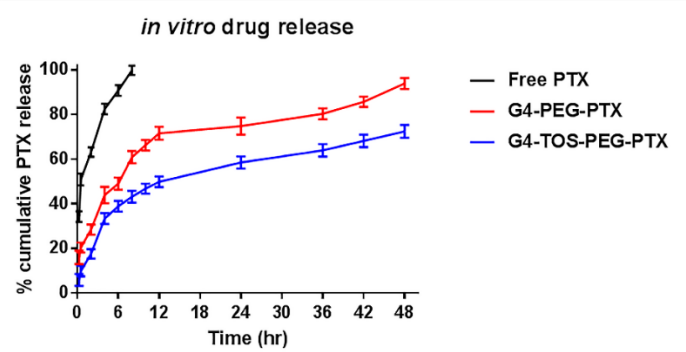

Figure 2.4. In vitro release study (pH 7.4) (each data point is expressed as mean ± SD; n = 3).

As shown in Figure 2.4, PTX was released faster (about 99%) within 8 h from PTX solution compared to dendrimer formulations. In contrast, G4-PEG-PTX and G4-TOS-PEG-PTX showed controlled release of PTX over 48 h. G4-PEG-PTX showed a PTX release of 74.83% after 24 h and 80.36% after 36 h. The α-TOS conjugated dendrimer had a better sustained drug releasing property compared to G4-PEG-PTX or free PTX alone, with a PTX release at 58.55% after 24 h and 63.97% after 36 h. The reason for the controlled release in G4-TOS-PEG-PTX is likely due to the attachment of α-TOS and PEG on the surface of the dendrimer. These attachments made the release path longer for the PTX, as well the partially hydrophobic coat over the dendrimers decreases the diffusion of PTX molecules from the dendrimeric cavity.

2.4.4 Hemolytic Toxicity Study

The hemolysis study was carried out to assess the biocompatibility of G4-PEG and G4-TOS-PEG for in vivo applications. The synthesized G4-PEG and G4-TOS-PEG showed negligible toxicity to the RBCs. The plain G4 showed more hemolysis at both of the concentrations (5 and 10 mg/mL) compared to G4-PEG and G4-TOS-PEG (Figure 2.5).

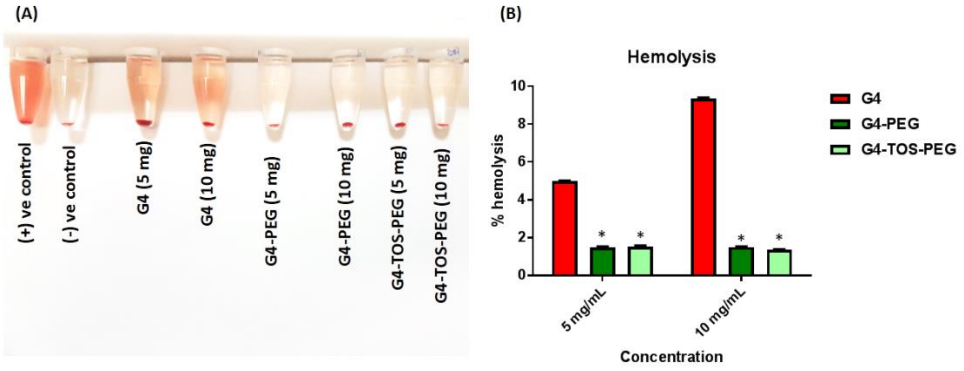

Figure 2.5. Hemolysis. (A) Percent hemolysis analyzed by the interaction between dendrimer conjugates and the RBCs. Data are represented as mean ± SD, n=3. The statistical significance of difference was assessed by ANOVA, and *p < 0.05. (B) Images of tubes containing centrifuged blood following treatment with formulations.

The attachment of PEG chains to the dendrimer molecules reduces the surface charge by providing a protective shield as compared to the plain G4. Moreover, modification with α-TOS on the G4 PAMAM dendrimer did not show any remarkable toxicity. The presence of surface amino groups and the associated cationic charge on dendrimers limits their applications in drug delivery due to the hemolytic and cytotoxic activity. Hence, the use of the G5 PAMAM dendrimer is limited in drug delivery applications, as a higher number of amino groups are present in G5 compared to the G4 PAMAM dendrimers. Attachment of PEG to the G4-TOS reduces the surface charge and improves the long circulation of nanocarriers. Conjugation of G5 dendrimers with α-TOS has been reported elsewhere (Zheng et al. 2014, Wang et al. 2017). However, PEGylation would reduce the side effects by effective charge neutralization.

2.4.5 Cellular Uptake by Flow Cytometry

The flow cytometry was carried out to assess the cellular internalization of the α-TOS-anchored dendrimer system.

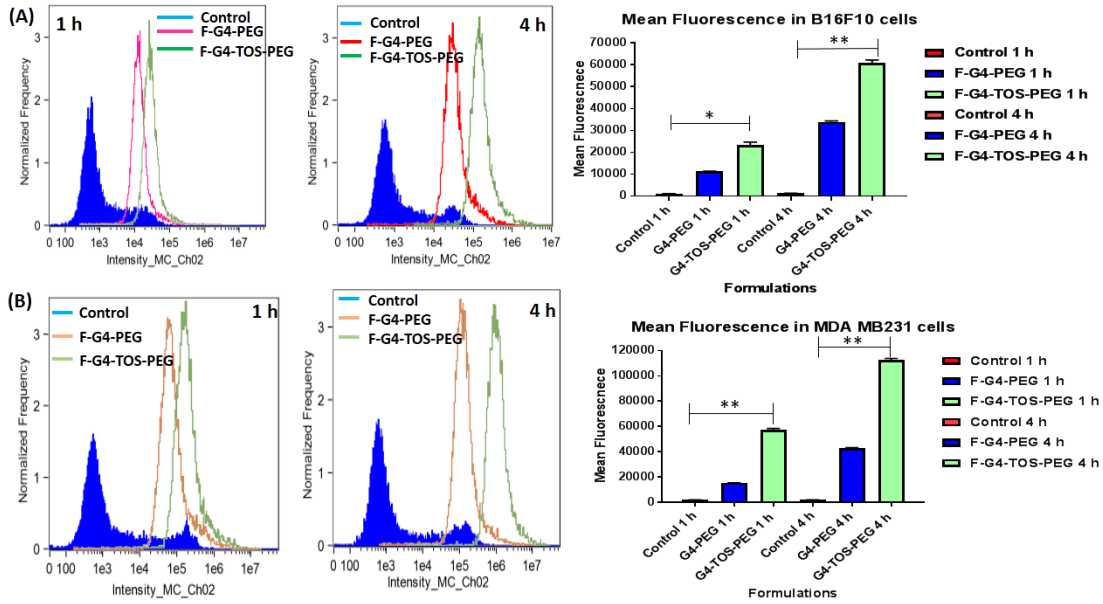

Figure 2.6. Cellular uptake of F-G4-PEG and F-G4-TOS-PEG in B16F10 (A) and MDA MB231 cells (B) measured by a flow cytometer at 1 and 4 h. The mean fluorescence data were plotted as bar graphs. The data were represented as mean ± SD, n = 3. The statistical significance of difference was evaluated by one-way ANOVA, and *p < 0.05 and **p < 0.01.

In this study, more mean fluorescence was observed in cells following F-G4-TOSPEG treatment compared to the treatment with F-G4-PEG (Figure 2.6). The α-TOS conjugation on the dendrimer surface facilitated the nanocarriers uptake, resulting in an increase in the internalized fluorescence, as indicated by the geometric mean of fluorescence. The histograms obtained from the flow cytometer are shown and the value of mean fluorescence is plotted as a bar graph in Figure 2.6. The internalization was time dependent in the case of both B16F10 and MDA-MB231 cells. The data indicated that MDA-MB231 cells were sensitive to the internalization of the α-TOS-conjugated dendrimer system compared to B16F10 cells.

2.4.6 Confocal Microscopy

Following the treatment of B16F10 and MDA MB231 cells with fluorescently labeled F-G4-PEG and F-G4-TOS-PEG for 1 and 4 h, the cells were visualized under a confocal microscope to assess the effect of α-TOS on the cellular internalization of the synthesized dendrimer conjugates.

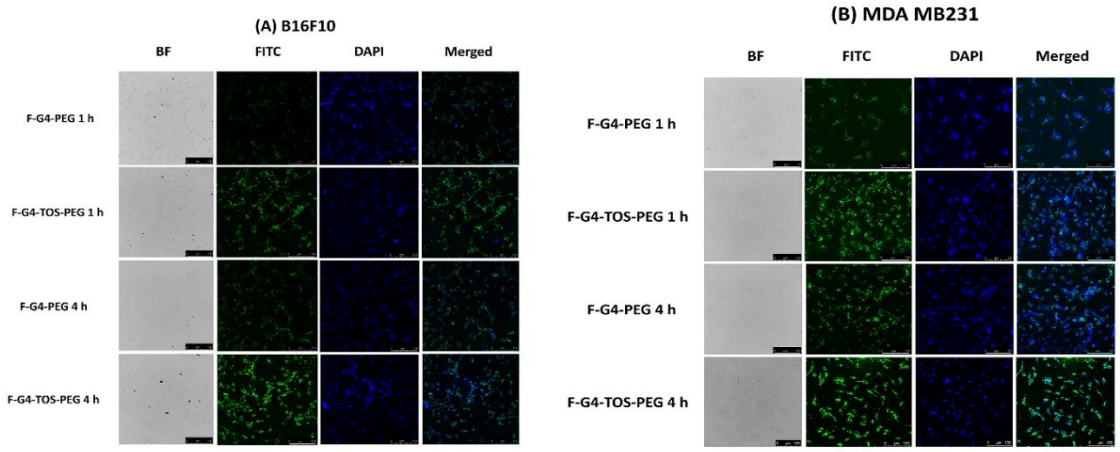

Figure 2.7. Confocal microscopic images of (A) B16F10 and (B) MDA MB231 cells following treatment with FITC-labeled G4-PEG and G4-TOS-PEG for 1−4 h to assess the cellular internalization potential of the nanocarriers.

Higher intensity of green fluorescence was observed in cytoplasm for F-G4-TOS-PEG compared to F-G4-PEG (Figure 2.7). These results are in corroboration with the data obtained using flow cytometry. The α-TOS-anchored dendrimer improved internalization into the cells as compared to F-G4-PEG at both tested time points of 1 and 4 h.

2.4.7 Cytotoxicity Study

The MTT assay was carried out to assess the cell viability of free PTX, PTX-loaded G4-PEG, and G4-TOS-PEG, in which both B16F10 and MDA MB231 cells were treated with formulations for 24 and 48 h at a PTX concentration in the range of 0−50 μg/mL. A time and concentration dependent decrease in cell viability was observed (Figure 2.8).

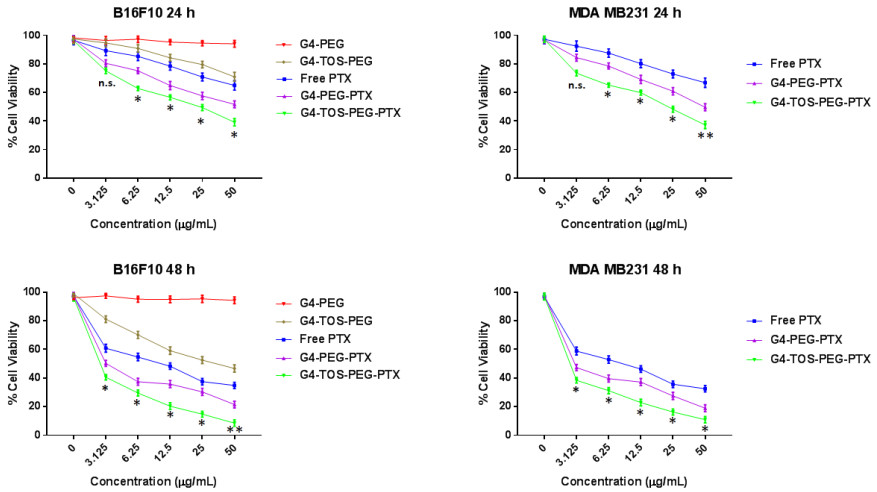

Figure 2.8. Percent cell viability of B16F10 and MDA MB231 cells treated with free PTX, Blank G4-PEG, Blank G4-TOS-PEG and PTX-loaded nanocarriers (at PTX concentrations at 0-50 µg/mL) and blank nanocarriers (without PTX loading) for 24 and 48 h (mean ± SD; n = 3). The significance of difference was calculated by one-way ANOVA. ** and * indicate $p < 0.01$ and 0.05, respectively.

As shown in Figure 2.8, G4-TOS-PEG-PTX showed the highest cell death by decreasing the cell viability to 37.21 ± 2.60% compared to 49.66 ± 2.43% following PTX-loaded G4-PEG and 66.85 ± 3.28% following free PTX treatment in MDA MB231 at the 24 h time point. At the 48 h time point, the cell viability of G4-TOS-PEG-PTX, G4-PEG-PTX, and free PTX was further reduced to 18.33 ± 2.19, 40.66 ± 2.03, and 60.45 ± 2.85%, respectively, in MDA MB231 cells, indicating a time dependent decrease in cellular viability. A similar cell viability profile was observed in B16F10 cells. Blank G4-PEG did not show significant cytotoxicity; however, G4-TOS-PEG demonstrated a cell viability of 70.94 ± 3.18 and 46.70 ± 2.49% after 24 and 48 h, respectively. Blank G4-TOS-PEG showed cytotoxicity due to the anticancer activity of TOS. PTX loaded G4-TOS-PEG and G4-PEG showed that the nanocarriers loaded with PTX were more cytotoxic compared to free PTX at all concentrations, as analyzed in both the tested time points and in both of the cell lines.

2.4.8 Apoptosis

The AnnexinV assay was performed to assess the extent of apoptosis induced by PTX as free drugs or dendrimeric formulations. Following a treatment, phosphatidylserine (PS), an early apoptotic marker, is exposed to the outer plasma membrane from inner membrane, which leads to the attraction of macrophages. The phenomena thus initiate the formation of phagocytized apoptotic bodies. FITCAnnexinV could bind to PS with a high affinity, which allows for the estimation of the induction of apoptosis by measuring the FITC fluorescence (Mulik et al. 2010). Moreover, PI binds specifically to necrotic bodies, which can also be measured simultaneously in a cell population. As shown in Figure 2.9, MDA MB 231 cells were treated with formulations at a PTX concentration of 25 μg/mL for 18 h. Signs of a late apoptosis of 11.6 ± 2.9% (Figure 2.9 B) were quantified in cells treated with free drug; whereas PTX-loaded G4-PEG and G4-TOS-PEG induced a late apoptosis of 27.3 ± 1.6 (Figure 2.9 C) and 40.7 ± 2.5% (Figure 2.9 D), respectively.

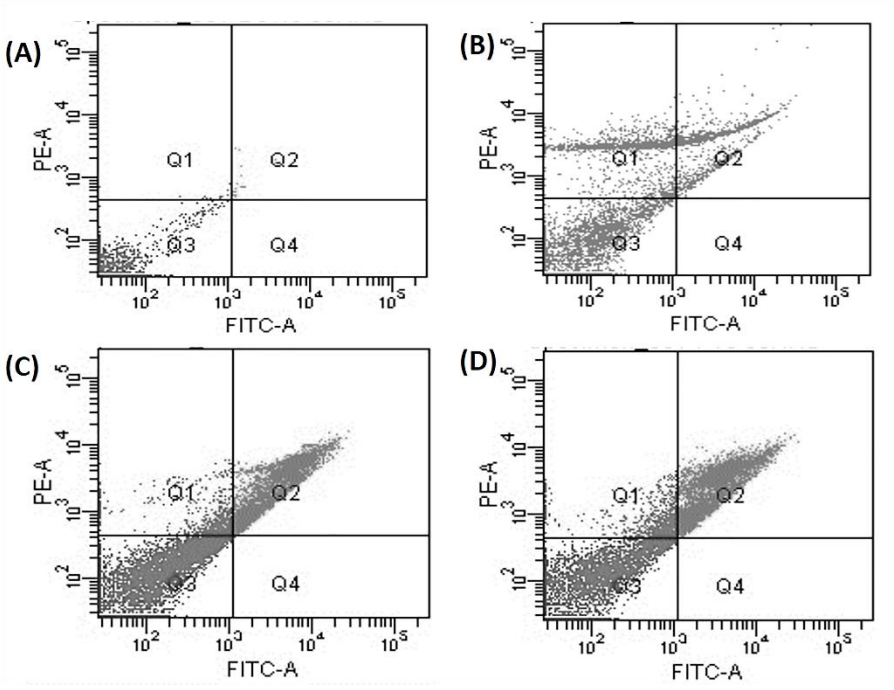

Figure 2.9. Quantitative assessment of apoptosis in MDA-MB231 cells induced by free PTX, G4-PEG-PTX, and G4-TOS-PEG-PTX as studied by the AnnexinV assay (Q1, necrotic cells; Q2, late apoptosis; Q3, live cells; and Q4, early apoptotic cells).

Both formulations induced a higher level of apoptosis compared to free PTX, which could be due to the enhanced cellular uptake of PTX via the nanocarrier extent, leading to enhanced therapeutic efficacy in treated cells. Additionally, the presence of α-TOS in the dendrimer system contributed to enhanced apoptotic action by various mechanisms (Ottino and Duncan 1997a, Ottino and Duncan 1997b, Malafa et al. 2002, Prasad, Cohrs, and Sharma 1990, Prochazka et al. 2013).

2.4.9 Penetration Efficiency in MDA MB231 3D Spheroids

3D spheroids have a natural morphology of cells, pH, redox gradients, and extracellular matrix, which makes them an alternative tool to simulate the microenvironment of in vivo tumors while studying the internalization of molecules into deep tumor tissue. The 3D spheroids improve the importance of in vitro data as compared to monolayers. Here, spheroids of MDA MB231 cells were visualized using a confocal microscope at varied focal lengths (Z-stack) following 1 and 4 h treatment to determine the penetration efficiency.

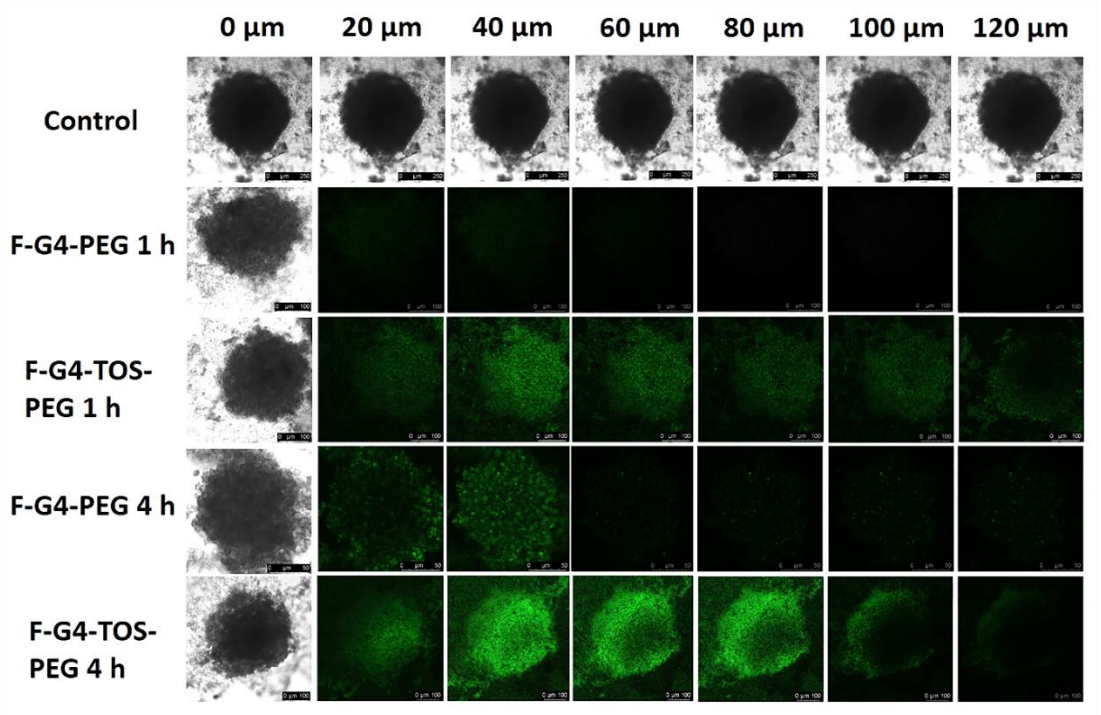

Figure 2.10. Penetration efficiency of fluorescent-labeled G4-PEG and G4-TOS-PEG in MDA MB231 3D spheroids at various depths (Z-stacks) observed using a confocal microscope following 1 and 4 h of incubation.

As shown in Figure 2.10, F-G4-TOS-PEG showed deeper penetration (toward center) in the 3D spheroids as compared to the fluorescently labelled G4-PEG in a time dependent manner. The α-TOS conjugation with the dendrimer improved the cellular internalization significantly, resulting in deeper tissue penetration into the spheroids, which evades the problem of the poor permeability of the nanocarriers into the tumor.

2.4.10 3D Spheroidal Uptake of Fluorescently Labeled Dendrimer Conjugates by Flow Cytometry

The spheroidal uptake of the fluorescently labeled G4-PEG and G4-TOS-PEG was quantified by analyzing the samples using a flow cytometer.

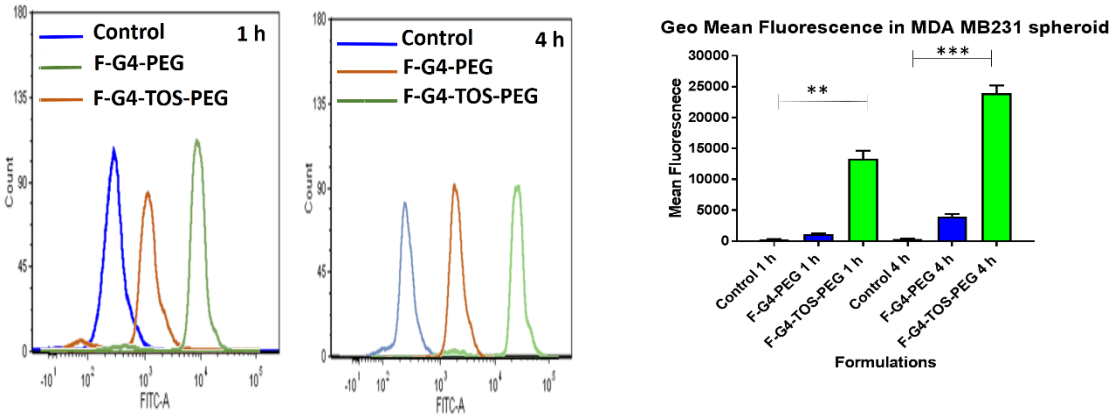

Figure 2.11. Quantitative evaluation of MDA MB231 3D spheroidal uptake of F-G4-PEG and F-G4-TOS-PEG by flow cytometry (data represented as mean ± SD; n = 3). The mean fluorescence data were plotted as bar graphs. The statistical significance of the difference between groups was assessed by ANOVA, and ***$p < 0.001$ and **$p < 0.01$.

The α-TOS-conjugated dendrimers were taken up by the spheroids to a much greater extent compared to the fluorescently labeled G4-PEG after 1 and 4 h (Figure 2.11), as is evident from the value of the mean fluorescence obtained using flow cytometry. The

same results were observed when the MDA MD231 3D spheroids as well as monolayer cells were analyzed qualitatively by confocal microscopy. The 3D spheroidal uptake study suggested that the α-TOS conjugation enhanced the cellular internalization significantly, resulting in deeper tissue penetration. This observation confirmed the importance of the surface modification of dendrimers with α-TOS, which maintained a balance of hydrophilicity and lipophilicity for enhanced absorption. Moreover, it could facilitate the cellular penetration via possible macromolecular interactions for enhanced cellular internalization.

2.4.11 Growth Inhibition of the MDA MB231 3D Spheroids

The treatment of free PTX and PTX-loaded dendrimer formulations to MDA MB231 3D spheroids was continued for 24 h to assess the treatment-mediated inhibition of spheroidal growth.

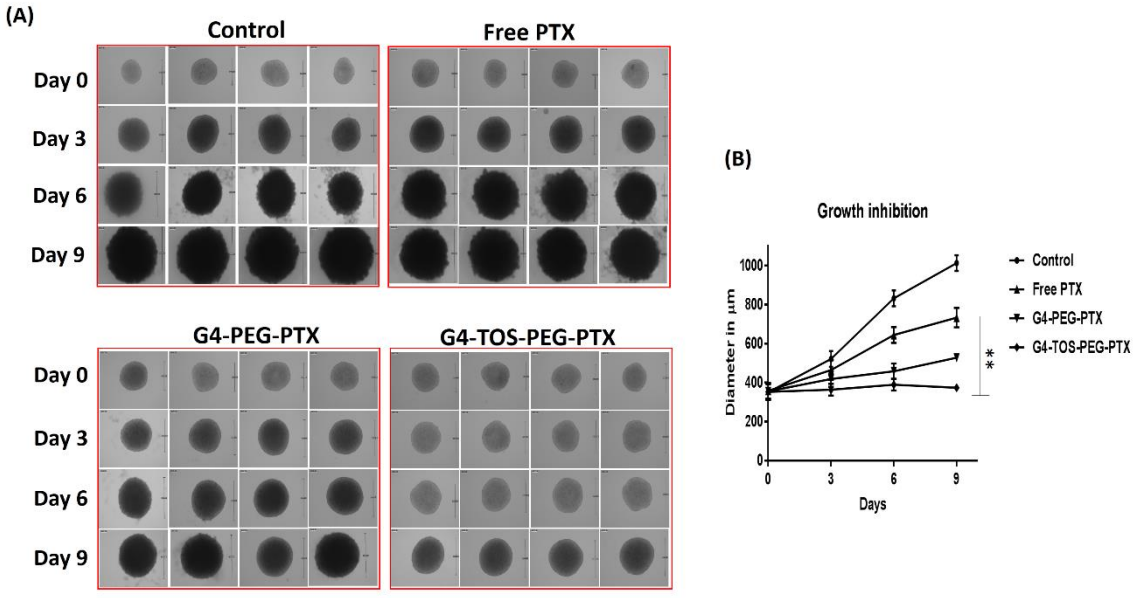

Figure 2.12. Spheroidal growth inhibition study. (A) Bright field microscopic images of MDA MB231 spheroids after treatment with free PTX, G4-PEG-PTX, and G4-TOS-PEG-PTX captured at day 0, 3, 6, and 9 at 10× magnification. (B) MDA MB231 spheroid growth inhibition was shown in a bar graph (mean of diameter in µm with standard deviation; n = 3). The statistical significance of the difference between the groups was assessed by one-way ANOVA. ** indicates $p < 0.01$.

As shown in Figure 2.12, the growth of the G4-TOS-PEG-PTX-treated spheroids was significantly more reduced than G4-PEG-PTX and free PTX-treated spheroids. Moreover, over the period of time, an increment in the diameter of untreated spheroids (size reached up to about 1000 μm) was observed, which was significantly larger in volume in comparison to the spheroids treated with dendrimer formulations as well as free PTX. The mean diameters of spheroids were found to be 1012.43 ± 40.81, 732.34 ± 50.10, 527.14 ± 20.13, and 373.20 ± 11.61 μm for the control, free PTX, PTX-loaded G4-PEG, and PTX-loaded G4-TOS-PEG, respectively, at 9 days. The data are shown as a line graph in Figure 2.12B. α-TOS facilitates the PTX to accumulate more in the 3D spheroids, which leads to the inhibition of the progression of their growth. Moreover, the 3D spheroidal growth inhibition study proves that the synthesized G4-TOS-PEG-PTX get internalized efficiently into the 3D spheroids over a period of time and increases the therapeutic action of PTX. Therefore, it can be concluded, that the α-TOS-anchored dendrimers have the potential to efficiently suppress the tumor growth in vivo based on the fact that the multicellular spheroids mimic the tumor microenvironment.

2.4.12 Tumor Localization of α-TOS-Anchored Dendrimer Conjugate in Tumor

The F-G4-TOS-PEG-treated tumor sections exhibited significantly higher green fluorescence compared to the F-G4-PEG-treated sections at both of the time points (8 and 24 h) (Figure 2.13).

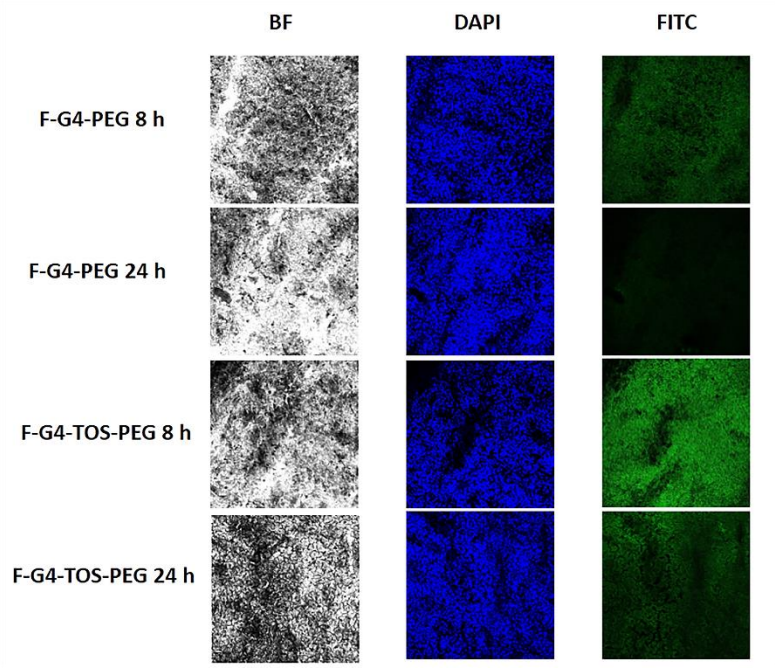

Figure 2.13. Tumor localization study. Fluorescence microscopic images of the B16F10 tumor sections showing the localization of fluorescently labeled G4-PEG and G4-TOS-PEG after the intraperitoneal administration at 10 mg/kg. Objective, 20X.

The strong localization efficiency could be due to the efficient permeation of the α-TOS-anchored nanocarriers into the interstitial extracellular matrix as well as efficient cellular internalization (Tan et al. 2017). Moreover, nanosized PEGylated dedrimeric nanocarriers accumulated into the tumor microenvironment by an EPR effect (Prabhu, Patravale, and Joshi 2015, Zhang et al. 2015, Feng and Mumper 2013, Blanco and Ferrari 2014, Wolinsky and Grinstaff 2008, Miele et al. 2009).

2.4.13 Tumor Inhibition Study

In the tumor inhibition study, combined treatment of the α-TOS-anchored dendrimer and PTX suppressed the growth of the tumor to a significantly higher extent (more than 4-fold) compared to the control (no treatment), free PTX, as well as G4-PEG-PTX (Figure 2.14 A). α-TOS could inhibit the tumor volume suppression by various proven mechanisms, including modification of activity of protein kinase C, blockage of the G1 cell cycle, increasing TGF-β type II receptor expression, and arresting the DNA

synthesis, which finally leads to enhancement of apoptosis (Ottino and Duncan 1997a, Ottino and Duncan 1997b, Malafa et al. 2002, Prasad, Cohrs, and Sharma 1990, Prochazka et al. 2013). It is also reported, that α-TOS imparts anticancer activity by the formation of the reactive oxygen species in the early apoptosis, which leads to mitochondrial destabilization (Prochazka et al. 2013). Suppression of tumor growth was also found significantly in G4-PEG-PTX as compared to free PTX. The possible reason could be more tumor accumulation, biodistribution, and cytotoxicity of the nanosized dendrimer conjugate (G4-PEG-PTX) by passive targeting (EPR effects) (Qin et al. 2011, Maruyama 2011).

Furthermore, the formulations did not show any toxicity in mice, as evidenced by no change in body weight throughout the study (Figure 2.14 B). At the end of the tumor volume reduction study, the tumors were isolated and weighed. The weight of the tumor in the G4-TOS-PEG-PTX-treated group was significantly lower compared to the control, G4-PEG-PTX, and free PTX-treated groups (Figure 2.14 C).

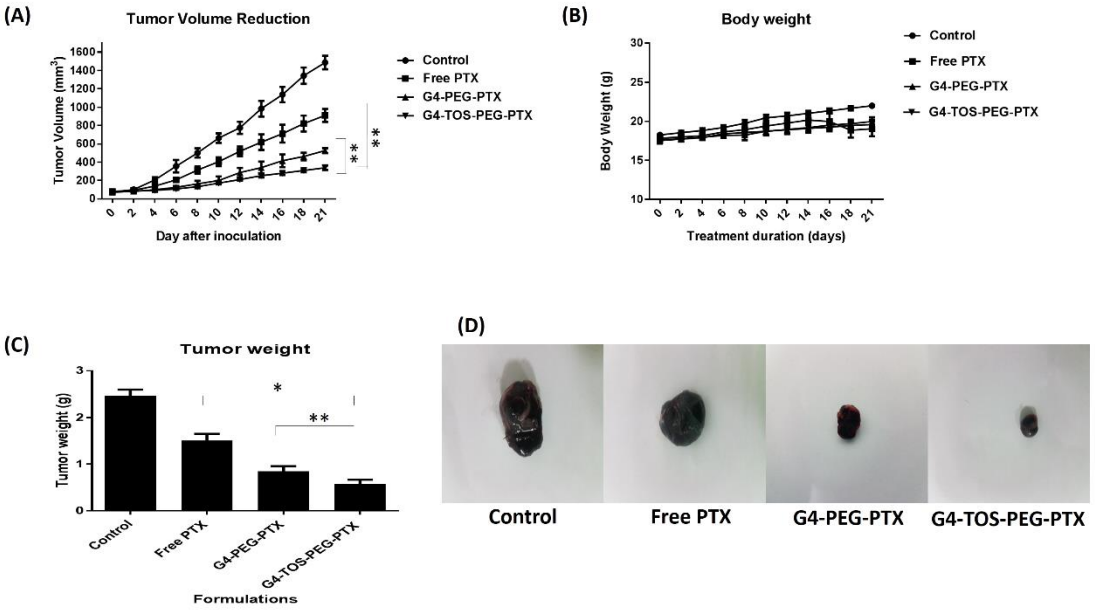

Figure 2.14. Evaluation of in vivo therapeutic efficacy of free PTX, PTX-loaded G4-TOS-PEG, and G4-PEG in B16F10 tumor bearing mice. (A) Graph representing the tumor volume reduction over time. (B) Graphical representation of the body weight over time. (C) A Bar graph representing tumor weight of

individual groups after study. (D) Images of tumors collected randomly from mice that received treatment as mentioned. The statistical significance of the difference between the groups was assessed by one-way ANOVA, and **p < 0.01 and *p < 0.05.

2.4.14 TUNEL Assay on Tumor Cryosections

The TUNEL assay is based on the principle of fragmentation of nuclear DNA by nucleases (activated by caspases), which induce the cell death. Terminal deoxynucleotidyl transferase catalyzes the addition of dUTP nucleotides to the free 3′ ends of fragmented DNA. dUTPs that are tagged with a chemical entity produce fluorescence or color of apoptotic cells (Kyrylkova et al. 2012).

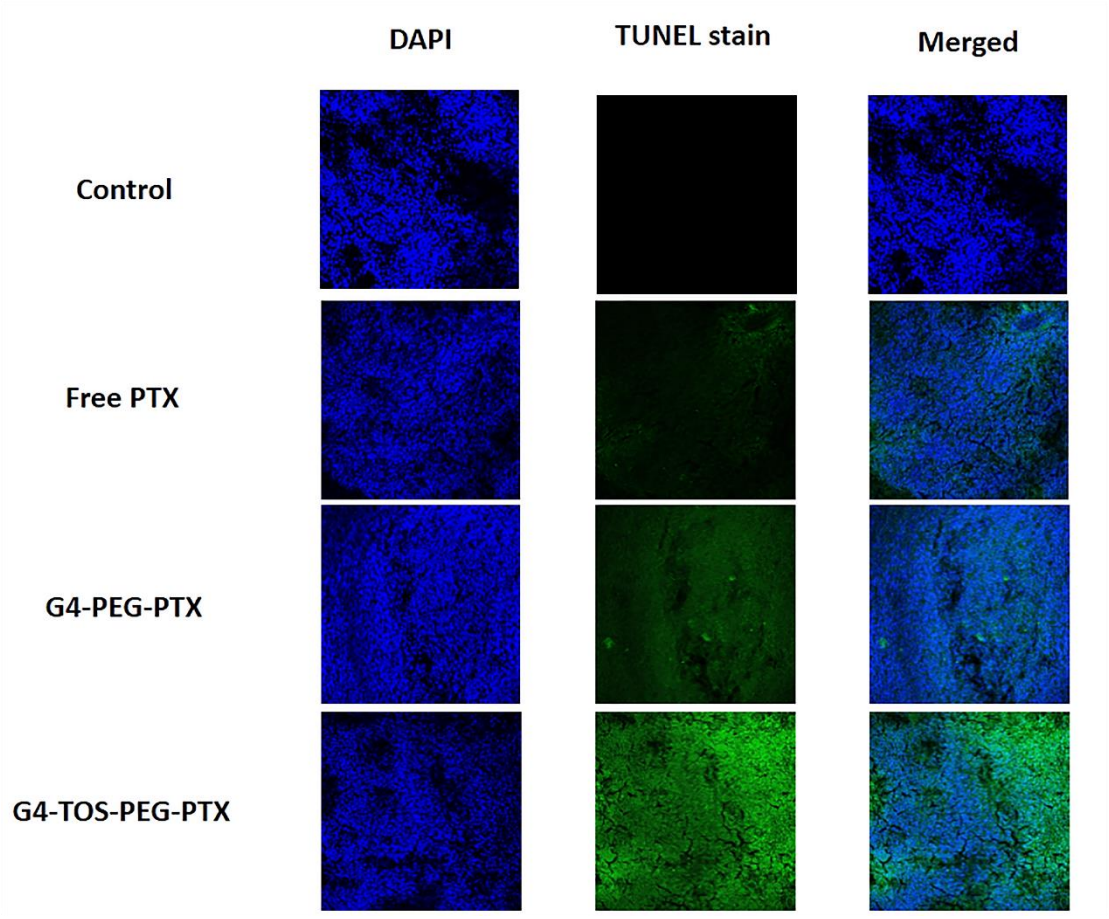

Figure 2.15. Detection of apoptosis by TUNEL assay in tumor cryosections treated with PTX formulations and free PTX as visualized by a fluorescence microscope. Magnification, 20X.

The presence of apoptotic bodies (indicated by strong green fluorescence) was significantly higher in tumor sections following G4-TOS-PEG treatment as compared to

the sections of other treatment groups (Figure 2.15). As stated earlier, α-TOS induced a higher extent of apoptosis leading to cell death; therefore, therapeutic action due to the combined effect of α-TOS and PTX was evident in apoptosis induction.

2.5 Conclusion

In this study, a newly synthesized α-TOS-conjugated PEGylated dendrimer was successfully developed as a delivery system for the improvement of the solubility of the chemotherapeutic drug PTX as well as to enhance its therapeutic efficacy. The developed dendrimeric conjugate entrapping PTX was characterized by proton NMR, hydrodynamic diameter, surface potential, %EE, and %DL. A hemolysis study revealed that the α-TOS-conjugated PEGylated dendrimer had negligible toxicity to RBCs. A cytotoxicity study in B16F10 and MDA MB231 cells demonstrated that the G4-TOS-PEG-PTX produced significantly higher cytotoxicity compared to G4-PEG-PTX and free PTX. Moreover, the α-TOS-conjugated dendrimers improved the internalization of dendrimer-based delivery systems into the monolayer cells as well as in the 3D spheroids. The apoptotic potential of G4-TOS-PEG-PTX was significantly higher compared to the other formulations, as determined by the AnnexinV assay. Deeper penetration was observed for F-G4-TOS-PEG into the 3D spheroids than that of the F-G4-PEG conjugate, as revealed by confocal microscopy and flow cytometry assays. Further, the α-TOS-conjugated dendrimer exhibited superior growth inhibition in 3D spheroids. F-G4-TOS-PEG accumulated in the tumor to a much greater extent compared to F-G4-PEG. An in vivo therapeutic efficacy study revealed that the tumor growth was suppressed with G4-TOS-PEG-PTX treatment to a greater extent compared to G4-PEG-PTX, free PTX, and saline-treated mice due to the induction of apoptosis, as evidenced by the TUNEL assay. Hence, the newly synthesized dendrimeric nanoconjugate could be a promising delivery

system for PTX or other hydrophobic chemotherapeutic drugs and could be utilized for the treatment of solid tumors.

References

Abu-Fayyad, Ahmed, Fathy Behery, Asmaa A Sallam, Saeed Alqahtani, Hassan Ebrahim, Khalid A El Sayed, Amal Kaddoumi, Paul W Sylvester, Jennifer L Carroll, and James A Cardelli. 2015. "PEGylated γ-tocotrienol isomer of vitamin E: synthesis, characterization, in vitro cytotoxicity, and oral bioavailability." *European Journal of Pharmaceutics and Biopharmaceutics* no. 96:185-195.

Biswas, Swati, Namita S Dodwadkar, Rupa R Sawant, Alexander Koshkaryev, and Vladimir P Torchilin. 2011. "Surface modification of liposomes with rhodamine-123-conjugated polymer results in enhanced mitochondrial targeting." *Journal of drug targeting* no. 19 (7):552-561.

Blanco, Elvin, and Mauro Ferrari. 2014. "Emerging nanotherapeutic strategies in breast cancer." *The Breast* no. 23 (1):10-18.

Chandrasekharan, Prashant, Dipak Maity, Cai Xian Yong, Kai-Hsiang Chuang, Jun Ding, and Si-Shen Feng. 2011. "Vitamin E (D-alpha-tocopheryl-co-poly (ethylene glycol) 1000 succinate) micelles-superparamagnetic iron oxide nanoparticles for enhanced thermotherapy and MRI." *Biomaterials* no. 32 (24):5663-5672.

Duhem, Nicolas, Fabienne Danhier, and Véronique Préat. 2014. "Vitamin E-based nanomedicines for anti-cancer drug delivery." *Journal of Controlled Release* no. 182:33-44.

Emami, Jaber, Mahboubeh Rezazadeh, Mahboubeh Rostami, Farshid Hassanzadeh, Hojjat Sadeghi, Abolfazl Mostafavi, Mohsen Minaiyan, and Afsaneh Lavasanifar. 2015. "Co-delivery of paclitaxel and α-tocopherol succinate by novel chitosan-based polymeric micelles for improving micellar stability and efficacious combination therapy." *Drug development and industrial pharmacy* no. 41 (7):1137-1147.

Feng, Lan, and Russell J Mumper. 2013. "A critical review of lipid-based nanoparticles for taxane delivery." *Cancer letters* no. 334 (2):157-175.

Fuchs, Sabine, Timo Kapp, Henning Otto, Torsten Schöneberg, Peter Franke, Ronald Gust, and A Dieter Schlüter. 2004. "A surface-modified dendrimer set for potential application as drug delivery vehicles: synthesis, in vitro toxicity, and intracellular localization." *Chemistry–A European Journal* no. 10 (5):1167-1192.

Gill, Kanwaldeep K, Amal Kaddoumi, and Sami Nazzal. 2012. "Mixed micelles of PEG2000-DSPE and vitamin-E TPGS for concurrent delivery of paclitaxel and parthenolide: enhanced chemosenstization and antitumor efficacy against non-small cell lung cancer (NSCLC) cell lines." *European journal of pharmaceutical sciences* no. 46 (1-2):64-71.

Gruber, Julia, Katrin Staniek, Christopher Krewenka, Rudolf Moldzio, Anjan Patel, Stefan Böhmdorfer, Thomas Rosenau, and Lars Gille. 2014. "Tocopheramine succinate and tocopheryl succinate: mechanism of mitochondrial inhibition and superoxide radical production." *Bioorganic & medicinal chemistry* no. 22 (2):684-691.

Guo, Yuanyuan, Jun Luo, Songwei Tan, Ben Oketch Otieno, and Zhiping Zhang. 2013. "The applications of Vitamin E TPGS in drug delivery." *European Journal of Pharmaceutical Sciences* no. 49 (2):175-186.

Kesharwani, Prashant, Virendra Gajbhiye, Rakesh K Tekade, and Narendra K Jain. 2011. "Evaluation of dendrimer safety and efficacy through cell line studies." *Current drug targets* no. 12 (10):1478-1497.

Kesharwani, Prashant, Keerti Jain, and Narendra Kumar Jain. 2014. "Dendrimer as nanocarrier for drug delivery." *Progress in Polymer Science* no. 39 (2):268-307.

Kline, K, W Yu, and BG Sanders. Vitamin E: mechanisms of action as tumor cell growth inhibitors Prasad KN Cole WC eds. Paper read at Proceedings of the International Conference on Nutrition and Cancer.

Kulhari, Hitesh, Deep Pooja, Shweta Shrivastava, Madhusudana Kuncha, VGM Naidu, Vipul Bansal, Ramakrishna Sistla, and David J Adams. 2016. "Trastuzumab-grafted PAMAM dendrimers for the selective delivery of anticancer drugs to HER2-positive breast cancer." *Scientific reports* no. 6:23179.

Kumari, Preeti, Sri Vishnu Kiran Rompicharla, Omkara Swami Muddineti, Balaram Ghosh, and Swati Biswas. 2018. "Transferrin-anchored poly (lactide) based micelles to improve anticancer activity of curcumin in hepatic and cervical cancer cell monolayers and 3D spheroids." *International journal of biological macromolecules* no. 116:1196-1213.

Kyrylkova, Kateryna, Sergiy Kyryachenko, Mark Leid, and Chrissa Kioussi. 2012. "Detection of apoptosis by TUNEL assay." In *Odontogenesis*, 41-47. Springer.

Malafa, Mokenge P, Frida D Fokum, Arian Mowlavi, Mary Abusief, and Michele King. 2002. "Vitamin E inhibits melanoma growth in mice." *Surgery* no. 131 (1):85-91.

Malik, Noeen, R Wiwattanapatapee, R Klopsch, K Lorenz, H Frey, JW Weener, EW Meijer, W Paulus, and R Duncan. 2000. "Dendrimers:: Relationship between structure and biocompatibility in vitro, and preliminary studies on the biodistribution of 125I-labelled polyamidoamine dendrimers in vivo." *Journal of Controlled Release* no. 65 (1-2):133-148.

Maruyama, Kazuo. 2011. "Intracellular targeting delivery of liposomal drugs to solid tumors based on EPR effects." *Advanced drug delivery reviews* no. 63 (3):161-169.

Miele, Evelina, Gian Paolo Spinelli, Ermanno Miele, Federica Tomao, and Silverio Tomao. 2009. "Albumin-bound formulation of paclitaxel (Abraxane® ABI-007) in the treatment of breast cancer." *International journal of nanomedicine* no. 4:99.

Muddineti, Omkara Swami, Preeti Kumari, Balaram Ghosh, Vladimir P Torchilin, and Swati Biswas. 2017. "d-α-Tocopheryl succinate/Phosphatidyl ethanolamine conjugated amphiphilic polymer-based Nanomicellar system for the efficient delivery of curcumin and to overcome multiple drug resistance in cancer." *ACS applied materials & interfaces* no. 9 (20):16778-16792.

Mulik, Rohit S, Jukka Mönkkönen, Risto O Juvonen, Kakasaheb R Mahadik, and Anant R Paradkar. 2010. "Transferrin mediated solid lipid nanoparticles containing curcumin: enhanced in vitro anticancer activity by induction of apoptosis." *International journal of pharmaceutics* no. 398 (1-2):190-203.

Nam, Joung-Pyo, Kyeong-Jae Lee, Joung-Woo Choi, Chae-Ok Yun, and Jae-Woon Nah. 2015. "Targeting delivery of tocopherol and doxorubicin grafted-chitosan polymeric micelles for cancer therapy: In vitro and in vivo evaluation." *Colloids and Surfaces B: Biointerfaces* no. 133:254-262.

Neuzil, Jiri, ZHAO Ming, Georg Ostermann, Martin Sticha, Nina Gellert, Christian Weber, John W Eaton, and Ulf T Brunk. 2002. "α-Tocopheryl succinate, an agent with

in vivo anti-tumour activity, induces apoptosis by causing lysosomal instability." *Biochemical Journal* no. 362 (3):709-715.

Ottino, P, and JR Duncan. 1997a. "Effect of vitamin E and indomethacin treatment on adenylate cyclase activity, PGE2 and cAMP levels in murine melanoma cells." *Prostaglandins, leukotrienes and essential fatty acids* no. 56 (2):143-149.

Ottino, Paulo, and John R Duncan. 1997b. "Effect of α-tocopherol succinate on free radical and lipid peroxidation levels in BL6 melanoma cells." *Free Radical Biology and Medicine* no. 22 (7):1145-1151.

Prabhu, Rashmi H, Vandana B Patravale, and Medha D Joshi. 2015. "Polymeric nanoparticles for targeted treatment in oncology: current insights." *International journal of nanomedicine* no. 10:1001.

Prasad, Kedar N, Randall J Cohrs, and Opendra K Sharma. 1990. "Decreased expressions of c-myc and H-ras oncogenes in vitamin E succinate induced morphologically differentiated murine B-16 melanoma cells in culture." *Biochemistry and Cell Biology* no. 68 (11):1250-1255.

Prochazka, Lubomir, Stepan Koudelka, Lan-Feng Dong, Jan Stursa, Jacob Goodwin, Jiri Neca, Josef Slavik, Miroslav Ciganek, Josef Masek, and Katarina Kluckova. 2013. "Mitochondrial targeting overcomes ABCA1-dependent resistance of lung carcinoma to α-tocopheryl succinate." *Apoptosis* no. 18 (3):286-299.

Qin, Yao, Huali Chen, Qianyu Zhang, Xiaoxiao Wang, Wenmin Yuan, Rui Kuai, Jie Tang, Li Zhang, Zhirong Zhang, and Qiang Zhang. 2011. "Liposome formulated with TAT-modified cholesterol for improving brain delivery and therapeutic efficacy on brain glioma in animals." *International journal of pharmaceutics* no. 420 (2):304-312.

Roberts, Jeanette C, Mahesh K Bhalgat, and Richard T Zera. 1996. "Preliminary biological evaluation of polyamidoamine (PAMAM) StarburstTM dendrimers." *Journal of Biomedical Materials Research: An Official Journal of The Society for Biomaterials and The Japanese Society for Biomaterials* no. 30 (1):53-65.

Rompicharla, Sri Vishnu Kiran, Preeti Kumari, Balaram Ghosh, and Swati Biswas. 2018. "Octa-arginine modified poly (amidoamine) dendrimers for improved delivery and

cytotoxic effect of paclitaxel in cancer." *Artificial cells, nanomedicine, and biotechnology*:1-13.

Tan, Songwei, Chenming Zou, Wei Zhang, Mingxing Yin, Xueqin Gao, and Qing Tang. 2017. "Recent developments in d-α-tocopheryl polyethylene glycol-succinate-based nanomedicine for cancer therapy." *Drug delivery* no. 24 (1):1831-1842.

Wang, Yunan, Wenwen Shen, Xiangyang Shi, Fanfan Fu, Yu Fan, Wanli Shen, Yini Cao, Qiang Zhang, and Rong Qi. 2017. "Alpha-Tocopheryl Succinate-Conjugated G5 PAMAM Dendrimer Enables Effective Inhibition of Ulcerative Colitis." *Advanced healthcare materials* no. 6 (14):1700276.

Wolinsky, Jesse B, and Mark W Grinstaff. 2008. "Therapeutic and diagnostic applications of dendrimers for cancer treatment." *Advanced drug delivery reviews* no. 60 (9):1037-1055.

Yu, Weiping, Qiao Yin Liao, Feras M Hantash, Bob G Sanders, and Kimberly Kline. 2001. "Activation of extracellular signal-regulated kinase and c-Jun-NH2-terminal kinase but not p38 mitogen-activated protein kinases is required for RRR-α-tocopheryl succinate-induced apoptosis of human breast cancer cells." *Cancer research* no. 61 (17):6569-6576.

Yu, Weiping, Bob G Sanders, and Kimberly Kline. 2002. "RRR-α--Tocopheryl Succinate Induction of DNA Synthesis Arrest of Human MDA-MB-435 Cells Involves TGF-β--Independent Activation of p21Waf1/Cip1." *Nutrition and cancer* no. 43 (2):227-236.

Zhang, Jimei, Chan Li, Xu Zhang, Shuaidong Huo, Shubin Jin, Fei-Fei An, Xiaodan Wang, Xiangdong Xue, CI Okeke, and Guiyun Duan. 2015. "In vivo tumor-targeted dual-modal fluorescence/CT imaging using a nanoprobe co-loaded with an aggregation-induced emission dye and gold nanoparticles." *Biomaterials* no. 42:103-111.

Zheng, Yun, Fanfan Fu, Mengen Zhang, Mingwu Shen, Meifang Zhu, and Xiangyang Shi. 2014. "Multifunctional dendrimers modified with alpha-tocopheryl succinate for targeted cancer therapy." *MedChemComm* no. 5 (7):879-885.

Chapter 3

Transferrin/α-tocopherol modified PAMAM Dendrimers for improved tumor targeting and anticancer activity of Paclitaxel

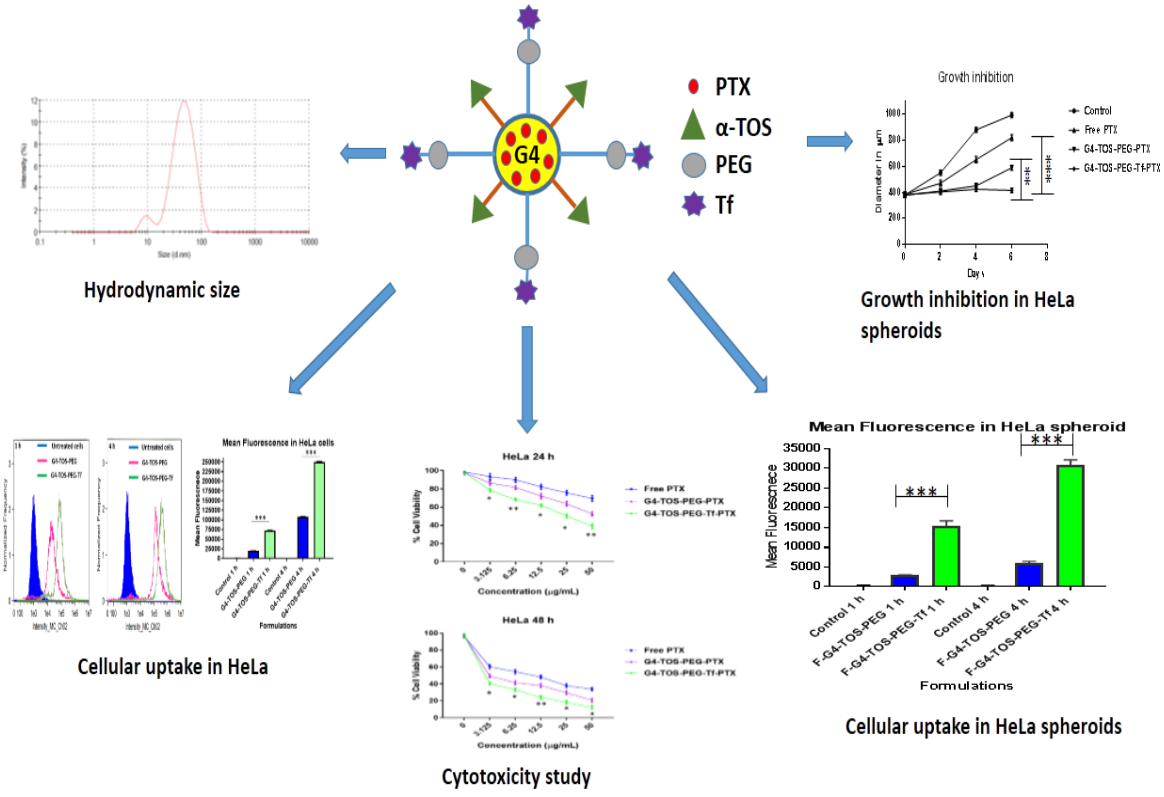

3.1 Abstract

Transferrin anchored, PEG and α-Tocopheryl Succinate (α-TOS) conjugated generation 4 dendrimer has been prepared in order to develop a tumor targeted delivery system of a hydrophobic chemotherapeutic agent, paclitaxel. The dendrimers were characterized physico-chemically for size, zeta and encapsulation ability. The cellular uptake, cytotoxicity potential and apoptosis of prepared nano-construct were evaluated in HeLa monolayer and 3D spheroids. G4-TOS-PEG-Tf demonstrated increased cellular uptake, cytotoxicity and apoptotic potential of PTX compared to free paclitaxel and G4-TOS-PEG-PTX. G4-TOS-PEG-Tf-PTX inhibited growth of HeLa spheroids significantly. The newly developed dendrimers hold promise as an efficient delivery system for paclitaxel or other hydrophobic chemotherapeutic agents for targeted delivery to tumors.

3.2 Introduction

Dendrimers are synthetic macromolecules which have nano-size, narrow polydispersity index, novel three dimensional architecture and high branching units originating from the central core. Poly (amidoamine) dendrimers (PAMAM) have gained interest over the decades to deliver small molecules, macromolecules, and genes to treat various diseases (Kesharwani, Jain, and Jain 2014, Prieto et al. 2014). However, the positively charged dendrimers are more toxic to the cells due to the presence of end group over the periphery of dendrimers (Malik et al. 2000). This toxicity can be overcome with suitable functionalization of the dendrimer surface (Ciolkowski et al. 2012, Kesharwani et al. 2011). The possibility of surface functionalization provides limitless possibility to tailor-made this drug delivery system for improving specific functions, including drug loading, tumor targetability and on-demand drug release.

α-Tocopheryl succinate (α-TOS) (Vitamin-E succinate) has been conjugated to polymers/drug delivery systems to utilize it as non-ionic surfactant or increase the efficiency of the DDS to load hydrophobic drugs efficiently (Gill, Kaddoumi, and Nazzal 2012, Chandrasekharan et al. 2011, Bhatt et al. 2019). α-TOS has proven its anticancer effects in various cancer cell lines by activating the apoptotic pathways (Abu-Fayyad et al. 2015, Emami et al. 2015, Nam et al. 2015, Gruber et al. 2014, Neuzil et al. 2002, Prasad et al. 2003, Yu et al. 2001, Muddineti et al. 2017). Moreover, α-TOS-conjugated ligands have demonstrated potential to overcome multiple drug resistance (MDR) induced by various anticancer drugs by inhibiting the drug efflux transporter, P-glycoprotein (P-gp) (Duhem, Danhier, and Préat 2014, Guo et al. 2013, Muddineti et al. 2017).

Over the past few years, modification of the surface of the nanocarriers using various targeting ligands has been performed to make the drug delivery systems actively targeted

to the tumor site or internalized more efficiently by the cancer cells thorough mechanism of receptor-mediated endocytosis (Hayashi et al. 2011, Sriraman et al. 2016, Zeng et al. 2010, Kulhari et al. 2016). Transferrin (Tf), a 78 kDa-monomeric glycoprotein which binds to transferrin receptor (TfR), a homodimeric type (II) transmembrane protein (Tortorella and Karagiannis 2014). The active role of Tf is to deliver iron in erythropoietic as well as proliferating cells. Rapid proliferation in cancer cells causes over-expression of TfR to meet iron demand. Therefore, surface modification of nanocarriers with Tf is a promising active tumor targeting approach, and proven its effectivity elsewhere. Various studies have revealed that cancer cells over-express (several hundred folds) the Tf receptors on metastatic and drug resistant tumors (Sriraman et al. 2016, Yue et al. 2012, Abouzeid et al. 2014, Chen et al. 2013). Therefore, the potential of active targeting of nanocarriers by anchoring transferrin on the surface of various drug delivery systems in order to improve the therapeutic efficacy of the loaded cargo have been investigated (Muddineti et al. 2018, Tortorella and Karagiannis 2014, Nam et al. 2013, Zhang et al. 2012, Muthu et al. 2015, Kumari et al. 2018, Li et al. 2012).

In this study, the Tf was conjugated over the surface of synthesized G4-TOS-PEG (Chapter 2) to improve the loading and targeting ability of PTX towards cancer cells. The multifunctional dendrimer conjugates were characterized physico-chemically, assessed for its targeting ability and cytotoxicity in human cervical epithelial cells (HeLa) in monolayers and in 3D spheroid model.

3.3 Materials and methods

3.3.1 Materials

The dendrimer Generation 4 Poly (amidoamine) (G4 PAMAM) was obtained from Dendritech Incorporation (MI, USA). The Paclitaxel (PTX) was provided as gift sample from Fresenius Kabi India Pvt., Ltd., India. Maleimide-polyethyleneglycol-N-

hydroxysuccinimidyl ester (mal-PEG-NHS ester, MW 2000 Da) was purchased from Jenkem Technology (USA). N-ethyl-di-isopropylamine (DIPEA) was procured from Avra Chemicals, Mumbai, India. The NHS-Fluorescein was purchased from Thermo Scientific (USA). α-tocopheryl succinate (α-TOS) was purchased from Sigma-Aldrich Chemicals (Bangalore, India). 1-ethyl-3-(3-dimethylaminopropyl) carbodiimide hydrochloride (EDC. HCl, 98%) and N-Hydroxysuccinimide (NHS, 98%) were procured from Sigma Aldrich Chemicals (USA). Dialysis membrane with MWCO 3.5 kDa, 12-14 kDa and 100 kDa was procured from Repligen Inc. (Massachusetts, USA).

HeLa cells were obtained from National Center for Cell Sciences (NCCS, Pune, India). Fetal bovine serum (FBS), Dulbecco's modified Eagle's media (DMEM) and penicillin/streptomycin were obtained from Himedia Laboratories (Mumbai, India). HeLa cells were grown in DMEM medium (DMEM complete medium with 10 percent FBS and 100 IU/mL of antibiotic solution) at 37 °C in 5% CO2 incubator.

3.3.2 Methods

3.3.2.1 Conjugation of TOS to G4 Poly (amidoamine) dendrimer

The synthesis scheme procedure was represented in Figure 3.1. The conjugation of TOS to G4 Poly (amidoamine) dendrimer was done through the reaction reported in previous literature (Bhatt et al. 2019). The acid group of α-TOS (9.341 mg, 17.6 μmol) was activated using EDC and NHS in excess in anhydrous dimethylformamide (DMF). Into the solution of G4-PAMAM dendrimer (3.52 μmol) in anhydrous DMF mixed with the base di isopropyl ethylamine, the activated α-TOS was added drop wise at room temperature. Under inert atmosphere, the mixture was kept for stirring overnight. The next day, DMF was removed by vacuum under rotary evaporator. The reaction mixture was dialyzed using regenerated cellulose membrane with MWCO 12-14 kDa and dried by lyophilisation to obtain pure G4-TOS.

3.3.2.2 Synthesis of PEGylated G4-TOS

To the solution of G4-TOS (3.391 μmol) in DMF, maleimide-PEG-NHS (33.91 μmol) (molar ratio of G4-TOS to Maleimide-PEG-NHS. 1:10) in DMF and 20 μl DIPEA was added. The reaction wascontinued for overnight under inert atmosphere. Following day, DMF was removed by rotary evaporator. Furhter, the product was purified by dialysis membrane with MWCO 12-14kD and dried by lyophilization to get pure G4-TOS-PEG.

3.3.2.3 Synthesis of Tf anchored G4-TOS-PEG

Thiolation of Tf was done using 2-iminothiolane hydrochloride in sodium borate buffer (pH 8.0) as per the instructions of Trout's reagent (Pierce, Thermo Fisher Scientific). Tf was incubated with Trout's reagent for 60 min. The number of thiol (-SH) groups present on the Tf was calculated using Ellmann's reagent (Ellman 1959). Thiolated Tf was coupled with G4-TOS-mal-PEG (at 10:1 ratio) in 10 mM HEPES buffer by incubating the reaction under mild stirring condition at 25°C for overnight. Then, the product was dialyzed using cellulose ester membrane of MWCO. 100 KDa using HEPES buffer for 8 h to get rid of unconjugated Tf.

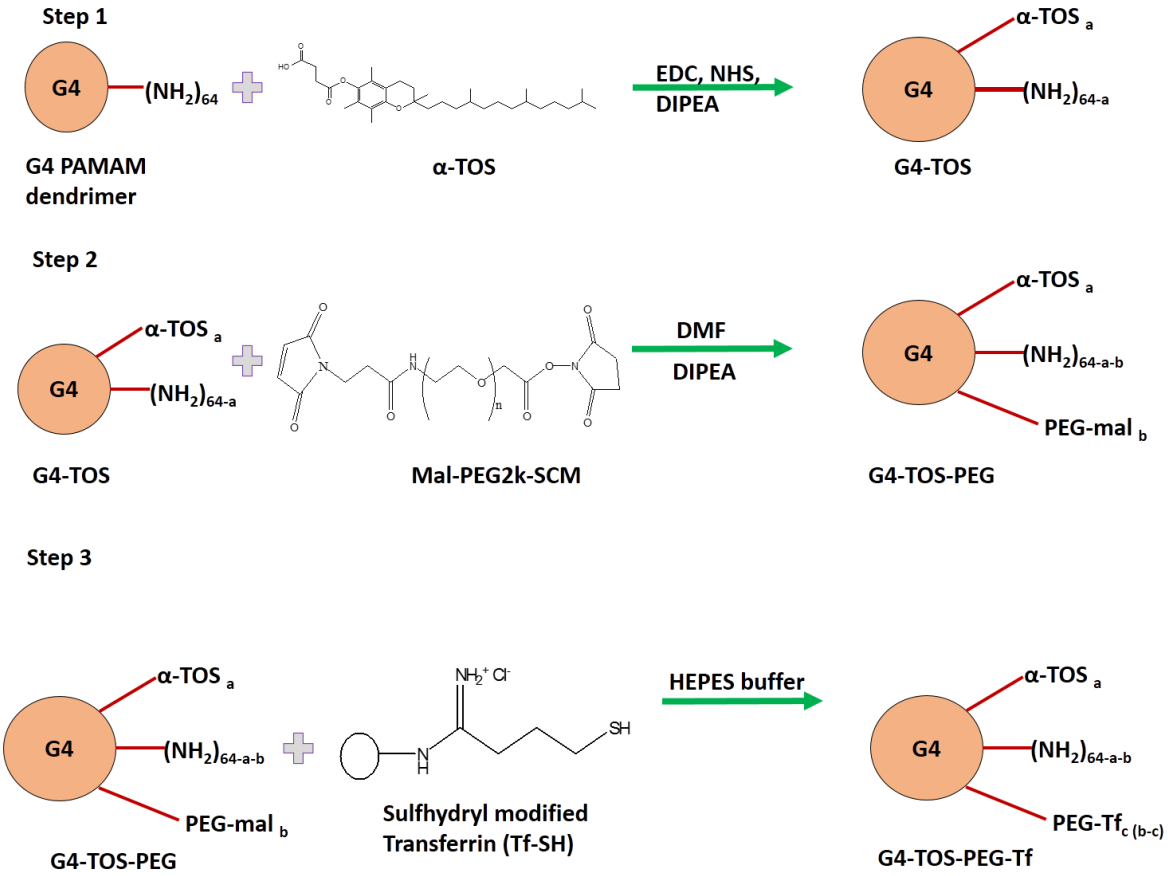

Figure 3.1. Schematic representation of the synthesis of α-tocopheryl succinate, poly (ethylene glycol) and G4-TOS-PEG-Tf.

3.3.3 ^{1}H NMR spectroscopy, Size exclusion chromatography (SEC), dynamic light scattering, transmission electron microscopy (TEM) of synthesized dendrimer conjugates

The ^{1}H NMR for the synthesized dendrimer conjugates was performed using NMR spectrometer (300 MHz, Bruker, USA) and Deuterium oxide (D2O) as the solvent. The SEC was performed to estimate the molecular weight of the synthesized Tf anchored G4-TOS-PEG conjugate (G4-TOS-PEG-Tf). The samples plain G4, G4-TOS, G4-TOS-PEG and G4-TOS-PEG-Tf were eluted through SEC column, Ultrahydrogel™ linear (7.8 mm × 300 mm) in Gel Permeation Chromatography system (Waters series). Milli-Q water was used as a mobile phase with flow rate of 0.7 ml/min. The pullulan standards were

run prior to analyze the dendrimer conjugates. The calibration curve was plotted using different molecular weight pullulan standards of molecular weight range 0.63×10^4, 0.98×10^4, 2.20×10^4, 4.71×10^4, 10.7×10^4, 20.1×10^4, 33.4×10^4, 64.2×10^4 Da. The data of relative molecular weight obtained from the SEC was represented in Table 3.1. The SEC chromatograms of plain G4, G4-TOS, G4-TOS-PEG and G4-TOS-PEG-Tf conjugates were depicted in Figure 3.3.

The hydrodynamic size, polydispersity index and zeta potential of the dendrimer conjugates was determined using a Malvern Zetasizer (Malvern Instruments, UK). The deionized water was used to dilute the dendrimer conjugates and the samples were assessed by photon correlation spectroscopy in Malvern zetasizer at room temperature. Further, the morphology of the synthesized dendrimer conjugate G4-TOS-PEG-PTX was determined using TEM analysis.

3.3.4 PTX loading in dendrimer

PTX in excess (5 mg) was added in dendrimer solution (25 mg) in PBS pH 7.4. The reaction mixture was sonicated for 1 min and kept overnight with gentle stirring. The PTX-loaded formulations were filtered through syringe filter (0.45 μm). Percentage drug loading (%DL) and encapsulation efficiency (%EE) of PTX were estimated by HPLC (Shimadzu, Japan). The flow rate was kept at 1 mL/min and λmax 227 nm. The drug was eluted out with the phosphate buffer saline, pH 7.4 and acetonitrile used as mobile phase. %EE and %DL of PTX-loaded dendrimer formulations were evaluated by the below equations:

$$\%EE = \frac{amount\ of\ drug\ in\ supernatant\ of\ dendrimer\ conjugate}{amount\ of\ drug\ added} \times 100$$

$$\%DL = \frac{amount\ of\ drug\ in\ supernatant\ of\ dendrimer\ conjugate}{amount\ of\ drug\ and\ dendrimer\ conjugate} \times 100$$

3.3.5 Fourier-transform infrared spectroscopy (FTIR) and X-ray diffractometry (XRD) analysis

The lyophilized G4-TOS-PEG-PTX and free PTX were accurately weighed and mixed with KBr to make the pellet. The pellet of lyophilized G4-TOS-PEG-PTX and free PTX was analyzed by FTIR spectrometer (FT/IR-4200, Jasco, USA) individually. The spectrum was recorded in range from 4000 to 400 cm^{-1}. The final spectrum of the G4-TOS-PEG-PTX was compared with free PTX to assess the spectral changes.

The XRD analysis of lyophilized G4-TOS-PEG-PTX and free PTX was carried out by X-Ray diffractometer (Rigaku Ultima IV, Japan) equipped with Copper anode (1.54 Å), current 30 mA and voltage 40 kV. The each samples were run with step size 0.02° and 2θ angle of 5–50° using scintillation counter detector. The final XRD diffractogram of the G4-TOS-PEG-PTX was compared with free PTX to assess any change in intensity using PDXL software.

3.3.6 In vitro PTX release study from dendrimers

In vitro release experiment was performed using dialysis method (Kulhari et al. 2016). PTX-loaded dendrimer formulations (equivalent to 2 mg of PTX) were filled in the dialysis bag (MWCO 2000), which was immersed in PBS, pH 7.4 (supplemented with 0.2 % Tween-80 for maintaining sink condition) and kept on magnetic stirring at 100 rpm at 37 °C. Then, 1 mL aliquot was taken from the release media at predetermined time points, and replaced with fresh medium. If necessary, the withdrawn aliquots were diluted, and filtered through a syringe filter (0.22 μm). The PTX release was estimated by HPLC following the same HPLC conditions mentioned above. The experiment was carried out in triplicate. The data were shown by plotting the graph of % cumulative release versus time (mean ± standard deviation, n = 3).

3.3.7 Cellular uptake in HeLa by flow cytometry

The cellular internalization of dendrimers in HeLa cells was evaluated quantitatively by flow cytometer (FlowSight, Millipore, USA). The cells were seeded in 6-well tissue culture plates at a cell density of 0.8 × 106 cells/ well and allowed the cells to attach overnight. Following day, the cells were treated with fluorescently labelled non-targeted G4-TOS-PEG and targeted G4-TOS-PEG-Tf at 20 μg/ml for 1 h and 4 h at 37 °C. To assess the mechanism of cellular internalization of dendrimers, the clathrin inhibitor chlorpromazine (CPZ) (30 μM) was added to the HeLa cells and the cells were incubated for 30 min at 37ºC/ 5% CO2 environment. Next, the cells were washed with phosphate buffer saline (pH 7.4) and fluorescently tagged dendrimers were added to the cells for 1-4 of incubation. Tf receptor-mediated cellular internalization of G4-TOS-PEG-Tf was assessed by pre-incubing the cells with free Transferrin (2 mg/mL) for 1 h before the treatment with G4-TOS-PEG-Tf. Following treatment, the cells were washed with phosphate buffer saline and trypsin were added for detachment of the cells from the well plate. Next, the cells were kept for centrifugation for 5 min at 1200 rpm. The obtained cell pellets were re-suspended in sterile phosphate buffer saline prior to analyze by flow cytometry at excitation wavelength of 488 nm using argon laser. The data obtained from flow cytometry were assessed in IDEAS software. The geo mean fluorescence of individual samples (triplicates) was shown as a bar graph.

3.3.8 Cellular uptake by confocal microscopy

The cellular uptake was determined qualitatively by confocal microscopy. HeLa cells were seeded in 12-well tissue culture plates onto circular coverslips at a cell density of 50000 cells/well. Following day, the cells were treated with non-targeted F-G4-TOS-PEG and targeted F-G4-TOS-PEG-Tf (20 μg/ml) and incubated for 1 h and 4 h at 37 °C. Similar to the flow cytometry study, the internalization pathway was assessed by adding the clathrin-mediated inhibitor chlorpromazine (CPZ) (30 μM) to the cells. The cells

were incubated for 30 min at 37 ºC in a CO2 incubator. In another experiment, Tf receptors were saturated by pre-incubation of HeLa cells with free Transferrin (2 mg/mL) for 1 h prior to the treatment with dendrimers for 1-4 h. After the treatment with formulations, the cells were washed with phosphate buffer saline three times, then treated with DAPI to stain the nucleus and kept in dark for 5 min. The para-formaldehyde solution was used to fix the cells. Following fixation, the treated coverslips were transferred on glass slides using Fluoromount-G medium. The slides were seen under confocal laser scanning microscope (Leica DMi8, Leica Microsystems, Germany) at 40X magnification using FITC and DAPI channels. The Image J software was used to process and analyze the captured images.

3.3.9 Cytotoxicity study

The cytotoxicity assay was performed to evaluate the cytotoxicity of free PTX and PTX loaded non-targeted and targeted dendrimer formulations in HeLa cells. The cells were seeded in 96-well sterile cell culture plates at cell density of 8000 cells/well in culture medium. Next day, the cellswere treated with free drug and drug loaded dendrimers (at paclitaxel concentrations of 0-50 µg/ml) and kept for 24 and 48 h at 37 °C. Free drug was dissolved in dimethyl sulfoxide, and further diluted with culture media (not more than 0.5% v/v in the final media). The culture media was removed after 24 and 48 h, and MTT reagent (50 µl) was added to the cells and kept for incubation for 4 h. MTT solution was removed from the plates, and the dimethyl sulfoxide was added. The optical density at 590 nm was checked by microplate reader instrument (Spectramax M4, Molecular Devices, California, USA). The reference absorption maxima was kept at 620 nm. The percentage cell viability was calculated by the below mentioned equation:

$$Percentage\ cell\ viability = \frac{\mathrm{Abs_{sample}}}{\mathrm{Abs_{control}}} \times 100$$

Where, Abssample = absorbance of the cells treated with free drug and drug loaded dendrimer formulations, and Abscontrol = absorbance of the control cells. The data were represented as the mean and standard deviation (triplicates).

3.3.10 Apoptosis assay

HeLa cells were seeded in 6-well plates at cell density of 1.2 × 106/well. The following day, cells were treated with free drug and drug loaded non-targeted dendrimer and drug loaded targeted dendrimer formulations at 25 μg/ml of paclitaxel concentration for 18 h and kept in the incubator at 37°C in 5% CO2 atmosphere. This study was carried out as per the protocol provided with Annexin V kit. Following a treatment period of 18 h, HeLa cells were washed with phosphate buffer saline and centrifuged to obtain cell pellets. The obtained cell pellets were again re-suspended in AnnexinV binding buffer (100 μl). Further, the cells were stained using 2 μl propidium iodide (PI) solution as well as 2 μl AnnexinV. Following 15 min of incubation in dark, AnnexinV buffer was added to all test samples and control tubes and assessed by using flow cytometry (Flowsight Amnis, Millipore, USA). The fluorescence of FITC (at 535 nm, Ch02) and propidium iodide (at 550 nm) was measured from the 10000 gated cells. The dot histogram plot for apoptosis data was obtained using IDEAS software. Early apoptosis as well as late apoptotic events were taken into consideration to analyze the magnitude of apoptosis induced in the cells.

3.3.11 Spheroid study

3.3.11.1 Formation of HeLa spheroids

Liquid overlay method was used to develop HeLa cancer cell spheroids as reported in previous literatures (Kumari et al. 2018, Rompicharla et al. 2018). Briefly, 1.5% w/v agar solution in serum free DMEM was prepared and sterilized. Next, the agarose solution (60 μL per well) was poured to the 96-well sterile plates to avoid cell attachment with the bottom surface of well plates. The plates were dried for 30 min before further use. 10000

cells per well were added in pre-coated agar plates. These plates were centrifuged at 1000 rpm for 15 min. The developed HeLa spheroids were seen daily under microscope.

3.3.11.2 Penetration efficiency in HeLa spheroids

HeLa cells were seeded at cell density of 1×104 cells/well into 8-well tissue culture plates to make the spheroids. The depth of penetration of fluorescently labelled dendrimers into the 3D HeLa spheroids was visualized by confocal microscope for 1 h as well as 4 h. Post incubation period, the spheroids were washed with phosphate buffer saline and then observed at 10X magnification under confocal microscope at different focal length (Z-stack). The images of the spheroids were taken and processed using Image J software.

3.3.11.3 HeLa 3D spheroid uptake by flow cytometry

HeLa spheroids (5 days old) were treated for 1 h and 4 h with non-targeted F-G4-TOS-PEG and targeted F-G4-TOS-PEG-Tf. For sufficient cell count, 12 spheroids were taken together as one replicate for both the time points. The spheroids were broken by AccutaseTM solution and were shaken moderately for 10 min. The suspension of the cells was moved to eppendorf tubes and fetal bovine serum was added. Following centrifugation, the supernatant was discarded and the cells were re-suspended in phosphate buffer saline to analyze by flow cytometer (BD Biosciences, USA). The mean fluorescence shown by non-targeted F-G4-TOS-PEG and targeted F-G4-TOS-PEG-Tf treated spheroids was plotted as a bar graph using Graph Pad prism 7 software. The FCS express software was used to analyze the data and to plot the histograms.

3.3.11.4 Assessment of growth inhibition of the HeLa spheroids

When the spheroids achieved proper integrity grown in 96-well plates, they were treated with free drug and drug loaded non-targeted and targeted dendrimer formulations, with paclitaxel concentration of 25 µg/mL. The growth media was replaced with fresh medium on alternate days. The spheroids were observed under bright field microscope (Leica,

Leica Microsystems, Germany) and the diameters of the spheroids were measured at predetermined time points (0, 2, 4 and 6 days) and the images were captured at 10X magnification. The mean diameter of 4 spheroids with standard deviation was shown quantitatively in Figure 3.12 (B).

3.3.11.5 Live/dead cell detection in HeLa spheroids

The live/dead cells in treated spheroids were detected using live/dead cells detection kit. Briefly, the treatment was given to the spheroids with following formulations, (i) free paclitaxel; (ii) paclitaxel loaded non-targeted G4-TOS-PEG; and (iii) paclitaxel loaded targeted G4-TOS-PEG-Tf, with 25 μg/mL of PTX concentration for 24 h. Next, calcein blue AM (2 μM) as well as propidium iodide (PI) (4 μM) were added to stain the spheroids. The stained spheroids were kept in incubation for 20 min at 37 ºC and was observed under fluorescence microscope using red and blue channels.

3.3.12 Statistics

All of the above experiments were performed in triplicates and the data are shown as mean and standard deviation (mean ± SD). The significance of difference between all the groups was evaluated by one-way ANOVA using Graph Pad prism software (GraphPad, Inc., California, USA). At p value < 0.05, the data were considered to be statistically significant.

3.4 Results and discussion

The presence of high number of surface amino groups and associated cationic charge on PAMAM dendrimers limits their applications in drug delivery due to their hemolytic toxicity, and other nonspecific toxicities. Anchoring of α-TOS to G4 was expected to enhance penetrability and solubility of poorly soluble chemotherapeutics drugs e.g. paclitaxel. Moreover, attachment of PEG to G4-TOS could reduce the surface charge, provide biocompatibility, and improve long circulation of the nanocarriers (Abedi-

Gaballu et al. 2018, Ghaffari et al. 2018). Here, TOS, PEG and Tf-modified G4 PAMAM dendrimer conjugate, G4-TOS-PEG-Tf has been prepared to load PTX efficiently to improve the solubility of PTX, and deliver it effectively to the tumor site as well as in the intracellular compartments via facile translocation through endocytosis. Vitamin-E could solubilize many hydrophobic drugs, and has been incorporated physically or covalently in various polymeric drug delivery systems for facile drug incorporation and improved loading (Chandrasekharan et al. 2011, Bhatt et al. 2019, Muddineti et al. 2018, Muddineti et al. 2017). Apart from its ability to solubilize various poorly water soluble drugs, α-TOS has proved its anticancer activity as an apoptosis inducer in a variety of human cancer cell lines (Bhatt et al. 2019, Abu-Fayyad et al. 2015, Emami et al. 2015, Nam et al. 2015, Gruber et al. 2014, Neuzil et al. 2002, Muddineti et al. 2017). Tf protein is considered as a stable and efficient tumor homing ligand, which has proved its ability to drag nanocarriers towards tumor by its anchorage on the nanocarriers surface (Kesharwani and Iyer 2015). As stated earlier, the selective accumulation is due to the high iron demand of the proliferating cancer cells that enables Tf-receptor mediated endocytic internalization of the nanocarriers.

3.4.1 Confirmation of synthesis of Tf anchored multifunctional dendrimer nano-construct

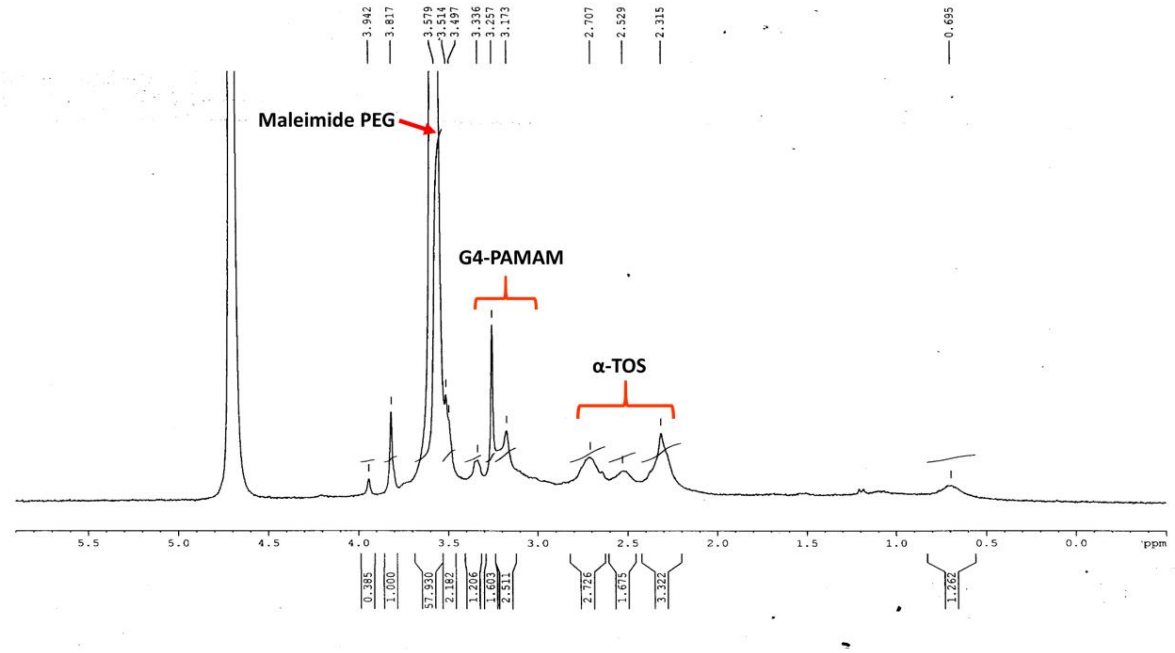

Figure 3.2. ^{1}H NMR spectra of G4-TOS-PEG in D2O at 300 MHz.

Figure 3.2 showed the proton NMR of the maleimide functionalized G4-TOS-PEG. The chemical shift at 3.5-3.9 in the NMR spectrum represented the protons of PEG chains. The chemical shift δ (ppm) at 3.1-3.5 are related to the G4 dendrimeric protons. The proton signals at chemical shift δ (ppm) 2.3-2.7 are related to the α-TOS protons. This confirms that TOS and maleimide PEG were conjugated to the G4 PAMAM dendrimer. Maleimide functionalization was required to conjugate the Tf via thiolation reaction.

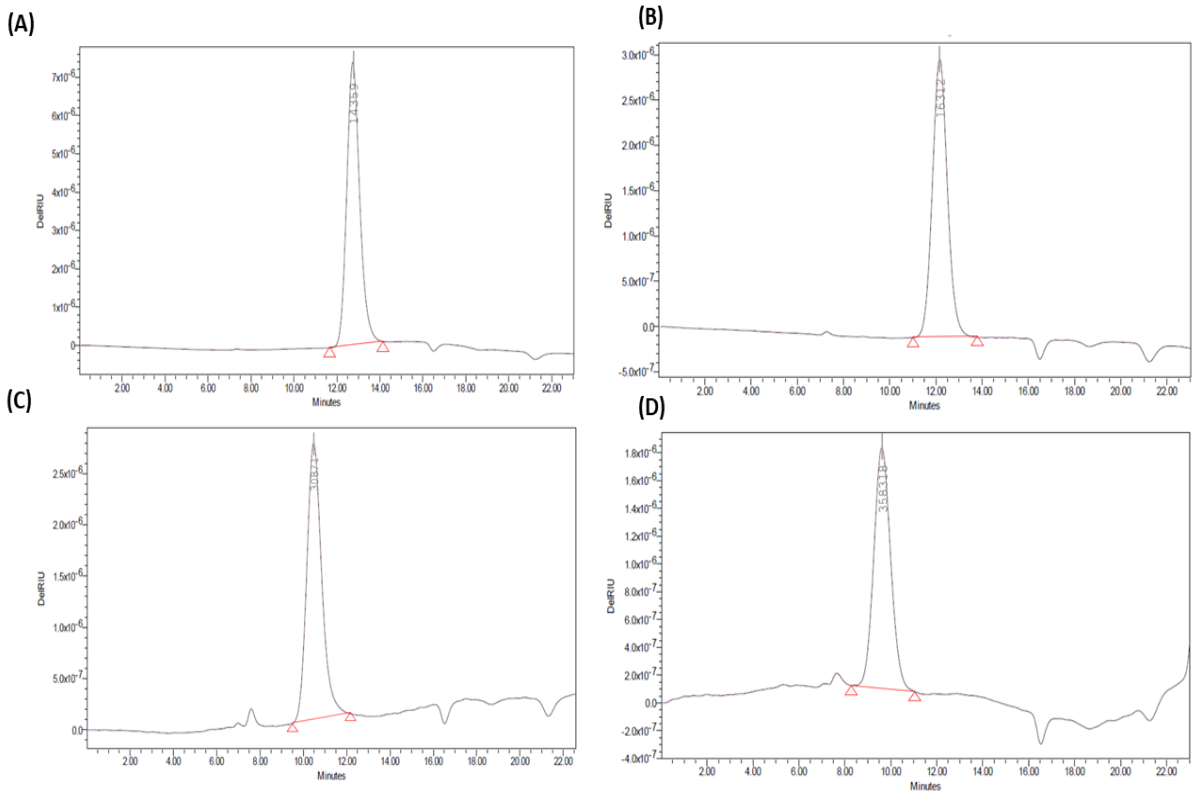

Figure 3.3. SEC chromatograms of synthesized dendrimer conjugates. (A) G4, (B) G4-TOS, (C) G4-TOS-PEG, (D) G4-TOS-PEG-Tf.

Conjugates	Molecular weight (Da)	Approximated No. of molecules attached to each G4 PAMAM dendrimer
G4	14359	-
G4-TOS	16312	3.67
G4-TOS-PEG	30871	7.27
G4-TOS-PEG-Tf	358318	4.19

Table 3.1. Molecular weight of each conjugates and estimated number of TOS, PEG and Tf attached to each PAMAM dendrimer obtained by SEC analysis.

The conjugation efficiency of TOS, maleimide PEG and Tf was estimated by size exclusion chromatography (SEC). SEC results showed that 3.67 molecules of TOS, 7.27 molecules of maleimide PEG and 4.19 molecules of Tf were conjugated to each G4 PAMAM dendrimer (Figure 3.3 and Table 3.1).

From the above Table 3.1, the molecular weight of plain G4 PAMAM dendrimer was found to be 14359 Da. The molecular weight of G4-TOS conjugate was found to be 16312 Da. The molecular weight of each TOS molecule is 530.79 Da. α-TOS of about 5 molar equivalents was taken to conjugate with each PAMAM dendrimer initially as mentioned in the method section. Hence, the TOS molecules got attached to each PAMAM dendrimer was calculated as follows:

$$\text{Number of TOS molecules attached to each PAMAM dendrimer} = \frac{(\text{molecular weight of G4} - \text{TOS conjugate}) - (\text{molecular weight of G4})}{molecular\ weight\ of\ each\ TOS\ molecules}$$

The molecular weight of G4-TOS-PEG conjugate was found to be 30871 Da. The molecular weight of each PEG molecule is 2000 Da. PEG of about 10 molar equivalents was taken to conjugate with each PAMAM dendrimer initially as mentioned in the method section. Hence, the PEG molecules got attached to each PAMAM dendrimer was calculated as follows:

$$\text{Number of PEG molecules attached to each PAMAM dendrimer} = \frac{(\text{molecular weight of G4} - \text{TOS} - \text{PEG conjugate}) - (\text{molecular weight of G4} - \text{TOS})}{molecular\ weight\ of\ each\ PEG\ molecules}$$

The molecular weight of G4-TOS-PEG-Tf conjugate was found to be 358318 Da. The molecular weight of each Tf molecule is 78000 Da. Tf of about 10 molar equivalents was taken to conjugate with each PAMAM dendrimer initially as mentioned in the method section. Hence, the Tf molecules got attached to each PAMAM dendrimer was calculated as follows:

$$\text{Number of Tf molecules attached to each PAMAM dendrimer} = \frac{(\text{molecular weight of G4} - \text{TOS} - \text{PEG} - \text{Tf conjugate}) - (\text{molecular weight of G4} - \text{TOS} - \text{PEG})}{molecular\ weight\ of\ each\ Tf\ molecules}$$

The NMR spectrum showed that the conjugation of TOS and PEG to the dendrimer to form G4-TOS-PEG was done successfully. The size exclusion chromatography confirmed the successful attachment of Tf molecules to the dendrimer surface.

3.4.2 Physicochemical characterization of dendrimer conjugates

Dendrimer conjugate	Size (nm)	PDI	Zeta potential (mV)	%EE	%DL
G4	13.69 ± 0.098	0.200 ± 0.002	+20.3 ± 0.58	-	-
G4-PEG-PTX	15.4 ± 0.084	0.177 ± 0.055	+14.7 ± 1.43	67.93 ± 2.46	10.32 ± 1.69
G4-TOS-PEG-PTX	30.42 ± 0.058	0.182 ± 0.089	+8.19 ± 0.39	80.35 ± 2.55	15.9 ± 1.23
G4-TOS-PEG-Tf-PTX	37.91 ± 0.069	0.266 ± 0.006	+2.44 ± 0.31	71.18 ± 2.38	13.04 ± 1.29

Table 3.2. Size, PDI, zeta potential, %EE and %DL values of PTX loaded dendrimer formulations and plain G4 dendrimer (Mean±SD, n=3)

The zeta potential of the dendrimers was measured after PTX loading to assess the surface properties after drug subsequent conjugation and drug loading as shown in Table 3.2. The zeta potential of plain G4 dendrimer was found to be +20.3 mV. Furthermore, the zeta potential was reduced to +14.7 mV following paclitaxel loading in PEGylated G4 (G4-PEG). The surface potential was reduced further to +8.19 mV following attachment with α-TOS. In final step, zeta potential was reduced to +2.44 following Tf-attachment. The hydrodynamic diameters of G4 PAMAM dendrimer, paclitaxel loaded G4-PEG, paclitaxel loaded non-targeted G4-TOS-PEG and PTX loaded targeted G4-TOS-PEG-Tf were 13.69 ± 0.098, 15.4 ± 0.084, 30.42 ± 0.058 and 37.91 ± 0.069 nm, respectively. The PTX loading was found to be 13.04 ± 1.29 %, 15.9 ± 1.23 % and 10.32 ± 1.69 % in G4-TOS-PEG-Tf, G4-TOS-PEG and G4-PEG, respectively as shown in Table 3.2.

Physico-chemical characterization revealedthat the zeta potential was reduced following PEG-attachment in G4-PEG. PEG is nonionic in nature, which reduces the positive surface charge of the dendrimer. The surface potential was reduced further following

attachment with α-TOS due to its anionic nature. In final step, zeta potential was reduced following Tf-attachment due to its shielding effect. The increase in % drug loading in case of G4-TOS-PEG than G4-PEG because α-TOS molecules was present on the surface of dendrimer, which could solubilize paclitaxel and provide an interior hydrophobic cavity for the entrapment of any poorly water soluble drugs. Further, PTX loading was decreased in G4-TOS-PEG-Tf, which could be due to bulkiness of Tf on the surface that limits the access of PTX into the interior dendrimer cavity.

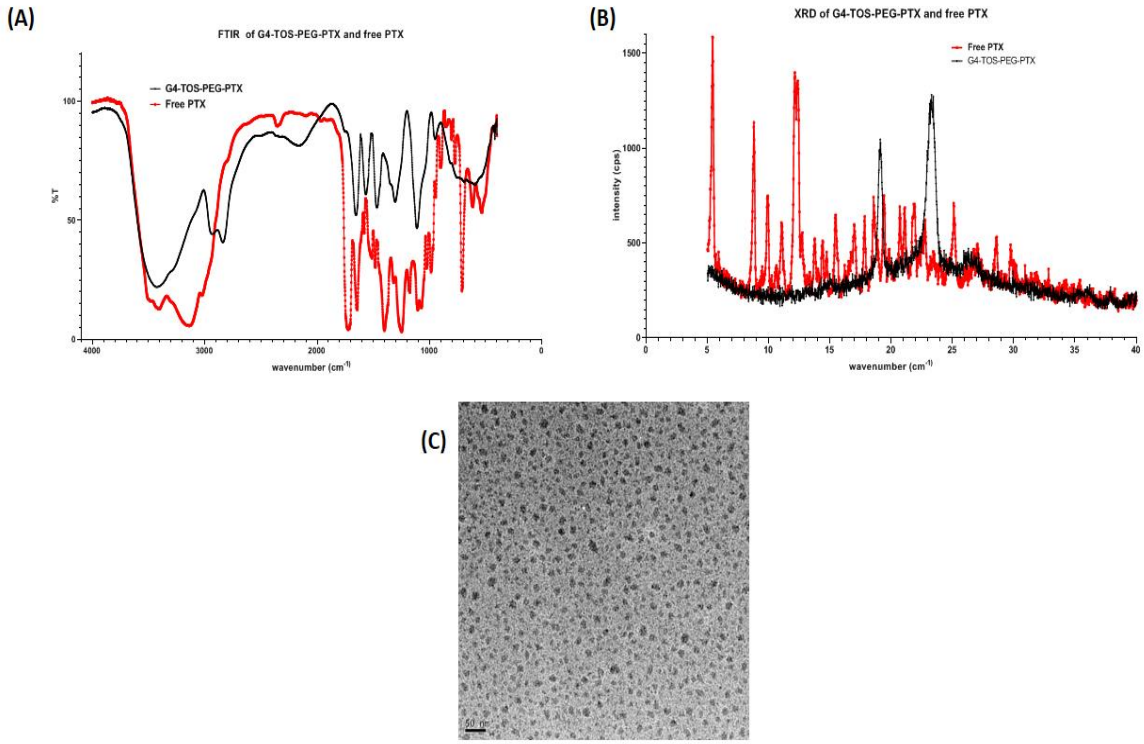

Figure 3.4. Free PTX and G4-TOS-PEG-PTX. (A) FTIR; (B) XRD; (C) TEM

The FTIR spectrum of free PTX (Figure 3.4 A) showed characteristic peaks at 1723 cm^{-1} (C=O group), 1644 cm^{-1} (-CONH2 group), 1247.7 cm^{-1} (C–O–O bending), 1072.2 cm^{-1} (C–O stretching), and 710.6 cm^{-1} (aromatic C–H). The FTIR spectrum of G4-TOS-PEG-PTX (Figure 3.4 A) showed characteristic peaks at 3425 cm^{-1}, which indicated the presence of -NH_2 groups on the surface. The absence of characteristic peaks of PTX in

the FTIR spectrum of G4-TOS-PEG-PTX revealed that the PTX was successfully encapsulated inside the TOS anchored PEGylated dendrimer. The FTIR spectrum of G4-TOS-PEG-PTX showed the characteristic peaks at 1653.7 cm^{-1} (C=O stretching) (amide-I) and 1566.9 cm^{-1} (N-H bending) (amide-II), which confirmed the formation of amide bond between G4 and TOS as well as G4 and PEG.

The free PTX showed typical diffraction peaks at 5.4°, 8.7°, 12.1° and 21.0°, suggesting that the drug was crystalline in nature (Figure 3.4 B). The G4-TOS-PEG-PTX showed the diffraction peaks at 19.08° and 23.2° (Figure 3.4 B). The absence of typical diffraction peaks of PTX in the diffractogram of G4-TOS-PEG-PTX confirmed that the PTX was converted into amorphous from. TEM analysis showed that the PTX loaded G4-TOS-PEG had spherical morphology and size in the nanometer range (Figure 3.4 C).

3.4.3 In vitro release study

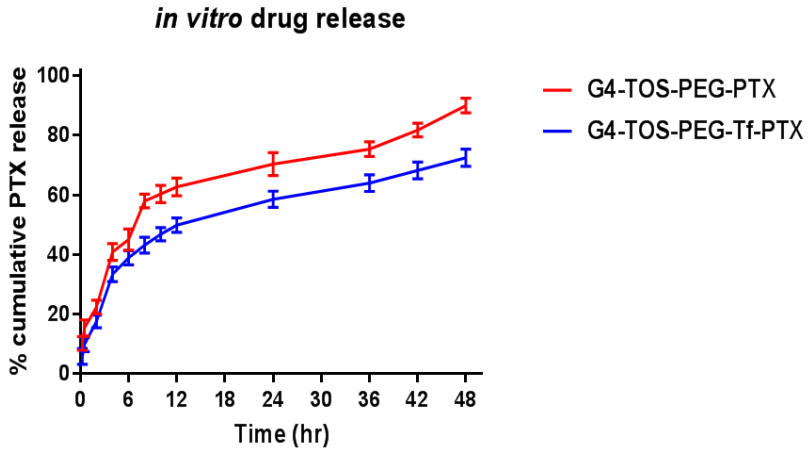

Figure 3.5. *In vitro* PTX release study in PBS (pH 7.4) (Mean ± SD; n = 3)

Drug release study of free PTX, PTX loaded Tf anchored dendrimer and non-Tf anchored dendrimer was carried out using PBS as the release medium (Figure 3.5). The plain PTX showed faster release within 8 h as compared to PTX loaded non-targeted G4-TOS-PEG and PTX loaded targeted G4-TOS-PEG-Tf. Whereas, PTX loaded non-targeted G4-TOS-

PEG and PTX loaded targeted G4-TOS-PEG-Tf showed controlled release behavior of drug over 48 h. G4-TOS-PEG showed PTX release of 70.30 and 89.93% after 24 h as well as 48 h, respectively. G4-TOS-PEG-Tf-PTX demonstrated PTX release of 58.55 and 72.45% after 24 h as well as 48 h, respectively. The attachment of Tf over the surface of the dendrimer created a barrier, which retarded drug release from the internal cavity.

3.4.4 Cellular uptake study by flow cytometer and confocal microscopy

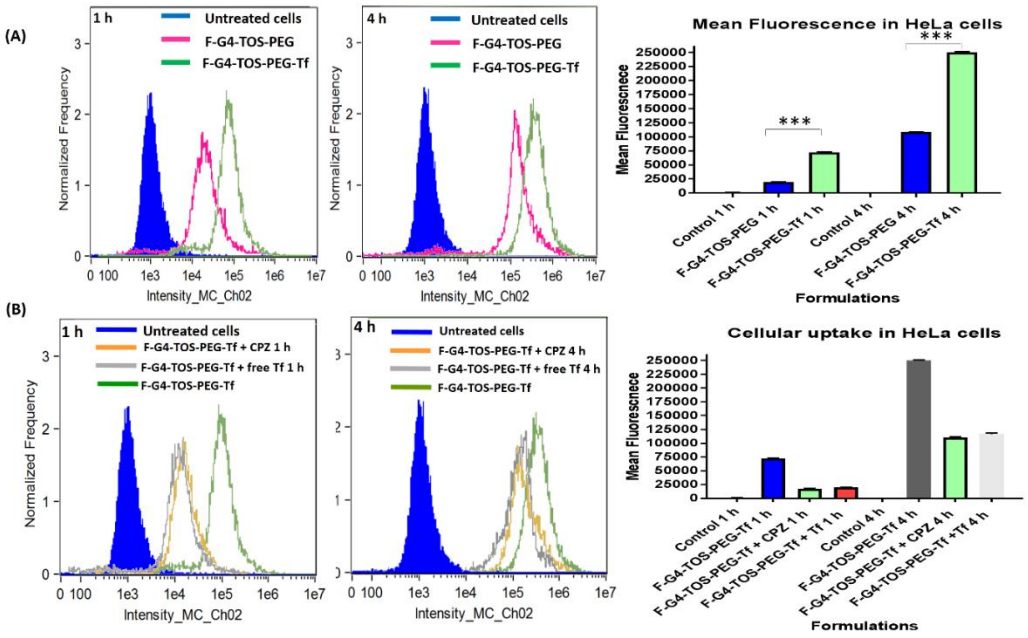

Figure 3.6. (A) cellular uptake study of FITC-labelled non-targeted G4-TOS-PEG and targeted G4-TOS-PEG-Tf in HeLa cells as assessed by flow cytometry instrument after 1 and 4 h (Mean ± standard deviation, triplicates). The bar graph represented the mean fluorescence observed. The statistical significance was assessed by applying one-way ANOVA, ***p<0.001. (B) assessment of cell internalization mechanism of fluorescently tagged non-targeted G4-TOS-PEG and targeted G4-TOS-PEG-Tf in HeLa cells assessed by flow cytometry instrument after 1 h and 4 h (Mean ± standard deviation, triplicates). The bar graph represented the mean fluorescence observed. CPZ : chlorpromazine; Tf : transferrin

This study was performed to evaluate the influence of Tf modification on the cellular internalization of multifunctional dendrimers. From the results, it was evident that more

uptake was observed in Tf anchored dendrimer at 1 h as well as 4 h time points compared to F-G4-TOS-PEG. Tf modification facilitated the cellular association of the dendrimers significantly. The geometric mean fluorescence was represented as histogram and bar graph as shown in Figure 3.6 (A).

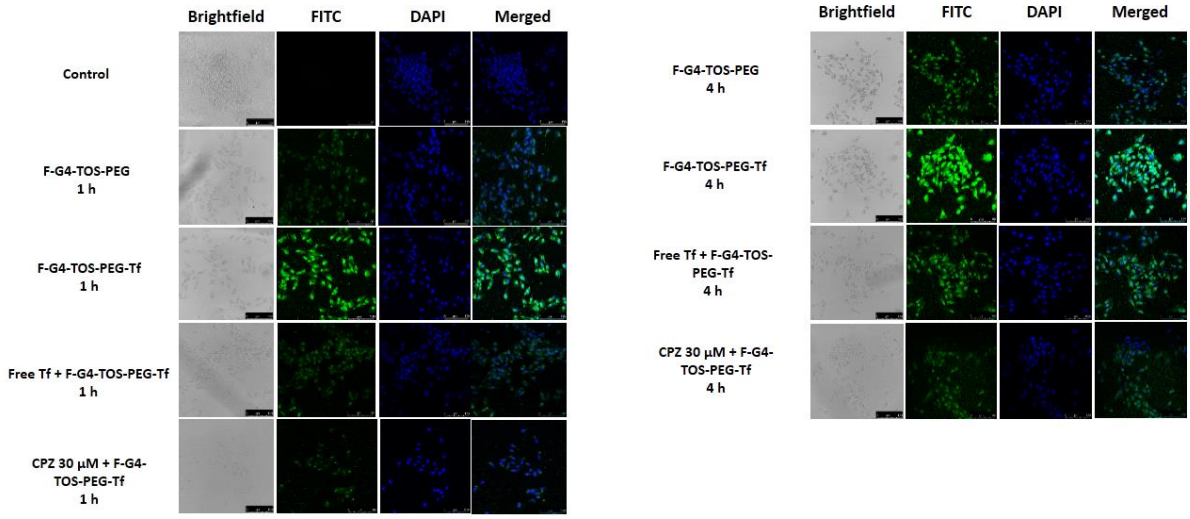

Figure 3.7. Cellular uptake and assessment of internalization mechanism of non-targeted G4-TOS-PEG and targeted G4-TOS-PEG-Tf in HeLa cells using confocal microscope. CPZ : chlorpromazine; Tf : transferrin

The cellular association of passively targeted F-G4-TOS-PEG and actively targeted F-G4-TOS-PEG-Tf was further evaluated using confocal microscopy. The intensity of associated fluorescence was higher for F-G4-TOS-PEG-Tf treated cells as compared to the cells treated with F-G4-TOS-PEG as shown in Figure 3.7. This confocal microscopy results are in accordance with the data acquired from the flow cytometry study. In order to determine the cellular internalization mechanism, the competitive inhibition of the cellular internalization was carried out by preincubation of the HeLa cells with free Tf which saturated the Tf receptors. The intensity of fluorescence as measured by using confocal microscopy and flow cytometry has been represented in Figure 3.6 (B) and Figure 3.7. Moreover, the internalization of F-G4-TOS-PEG-Tf was decreased

significantly following CPZ (clathrin-mediated endocytosis inhibitor) pre-treatment as shown in Figure 3.6 (B) and Figure 3.7.

Chlorpromazine is a cationic amphiphilic drug which inhibits the function of AP2, one of the key adaptor proteins in clathrin-mediated endocytosis. Chlorpromazine is also known to trap receptors inside the endosomes, thus blocking their recycling. Therefore, this compound interferes with clathrin-mediated endocytosis at multiple levels (Francia et al. 2019).

Cellular uptake study proved that the conjugation of α-TOS and Tf molecules over the surface of G4 PAMAM dendrimer enhanced the uptake of nanocarriers resulting in increase in the geo mean fluorescence acquired from flow cytometry. Confocal microscopic observation of cells corroborated the flow cytometric data. Further, fluorescence intensity decreased following pre-treatment with Tf, which could be due to the inaccessibility of the Tf receptors for F-G4-TOS-PEG-Tf due to the presaturation. The result clearly indicated that the internalization of Tf-anchored dendrimers was via the interaction with the Tf-receptors, over-expressed on the surface of the HeLa cells. Moreover, the internalization of F-G4-TOS-PEG-Tf was decreased significantly following CPZ (clathrin-mediated endocytosis inhibitor) pre-treatment, which indicated that the internalization of F-G4-TOS-PEG-Tf could be via clathrin-mediated endocytosis pathway. Overall, Tf-modification in G4-TOS-PEG-Tf targeted the nano-conjugate efficiently to the Tf-receptor over-expressing cancer cells.

3.4.6 Cytotoxicity study

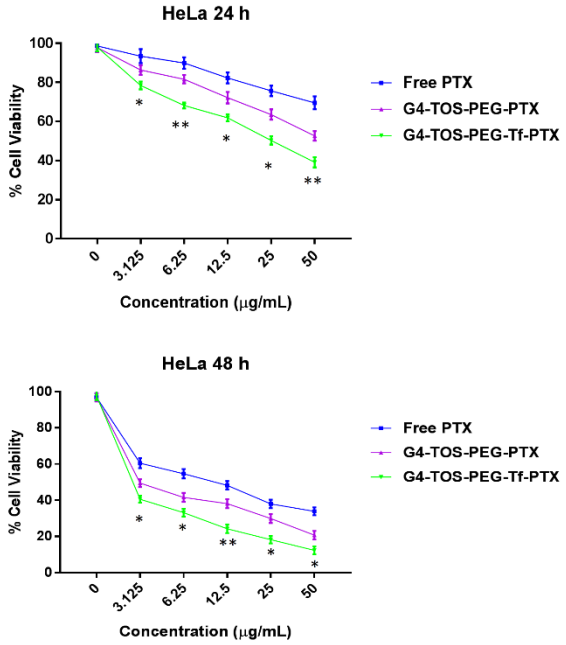

Figure 3.8. % cell viability of HeLa cells treated with free drug and drug loaded dendrimer conjugates (Mean with standard deviation; triplicates). The statistical significance was analyzed by applying one-way ANOVA test, ** and * represented $p < 0.01$ and 0.05, respectively.

Cell viability following the treatment with free drug and drug-loaded dendrimer conjugates was measured to determine the in vitro therapeutic efficacy. As shown in Figure 3.8, the time as well as concentration dependent cytotoxicity in Hela cells was observed in all the time points following all the treatments. Treatment with G4-TOS-PEG-Tf-PTX as well as G4-TOS-PEG-PTX at paclitaxel concentration of 50 µg/mL showed cell viability of 39.12±2.6 and 52.66 ± 2.43 %, respectively following 24 h treatment as compared to free PTX (69.58±3.28%). The further reduction in cell viability of paclitaxel loaded actively targeted G4-TOS-PEG-Tf, PTX loadedpassively targeted G4-TOS-PEG and free paclitaxel was found to be 12.29±2.23%, 20.69±2.39%, and 33.85±2.18% respectively after 48 h. Cell viability study showed that the Tf attachment in G4-TOS-PEG-Tf-PTX promoted the cellular internalization of dendrimer conjugates,

which liberated the entrapped PTX efficiently and resulted in decreased cell viability as compared to the treatment with free PTX and G4-TOS-PEG-PTX.

3.4.7 Apoptosis assay

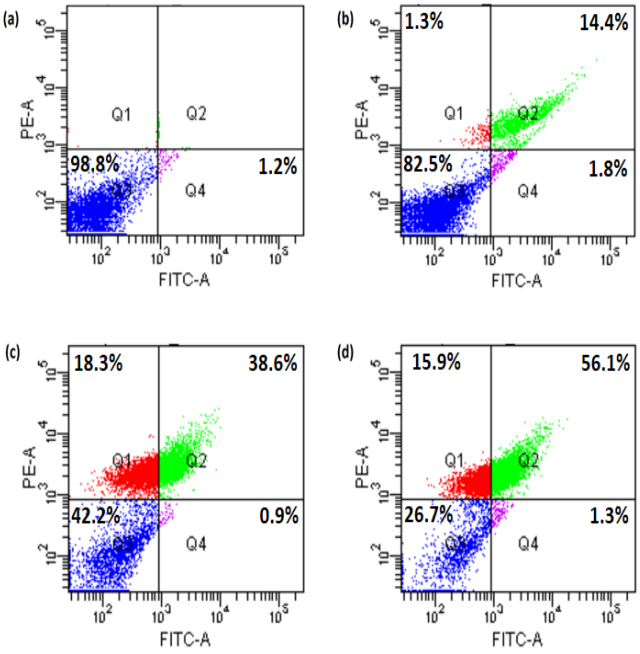

Figure 3.9. Quantitative assessment of apoptosis. (a) control, (b) free paclitaxel, (c) PTX loaded non-targeted G4-TOS-PEG, (d) paclitaxel loaded targeted G4-TOS-PEG-Tf assessed by AnnexinV reagent. (Q1 denotes necrotic cells population, Q2 denotes late apoptotic population, Q3 denotes live cells population, Q4 denotes early apoptotitc population)

Induction of apoptosis following treatment with PTX was determined by Annexin V assay. Upon activation of apoptotic pathway in the cells, phosphatidylserine (PS) translocates outside the plasma membrane by attracting macrophages which initiates the formation of apoptotic bodies. AnnexinV, a ligand of PS binds specifically to PS, which could be detected by its tagged fluorescence. Furhtermore, propidium iodide (PI) binds to necrotic cells (Rompicharla et al. 2018). As shown in Figure 3.9, free PTX induced apoptosis of 15.2 ± 2.4 %, whereas targeted dendrimer (G4-TOS-PEG-PTX-Tf) and nontargeted (G4-TOS-PEG-PTX) induced the total apoptosis of 56.3 ± 1.4 and 37.3 ±

2.2 %, respectively. In control cells, no apoptosis or necrosis was observed. Moreover, both the formulations showed more induciton in apoptosis compared to free paclitaxel. Tf anchored dendrimers targeted cancer cells and got internalized efficiently which resulted in enhanced intracellular PTX availability leading to induction of apoptosis to a greater extent compared to freepaclitaxel and G4-TOS-PEG-PTX. Furthermore, the apoptotic action could would be due to the combine effect of simultaneous delivery of α-TOS and paclitaxel intracellularly.

3.4.8 Penetration efficiency in HeLa spheroids

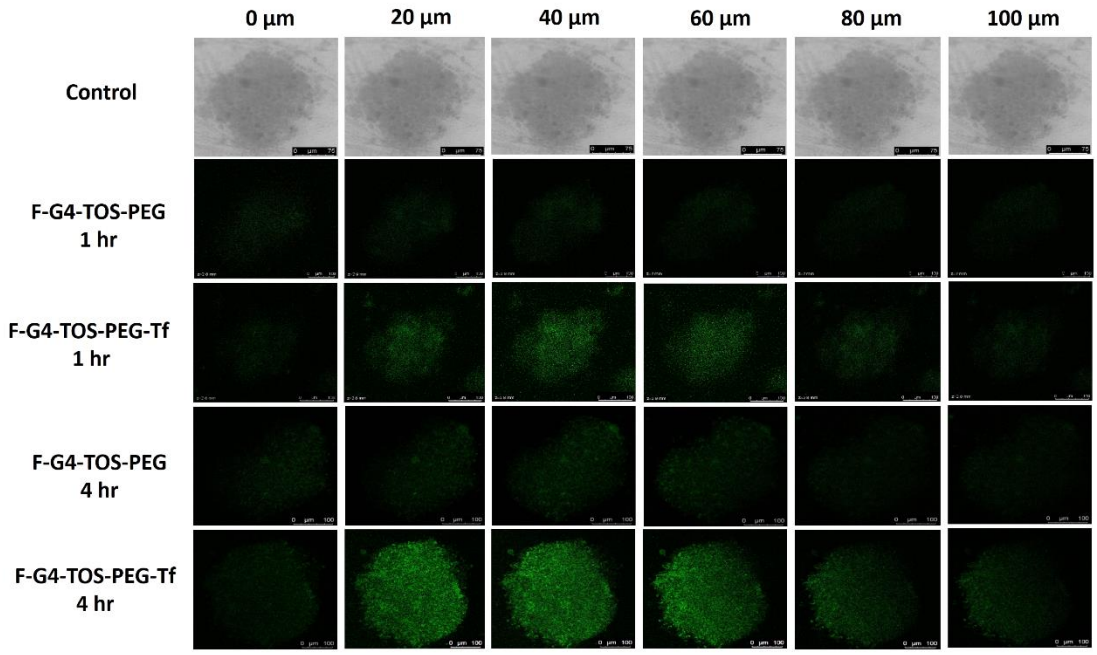

Figure 3.10. Penetration efficiency of fluorescently tagged G4-TOS-PEG as well as G4-TOS-PEG-Tf in HeLa spheroids at different depths visualized under confocal laser scanning microscope after 1 h and 4 h time points.

In this penetration study, the HeLa spheroids were visualized under confocal microscope at different depths (Z-stack) after 1 and 4 h. Tf anchored dendrimer conjugate showed more permeation as indicated by more fluorescence towards center in the 3D spheroids

in comparison to non-Tf anchored G4-TOS-PEG over the period of time as shown in Figure 3.10. The penetration efficiency study in 3D soheroids proved that the Tf/TOS attachment in dendrimer enhanced deeper tissue penetration in the 3D spheroids. Penetration of nanomedicines to the solid tumor mass is challenging, which limit their therapeutic potential. However, it is evident from the study that the actively targeted dendrimer system with Tf-attachment on the surface could penetrate in deeper tumor tissues and deliver the loaded cargo.

3.4.9 Uptake study of spheroids treated with dendrimer conjugates

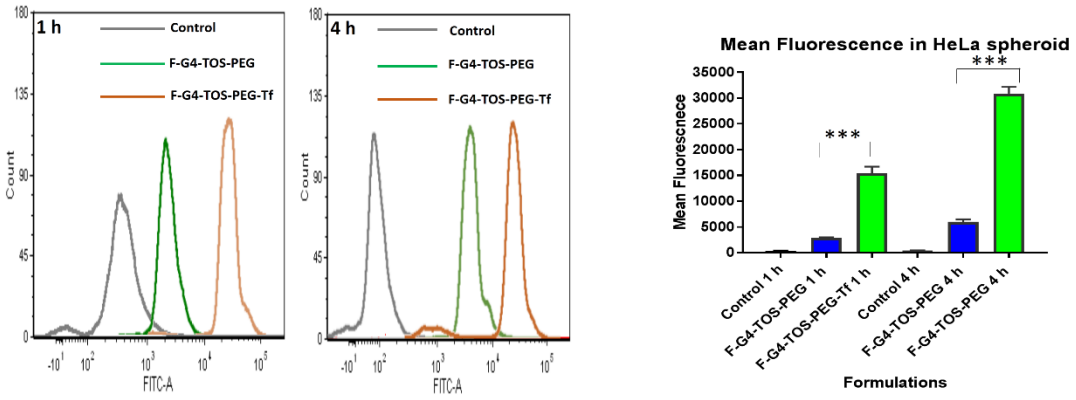

Figure 3.11. Quantitative evaluation of uptake in HeLa spheroid treated with non-targeted F-G4-TOS-PEG and targeted F-G4-TOS-PEG-Tf as analyzed by flow cytometer (Mean and standard deviation; n = 3). The bar graph represented the mean fluorescence observed. The statistical significance between all the groups was carried out by applying one-way ANOVA test, ***$p < 0.001$.

The cellular internalization into HeLa spheroid was carried out by assessing the samples using flow cytometry. From the Figure 3.11, it was observed that the Tf anchored dendrimer conjugate was taken up into the spheroids more efficiently as compared to the fluorescently labelled non-Tf anchored G4-TOS-PEG at both, 1 and 4 h time points. These results supported the observations of cellular uptake when the HeLa spheroids and monolayer cells were visualized using confocal microscopy.

3.4.10 Assessment of Growth inhibition in 3D spheroids of HeLa

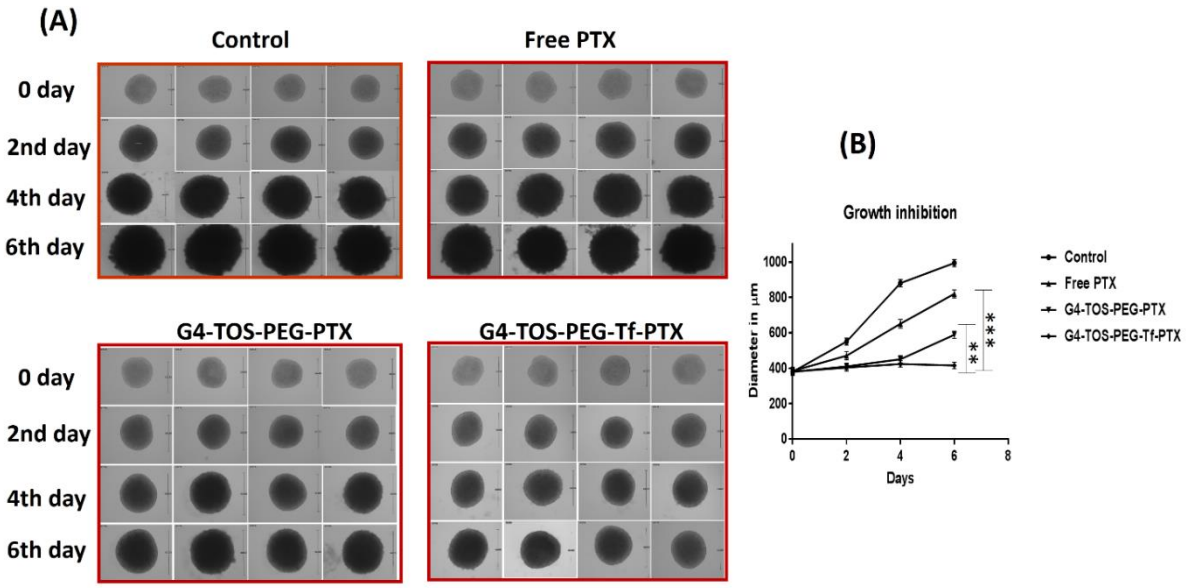

Figure 3.12. (A) Brightfield images of HeLa spheroids after treatment with free drug and drug loaded dendrimer conjugates. The images were captured at 0th Day, 2nd day, 4th day and 6th day at 10X magnification. (B) Representation of growth inhibition of HeLa spheroids as bar graph. The statistical significance between all the groups was assessed by applying one-way ANOVA test, ***$p < 0.001$ and **$p<0.01$.

The spheroid growth inhibition was assessed by checking the diameter of HeLa spheroids when the spheroids were incubated with free paclitaxel as well as paclitaxel loaded dendrimer formulations for 24 h. The diameter of HeLa spheroids were measured on zero day, second day, fourth day and sixth day by inverted microscope. The bright field images were taken and the data had been shown in Figure 3.12 (A). The progression of growth of the spheroids treated with PTX loaded targeted G4-TOS-PEG-Tf was retarded significantly compared to the spheroids treated non-Tf anchored PTX loaded dendrimer and free paclitaxel. The average diameter of spheroids was found to be 994.34 ± 20.18, 820.34 ± 23.51, 589.41 ± 20.56, and 415.94 ± 18.51 µm for control group, free paclitaxel group, PTX loaded non-targeted G4-TOS-PEG group and paclitaxel loaded targeted G4-

TOS-PEG-Tf group treatment, respectively at the end of 6 days. These data are shown in the line graph plotted between the diameters versus days as shown in Figure 3.12 (B). Further, the growth inhibition study in HeLa 3D spheroids revealed that the Tf-anchorage on the dendrimer surface promoted active targeting of the conjugate, whereas presence of both TOS and PTX caused effective spheroid volume regression by cell killing.

3.4.11 Live and Dead cell detection in HeLa spheroids

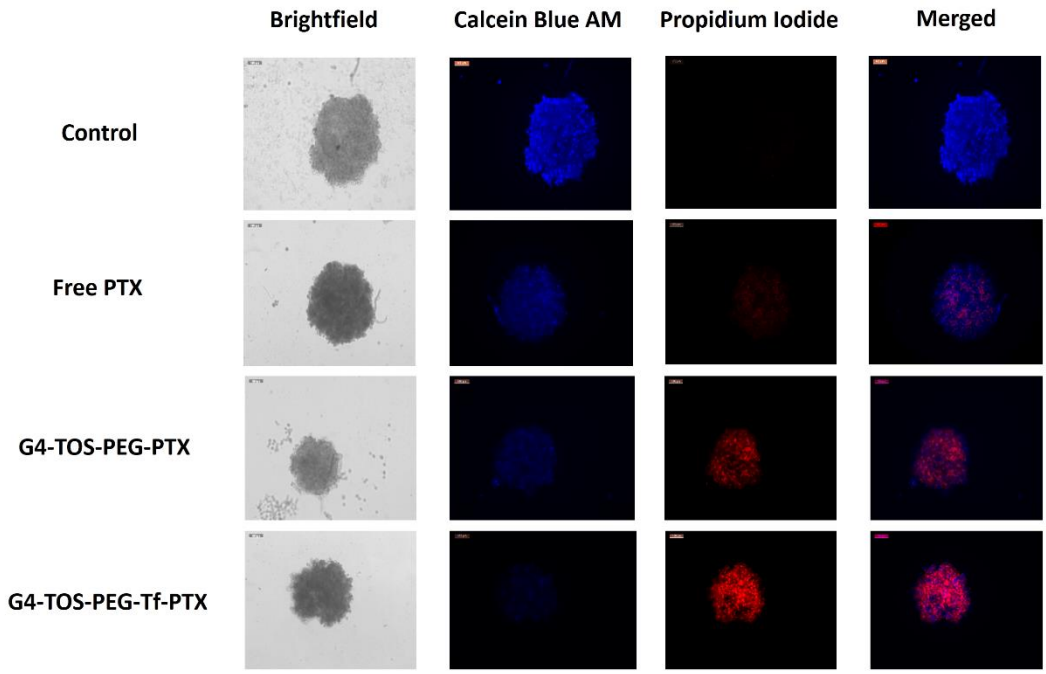

Figure 3.13. LIVE/DEAD cell assay of HeLa cells treated with free drug and drug loaded dendrimer conjugates

To elucidate whether the spheroid growth inhibition is caused by the cell death induced by the treatment, live and dead cell detection assay was performed on treated spheroids. After theformulation treatment, live/dead cell populations in HeLa spheroids were visualized after incubating the soheroids with calcein blue reagent. The blue fluorescence was produced when the live cells internalized the calcein blue. The ester bond in calcein blue AM is broken by the intracellular estersses to liberate the dye that emits blue fluorescence. Moreover, PI stains the dead cells. G4-TOS-PEG-Tf-PTX showed more

red fluorescence than PTX loaded non-targeted G4-TOS-PEG and free paclitaxel as shown in Figure 3.13. The dead cell population was observed mostly on the periphery of spheroids treated with free PTX in life/dead cells assay, which indicated that free PTX was unable to penetrate deeper in HeLa spheroid. The dead cell population was observed evidently in the core as well as periphery of the spheroids treated with G4-TOS-PEG-Tf-PTX and G4-TOS-PEG-PTX, which revealed that both the formulations had the ability to penetrate towards the central core. Tf/TOS-dual attachment to the dendrimer promoted better penetration of dendrimers in deep spheroid tissues causing cell death.

3.5 Conclusion

Here, an actively tumor-targeted polymer, Tf anchored α-TOS conjugated PEGylated dendrimer, G4-TOS-PEG-Tf was synthesized and loaded with practically insoluble anticancer drug, paclitaxel. The new multifunctional dendrimer was characterized using 1H NMR and the hydrodynamic size, zeta potential, %EE and %DL were determined. G4-TOS-PEG-Tf was readily taken up by the clathrin-dependent transferrin receptor-mediated endocytosis process. Cell viability study in HeLa cells revealed that the paclitaxel loaded targeted G4-TOS-PEG-Tf demonstrated significantly higher cytotoxicity compared to non-targeted G4-TOS-PEG-PTX and free paclitaxel. Moreover, Tf attachment to α-TOS anchored dendrimer enhanced the cellular uptake in 3D spheroids. Apoptosis inducing potential of PTX was higher when delivered using targeted G4-TOS-PEG-Tf compared to non-targeted G4-TOS-PEG or free administration as confirmed by AnnexinV assay. Penetration efficiency into 3D spheroids was higher for G4-TOS-PEG-Tf than G4-TOS-PEG as assessed by confocal laser scanning microscopy and flow cytometry study. Moreover, G4-TOS-PEG-Tf-PTX showed superior inhibitory effect in the growth of spheroids. While the developed dendrimer nanoconjugate loaded and delivered PTX successfully due to the PTX

modification on its surface, moreover, the combined delivery of TOS and PTX produced significant cytotoxicity in HeLa cells. Conclusively, the newly synthesized dendrimer-based PTX delivery system proved to be promising for further exploration to be utilized in the treatment of Tf-over-expressing tumors.

References

Abedi-Gaballu, Fereydoon, Gholamreza Dehghan, Maryam Ghaffari, Reza Yekta, Soheil Abbaspour-Ravasjani, Behzad Baradaran, Jafar Ezzati Nazhad Dolatabadi, and Michael R Hamblin. 2018. "PAMAM dendrimers as efficient drug and gene delivery nanosystems for cancer therapy." *Applied materials today* no. 12:177-190.

Abouzeid, Abraham H, Niravkumar R Patel, Can Sarisozen, and Vladimir P Torchilin. 2014. "Transferrin-targeted polymeric micelles co-loaded with curcumin and paclitaxel: efficient killing of paclitaxel-resistant cancer cells." *Pharmaceutical research* no. 31 (8):1938-1945.

Abu-Fayyad, Ahmed, Fathy Behery, Asmaa A Sallam, Saeed Alqahtani, Hassan Ebrahim, Khalid A El Sayed, Amal Kaddoumi, Paul W Sylvester, Jennifer L Carroll, and James A Cardelli. 2015. "PEGylated γ-tocotrienol isomer of vitamin E: synthesis, characterization, in vitro cytotoxicity, and oral bioavailability." *European Journal of Pharmaceutics and Biopharmaceutics* no. 96:185-195.

Bhatt, Himanshu, Sri Vishnu Kiran Rompicharla, Balaram Ghosh, and Swati Biswas. 2019. "α-tocopherol succinate anchored PEGylated Poly (Amidoamine) Dendrimer for the Delivery of Paclitaxel: Assessment of in vitro and in-vivo therapeutic efficacy." *Molecular pharmaceutics*.

Chandrasekharan, Prashant, Dipak Maity, Cai Xian Yong, Kai-Hsiang Chuang, Jun Ding, and Si-Shen Feng. 2011. "Vitamin E (D-alpha-tocopheryl-co-poly (ethylene glycol) 1000 succinate) micelles-superparamagnetic iron oxide nanoparticles for enhanced thermotherapy and MRI." *Biomaterials* no. 32 (24):5663-5672.

Chen, Han, Tong Zhang, Zhimin Zhou, Man Guan, Jingjie Wang, Lingrong Liu, and Qiqing Zhang. 2013. "Enhanced uptake and cytotoxity of folate-conjugated mitoxantrone-loaded micelles via receptor up-regulation by dexamethasone." *International journal of pharmaceutics* no. 448 (1):142-149.

Ciolkowski, Michal, Johannes F Petersen, Mario Ficker, Anna Janaszewska, Jørn B Christensen, Barbara Klajnert, and Maria Bryszewska. 2012. "Surface modification of PAMAM dendrimer improves its biocompatibility." *Nanomedicine: Nanotechnology, Biology and Medicine* no. 8 (6):815-817.

Duhem, Nicolas, Fabienne Danhier, and Véronique Préat. 2014. "Vitamin E-based nanomedicines for anti-cancer drug delivery." *Journal of Controlled Release* no. 182:33-44.

Ellman, George L. 1959. "Tissue sulfhydryl groups." *Archives of biochemistry and biophysics* no. 82 (1):70-77.

Emami, Jaber, Mahboubeh Rezazadeh, Mahboubeh Rostami, Farshid Hassanzadeh, Hojjat Sadeghi, Abolfazl Mostafavi, Mohsen Minaiyan, and Afsaneh Lavasanifar. 2015. "Co-delivery of paclitaxel and α-tocopherol succinate by novel chitosan-based polymeric micelles for improving micellar stability and efficacious combination therapy." *Drug development and industrial pharmacy* no. 41 (7):1137-1147.

Francia, Valentina, Catharina Reker-Smit, Guido Boel, and Anna Salvati. 2019. "Limits and challenges in using transport inhibitors to characterize how nano-sized drug carriers enter cells." *Nanomedicine* no. 14 (12):1533-1549.

Ghaffari, Maryam, Gholamreza Dehghan, Fereydoon Abedi-Gaballu, Soheila Kashanian, Behzad Baradaran, Jafar Ezzati Nazhad Dolatabadi, and Dusan Losic. 2018. "Surface functionalized dendrimers as controlled-release delivery nanosystems for tumor targeting." *European Journal of Pharmaceutical Sciences*.

Gill, Kanwaldeep K, Amal Kaddoumi, and Sami Nazzal. 2012. "Mixed micelles of PEG2000-DSPE and vitamin-E TPGS for concurrent delivery of paclitaxel and parthenolide: enhanced chemosenstization and antitumor efficacy against non-small cell lung cancer (NSCLC) cell lines." *European journal of pharmaceutical sciences* no. 46 (1-2):64-71.

Gruber, Julia, Katrin Staniek, Christopher Krewenka, Rudolf Moldzio, Anjan Patel, Stefan Böhmdorfer, Thomas Rosenau, and Lars Gille. 2014. "Tocopheramine succinate and tocopheryl succinate: mechanism of mitochondrial inhibition and superoxide radical production." *Bioorganic & medicinal chemistry* no. 22 (2):684-691.

Guo, Yuanyuan, Jun Luo, Songwei Tan, Ben Oketch Otieno, and Zhiping Zhang. 2013. "The applications of Vitamin E TPGS in drug delivery." *European Journal of Pharmaceutical Sciences* no. 49 (2):175-186.

Hayashi, Teruo, Shang-Yi Tsai, Tomohisa Mori, Michiko Fujimoto, and Tsung-Ping Su. 2011. "Targeting ligand-operated chaperone sigma-1 receptors in the treatment of neuropsychiatric disorders." *Expert opinion on therapeutic targets* no. 15 (5):557-577.

Kesharwani, Prashant, Virendra Gajbhiye, Rakesh K Tekade, and Narendra K Jain. 2011. "Evaluation of dendrimer safety and efficacy through cell line studies." *Current drug targets* no. 12 (10):1478-1497.

Kesharwani, Prashant, and Arun K Iyer. 2015. "Recent advances in dendrimer-based nanovectors for tumor-targeted drug and gene delivery." *Drug discovery today* no. 20 (5):536-547.

Kesharwani, Prashant, Keerti Jain, and Narendra Kumar Jain. 2014. "Dendrimer as nanocarrier for drug delivery." *Progress in Polymer Science* no. 39 (2):268-307.

Kulhari, Hitesh, Deep Pooja, Shweta Shrivastava, Madhusudana Kuncha, VGM Naidu, Vipul Bansal, Ramakrishna Sistla, and David J Adams. 2016. "Trastuzumab-grafted PAMAM dendrimers for the selective delivery of anticancer drugs to HER2-positive breast cancer." *Scientific reports* no. 6:23179.

Kumari, Preeti, Sri Vishnu Kiran Rompicharla, Omkara Swami Muddineti, Balaram Ghosh, and Swati Biswas. 2018. "Transferrin-anchored poly (lactide) based micelles to improve anticancer activity of curcumin in hepatic and cervical cancer cell monolayers and 3D spheroids." *International journal of biological macromolecules* no. 116:1196-1213.

Li, Yan, Hai He, Xinru Jia, Wan-Liang Lu, Jinning Lou, and Yen Wei. 2012. "A dual-targeting nanocarrier based on poly (amidoamine) dendrimers conjugated with transferrin and tamoxifen for treating brain gliomas." *Biomaterials* no. 33 (15):3899-3908.

Malik, Noeen, R Wiwattanapatapee, R Klopsch, K Lorenz, H Frey, JW Weener, EW Meijer, W Paulus, and R Duncan. 2000. "Dendrimers:: Relationship between structure and biocompatibility in vitro, and preliminary studies on the biodistribution of 125I-labelled polyamidoamine dendrimers in vivo." *Journal of Controlled Release* no. 65 (1-2):133-148.

Muddineti, Omkara Swami, Preeti Kumari, Balaram Ghosh, and Swati Biswas. 2018. "Transferrin-Modified Vitamin-E/Lipid Based Polymeric Micelles for Improved Tumor Targeting and Anticancer Effect of Curcumin." *Pharmaceutical research* no. 35 (5):97.

Muddineti, Omkara Swami, Preeti Kumari, Balaram Ghosh, Vladimir P Torchilin, and Swati Biswas. 2017. "d-α-Tocopheryl succinate/Phosphatidyl ethanolamine conjugated amphiphilic polymer-based Nanomicellar system for the efficient delivery of curcumin and to overcome multiple drug resistance in cancer." *ACS applied materials & interfaces* no. 9 (20):16778-16792.

Muthu, Madaswamy S, Rajaletchumy Veloo Kutty, Zhentao Luo, Jianping Xie, and Si-Shen Feng. 2015. "Theranostic vitamin E TPGS micelles of transferrin conjugation for targeted co-delivery of docetaxel and ultra bright gold nanoclusters." *Biomaterials* no. 39:234-248.

Nam, Joung-Pyo, Kyeong-Jae Lee, Joung-Woo Choi, Chae-Ok Yun, and Jae-Woon Nah. 2015. "Targeting delivery of tocopherol and doxorubicin grafted-chitosan polymeric micelles for cancer therapy: In vitro and in vivo evaluation." *Colloids and Surfaces B: Biointerfaces* no. 133:254-262.

Nam, Joung-Pyo, Seong-Cheol Park, Tae-Hun Kim, Jae-Yeang Jang, Changyong Choi, Mi-Kyeong Jang, and Jae-Woon Nah. 2013. "Encapsulation of paclitaxel into lauric acid-O-carboxymethyl chitosan-transferrin micelles for hydrophobic drug delivery and site-specific targeted delivery." *International journal of pharmaceutics* no. 457 (1):124-135.

Neuzil, Jiri, ZHAO Ming, Georg Ostermann, Martin Sticha, Nina Gellert, Christian Weber, John W Eaton, and Ulf T Brunk. 2002. "α-Tocopheryl succinate, an agent with in vivo anti-tumour activity, induces apoptosis by causing lysosomal instability." *Biochemical Journal* no. 362 (3):709-715.

Prasad, Kedar N, Bipin Kumar, Xiang-Dong Yan, Amy J Hanson, and William C Cole. 2003. "α-tocopheryl succinate, the most effective form of vitamin E for adjuvant cancer treatment: a review." *Journal of the American College of Nutrition* no. 22 (2):108-117.

Prieto, Maria Jimena, Nahuel Eduardo del Rio Zabala, Cristian Hernan Marotta, Hector Carreno Gutierrez, Rosario Arevalo Arevalo, Nadia Silvia Chiaramoni, and Silvia del Valle Alonso. 2014. "Optimization and in vivo toxicity evaluation of G4. 5 pamam dendrimer-risperidone complexes." *PloS one* no. 9 (2):e90393.

Rompicharla, Sri Vishnu Kiran, Preeti Kumari, Balaram Ghosh, and Swati Biswas. 2018. "Octa-arginine modified poly (amidoamine) dendrimers for improved delivery and cytotoxic effect of paclitaxel in cancer." *Artificial cells, nanomedicine, and biotechnology*:1-13.

Sriraman, Shravan Kumar, Jiayi Pan, Can Sarisozen, Ed Luther, and Vladimir Torchilin. 2016. "Enhanced cytotoxicity of folic acid-targeted liposomes co-loaded with C6 ceramide and doxorubicin: in vitro evaluation on HeLa, A2780-ADR, and H69-AR cells." *Molecular pharmaceutics* no. 13 (2):428-437.

Tortorella, Stephanie, and Tom C Karagiannis. 2014. "Transferrin receptor-mediated endocytosis: a useful target for cancer therapy." *The Journal of membrane biology* no. 247 (4):291-307.

Yu, Weiping, Qiao Yin Liao, Feras M Hantash, Bob G Sanders, and Kimberly Kline. 2001. "Activation of extracellular signal-regulated kinase and c-Jun-NH2-terminal kinase but not p38 mitogen-activated protein kinases is required for RRR-α-tocopheryl succinate-induced apoptosis of human breast cancer cells." *Cancer research* no. 61 (17):6569-6576.

Yue, Jun, Shi Liu, Rui Wang, Xiuli Hu, Zhigang Xie, Yubin Huang, and Xiabin Jing. 2012. "Transferrin-conjugated micelles: enhanced accumulation and antitumor effect for transferrin-receptor-overexpressing cancer models." *Molecular pharmaceutics* no. 9 (7):1919-1931.

Zeng, Xuan, Yun-Xia Sun, Wei Qu, Xian-Zheng Zhang, and Ren-Xi Zhuo. 2010. "Biotinylated transferrin/avidin/biotinylated disulfide containing PEI bioconjugates mediated p53 gene delivery system for tumor targeted transfection." *Biomaterials* no. 31 (17):4771-4780.

Zhang, Pengcheng, Luojuan Hu, Qi Yin, Zhiwen Zhang, Linyin Feng, and Yaping Li. 2012. "Transferrin-conjugated polyphosphoester hybrid micelle loading paclitaxel for brain-targeting delivery: synthesis, preparation and in vivo evaluation." *Journal of controlled release* no. 159 (3):429-434.

Chapter 4

Cell Penetrating Peptide and α-Tocopherol Conjugated Poly(amidoamine) Dendrimers for Improved Delivery and Anticancer Activity of Loaded Paclitaxel

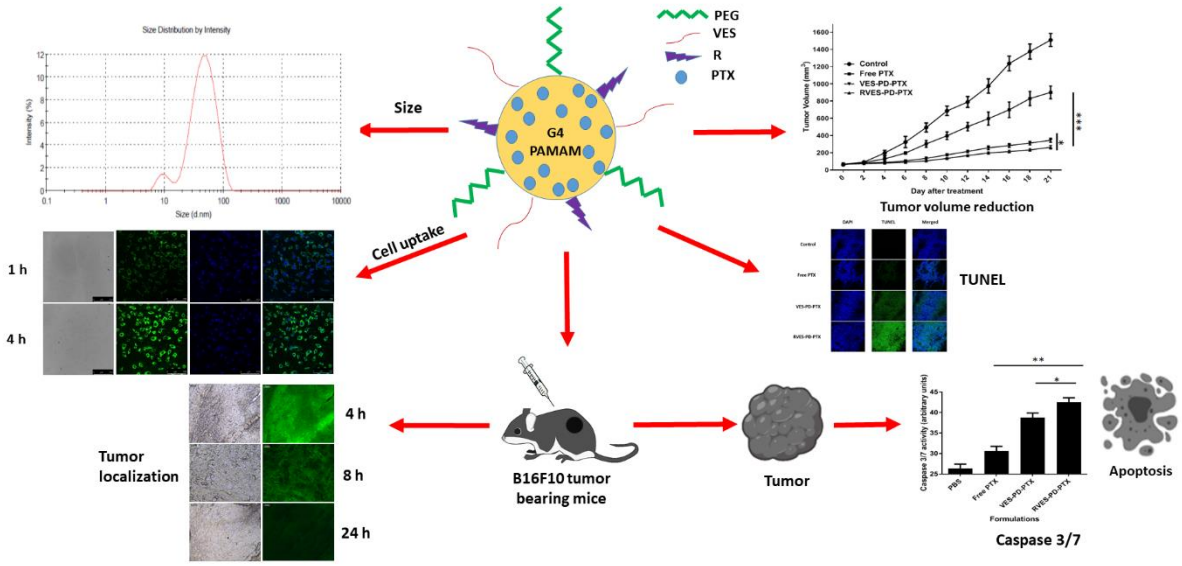

4.1 Abstract

Even though existing chemotherapeutic agents, including paclitaxel (PTX) possess superior anticancer activity, their application is limited due to extreme hydrophobicity. Here, a dendrimers-based nanoparticles system has been prepared for improved delivery of loaded paclitaxel to the tumor. The cell penetrating peptide, Octa-arginine (R) and Vitamin-E Succinate (VES) had been conjugated to the PEGylated generation 4 polyamidoamine dendrimer (D) to form RVES-PD. The synthesized polymers had been characterized by 1NMR, IR, and gel permeation chromatography. The PTX-loaded RVES-PD (RVES-PD-PTX) was physico-chemically characterized for particle size, zeta potential analysis, drug loading, release, and encapsulation studies. The cellular uptake, and cytotoxicity, and apoptosis determination studies were carried out in human lung cancer cells (A549) in monolayers, and spheroids, respectively. In vivo antitumor efficacy of RVES-PD-PTX was determined using B16F10-tumor bearing mice. The results indicated that the RVES-PD nanoparticles were taken up by cancer cells effectively and demonstrated improved cellular translocation compared to non-targeted VES-PD. The cytotoxicity study revealed that the RVES-PD-PTX exhibited highest cytotoxicity of PTX compared to non-targeted, VES-PD-PTX and free PTX at PTX concentration range of 0-50 µg/mL. RVES-PD-PTX induced apoptosis as analyzed by Annexin V assay and suppressed the growth of spheroids to the highest extent compared to VES-PD-PTX and free PTX. Further, the bio-distribution study indicated that the RVES-PD had higher accumulation in tumor compared to VES-PD. The in vivo experiment using B16F10 tumor bearing mice demonstrated that the RVES-PD treatment resulted in highest rate of tumor volume reduction and apoptosis primarily by upregulating the caspase 3/7 to the highest extent compared to VES-PD and free PTX. In conclusion, the developed RVES-PD could load PTX, showed efficient cell

penetration and improved PTX-mediated cytotoxicity in all tested in vitro and in vivo assay systems. The results strongly suggest further exploration of this developed PTX-nano-formulation in cancer treatment.

4.2 Introduction

Use of nanoscale materials (5-150 nm diameter) as drug delivery cargo offers multiple advantages over conventional free drug administration. Nanomaterials improve the solubility of hydrophobic drugs, minimize non-specific interaction of drug, delay drug clearance from body, enhance tissue penetration, and passively target the drug at the tumor site by Enhanced Permeability and Retention (EPR) effect. Various nanoparticles have been tried for anticancer drug delivery, including liposomes, polymeric micelles, solid lipid nanoparticles, inorganic nanoparticles, drug-polymer conjugates, and spherical polymers such as dendrimers (Min et al. 2015, Sethi et al. 2014, Au et al. 2015). Dendrimers are nano-sized, synthetic, monodisperse systems, which possess well-defined geometrical branching units. Dendrimers are highly hydrophilic with superior biocompatibility (Kesharwani, Jain, and Jain 2014, Kesharwani et al. 2011, Barrière et al. 2012). Dendrimers possess a large number of functional groups on the surface, which increases in numbers with generations. The surface functional groups could be derivatized with various ligands for improving their functional activities, such as improving drug loading, enhancing tissue penetration, and targeting ability of nanocarriers to the cancer cells (D'Emanuele and Attwood 2005, Tekade, Kumar, and Jain 2008, Tekade et al. 2008). However, due to the presence of large number of functional groups, dendrimers encounter non-specific interactions in circulation leading to toxicity. Usually, the -NH_2 terminated Poly(amidoamine) and Poly(propyleneimine) dendrimers have shown the concentration-dependent toxicity and hemolysis as compared to neutral or negatively charged dendrimers (Malik et al. 2000, Roberts, Bhalgat, and Zera 1996, Jevprasesphant et al. 2003, Padilla De Jesús et al. 2002). However, the toxicity of positively charged dendrimers could be reduced by modifying the surface with acetyl groups, polyethylene glycol (PEG) etc (Malik et al. 2000,

Jevprasesphant et al. 2003, Chen et al. 2004, Kesharwani et al. 2011, Padilla De Jesús et al. 2002, Ihre et al. 2002).

Vitamin-E succinate (VES) has been conjugated to variety of drug delivery systems to achieve multiple benefits in cancer therapy (Gill, Kaddoumi, and Nazzal 2012, Chandrasekharan et al. 2011, Abu-Fayyad et al. 2015, Emami et al. 2015, Nam et al. 2015, Gruber et al. 2014, Neuzil et al. 2002, Prasad et al. 2003, Yu et al. 2001, Muddineti et al. 2018, Bhatt et al. 2019). VE solubilizes many hydrophobic agents, therefore, incorporation of VE in the micellar core improves solubility of many anticancer drugs. VE and its derivatives demonstrated anticancer activity by induction of apoptotic pathways (Muddineti, Ghosh, and Biswas 2017). Moreover, VES has the ability to inhibit the drug efflux transporters such as P-glycoprotein, and multiple drug resistance proteins (Duhem, Danhier, and Préat 2014, Guo et al. 2013, Muddineti et al. 2017).

A major issue with existing chemotherapy is the ineffective penetration of drug molecules into the tumor (Ruoslahti 2017). Penetration into cancer tissues is a noteworthy concern with nanoparticles as well. The poor penetrability could be due to the fact that the tumor micro-environment is made of dense connective tissue stroma which retards free movement of drug molecules into the tumor cells (Ruoslahti 2017, Uchida et al. 2011). Moreover, the leaky vasculature in the tumor forms a high osmotic pressure zone within the tumor not allowing fluid to penetrate in, and hence, the chemotherapeutics cannot enter freely (Golombek et al. 2018). Moreover, compact mass of solid tumors stands impermeable to chemotherapeutic agent to enter into the core. Due to this, the accumulation of sub-optimum concentration of drug in the tumor enables cancer cells to develop drug resistance.(Ruoslahti 2017). This situation can be addressed by using a class of peptides called cell penetrating peptides (CPPs). The

advantage of CPPs is their capability to deliver cargos through the cell membrane, which are many times higher than their own molecular weight. Cell-penetrating peptides (CPPs) are extensively used as an attachment to impermeable macromolecules or nanocarriers to translocate them intracellularly (Dissanayake et al. 2017, Liu et al. 2015, Li et al. 2016). In this regard, Octa-arginine (R), a CPP containing 8 arginine residues enhanced cellular uptake of various nanocarriers in previous studies (Yamada, Hashida, and Harashima 2015, Biswas et al. 2013, Kitagishi et al. 2015, Rompicharla et al. 2018a).

In this study, the octa-arginine (R) was conjugated over the surface of synthesized G4-TOS-PEG (Chapter 2) via step-by step synthesis procedure and loaded with an anticancer drug, PTX to improve the loading and targeting ability of PTX towards cancer cells. The multifunctional dendrimer conjugates were characterized physico-chemically, assessed for its ability for intracellular translocation and cytotoxicity in human alveolar basal epithelial lung carcinoma cells (A549) in monolayers and in a 3D spheroid model. Further, the therapeutic efficacy of paclitaxel loaded multifunctional dendrimer was evaluated *in vivo* using B16F10 tumor bearing mice.

4.3 Materials and methods

4.3.1 Materials

The poly(amidoamine) dendrimer of Generation 4 (D) was obtained from Dendritech Inc. (MI, USA). The Paclitaxel (PTX) was provided as a gift sample from Fresenius Kabi India Pvt., Ltd. Methoxy-polyethyleneglycol-N-hydroxysuccinimidyl ester (m-PEG-SCM ester, MW 2000 Da) was purchased from Jenkem Technology (USA). N-ethyl-di-isopropylamine (DIPEA) was procured from Avra Chemicals, Mumbai, India. The NHS-Fluorescein was purchased from Thermo Scientific (USA). Vitamin-E succinate (VES) was purchased from Sigma-Aldrich (Bangalore, India). The peptide,

octa-arginine was custom synthesized from GCC Biotech India Pvt. Ltd. (Kolkata, India). The 1-ethyl-3-(3-dimethylaminopropyl) carbodiimide hydrochloride (EDC. HCl) and N-Hydroxysuccinimide (NHS) were purchased from Merck (Germany). Accutase™ and Fluoromount-G were purchased from Himedia Laboratories (Mumbai, India). Dialysis membrane with MWCO 3.5 kDa, 12-14 kDa was procured from Repligen Inc. (Massachusetts, USA).

A549 and B16F10 cells were obtained from National Center for Cell Sciences (NCCS, Pune, India). Fetal bovine serum (FBS), DMEM F-12 and penicillin/streptomycin were purchased from Himedia Laboratories (Mumbai, India). A549 cells were sub-cultured in DMEM F-12 medium (DMEM complete medium with 10 % FBS and 100 IU/mL of antibiotic solution) in a CO_2 incubator regulated at 37 °C and 5% CO_2.

4.3.2 Methods

4.3.2.1 Synthesis of VES-D

The synthesis procedure was represented in Figure 4.1. The conjugation of VES to G4 PAMAM dendrimer was done through the reaction reported in previous literature (Bhatt et al. 2019). The acid group of VES (9.341 mg, 17.6 µmol) was activated using EDC and NHS in 3 moles equivalent excess in presence of diisopropyl ethylamine (DIPEA) in anhydrous dimethylformamide (DMF). Into the solution of G4-PAMAM dendrimer (3.52 µmol) in anhydrous DMF, the activated VES was added dropwise at room temperature. The mixture was kept in stirring condition for overnight. The following day, DMF was removed by vacuum under rotary evaporator. The reaction mixture was dialyzed using regenerated cellulose membrane (MWCO 12-14 kDa) and dried by using lyophilization technique.

4.3.2.2 Synthesis of VES-PD

To the solution of VES-D (50 mg) in DMF, mPEG-NHS (67.82 mg) and 20 µl DIPEA was added. The reaction was continued for overnight under inert atmosphere. The following day, DMF was removed using rotary evaporator. Further, the product was purified by dialysis technique using regenerated cellulose membrane with molecular weight cut-off, 12-14kD. Pure VES-PD in solid form was obtained by lyophilizing the dialysate**.**

4.3.2.3 Synthesis of RVES-PD

Octa-arginine (4.08 µmol, 4.298 mg) was activated using EDC and NHS in excess in presence of DIPEA in anhydrous dimethylformamide (DMF) for 2 h. VES-PD (molar ratio of VES-PD to R: 1:3) was added dropwise to the reaction mixture. The crude reaction mixture was stirred overnight at room temperature under nitrogen atmosphere. The solvent was evaporated, and the crude product was purified by dialysis and lyophilized to obtain solid RVES-PD.

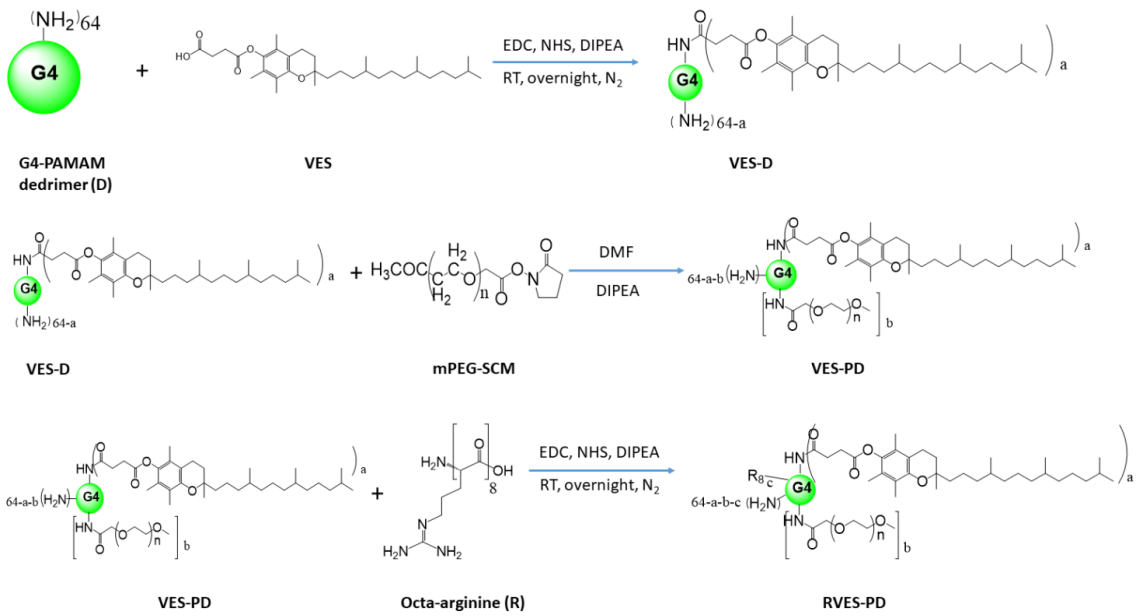

Figure 4.1. Scheme for the synthesis of RVES-PD.

4.3.3 Characterization of the synthesized polymers.

The ^{1}H NMR spectrum in Deuterium oxide (D_2O) was obtained by using NMR spectrometer (300 MHz, Bruker, USA). Gel permeation chromatography was carried out using Ultrahydrogel™ linear size exclusion column (7.8 mm × 300 mm) in SEC system (Waters series). The calibration curve was plotted using different molecular weight pullulan standards of molecular weight range 0.63×10^4, 0.98×10^4, 2.20×10^4, 4.71×10^4, 10.7×10^4, 20.1×10^4, 33.4×10^4, 64.2×10^4 Da. The hydrodynamic size, polydispersity index and zeta potential of the dendrimer nano-conjugate RVES-PD was measured using a Malvern Zetasizer (Malvern Instruments, UK). The samples were assessed by photon correlation spectroscopy in Malvern zetasizer at room temperature. The deionized water was used to dilute the dendrimer conjugates.

4.3.4 PTX loading in dendrimer

PTX in excess (5 mg) was added into the VES-PD or RVES-PD solution (25 mg/mL) in PBS, pH 7.4. The reaction mixture was sonicated for 1 min and kept overnight with gentle stirring. The VES-PD-PTX or RVES-PD-PTX formulations were passed through syringe filter (0.45 μm). Percentage drug loading (%DL) and encapsulation efficiency (%EE) of PTX were estimated by HPLC (Shimadzu, Japan). The PTX was liberated from VES-PD/RVES-PD by dissolving the polymers in methanol. The flow rate was kept at 1 mL/min and λ_{max} 227 nm. The drug was eluted out with the mobile phase of phosphate buffer saline, pH 7.4 and acetonitrile (Bhatt et al. 2019). The percent encapsulation efficiency (% EE) andpercent drug loading (% DL) of VES-PD-PTX or RVES-PD-PTX were determined following the equations:

$$\%EE = \frac{\text{drug amount present in supernatant of dendrimer conjugate}}{\text{initial drug amount added}} \times 100$$

$$\%\text{DL} = \frac{\text{drug amount present in supernatant of dendrimer conjugate}}{\text{initial drug amount drug and dendrimer conjugate added}} \times 100$$

4.3.5 *In vitro* PTX release study from VES-PD-PTX and RVES-PD-PTX

The i*n vitro* release experiment was performed using dialysis method (Kulhari et al. 2016). VES-PD-PTX and RVES-PD-PTX formulations (equivalent to 2 mg of PTX) were filled in a dialysis bag (MWCO 2000), which was immersed in PBS, pH 7.4 (supplemented with 0.2 % Tween-80 for maintaining sink condition). The solution was stirred continuously at 100 rpm at 37 °C. Then, 1 mL of aliquot was taken from the release media at predetermined time points, and replaced with fresh medium. The PTX release was estimated by HPLC following the same HPLC conditions as mentioned above. The experiment was carried out in triplicate. The data were shown by plotting the graph of % cumulative release versus time (mean ± standard deviation, triplicates).

4.3.6 Cellular uptake in A549 by flow cytometry

The cellular internalization of dendrimers in A549 cells was evaluated quantitatively by flow cytometer (FlowSight, Millipore, USA). The cells were seeded in 6-well tissue culture plates at a cell density of 1×10^6 cells/ well. The cells were allowed to attach for overnight. The following day, cells were treated with fluorescently labelled (FITC) VES-PD and RVES-PD at dendrimer concentration of 20 µg/ml for 1 h and 4 h. Next, the cells were washed using phosphate buffer saline (pH 7.4). Trypsin was added for detachment of the cells from the well plate. Next, the cells were kept for centrifugation for 5 min at 1200 rpm. The cell pellets obtained by centrifugation were re-suspended in sterile PBS prior to analyzing the cells by flow cytometry (excitation wavelength of 488 nm using argon laser). The data obtained from flow cytometry were assessed in IDEAS software. The geo mean fluorescence values of individual samples (triplicates) was shown as a bar graph.

4.3.7 Cellular uptake by confocal microscopy

The cellular uptake was determined qualitatively by confocal microscopy. A549 cells were seeded in 12-well tissue culture plates onto circular coverslips at a cell density of 50000 cells/well. Following day, the cells were incubated with fluorescently labelled (FITC) VES-PD and RVES-PD (20 µg/ml) and incubated for 1 h and 4 h. The major uptake mechanism of CPP mediated nano-carriers is through the macropinocytosis. Hence, the internalization pathway was assessed by adding the macropinocytosis inhibitor Amiloride (1 mM) to the cells. The cells were incubated for 30 min at 37 ºC in a CO_2 incubator. After the treatment with formulations, the cells were washed with phosphate buffer saline three times, then treated with DAPI to stain the nucleus and kept in dark for 5 min. The para-formaldehyde solution was used to fix the cells. Following fixation, the treated coverslips were transferred on glass slides using Fluoromount-G medium. The slides were seen under confocal laser scanning microscope (Leica DMi8, Leica, Germany) at 40X magnification using FITC and DAPI channels. The *Image J* software was used to process and analyze the captured images.

4.3.8 Cytotoxicity assessment

The MTT assay was performed to evaluate the cytotoxic potential of free PTX, VES-PD-PTX and RVES-PD-PTX in A549 cells. The cells were seeded in 96-well sterile cell culture plates at cell density of 10000 cells/well in culture medium. Next day, the cells were treated with free PTX, VES-PD-PTX and RVES-PD-PTX (at PTX concentrations of 0-50 µg/ml) and kept for 24 and 48 h at 37 °C. Free PTX was dissolved in dimethyl sulfoxide, and further diluted with culture media (not more than 0.5% v/v in the final media). The culture media was removed after 24 and 48 h, and MTT reagent (50 µl) was added to the cells and kept for incubation for 4 h. MTT solution was removed from the plates, and the dimethyl sulfoxide was added for the dissolution of MTT reagent. The optical density at 590 nm was checked by microplate

reader instrument (Spectramax M4, Molecular Devices, San Jose, USA). The reference absorption maxima were kept at 620 nm. The percentage cell viability was calculated by the below mentioned equation:

$$\text{Percentage cell viability} = Abs_{sample} / Abs_{control} \times 100$$

Where, Abs_{sample} = absorbance of the cells treated with free drug and drug loaded dendrimer formulations, and $Abs_{control}$ = absorbance of the control cells. The data were represented as the mean and standard deviation (triplicates).

4.3.9 Annexin V assay

A549 cells were seeded in 6-well plates at a cell density of 1×10^6/well. The following day, cells were treated with free PTX, VES-PD-PTX and RVES-PD-PTX at 20 µg/ml of PTX concentration for 18 h and kept in the incubator at 37 °C in 5% CO_2 atmosphere. This study was carried out as per the protocol provided with Annexin V assay kit. In brief, after the treatment for 18 h, A549 cells were washed with phosphate buffer saline and centrifuged to obtain cell pellets. The pellets were again re-suspended in AnnexinV binding buffer (100 µl). Further, the cells were stained using 2 µl propidium iodide (PI) solution as well as 2 µl Annexin V solution. Following 15 min of incubation in dark, AnnexinV buffer was added to all test samples and control tubes and assessed by using flow cytometry (Flowsight Amnis, Millipore, USA). The fluorescence of FITC (at 535 nm, Ch02) and propidium iodide (at 550 nm) was measured from the 10000 gated cells. The dot histogram plot for apoptosis data was obtained using IDEAS software. Early apoptosis as well as late apoptotic events were taken into consideration to analyze the magnitude of apoptosis induced in the cells.

4.3.10 Spheroid study

4.3.10.1 *Formation of A549 spheroids*

Liquid overlay method was used to develop A549 cancer cell spheroids as reported in previous literatures (Kumari et al. 2018, Rompicharla et al. 2018b). Briefly, 1.5% w/v agar solution in serum free DMEM was prepared and sterilized. Next, the agarose solution (60 µL per well) was poured to the 96-well sterile plates to avoid cell attachment with the bottom surface of the well plates. The plates were dried for 30 min before further use. 10000 cells per well were added in the pre-coated agar plates. These plates were centrifuged at 1000 rpm for 15 min. The developed A549 spheroids were seen daily under microscope.

4.3.10.2 *Penetration efficiency in A549 spheroids*

A549 cells were seeded at the cell density of 1×10^4 cells/well into 8-well tissue culture plates to make the spheroids. The depth of penetration of fluorescently labelled dendrimers into the A549 spheroids was visualized by confocal microscope for 1 h and 4 h. Following incubation, the spheroids were washed with phosphate buffer saline and observed at 10X magnification under confocal microscope at different focal length (Z-stack). The images of the spheroids were taken and processed using *Image J* software.

4.3.10.3 *A549 spheroidal uptake of dendrimers by flow cytometry*

A549 spheroids (5 days old) were treated for 1 h and 4 h with fluorescently labelled RVES-PD and VES-PD. For sufficient cell count, 12 spheroids were taken together as one replicate for both the time points. The spheroids were broken by using Accutase™ solution and shaking moderately for 10 min. The suspension of the cells was taken in eppendorf tubes and fetal bovine serum was added. Following centrifugation, the supernatant was discarded and the cells were re-suspended in phosphate buffer saline to analyze by using flow cytometer (Amnis, Millipore, USA). The mean fluorescence shown by RVES-PD and VES-PD treated spheroids was plotted as a bar graph using

Graph Pad prism 7 software. The FCS express software was used to analyze the data and to plot the histograms.

4.3.10.4 *Assessment of growth inhibition in A549 spheroids*

When the spheroids achieved proper integrity grown in 96-well plates, they were treated with free PTX, VES-PD-PTX and RVES-PD-PTX, with 25 µg/mL of paclitaxel concentration. The growth media was replaced with fresh medium on alternate days. The spheroids were observed under bright field microscope (Leica, Leica Microsystems, Germany) and the diameters of the spheroids were measured at predetermined time points (0, 2, 4 and 6 days). The images were taken at 10X magnification. The mean diameter of 4 spheroids with standard deviation was shown quantitatively in Figure 4.10 B.

4.3.11 *In vivo* therapeutic efficacy

The therapeutic efficacy of free PTX, VES-PD-PTX and RVES-PD-PTX formulations was assessed in female C57BL/6 mice (6−8 week, 18−22 g) obtained from the Vivo Biotech Pvt. Ltd, Hyderabad, India. The animals were adapted for 1 week at in-housed conditions of 19−25 °C with nocturnal−diurnal cycles with a relative humidity of 50−60% with free access to food and water. The anti-tumor efficacy was carried out according to the approved protocol from the Institutional Animal Ethics Committee. The murine melanoma cells B16F10 (1×10^6) suspended in PBS was injected subcutaneously to develop the xenograft tumor model in mice. The animals were scrutinized for 10−15 days for the presence of a solid tumor. Once palpable solid tumor was formed, the tumor volume (length × $width^2$)/2) and body weight was measured using the digital vernier caliper.

4.3.11.1 Biodistribution of multifunctional dendrimer nano-conjugates

The animals were separated into two groups (n=5) when the average tumor volume was reached up to 200 mm^3. The fluorescently labeled dendrimer formulations were injected to the tumor bearing mice at dendrimer concentration of 10 mg/ kg in PBS intra-peritoneally. The tumors, heart, kidney, lungs, spleen and liver were isolated after sacrificing the mice at 4, 8 and 24 h using CO_2. The tissue sections were washed with PBS (pH 7.4), immersed in tissue freezing media and kept in -80 °C freezer. Next, these frozen sections of all tissues were cryo-sectioned (5 μm thickness) by a Cryotome instrument (Leica, Germany), mounted on glass slides, washed with phosphate buffer saline, and fixed using 4% para-formaldehyde solution. The sections were visualized under fluorescence microscope at 20X magnification.

4.3.11.2 Tumor volume reduction Study

The tumor bearing mice were divided into four different groups when the tumor volume was reached at 50−100 mm^3. Free PTX, VES-PD-PTX and RVES-PD-PTX were injected at PTX dose of 10 mg/kg/day intra-peritoneally to the tumor bearing mice. Polysorbate 80 and ethanol was used to dissolve free PTX and diluted with PBS if necessary (Sparreboom et al. 1996). The groups of the animals were as follows: (a) controls, (b) free PTX, (c) VES-PD-PTX, and (d) RVES-PD-PTX (no of animals in each group, n=6). The dosing of free drug and formulations was performed on alternate days till 10 days (5 times injections). The tumor volume and body weight of the mice were noted every alternate day for all groups for 21 days. After the study period, the mice were sacrificed by cervical dislocation, and the weight of the tumors was taken.

4.3.11.3 Caspase 3/7 activity in tumor

The level of Caspase 3/7 in isolated tumors was determined by using Apo-ONE Homogeneous Caspase-3/7 assay kit (Promega) following manufacturer's instruction. A small portion of tumors was cut, and homogenized using a bead tissue homogenizer

(Minilys, Bertin Technologies, USA) in PBS, pH 7.4. Micro BCA protein assay was performed to measure the protein content in the tissue. Next, 25 µg of protein in 100 µL of PBS was added to 96-well plate. The caspase substrate was added into the tissue solutions according to the manufacturer's protocol and kept at room temperature for 6 h. The fluorescence was measured by the microplate reader at excitation 499 and emission 521 nm. The fluorescence values were directly proportional to the amount of caspase 3/7 release and graph was plotted.

4.3.11.4 TUNEL assay

Measurement of the apoptotic effect following treatment with multifunctional dendrimers was carried out in frozen tumor sections by using TUNEL assay. The tumor sections (5 µm) were taken using Cryotome, mounted on superfrost plus slides. The cryo-sections were fixed using 4 % para-paraformaldehyde solution for 10 min at room temperature. TUNEL assay was done on the sections using TUNEL detection kit according to the manufacturer's instructions. The apoptotic cells in the sections as stained by TUNEL assay reagent were visualized under fluorescence microscope.

4.3.12 Statistics

All of the above *in vitro* studies were executed in triplicates (n=3) and the data are shown as mean and standard deviation (mean ± SD). The animal experiment was performed using 6 animals in each treatment group (n=5, or 6). The significance between all the groups was determined by one-way analysis of variance using Graph Pad prism software. The experimental data were considered significant at p value < 0.05.

4.4 Results and discussion

4.4.1 Confirmation of synthesis of RVES-PD nano-construct

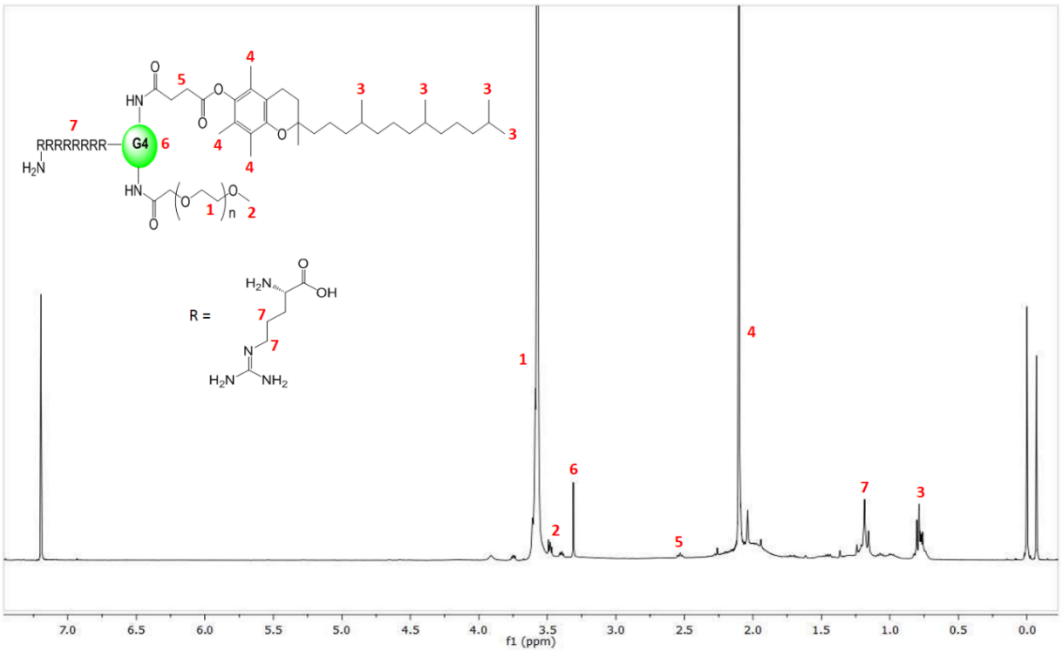

Figure 4.2. Proton nuclear magnetic resonance spectrum of RVES-PD in $CDCl_3$ at 300 MHz

Dendrimer, a hyper branched molecule with defined architecture has gained attention in various biomedical applications, including drug delivery research since 1990s following its inception in 1980s. Dendrimers improve the solubility, stability and bioavailability of various anticancer drugs. The major advantage with dendrimers is the scope as well as the ease of surface functionalization, which enables covalent attachment of drugs, or other ligands to modulate drug loading, release, tumor targetability and minimize non-specific interaction of the nano-construct in systemic circulation (Dehshahri and Sadeghpour 2015, Palmerston Mendes, Pan, and Torchilin 2017). Here, we design development of a multifunctional dendrimer nano-construct conjugating PEG, α-TOS- and R-on the surface. The attachment of PEG on the surface of dendrimer would improve its hydrophilicity, minimize non-specific interaction by reducing the surface charge, and prolong blood circulation, which would lead to passive targeting of the nano-sized dendrimers to tumor region via EPR effect. The presence of

α-TOS on the surface would improve its capacity to load hydrophobic drugs, and provide therapeutic benefits in cancer treatment. Anchorage of cell penetrating peptide, R8 would promote facile intracellular translocation of this macromolecule, therefore, would increase therapeutic efficacy of the loaded PTX.

Following synthesis of the modified dendrimers following Figure 4.1, the conjugation of VES, PEG and octa-arginine was confirmed by analyzing the NMR spectrum of RVES-PD (Figure 4.2). NMR signals at 0.75 ppm, 2.25 and 2.5 ppm confirmed the presence of VES. Sharp singlet at 1.2 ppm confirmed the conjugation of octa-arginine to the dendrimer. The peaks at 3.5 ppm and 3.3 ppm was from the protons of PEG moiety and dendrimer, respectively. All NMR signals acknowledged the successful conjugation of VES, PEG and octa-arginine onto the dendrimer surface.

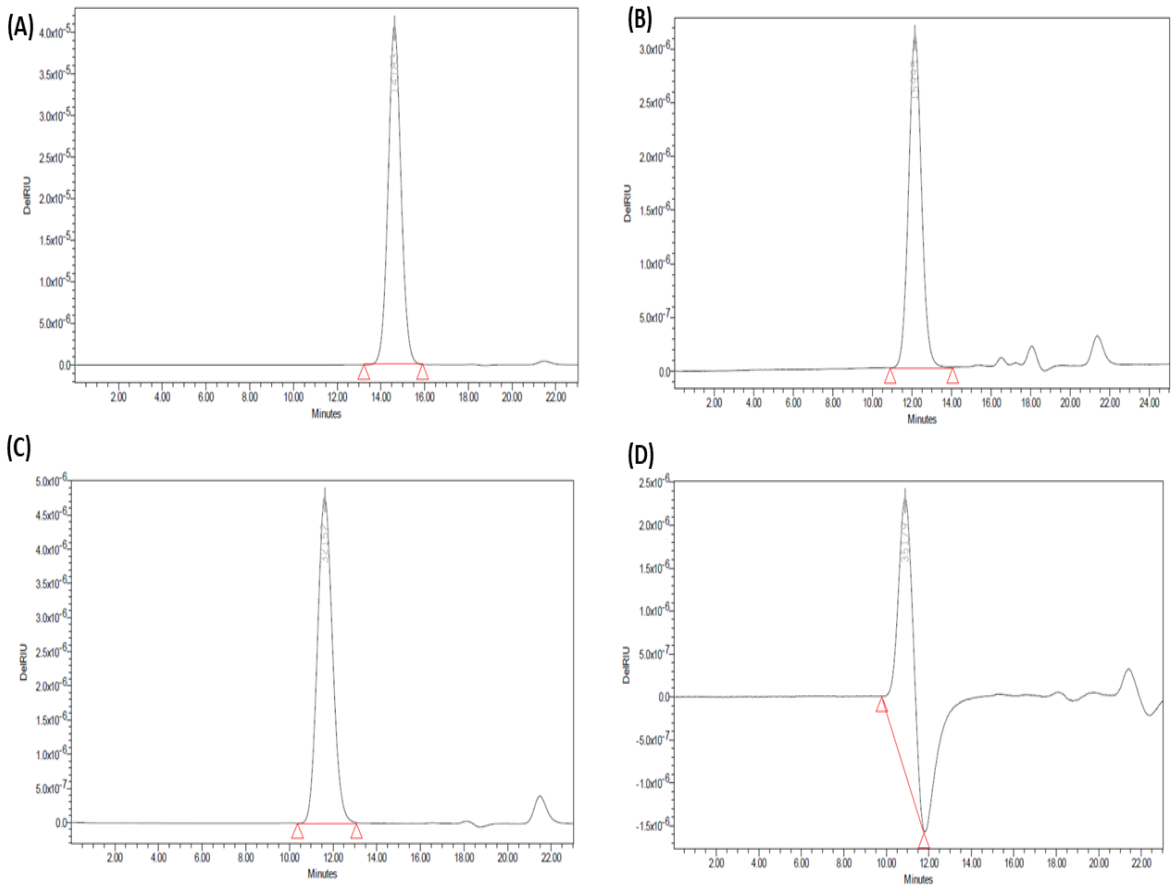

Figure 4.3. SEC chromatograms of synthesized dendrimer conjugates. (A) G4 PAMAM dendrimer, (B) VES-D, (C) VES-PD, (D) RVES-PD.

Conjugates	Molecular weight (Da)	Approximated No. of molecules attached to each G4 PAMAM dendrimer
G4	14183	-
VES-D	15995	3.41
VES-PD	32152	8.07
RVES-PD	35179	2.40

Table 4.1. Relative molecular weight of each conjugate and estimation of the number of VES, PEG and octa-arginine attached to each PAMAM dendrimer obtained by SEC analysis.

The increase in the molecular weights of the dendrimers upon each conjugation was determined by performing size exclusion chromatography (SEC). The SEC graphs and relative molecular weight are reported in Figure 4.3 and Table 4.1. As shown in Figure 4.3 (A), Figure 4.3 (B), Figure 4.3 (C) and Figure 4.3 (D), 3.41 molecules of VES, 8.07 molecules of PEG and 2.40 molecules of octa-arginine were conjugated on each dendrimer molecule.

From the above Table 4.1, the molecular weight of plain G4 PAMAM dendrimer was found to be 14183 Da. The molecular weight of VES-D conjugate was found to be 15995 Da. The molecular weight of each VES molecule is 530.79 Da. VES of about 5 molar equivalents was taken to conjugate with each PAMAM dendrimer initially as mentioned in the method section. Hence, the VES molecules got attached to each PAMAM dendrimer was calculated as follows:

$$\text{Number of TOS molecules attached to each PAMAM dendrimer} = \frac{(\text{molecular weight of VES} - \text{D conjugate}) - (\text{molecular weight of G4})}{molecular\ weight\ of\ each\ VES\ molecules}$$

The molecular weight of VES-PD conjugate was found to be 32152 Da. The molecular weight of each PEG (P) molecule is 2000 Da. PEG of about 10 molar equivalents was taken to conjugate with each PAMAM dendrimer initially as mentioned in the method section. Hence, the PEG molecules got attached to each PAMAM dendrimer was calculated as follows:

$$\text{Number of PEG molecules attached to each PAMAM dendrimer} = \frac{(\text{molecular weight of VES} - \text{PD conjugate}) - (\text{molecular weight of VES} - \text{D})}{molecular\ weight\ of\ each\ PEG\ molecules}$$

The molecular weight of RVES-PD conjugate was found to be 35179 Da. The molecular weight of each octa-arginine (R) molecule is 1261 Da. Octa-arginine of about 3 molar equivalents was taken to conjugate with each PAMAM dendrimer initially as mentioned in the method section. Hence, the octa-arginine molecules got attached to each PAMAM dendrimer was calculated as follows:

$$\text{Number of R molecules attached to each PAMAM dendrimer} = \frac{(\text{molecular weight of RVES} - \text{PD conjugate}) - (\text{molecular weight of VES} - \text{PD})}{molecular\ weight\ of\ each\ octa - arginine\ molecules}$$

4.4.2 Physicochemical characterization of dendrimer conjugates

Dendrimer conjugates	Size (nm)	PDI	Zeta potential (mV)	%EE	%DL (% w/w)
Plain dendrimer	13.56 ± 0.072	0.193 ± 0.003	+18.6 ± 0.41	-	-
VES-PD-PTX	29.85 ± 0.013	0.189 ± 0.057	+7.25 ± 0.28	81.21 ± 1.80	15.3 ± 1.09
RVES-PD-PTX	38.14 ± 0.053	0.197 ± 0.008	+9.58 ± 0.42	73.58 ± 2.27	12.48 ± 1.75

Table 4.2. Size, polydispersity index, zeta potential, % encapsulation efficiency and % drug loading values of various dendrimer nano-constructs (Mean ± standard deviation, n=3)

The physico-chemical characterizations of PTX-loaded, VES-PD-PTX, and RVES-PD-PTX were carried out and the data had been represented in Table 4.2. The zeta potential of plain G4 PAMAM dendrimer was found to be +18.6 ± 0.41 mV. After VES/PEG

conjugation and PTX-loading, the zeta potential was decreased to +7.25 ± 0.28 mV. The non-ionic PEG and anionic VES decreased the overall zeta potential in the conjugated dendrimer. Further, conjugation with cationic peptide, R8 increased the surface potential of RVES-PD.

The hydrodynamic diameters of plain dendrimer, VES-PD-PTX and RVES-PD-PTX were 13.56 ± 0.072, 29.85 ± 0.013 and 38.14 ± 0.053, respectively. The increase in the diameter was due to the conjugation of VES, PEG, octa-arginine on the surface, and PTX loading. The PTX loading efficiency was 15.3 ± 1.09 % w/w and 12.48 ± 1.75 % w/w in VES-PD-PTX and RVES-PD-PTX, respectively. The PTX loading in dendrimer was dependent on the non-covalent interactions between PTX and dendrimer formulations. The percent drug loading of PTX was increased in VES-PD as VES could improve the solubility of PTX by providing an internal hydrophobic space. In contrast, % drug loading of PTX was decreased in RVES-PD due to the attachment of octa-arginine, which provided limited access to PTX to go inside the dendrimer cavity.

4.4.3 *In vitro* drug release study

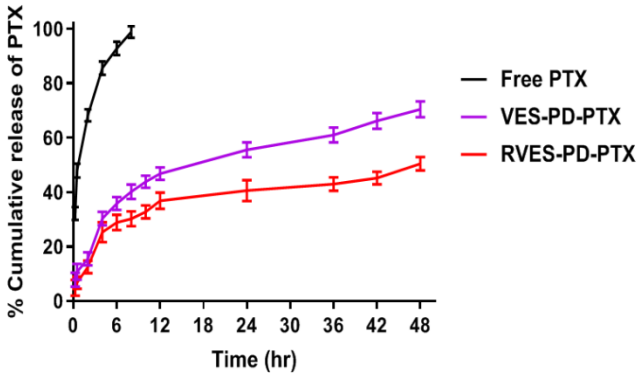

Figure 4.4. *In vitro* drug release study. Release of PTX from RVES-PD and VES-PD at pH 7.4 (Mean ± SD; n = 3)

Drug release study of RVES-PD and VES-PD formulations was performed using PBS pH 7.4 (Figure 4.4). The plain PTX showed faster release (92.79 ± 2.45 %) within 6 h

while PTX showed controlled release behavior of drug over 48 h when loaded into RVES-PD and VES-PD. VES-PD showed cumulative PTX release of 55.57 and 70.45%, whereas RVES-PD showed PTX release of 40.55 and 51.23 % in 24, and 48 h, respectively. The attachment of VES, PEG and octa-arginine over the dendrimer surface provided a shielding effect, which retarded the release of PTX. During initial hours, a nonlinear release profile was observed followed by controlled release later. The possible reason for the controlled release could be due to the entrapment of the paclitaxel molecules in the hydrophobic core of the dendrimer which acts as a reservoir to retain the paclitaxel molecules.

4.4.4 Cellular uptake study by flow cytometer and confocal microscopy

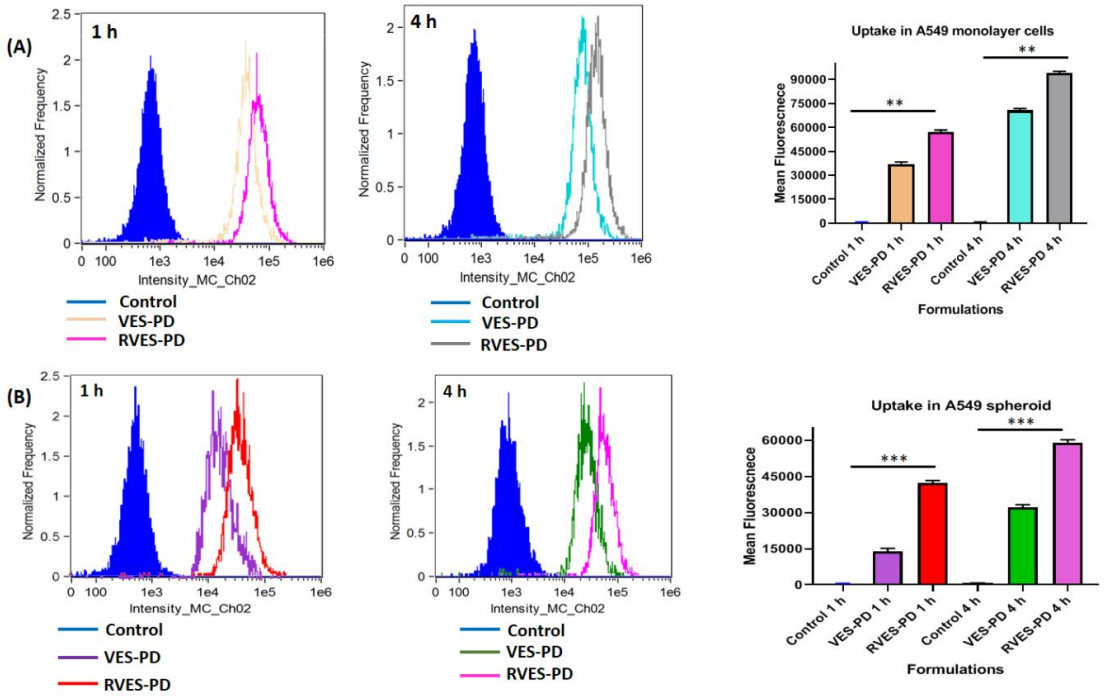

Figure 4.5. cell uptake study in monolayers and spheroids. (A) Flow cytometry analysis of cellular uptake of FITC-labelled RVES-PD and VES-PD in A549 cells. (B) Uptake of FITC-RVES-PD and VES-PD in A549 spheroids analyzed by flow cytometry. Data in graph is represented as mean ± standard deviation performed in triplicates. The bar graph represented the mean fluorescence observed. The significance was assessed by applying one-way analysis of variance, ***$p<0.001$.

The cellular uptake study was carried out to evaluate the influence of octa-arginine attachment on the cellular uptake of the dendrimers. As shown in Figure 4.5, RVES-PD had higher accumulation in cells compared to VES-PD. The geometric mean fluorescence was 37131.26 ± 1221.41 and 70745.70 ± 1150.23 for cells treated with VES-PD, which was increased to 57206.22 ± 1195.3 and 94032.57 ± 1056.21 for RVES-PD treated cells in 1 and 4 h, respectively (Figure 4.5 A). Similar observation was registered in spheroids, where the mean florescence of VES-PD, and RVES-PD treated cells were 13896.31 ± 1243.78, 32087 ± 950.11, and 42138 ± 1095.53, 59083 ± 1126.76 in 1, and 4 h, respectively. The octa-arginine attachment enhanced the cellular association of the RVES-PD conjugate significantly compared to VES-PD. Octa-arginine has demonstrated its potential to carry various macromolecules inside the cells (van Oppen et al. 2019). In a recent study, elastin like polypeptide-based nanoparticles were prepared with controlled density of octa-arginine on the surface (van Oppen et al. 2019, Liu et al. 2017). In our previous study, octa-arginine-modified PEGylated PAMAM dendrimers were prepared, where PTX was conjugated on the surface of the dendrimer (Rompicharla et al. 2018c). In order to determine the cellular internalization mechanism of RVES-PD, the competitive inhibition of the cellular internalization was performed by pre-incubation of A549 cells with micropinocytosis inhibitor, amiloride (1mM). Amiloride inhibits macropinocytosis by blocking Na^+/H^+ exchanger and by lowering the sub-membranous pH. The intensity of fluorescence for this study has been represented in Figure 4.6. It was observed that the internalization of RVES-PD was decreased significantly following Amiloride pre-treatment.

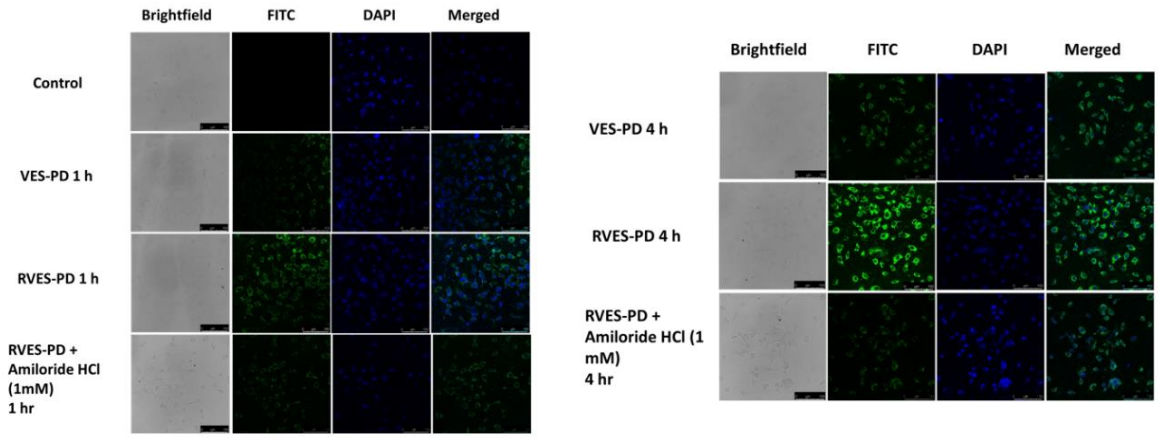

Figure 4.6. Cellular uptake and assessment of internalization mechanism of VES-PD and RVES-PD in A549 cells using confocal microscope.

The mechanism behind the higher octa-arginine mediated uptake is the non-clathrin and non-caveolar mediated endocytosis, called micropinocytosis. When the cell penetrating peptides are attached to large cargos (molecular weight >30,000 Da), the internalization by macropinocytosis involves the formation of macropinosomes (>1 μm). The macropinosoms tend to completely merge with the lysosomes, tend to be recycled and prevents the nanocarriers from lysosomal degradation (Meier et al. 2002, Swanson and Watts 1995, Wadia, Stan, and Dowdy 2004).

4.4.5 Cytotoxicity study

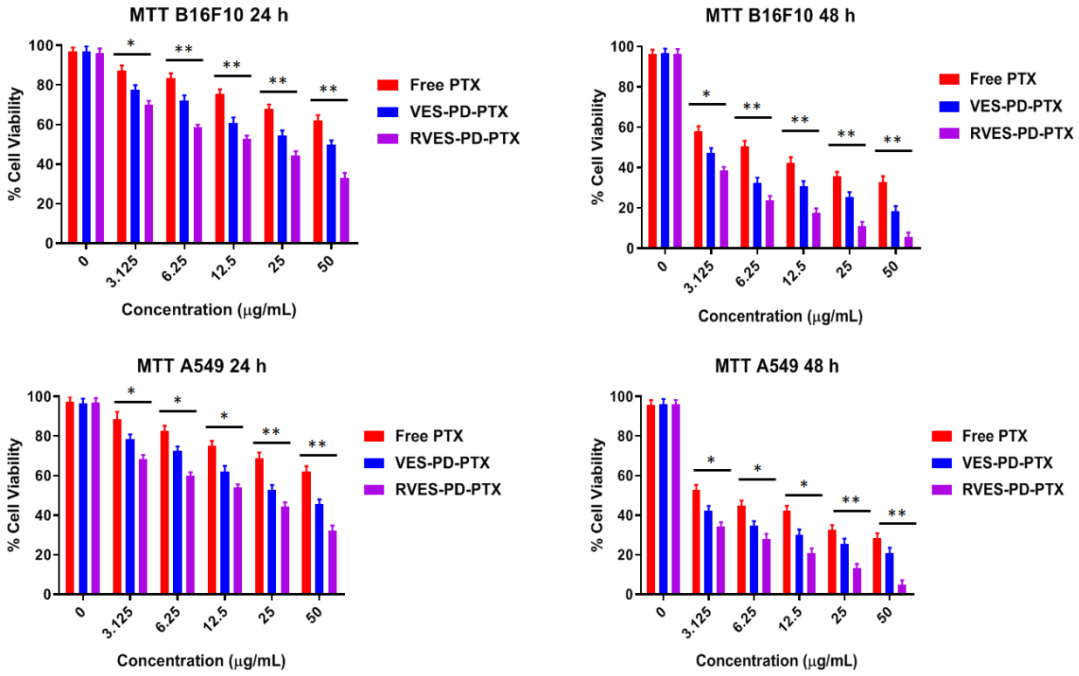

Figure 4.7. Determination of cell viability by MTT assay performed using B16F10 and A549 cells. Percent cell viability of A549 and B16F10 cells incubated with free PTX, VES-PD-PTX and RVES-PD-PTX was determined at 24 and 48 h post incubation (n=3, mean with standard deviation). The statistical significance was analyzed by applying one-way analysis of variance test, ** and * represented $p < 0.01$ and 0.05, respectively.

As shown in Figure 4.7, the cell viability decreased significantly with RVES-PD-PTX treatment compared to the treatment with VES-PD-PTX and free PTX. The RVES-PD-PTX, VES-PD-PTX, and free PTX demonstrated cell viability of 32.21 ± 2.58, 45.66 ± 2.34, and 61.85 ± 2.98 % respectively at 24 h at the PTX concentration of 50 µg/mL. Further decrease in cell viability was observed with RVES-PD-PTX (4.92 ± 2.28%) as compared to VES-PD-PTX (20.96 ± 2.69 %) and free PTX (28.58 ± 2.36 %) at the PTX concentration of 50 µg/mL at 48 h. Cell viability study demonstrated that the octa-arginine attachment in RVES-PD-PTX promoted higher cellular internalization and resulted in decreased cell viability compared to free PTX and VES-PD-PTX. Another reason of obtaining cytotoxicity in RVES-PD-PTX would be due to the anticancer effect of VES.

4.4.6 Apoptosis assay

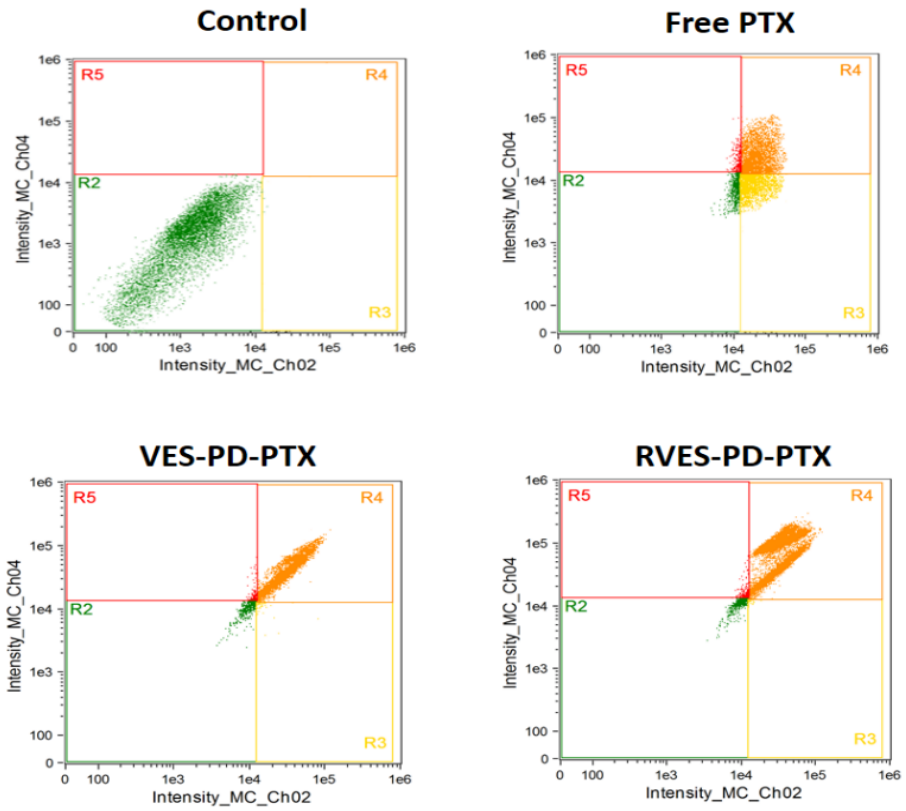

Figure 4.8. Annexin V assay. Quantitative assessment of apoptosis in A549 cells induced by RVES-PD-PTX, VES-PD-PTX and free PTX. R5-R2 denote necrotic, late apoptotic, early apoptotic, and live cells population, respectively.

Upon activation of the apoptotic pathway in the cells following treatment, phosphatidylserine (PS) translocates outside the plasma membrane to attract macrophages, which initiates the formation of apoptotic bodies. AnnexinV, a specific ligand of PS binds specifically to PS, which could be detected by its tagged fluorescence. The assay also uses propidium iodide (PI), which binds to the necrotic cells. As shown in Figure 4.8, the free PTX induced apoptosis of 26.9 ± 1.6 %, whereas RVES-PD-PTX and VES-PD-PTX induced the total apoptosis of 49.85 ± 2.14 and 36.51 ± 2.28 %, respectively. The higher level of cytotoxicity produced by RVES-PD-PTX was due to the induction of apoptosis to higher extent compared to VES-PD and

free PTX. The significant improvement in apoptotic percentage could be be due to the improved internalization of the R8-conjugated nanomedicine, which increased the delivery of PTX in deeper tumor tissues.

4.4.7 Penetration efficiency in A549 spheroids

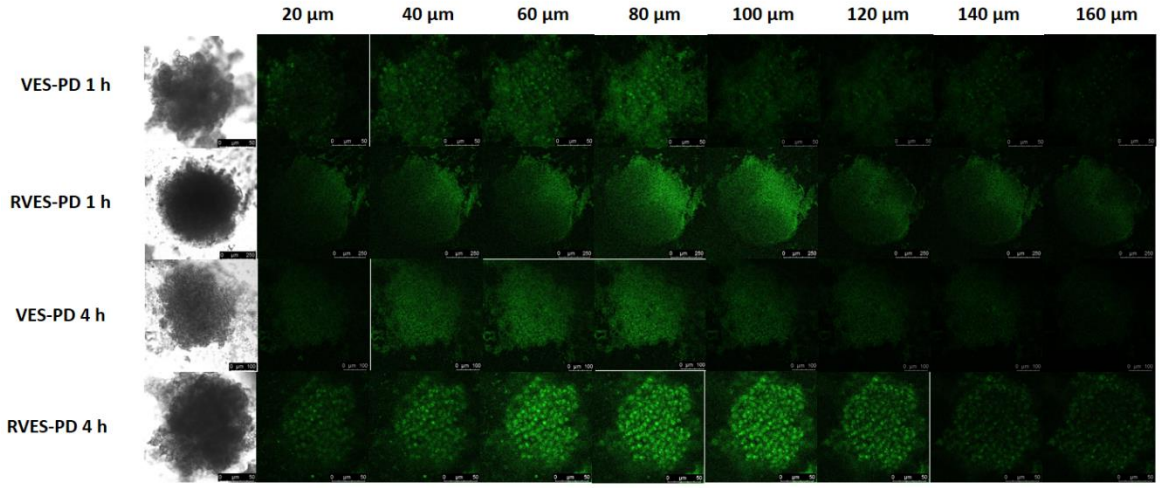

Figure 4.9. Penetration efficiency of fluorescently tagged RVES-PD and VES-PD in A549 spheroids at different depths visualized under confocal laser scanning microscope following 1 h and 4 h incubation.

Spheroids are three dimensional *in vitro* cell culture system that closely mimic several features of *in vivo* tumor growth such as growth rate, close proximity of cells during growth, cellular heterogeneity and cell-cell signalling, development of necrotic core, higher rate of proliferation of the peripheral cells than the core region, deposition of extracellular matrix, similar gene expressions, and multiple drug resistance (Costa et al. 2016). Due to its close resemblance to *in vivo* tumor, 3D spheroids are promisingly used to screen various anticancer therapeutic modalities. In the penetration study, the A549 spheroids were visualized under confocal microscope at different depths (Z-stack) after 1 and 4 h of treatment. RVES-PD showed more permeation as indicated by higher intensity of fluorescence towards center in the 3D spheroids in comparison to VES-PD at both the time points (Figure 4.9). The penetration efficiency study in 3D spheroids proved that the R/VES attachment in dendrimer enhanced deeper tissue

penetration in the 3D spheroids. Penetration of nanomedicines to the solid tumor mass is challenging, which limit their therapeutic potential. However, it is evident from the study that the RVES-PD system with R/VES attachment on the surface could improve the permeability of dendrimers to deeper tumor tissues (Rompicharla et al. 2018a).

4.4.8 Growth inhibition of A549 spheroids

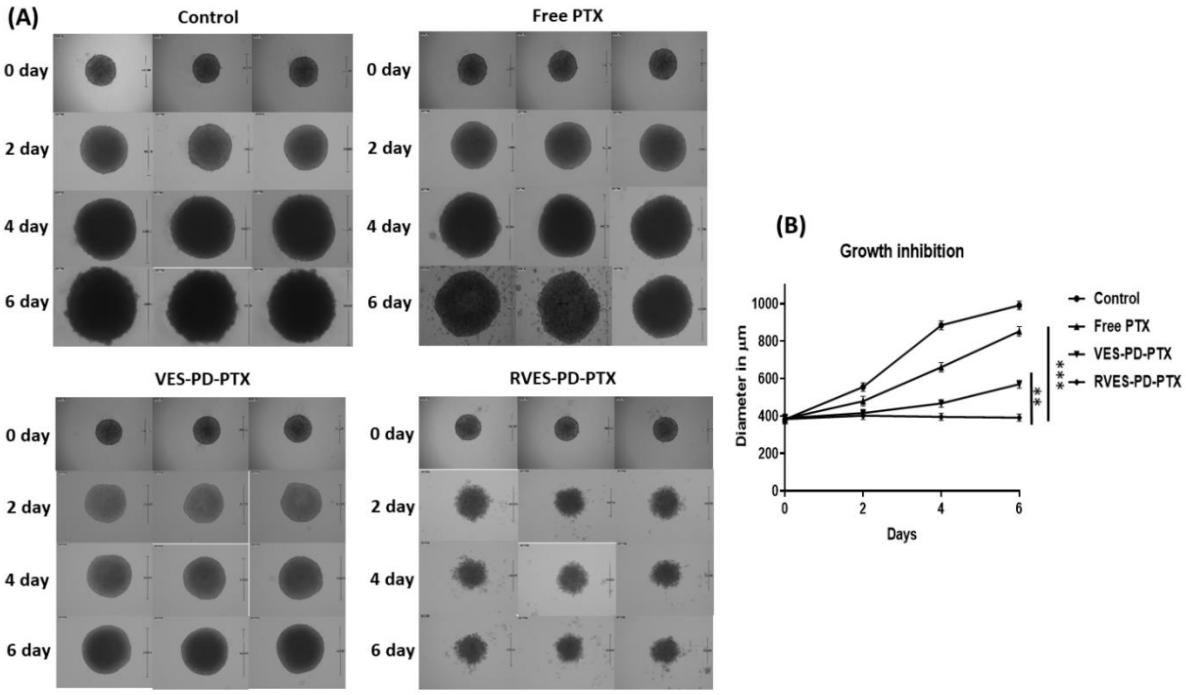

Figure 4.10. Growth inhibition of A549 spheroids following treatment. (A) Bright field images of A549 spheroids after treatment with free PTX, VES-PD-PTX and RVES-PD-PTX. The images were captured at 0, 2, 4 and 6 th day at 10X magnification. (B) Graphical representation of the growth inhibition of A549 spheroids. The significance between all the groups was assessed by one-way analysis of variance test, ***$p < 0.001$ and **$p<0.01$.

The bright field images of spheroids treated with free PTX, VES-PD-PTX, and RVES-PD-PTX at PTX concentration of 25 µg/mL has been represented in Figure 4.10 (A). The progression of growth of the spheroids treated with RVES-PD-PTX was retarded significantly compared to the spheroids treated with VES-PD-PTX and free PTX. The average diameter of spheroids was found to be 990.34 ± 23.2, 852.34 ± 25.58, 569.41

± 21.35, and 390.94 ± 18.15 μm for control, free PTX, VES-PD-PTX and RVES-PD-PTX treatment, respectively at the end of 6 days. These data are shown in the line graph plotted between the diameters versus days as shown in Figure 4.10 (B). R/VES-modified dendrimers translocated PTX more efficiently resulting in superior growth inhibitory effect. R8 facilitated PTX to accumulate in the spheroids thereby inhibiting the spheroid growth progression. Moreover, the cellular uptake data also corroborated that the RVES-PD gets internalized significantly into the spheroids which improved availability of the PTX in tumor.

4.4.9 Biodistribution of multifunctional dendrimer conjugates

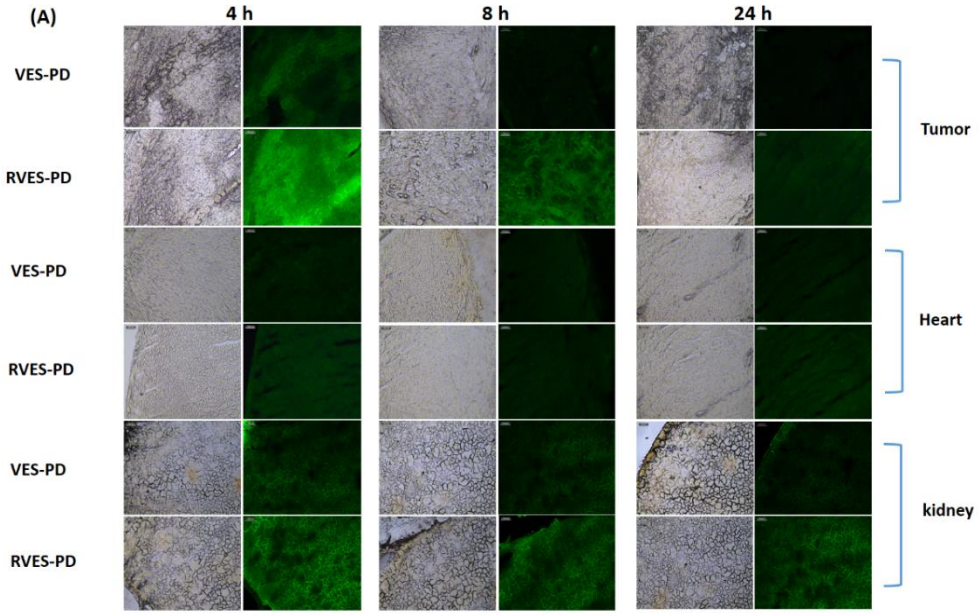

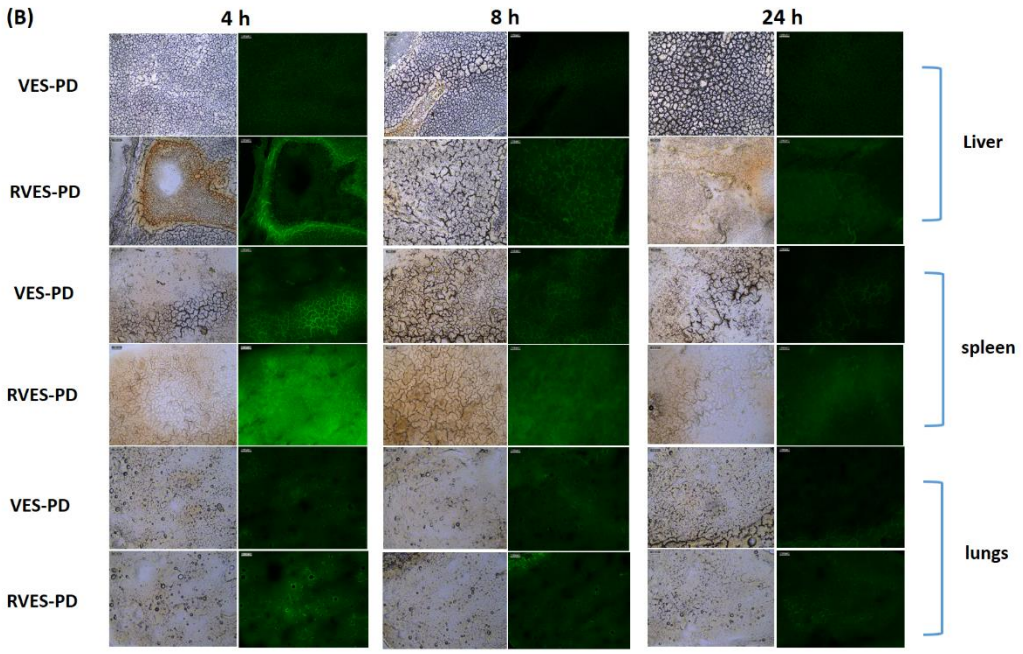

Figure 4.11. Biodistribution of dendrimer nano-constructs. (A) Fluorescence microscopic images of tumor, heart and kidney sections isolated from the mice treated with FITC-labeled VES-PD and RVES-PD for 4, 8 and 24 h. (B) Fluorescence microscopic images of liver, spleen and lungs sections isolated from the mice treated with FITC-labeled VES-PD and RVES-PD for 4, 8 and 24 h. Tumor sections are visualized at 20 X objective.

The RVES-PD treated sections showed fluorescence intensity more prominent in all organs and tumor than other treatment groups at all the time points (4, 8 and 24 h) (Figure 4.11). The strong localization effect may be attributed to the efficient penetration of the RVES-PD into the interstitial extracellular matrix and cells (Tan et al. 2017, Biswas et al. 2013). Furthermore, it is evident that amine terminated dendrimers localize in higher concentration in spleen, kidney and liver (Labieniec-Watala and Watala 2015, Agashe et al. 2007). The targeting ligand was not attached to the developed nano-carriers and hence they are accumulating in all the tissues including tumor. The justification behind prominent accumulation of RVES-PD in tumor could be the EPR effect as well the efficiency of R8 to deliver macromolecular cargo inside the cells (Prabhu, Patravale, and Joshi 2015, Wolinsky and Grinstaff 2008, Bhatt et al.

2019). It is evident that dendrimers with high positive charge and smaller size appear to clear rapidly from plasma which limits their application in drug-delivery (Kaminskas, Boyd, and Porter 2011). Attaching the anionic group like VES and neutral group like PEG reduces the renal clearance as macromolecules (molecular weight ≥ 25 kDa) could not be eliminated through glomerular filtration (Kaminskas, Boyd, and Porter 2011). Moreover, PEG cloud on the dendrimer surface enables dendrimers to evade recognition by reticulo-endothelial system and as a result, prolong the systemic circulation of the nanocarriers. The prolong systemic stay of the dendrimers eventually allow them to accumulate in the tumor site by EPR effect (Labieniec-Watala and Watala 2015, Kaminskas, Boyd, and Porter 2011). Moreover, attaching various ligands on the nanocarriers surface increases their hydrodynamic diameter, and reduces their chance of renal clearance (Labieniec-Watala and Watala 2015).

4.4.10 Therapeutic efficacy study

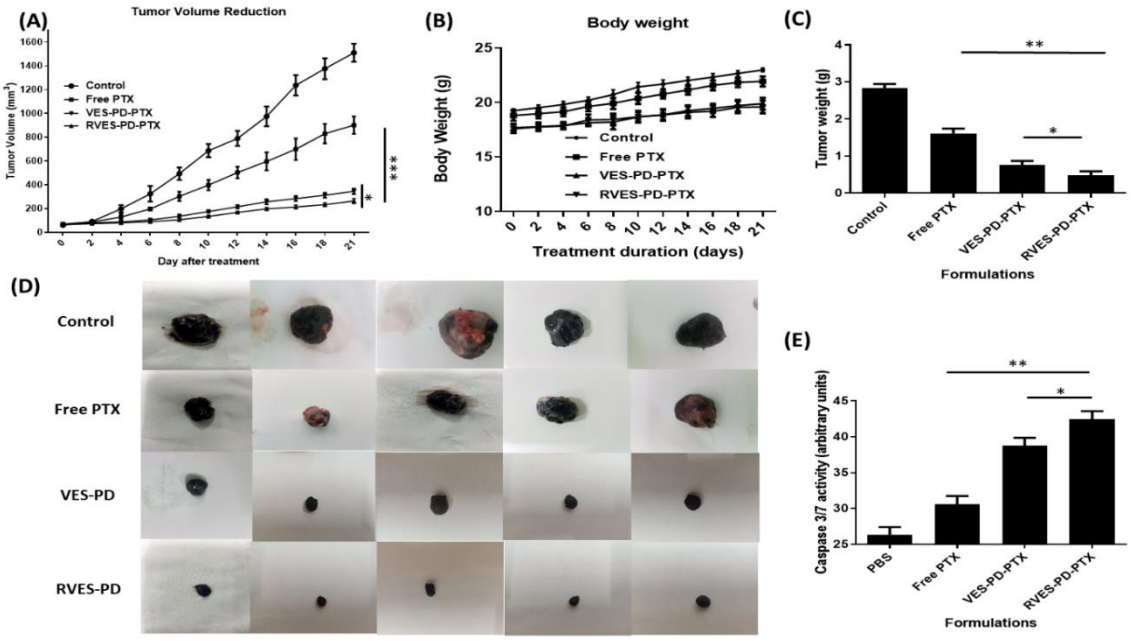

Figure 4.12. Assessment of therapeutic efficacy of RVES-PD-PTX, VES-PD-PTX and free PTX in B16F10 tumor bearing C57Bl/6 mice. Graphical representation of (A) tumor volume vs. days during treatment, (B) Measurement of body weight during treatment, and (C) The average weight of tumors

isolated from various treatment groups. (D) Representative tumors isolated from animals' post treatment, (E) Measurement of caspase 3/7 levels in tumor homogenates. The significance between the groups was evaluated by one-way analysis of variance, where ***$p < 0.001$, **$p < 0.01$ and *$p < 0.05$.

In the tumor volume reduction study, it was observed that the treatment of tumor bearing mice with VES-PD-PTX and RVES-PD-PTX reduced their tumor volume more effectively compared to the treatment with free PTX (Figure 4.12 (A). There was significant difference ($p<0.05$) in the tumor volumes between VES-PD-PTX and RVES-PD-PTX treatment, the latter being more effective therapeutically. The data clearly supports the in vitro study results and proved that the dendrimer macromolecules, functionalized with PEG, VES, and octa-arginine could deliver the therapeutic cargo effectively to the tumor, and produce anticancer effect. Moreover, no significant change in body weight (Figure 4.12 B) was observed throughout the study, which proved that the tested formulations are safe in mice. The average weight of isolated tumors obtained after sacrificing the animals and tumor morphology are shown in Figure 4.12 (C) and (D). The data clearly demonstrated the superior therapeutic effect of RVES-PD-PTX compared to VES-PD-PTX. Moreover, the expression level of caspase 3/7 in isolated tumors were analyzed, and the data was represented in Figure 4.12 (E). The result demonstrated that the expression of caspase 3/7 was upregulated in all the treatment groups compared to PBS. The RVES-PD-PTX treatment caused highest upregulation of the apoptotic marker in tumors. Nest, TUNEL assay was performed to determine the extent of apoptosis induced in tumors following treatment with free PTX, VES-PD-PTX, and RVES-PD-PTX. As shown in Figure 4.13, the presence of apoptotic cells was significantly higher in tumor sections isolated from RVES-PD-PTX-treated groups as indicated by increased green fluorescence.

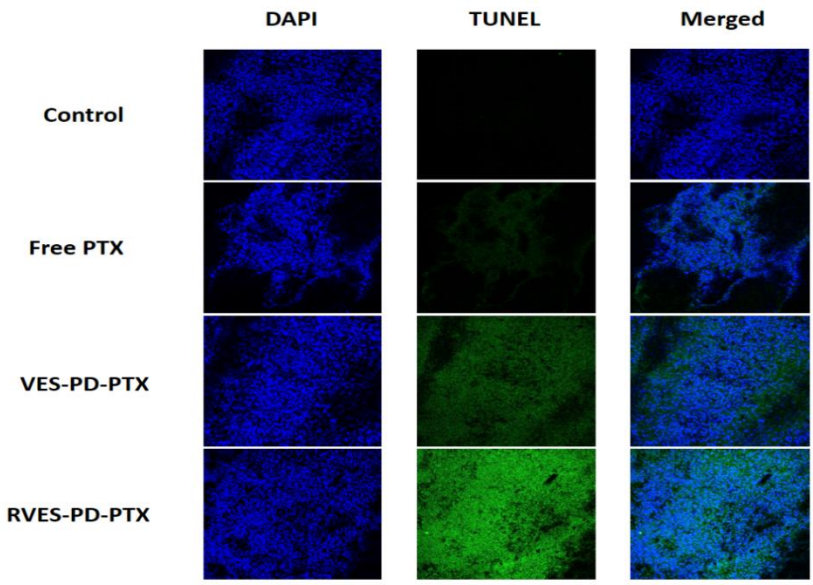

Figure 4.13. Determination of apoptosis by TUNEL assay. The treated tumor sections are visualized under fluorescence microscope with 20X magnification.

4.5 Conclusion

A multifunctional generation 4 PAMAM dendrimer nano-construct has been prepared by conjugating VES, PEG, and a cell penetrating peptide, octa-arginine at approximate molar ratio of dendrimer: VES: PEG: octa-arginine: 1: 3.4: 8.0: 2.4. VES, PEG, and octa-arginine was envisioned to improve solubility of encapsulated hydrophobic drug, prolong systemic circulation, and improve intracellular translocation of the macromolecule loaded with the chemotherapeutic agent, paclitaxel, respectively. The nano-scaffold, RVES-PD-PTX was able to translocate efficiently through the cancer cells in monolayers and spheroids and the internalization was via majorly via micropinocytosis, mediated by octa-arginine. The increased translocation of dendrimers brought loaded PTX intracellularly to a high concentration, which improved the cytotoxicity. RVES-PD-PTX inhibited the growth of A549 spheroids as well as the murine melanoma tumors by inducing apoptosis. Overall, the developed multifunctional dendrimer system significantly improved the therapeutic efficacy of

PTX, and therefore, could be utilized as a promising chemotherapeutic agent to achieve PTX-mediated superior anticancer effect to treat solid tumors.

References

Abu-Fayyad, Ahmed, Fathy Behery, Asmaa A Sallam, Saeed Alqahtani, Hassan Ebrahim, Khalid A El Sayed, Amal Kaddoumi, Paul W Sylvester, Jennifer L Carroll, and James A Cardelli. 2015. "PEGylated γ-tocotrienol isomer of vitamin E: Synthesis, characterization, in vitro cytotoxicity, and oral bioavailability." *European Journal of Pharmaceutics and Biopharmaceutics* no. 96:185-195.

Agashe, Hrushikesh B, Anil Kumar Babbar, Sanyog Jain, Rakesh Kumar Sharma, Anil Kumar Mishra, Abhay Asthana, Minakshi Garg, Tathagata Dutta, and Narendra Kumar Jain. 2007. "Investigations on biodistribution of technetium-99m-labeled carbohydrate-coated poly (propylene imine) dendrimers." *Nanomedicine: Nanotechnology, Biology and Medicine* no. 3 (2):120-127.

Au, Kin Man, Yuanzeng Min, Xi Tian, Longzhen Zhang, Virginia Perello, Joseph M Caster, and Andrew Z Wang. 2015. "Improving cancer chemoradiotherapy treatment by dual controlled release of wortmannin and docetaxel in polymeric nanoparticles." *ACS nano* no. 9 (9):8976-8996.

Barrière, Clément, Virginie Latour, Pierre Fau, Anne-Marie Caminade, and Cédric-Olivier Turrin. 2012. "Low generation PEGylated phosphorus-containing dendrons with phosphonate anchors." *Tetrahedron Letters* no. 53 (15):1908-1911.

Bhatt, Himanshu, Sri Vishnu Kiran Rompicharla, Balaram Ghosh, and Swati Biswas. 2019. "α-tocopherol succinate-anchored PEGylated Poly (amidoamine) dendrimer for the delivery of paclitaxel: assessment of in vitro and in vivo therapeutic efficacy." *Molecular pharmaceutics* no. 16 (4):1541-1554.

Biswas, Swati, Pranali P Deshpande, Federico Perche, Namita S Dodwadkar, Shailendra D Sane, and Vladimir P Torchilin. 2013. "Octa-arginine-modified pegylated

liposomal doxorubicin: an effective treatment strategy for non-small cell lung cancer." *Cancer letters* no. 335 (1):191-200.

Chandrasekharan, Prashant, Dipak Maity, Cai Xian Yong, Kai-Hsiang Chuang, Jun Ding, and Si-Shen Feng. 2011. "Vitamin E (D-alpha-tocopheryl-co-poly (ethylene glycol) 1000 succinate) micelles-superparamagnetic iron oxide nanoparticles for enhanced thermotherapy and MRI." *Biomaterials* no. 32 (24):5663-5672.

Chen, Hui-Ting, Michael F Neerman, Alan R Parrish, and Eric E Simanek. 2004. "Cytotoxicity, hemolysis, and acute in vivo toxicity of dendrimers based on melamine, candidate vehicles for drug delivery." *Journal of the American Chemical Society* no. 126 (32):10044-10048.

Costa, Elisabete C., André F. Moreira, Duarte de Melo-Diogo, Vítor M. Gaspar, Marco P. Carvalho, and Ilídio J. Correia. 2016. "3D tumor spheroids: an overview on the tools and techniques used for their analysis." *Biotechnology Advances* no. 34 (8):1427-1441. doi: https://doi.org/10.1016/j.biotechadv.2016.11.002.

D'Emanuele, Antony, and David Attwood. 2005. "Dendrimer–drug interactions." *Advanced drug delivery reviews* no. 57 (15):2147-2162.

Dehshahri, Ali, and Hossein Sadeghpour. 2015. "Surface decorations of poly(amidoamine) dendrimer by various pendant moieties for improved delivery of nucleic acid materials." *Colloids and Surfaces B: Biointerfaces* no. 132:85-102. doi: https://doi.org/10.1016/j.colsurfb.2015.05.006.

Dissanayake, Shama, William A Denny, Swarna Gamage, and Vijayalekshmi Sarojini. 2017. "Recent developments in anticancer drug delivery using cell penetrating and tumor targeting peptides." *Journal of Controlled Release* no. 250:62-76.

Duhem, Nicolas, Fabienne Danhier, and Véronique Préat. 2014. "Vitamin E-based nanomedicines for anti-cancer drug delivery." *Journal of Controlled Release* no. 182:33-44.

Emami, Jaber, Mahboubeh Rezazadeh, Mahboubeh Rostami, Farshid Hassanzadeh, Hojjat Sadeghi, Abolfazl Mostafavi, Mohsen Minaiyan, and Afsaneh Lavasanifar. 2015. "Co-delivery of paclitaxel and α-tocopherol succinate by novel chitosan-based polymeric micelles for improving micellar stability and efficacious combination therapy." *Drug development and industrial pharmacy* no. 41 (7):1137-1147.

Gill, Kanwaldeep K, Amal Kaddoumi, and Sami Nazzal. 2012. "Mixed micelles of PEG2000-DSPE and vitamin-E TPGS for concurrent delivery of paclitaxel and parthenolide: enhanced chemosenstization and antitumor efficacy against non-small cell lung cancer (NSCLC) cell lines." *European journal of pharmaceutical sciences* no. 46 (1-2):64-71.

Golombek, Susanne K, Jan-Niklas May, Benjamin Theek, Lia Appold, Natascha Drude, Fabian Kiessling, and Twan Lammers. 2018. "Tumor targeting via EPR: Strategies to enhance patient responses." *Advanced drug delivery reviews* no. 130:17-38.

Gruber, Julia, Katrin Staniek, Christopher Krewenka, Rudolf Moldzio, Anjan Patel, Stefan Böhmdorfer, Thomas Rosenau, and Lars Gille. 2014. "Tocopheramine succinate and tocopheryl succinate: mechanism of mitochondrial inhibition and superoxide radical production." *Bioorganic & medicinal chemistry* no. 22 (2):684-691.

Guo, Yuanyuan, Jun Luo, Songwei Tan, Ben Oketch Otieno, and Zhiping Zhang. 2013. "The applications of Vitamin E TPGS in drug delivery." *European Journal of Pharmaceutical Sciences* no. 49 (2):175-186.

Ihre, Henrik R, Omayra L Padilla De Jesús, Francis C Szoka, and Jean MJ Fréchet. 2002. "Polyester dendritic systems for drug delivery applications: design, synthesis, and characterization." *Bioconjugate chemistry* no. 13 (3):443-452.

Jevprasesphant, R, J Penny, R Jalal, D Attwood, NB McKeown, and A D'emanuele. 2003. "The influence of surface modification on the cytotoxicity of PAMAM dendrimers." *International journal of pharmaceutics* no. 252 (1-2):263-266.

Kaminskas, Lisa M, Ben J Boyd, and Christopher JH Porter. 2011. "Dendrimer pharmacokinetics: the effect of size, structure and surface characteristics on ADME properties." *Nanomedicine* no. 6 (6):1063-1084.

Kesharwani, Prashant, Virendra Gajbhiye, Rakesh K Tekade, and Narendra K Jain. 2011. "Evaluation of dendrimer safety and efficacy through cell line studies." *Current drug targets* no. 12 (10):1478-1497.

Kesharwani, Prashant, Keerti Jain, and Narendra Kumar Jain. 2014. "Dendrimer as nanocarrier for drug delivery." *Progress in Polymer Science* no. 39 (2):268-307.

Kitagishi, Hiroaki, Fumihiko Chai, Shigeru Negi, Yukio Sugiura, and Koji Kano. 2015. "Supramolecular intracellular delivery of an anionic porphyrin by octaarginine-conjugated per-O-methyl-β-cyclodextrin." *Chemical Communications* no. 51 (12):2421-2424.

Kulhari, Hitesh, Deep Pooja, Shweta Shrivastava, Madhusudana Kuncha, VGM Naidu, Vipul Bansal, Ramakrishna Sistla, and David J Adams. 2016. "Trastuzumab-grafted PAMAM dendrimers for the selective delivery of anticancer drugs to HER2-positive breast cancer." *Scientific reports* no. 6:23179.

Kumari, Preeti, Sri Vishnu Kiran Rompicharla, Omkara Swami Muddineti, Balaram Ghosh, and Swati Biswas. 2018. "Transferrin-anchored poly (lactide) based micelles to improve anticancer activity of curcumin in hepatic and cervical cancer cell monolayers

and 3D spheroids." *International journal of biological macromolecules* no. 116:1196-1213.

Labieniec-Watala, Magdalena, and Cezary Watala. 2015. "PAMAM dendrimers: destined for success or doomed to fail? Plain and modified PAMAM dendrimers in the context of biomedical applications." *Journal of pharmaceutical sciences* no. 104 (1):2-14.

Li, Yuhuan, Robert J Lee, Kongtong Yu, Ye Bi, Yuhang Qi, Yating Sun, Yujing Li, Jing Xie, and Lesheng Teng. 2016. "Delivery of siRNA using lipid nanoparticles modified with cell penetrating peptide." *ACS applied materials & interfaces* no. 8 (40):26613-26621.

Liu, Chang, Qi Lan, Wei He, Changlu Nie, Chunjuan Zhang, Tonghua Xu, Tongying Jiang, and Siling Wang. 2017. "Octa-arginine modified lipid emulsions as a potential ocular delivery system for disulfiram: A study of the corneal permeation, transcorneal mechanism and anti-cataract effect." *Colloids and Surfaces B: Biointerfaces* no. 160:305-314. doi: https://doi.org/10.1016/j.colsurfb.2017.08.037.

Liu, Yayuan, Ling Mei, Qianwen Yu, Chaoqun Xu, Yue Qiu, Yuting Yang, Kairong Shi, Qianyu Zhang, Huile Gao, and Zhirong Zhang. 2015. "Multifunctional tandem peptide modified paclitaxel-loaded liposomes for the treatment of vasculogenic mimicry and cancer stem cells in malignant glioma." *ACS applied materials & interfaces* no. 7 (30):16792-16801.

Malik, Noeen, R Wiwattanapatapee, R Klopsch, K Lorenz, H Frey, JW Weener, EW Meijer, W Paulus, and R Duncan. 2000. "Dendrimers:: Relationship between structure and biocompatibility in vitro, and preliminary studies on the biodistribution of 125I-labelled polyamidoamine dendrimers in vivo." *Journal of Controlled Release* no. 65 (1-2):133-148.

Meier, Oliver, Karin Boucke, Silvija Vig Hammer, Stephan Keller, Robert P Stidwill, Silvio Hemmi, and Urs F Greber. 2002. "Adenovirus triggers macropinocytosis and endosomal leakage together with its clathrin-mediated uptake." *The Journal of cell biology* no. 158 (6):1119-1131.

Min, Yuanzeng, Joseph M Caster, Michael J Eblan, and Andrew Z Wang. 2015. "Clinical translation of nanomedicine." *Chemical reviews* no. 115 (19):11147-11190.

Muddineti, Omkara Swami, Balaram Ghosh, and Swati Biswas. 2017. "Current trends in the use of vitamin E-based micellar nanocarriers for anticancer drug delivery." *Expert Opinion on Drug Delivery* no. 14 (6):715-726. doi: 10.1080/17425247.2016.1229300.

Muddineti, Omkara Swami, Preeti Kumari, Balaram Ghosh, and Swati Biswas. 2018. "Transferrin-modified vitamin-E/lipid based polymeric micelles for improved tumor targeting and anticancer effect of curcumin." *Pharmaceutical research* no. 35 (5):97.

Muddineti, Omkara Swami, Preeti Kumari, Balaram Ghosh, Vladimir P Torchilin, and Swati Biswas. 2017. "d-α-Tocopheryl succinate/Phosphatidyl ethanolamine conjugated amphiphilic polymer-based Nanomicellar system for the efficient delivery of curcumin and to overcome multiple drug resistance in cancer." *ACS applied materials & interfaces* no. 9 (20):16778-16792.

Nam, Joung-Pyo, Kyeong-Jae Lee, Joung-Woo Choi, Chae-Ok Yun, and Jae-Woon Nah. 2015. "Targeting delivery of tocopherol and doxorubicin grafted-chitosan polymeric micelles for cancer therapy: In vitro and in vivo evaluation." *Colloids and Surfaces B: Biointerfaces* no. 133:254-262.

Neuzil, Jiri, ZHAO Ming, Georg Ostermann, Martin Sticha, Nina Gellert, Christian Weber, John W Eaton, and Ulf T Brunk. 2002. "α-Tocopheryl succinate, an agent with

in vivo anti-tumour activity, induces apoptosis by causing lysosomal instability." *Biochemical Journal* no. 362 (3):709-715.

Padilla De Jesús, Omayra L, Henrik R Ihre, Lucie Gagne, Jean MJ Fréchet, and Francis C Szoka. 2002. "Polyester dendritic systems for drug delivery applications: in vitro and in vivo evaluation." *Bioconjugate chemistry* no. 13 (3):453-461.

Palmerston Mendes, Livia, Jiayi Pan, and Vladimir P. Torchilin. 2017. "Dendrimers as Nanocarriers for Nucleic Acid and Drug Delivery in Cancer Therapy." *Molecules* no. 22 (9):1401.

Prabhu, Rashmi H, Vandana B Patravale, and Medha D Joshi. 2015. "Polymeric nanoparticles for targeted treatment in oncology: current insights." *International journal of nanomedicine* no. 10:1001.

Prasad, Kedar N, Bipin Kumar, Xiang-Dong Yan, Amy J Hanson, and William C Cole. 2003. "α-tocopheryl succinate, the most effective form of vitamin E for adjuvant cancer treatment: a review." *Journal of the American College of Nutrition* no. 22 (2):108-117.

Roberts, Jeanette C, Mahesh K Bhalgat, and Richard T Zera. 1996. "Preliminary biological evaluation of polyamidoamine (PAMAM) StarburstTM dendrimers." *Journal of Biomedical Materials Research: An Official Journal of The Society for Biomaterials and The Japanese Society for Biomaterials* no. 30 (1):53-65.

Rompicharla, Sri Vishnu Kiran, Preeti Kumari, Balaram Ghosh, and Swati Biswas. 2018a. "Octa-arginine modified poly (amidoamine) dendrimers for improved delivery and cytotoxic effect of paclitaxel in cancer." *Artificial cells, nanomedicine, and biotechnology* no. 46 (sup2):847-859.

Rompicharla, Sri Vishnu Kiran, Preeti Kumari, Balaram Ghosh, and Swati Biswas. 2018b. "Octa-arginine modified poly (amidoamine) dendrimers for improved delivery

and cytotoxic effect of paclitaxel in cancer." *Artificial cells, nanomedicine, and biotechnology*:1-13.

Rompicharla, Sri Vishnu Kiran, Preeti Kumari, Balaram Ghosh, and Swati Biswas. 2018c. "Octa-arginine modified poly(amidoamine) dendrimers for improved delivery and cytotoxic effect of paclitaxel in cancer." *Artificial Cells, Nanomedicine, and Biotechnology* no. 46 (sup2):847-859. doi: 10.1080/21691401.2018.1470527.

Ruoslahti, Erkki. 2017. "Tumor penetrating peptides for improved drug delivery." *Advanced drug delivery reviews* no. 110:3-12.

Sethi, Manish, Rohit Sukumar, Shrirang Karve, Michael E Werner, Edina C Wang, Dominic T Moore, Sonya R Kowalczyk, Liangfang Zhang, and Andrew Z Wang. 2014. "Effect of drug release kinetics on nanoparticle therapeutic efficacy and toxicity." *Nanoscale* no. 6 (4):2321-2327.

Sparreboom, Alex, Olaf van Tellingen, Willem J Nooijen, and Jos H Beijnen. 1996. "Nonlinear pharmacokinetics of paclitaxel in mice results from the pharmaceutical vehicle Cremophor EL." *Cancer research* no. 56 (9):2112-2115.

Swanson, Joel A, and Colin Watts. 1995. "Macropinocytosis." *Trends in cell biology* no. 5 (11):424-428.

Tan, Songwei, Chenming Zou, Wei Zhang, Mingxing Yin, Xueqin Gao, and Qing Tang. 2017. "Recent developments in d-α-tocopheryl polyethylene glycol-succinate-based nanomedicine for cancer therapy." *Drug Delivery* no. 24 (1):1831-1842.

Tekade, Rakesh Kumar, Tathagata Dutta, Abhishek Tyagi, Alok Chandra Bharti, Bhudev Chandra Das, and Narendra Kumar Jain. 2008. "Surface-engineered dendrimers for dual drug delivery: a receptor up-regulation and enhanced cancer targeting strategy." *Journal of drug targeting* no. 16 (10):758-772.

Tekade, Rakesh Kumar, Palanirajan Vijayaraj Kumar, and Narendra Kumar Jain. 2008. "Dendrimers in oncology: an expanding horizon." *Chemical reviews* no. 109 (1):49-87.

Uchida, Masaki, Hisanori Kosuge, Masahiro Terashima, Deborah A Willits, Lars O Liepold, Mark J Young, Michael V McConnell, and Trevor Douglas. 2011. "Protein cage nanoparticles bearing the LyP-1 peptide for enhanced imaging of macrophage-rich vascular lesions." *ACS nano* no. 5 (4):2493-2502.

van Oppen, Lisanne M. P. E., Jan Pille, Christiaan Stuut, Marleen van Stevendaal, Lisa N. van der Vorm, Jan A. M. Smeitink, Werner J. H. Koopman, Peter H. G. M. Willems, Jan C. M. van Hest, and Roland Brock. 2019. "Octa-arginine boosts the penetration of elastin-like polypeptide nanoparticles in 3D cancer models." *European Journal of Pharmaceutics and Biopharmaceutics* no. 137:175-184. doi: https://doi.org/10.1016/j.ejpb.2019.02.010.

Wadia, Jehangir S, Radu V Stan, and Steven F Dowdy. 2004. "Transducible TAT-HA fusogenic peptide enhances escape of TAT-fusion proteins after lipid raft macropinocytosis." *Nature medicine* no. 10 (3):310.

Wolinsky, Jesse B, and Mark W Grinstaff. 2008. "Therapeutic and diagnostic applications of dendrimers for cancer treatment." *Advanced drug delivery reviews* no. 60 (9):1037-1055.

Yamada, Yuma, Masahiro Hashida, and Hideyoshi Harashima. 2015. "Hyaluronic acid controls the uptake pathway and intracellular trafficking of an octaarginine-modified gene vector in CD44 positive-and CD44 negative-cells." *Biomaterials* no. 52:189-198.

Yu, Weiping, Qiao Yin Liao, Feras M Hantash, Bob G Sanders, and Kimberly Kline. 2001. "Activation of extracellular signal-regulated kinase and c-Jun-NH2-terminal kinase but not p38 mitogen-activated protein kinases is required for RRR-α-tocopheryl

succinate-induced apoptosis of human breast cancer cells." *Cancer research* no. 61 (17):6569-6576.

Chapter 5

Comparison of Paclitaxel loaded dendrimers

5.1 Introduction

In the present research work, it was aimed to deliver a chemotherapeutic agent, paclitaxel (PTX) whose therapeutic potential is limited by its poor physicochemical properties, by loading into PAMAM dendrimers physically. PAMAM dendrimers were modified with α-TOS to improve the therapeutic potential of PTX intracellularly. Furthermore, PAMAM dendrimers were modified on surface with Transferrin, which actively targets the Transferrin uptake receptors overexpressed on the surface of cancer cells. Further, to improve the delivery of PTX intracellularly, PAMAM dendrimers are modified on surface with a cell penetrating peptide (CPP), octa-arginine (R8). PEGylation was performed to reduce the toxicity of positively charged PAMAM dendrimers and extend the blood circulation time. The dendrimers were fluorescently labelled for experiments which need fluorescence measurement. The proton NMR spectra of each dendrimer nano-conjugates confirmed the successful conjugation of different functional moieties. Moreover, the GPC analysis revealed an approximate number of molecules attached per PAMAM dendrimer molecule. The physico-chemical characterization confirmed the formation of conjugates. The PTX-loaded dendrimer conjugates were evaluated in monolayers and 3D spheroids to assess the therapeutic potential of PTX. The antitumor efficacy of free PTX and various PTX-loaded dendrimers was successfully evaluated in tumor bearing xenografted mice. The developed dendrimer-based formulations are non-specific for any cancer. Hence, various cell lines like MDA-MB231, HeLa and A549 were used to test therapeutic efficacy of developed formulations.

5.2 Comparison of particle size, zeta potential, EE%, DL% and *in-vitro* release

The particle size, zeta potential, EE% and DL% of the optimized formulations of G4-PEG-PTX, G4-TOS-PEG-PTX, G4-TOS-PEG-Tf-PTX, and RVES-PD-PTX are given

in the Table 5.1. The particle size was increased after each successful conjugation over the surface of dendrimer. The PTX loading was found to be increased in case of G4-TOS-PEG because TOS helped in the solubilization of PTX while drug loading was found to be decreased in case of G4-TOS-PEG-Tf-PTX and RVES-PD-PTX which could be due to steric hindrance of Tf or octa-arginine on the surface that limits the access of PTX into the interior dendrimer cavity. The increase in %DL in the case of G4-TOS-PEG could be due to the presence of α-TOS on the surface of the dendrimer, which could solubilize PTX and facilitate entrapment of PTX in the dendrimer. Further, the surface charge was reduced after each successful conjugation over the dendrimer surface due to the non-ionic nature of PEG and anionic nature of α-TOS but in case of RVES-PD-PTX the zeta potential was increased due to cationic nature of octa-arginine.

Table 5.1. Physical characteristics of PTX loaded dendrimer conjugates

Physical characteristics	G4-PEG-PTX	G4-TOS-PEG-PTX	G4-TOS-PEG-Tf-PTX	RVES-PD-PTX
Particle size (nm)	15.39 ± 0.06	31.19 ± 0.07	37.91 ± 0.069	38.14 ± 0.053
PDI	0.233 ± 0.104	0.150 ± 0.092	0.266 ± 0.006	0.197 ± 0.008
Zeta potential (mV)	10.4 ± 1.11	5.32 ± 0.37	2.44 ± 0.31	9.58 ± 0.42
Entrapment efficiency (%)	65.79 ± 3.11	78.33 ± 2.81	71.18 ± 2.38	73.58 ± 2.27
Drug loading (%)	10.49 ± 1.31	14.93 ± 1.64	13.04 ± 1.29	12.48 ± 1.75

In-vitro drug release study revealed that free PTX was released faster (about 99%) within 8 h from PTX solution compared to dendrimer formulations. In contrast, G4-PEG-PTX and G4-TOS-PEG-PTX showed ~ 82% and ~ 70% release of PTX over 48 h. G4-TOS-PEG-Tf-PTX demonstrated PTX release of ~ 62.45% over 48 h. RVES-PD showed PTX release of ~ 51% in 48 h. The reason for the controlled release in each dendrimer conjugate is likely due to the attachment of α-TOS, PEG, Tf and octa-

arginine on the surface of the dendrimer. These attachments made the release path longer for the PTX, as well the partially hydrophobic coat over the dendrimers decreases the diffusion of PTX molecules from the dendrimeric cavity.

5.3 Comparison of cell uptake, cytotoxicity, apoptosis and growth inhibition of spheroids

The α-TOS or Tf or acta-arginine conjugation on the dendrimer surface facilitated the nanocarriers uptake, resulting in an increase in the internalized fluorescence, as indicated by the geometric mean of fluorescence. As shown in Figure 2.8, G4-TOS-PEG-PTX showed the highest cell death by decreasing the cell viability to 37.21 ± 2.60% compared to 49.66 ± 2.43% following PTX-loaded G4-PEG and 66.85 ± 3.28% following free PTX treatment in MDA MB231 at the 24 h time point. At the 48 h time point, the cell viability of G4-TOS-PEG-PTX, G4-PEG-PTX, and free PTX was further reduced to 18.33 ± 2.19, 40.66 ± 2.03, and 60.45 ± 2.85%, respectively, in MDA MB231 cells, indicating a time dependent decrease in cellular viability. Treatment with G4-TOS-PEG-Tf-PTX as well as G4-TOS-PEG-PTX at paclitaxel concentration of 50 µg/mL showed cell viability of 39.12±2.6 and 52.66 ± 2.43 %, respectively following 24 h treatment as compared to free PTX (69.58±3.28%). The further reduction in cell viability of paclitaxel loaded actively targeted G4-TOS-PEG-Tf, PTX loadedpassively targeted G4-TOS-PEG and free paclitaxel was found to be 12.29±2.23%, 20.69±2.39%, and 33.85±2.18% respectively after 48 h. The RVES-PD-PTX, VES-PD-PTX, and free PTX demonstrated cell viability of 32.21 ± 2.58, 45.66 ± 2.34, and 61.85 ± 2.98 % respectively at 24 h at the PTX concentration of 50 µg/mL. Further decrease in cell viability was observed with RVES-PD-PTX (4.92 ± 2.28%) as compared to VES-PD-PTX (20.96 ± 2.69 %) and free PTX (28.58 ± 2.36 %) at the PTX concentration of 50 µg/mL at 48 h. Signs of a late apoptosis of 11.6 ± 2.9% (Figure 2.9 B) were quantified

in cells treated with free drug; whereas PTX-loaded G4-PEG and G4-TOS-PEG induced a late apoptosis of 27.3 ± 1.6 (Figure 2.9 C) and 40.7 ± 2.5% (Figure 2.9 D), respectively. As shown in Figure 3.9, free PTX induced apoptosis of 15.2 ± 2.4 %, whereas targeted dendrimer (G4-TOS-PEG-PTX-Tf) and nontargeted (G4-TOS-PEG-PTX) induced the total apoptosis of 56.3 ± 1.4 and 37.3 ± 2.2 %, respectively. As shown in Figure 4.8, the free PTX induced apoptosis of 26.9 ± 1.6 %, whereas RVES-PD-PTX and VES-PD-PTX induced the total apoptosis of 49.85 ± 2.14 and 36.51 ± 2.28 %, respectively. The higher level of cytotoxicity and apoptosis compared to free PTX was due to the improved internalization of the different nanocarriers by attaching various ligands over the dendrimer surface, which increased the accumulation of PTX inside the cells. The mean diameters of spheroids were found to be 1012.43 ± 40.81, 732.34 ± 50.10, 527.14 ± 20.13, and 373.20 ± 11.61 μm for the control, free PTX, PTX-loaded G4-PEG, and PTX-loaded G4-TOS-PEG, respectively, at 9 days. The data are shown as a line graph in Figure 2.12B. The average diameter of spheroids was found to be 994.34 ± 20.18, 820.34 ± 23.51, 589.41 ± 20.56, and 415.94 ± 18.51 μm for control group, free paclitaxel group, PTX loaded non-targeted G4-TOS-PEG group and paclitaxel loaded targeted G4-TOS-PEG-Tf group treatment, respectively at the end of 6 days. These data are shown in the line graph plotted between the diameters versus days as shown in Figure 3.12 (B). The average diameter of spheroids was found to be 990.34 ± 23.2, 852.34 ± 25.58, 569.41 ± 21.35, and 390.94 ± 18.15 μm for control, free PTX, VES-PD-PTX and RVES-PD-PTX treatment, respectively at the end of 6 days. These data are shown in the line graph plotted between the diameters versus days as shown in Figure 4.10 (B). α-TOS or Tf or octa-arginine facilitates the PTX to accumulate more in the 3D spheroids, which leads to the inhibition of the progression of their growth. Moreover, the 3D spheroidal growth inhibition study proves that the

synthesized multifunctional dendrimer conjugates get internalized efficiently into the 3D spheroids over a period of time and increases the therapeutic action of PTX. Therefore, it can be concluded, that the synthesized multifunctional dendrimers have the potential to efficiently suppress the tumor growth in vivo based on the fact that the multicellular spheroids mimic the tumor microenvironment.

5.4 Comparison of tumor volume reduction in B16F10 tumor-bearing C57Bl/6 mice

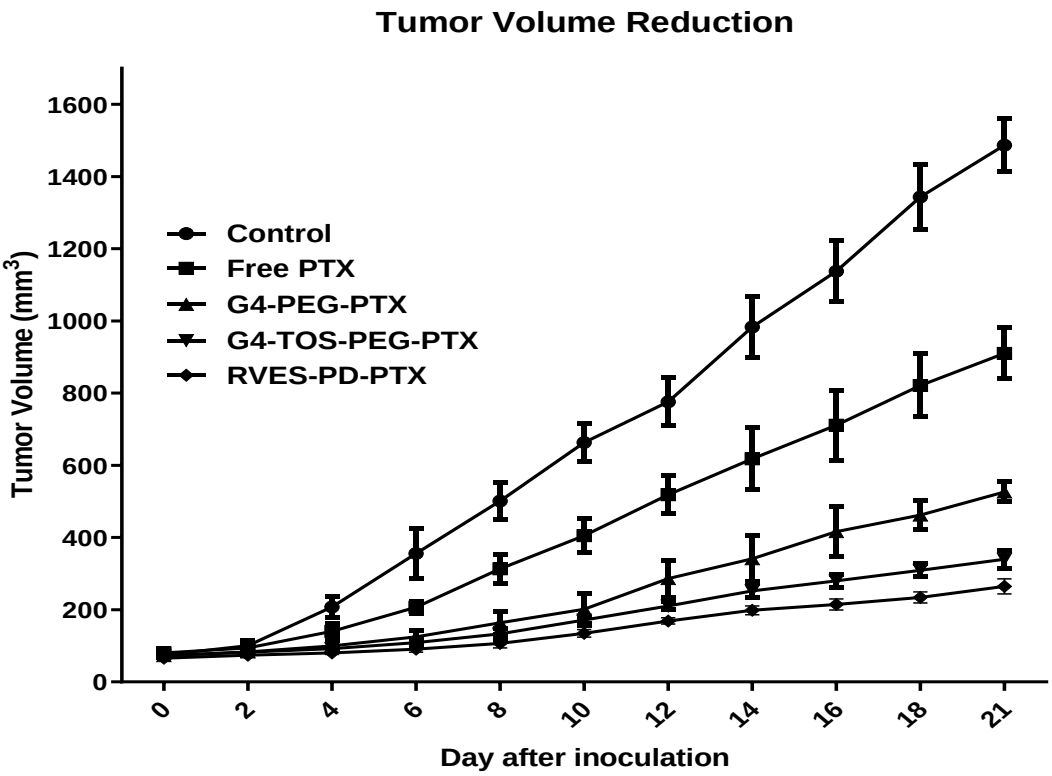

Figure 5.1 Graph representing the tumor volume reduction of different dendrimer based formulations over time.

In the tumor inhibition study, combined treatment of the α-TOS-anchored dendrimer and PTX suppressed the growth of the tumor to a significantly higher extent (more than 4-fold) compared to the control (no treatment), free PTX, as well as G4-PEG-PTX (Figure 5.1). α-TOS could inhibit the tumor volume suppression by various proven mechanisms. There was significant difference ($p<0.05$) in the tumor volumes between

VES-PD-PTX and RVES-PD-PTX treatment, the latter being more effective therapeutically (Figure 5.1 and Figure 4.12). The data clearly supports the in vitro study results and proved that the dendrimer macromolecules, functionalized with PEG, VES, and octa-arginine could deliver the therapeutic cargo effectively to the tumor, and produce anticancer effect. The possible reason could be more tumor accumulation, biodistribution, and cytotoxicity of the nanosized dendrimer conjugate by passive targeting (EPR effects).

5.5 Conclusion

The above-mentioned *in vivo* studies of all of the dendrimer based nanocarriers revealed that RVES-PD-PTX is relatively better in terms of providing more tumor volume reduction and thereby improving anti-cancer activity of PTX. However, all of the three dendrimer based nanocarriers have showed better performance compared to conventional formulations of the drug. Yet it is expected that the synthesized Tf anchored dendrimer conjugate G4-TOS-PEG-Tf will show better performance than any other developed conjugates in *in vivo* studies which needs to be further explored in future because ligand mediated nanocarriers are up taken in to the tumor cells by active targeting mechanism.

Chapter 6

Conclusion

6. Conclusion

The use of chemotherapeutic agents is limited clinically due to their poor pharmacokinetic properties, toxicity and stability issues although they are potent. Therefore, there is need to develop delivery system capable of delivering drug efficiently. Various polymers have been identified as drug delivery nanocarriers but lack of well-defined chemical structures is a major drawback associated with them. Hence, nanotechnology came as emerging field to overcome these problems and to improve physicochemical and biological properties of chemotherapeutic agents by increasing drug solubilisation, bioavailability, and drug targeting potential. PAMAM dendrimers have taken considerable attention in the field of drug delivery to achieve controlled drug delivery due to their well-defined architecture, size and monodispersity. PAMAM dendrimers have been explored to deliver anti-cancer agents either by physical entrapment in the internal cavities or by covalently conjugating them to the wide variety and number of functional groups they offer.

The current study was aimed to deliver a chemotherapeutic agent, paclitaxel (PTX) whose therapeutic potential is limited by its poor physicochemical properties, by loading into PAMAM dendrimers physically. PAMAM dendrimers were modified with α-TOS to improve the therapeutic potential of PTX intracellularly. Furthermore, PAMAM dendrimers were modified on surface with Transferrin, which actively targets the Transferrin uptake receptors overexpressed on the surface of cancer cells. Further, to improve the delivery of PTX intracellularly, PAMAM dendrimers are modified on surface with a cell penetrating peptide (CPP), octa-arginine (R8). PEGylation was performed to reduce the toxicity of positively charged PAMAM dendrimers and extend the blood circulation time. The dendrimers were fluorescently labelled for experiments which need fluorescence measurement. The proton NMR spectra of each dendrimer

nano-conjugates confirmed the successful conjugation of different functional moieties. Moreover, the GPC analysis revealed an approximate number of molecules attached per PAMAM dendrimer molecule. The physico-chemical characterization confirmed the formation of conjugates. The PTX-loaded dendrimer conjugates were evaluated in monolayers and 3D spheroids to assess the therapeutic potential of PTX. The antitumor efficacy of free PTX and various PTX-loaded dendrimers was successfully evaluated in tumor bearing xenografted mice. The developed dendrimer-based formulations are non-specific for any cancer. Hence, various cell lines like MDA-MB231, HeLa and A549 were used to test therapeutic efficacy of developed formulations.

In the first objective of the work, α-TOS was attached over the surface of PAMAM dendrimer to deliver PTX intracellularly to triple negative breast cancer (MDA MB231) cells. The synthesized nano-conjugates was found to be non-toxic to red blood cells in haemolytic assay. The cellular internalization and association of G4-TOS-PEG in vitro was significantly higher than the unmodified conjugate (G4-PEG) as evaluated by confocal microscopy and flow cytometry. The cytotoxicity results revealed that G4-TOS-PEG dendrimer conjugates showed maximum cytotoxicity to cancer cells in comparison to free drug after 24 h and 48 h treatment. Further, the G4-TOS-PEG-PTX induced higher apoptosis in MDA MB231 cells which can be attributed to the greater cellular uptake and hence more availability of drug in the cells. Moreover, the dendrimer conjugates were evaluated in 3D multicellular MDA MB231 spheroids. The ability of α-TOS to internalize deeper into the tissues has resulted in increased permeation, uptake, growth inhibition, and cytotoxicity of TOS-modified dendrimer conjugates over G4-PEG-PTX and free PTX in the spheroid model. In animal experiments, the strong localization efficiency of G4-TOS-PEG could be due to the efficient permeation of the α-TOS-anchored nanocarriers into the interstitial extracellular matrix as well as efficient cellular

internalization. In the tumor inhibition study, combined treatment of the α-TOS-anchored dendrimer and PTX suppressed the growth of the tumor to a significantly higher extent compared to the control free PTX and G4-PEG-PTX. The presence of apoptotic bodies was significantly higher tumor sections following G4-TOS-PEG treatment as compared to the sections of other treatment groups.

In the second objective of the work, Transferrin, a ligand has been tagged on surface of α-TOS modified PAMAM dendrimers to actively target the cancer cells overexpressing Transferrin receptors (HeLa). The Tf receptors are overexpressed in the HeLa cells. Hence, HeLa cells were used to test our developed formulations by doing various cell-based studies. GPC results revealed an attachment of around 4.19 molecules of Transferrin per PAMAM dendrimer. The active targeting of cancer cells by Transferrin has significantly improved the cellular uptake and cytotoxicity caused by G4-TOS-PEG-PTX-Tf over G4-TOS-PEG-PTX, G4-PEG-PTX and free PTX. Saturation of Transferrin receptors by excess free Transferrin revealed that the uptake mechanism was receptor mediated. Also, due to the cationic nature of the dendrimer conjugates, adsorptive endocytosis also adds to the uptake mechanisms. Moreover, the evaluation in multicellular HeLa cell spheroids resulted in Transferrin tagged conjugates being more effective in therapeutic outcome by inhibition of spheroid growth and cell killing. The designed Transferrin dendrimer nano-conjugate is selective to cancer cells overexpressing Transferrin receptors and can minimize non-specific toxicities.

In the third objective of the work, a cell penetrating peptide, octa-arginine (R8) was attached over the surface of α-TOS modified dendrimer to deliver PTX intracellularly to human lung carcinoma (A549) cells. The synthesized dendrimer nano-conjugate (RVES-PD) was uptaken significantly into the A549 cells than the unmodified conjugate. The RVES-PD was internalized into the cells by macropinicytosis confirmed by Amiloride

inhibitor. The cytotoxicity study revealed that R8 modified dendrimer conjugates showed maximum cytotoxicity to cancer cells in comparison to free drug after 24 h and 48 h treatment. Furthermore, the RVES-PD-PTX induced higher apoptosis in A549 cells which can be attributed to the greater cellular uptake and hence more availability of drug in the cells. Moreover, the R8 modified dendrimer conjugates were evaluated in 3D multicellular A549 spheroids. The ability of R8 to internalize deeper into the tissues has resulted in increased permeation, uptake, growth inhibition, and cytotoxicity of R8-modified dendrimer conjugates over VES-PD and free PTX in the spheroid model. Biodistribution study conducted tumor bearing mice revealed that the RVES-PD treated sections showed fluorescence intensity more prominent in all organs and tumor than other treatment groups at all the time points (4, 8 and 24 h) due to the EPR effect as well the efficiency of R8 to deliver macromolecular cargo inside the cells. In the tumor volume reduction study, it was observed that the treatment of tumor bearing mice with VES-PD-PTX and RVES-PD-PTX reduced their tumor volume more effectively compared to the treatment with free PTX. The RVES-PD-PTX treatment caused highest upregulation of the apoptotic markers Caspase 3 and 7 in tumors. The presence of apoptotic cells was significantly higher in tumor sections isolated from RVES-PD-PTX-treated groups as indicated by increased green fluorescence.

Overall, the developed multifunctional dendrimer nano-conjugates could be a promising treatment strategy for the delivery of poorly soluble chemotherapeutic agents to cancer tissues.

Future Scope of Work

The 20th century has mushroomed remarkable innovations in polymer synthesis and advancement in the design of biodegradable and biocompatible polymeric macromolecules. Initially very few researchers were interested in developing aesthetic pleasing macromolecules but later on it was understood that dendritic macromolecules have something very special to offer. In this context, the dendrimers have been explored as one of the most promising and innovative polymeric nanocarriers in the delivery of different bioactives *i.e.* drugs, oligonucleotides, enzymes and vaccines.

Dendrimers are synthetic macromolecules having high branching points, three-dimensional globular shape, monodispersity and nanometric size range (1-100 nm) which provides a well-defined branched structure with globular shape and a large number of surface groups that can be modified which offer a template in the field of drug delivery. The surface of dendrimers can be tailored to attach various ligands or peptides such as cell penetrating peptides along with receptor specific targeting ligands together which offer different functions making them dual-targeted delivery systems. These exclusive properties like molecular uniformity, multifunctional end groups and occurrence of numerous internal cavities make dendrimers appropriate for various pharmaceutical and biomedical applications.

The developed dendrimer-based delivery system can be further explored to deliver other chemotherapeutic agents which possess poor physico-chemical properties which hampers its potential to be in clinic. The future exploration will focus on the covalent conjugation of drugs (prodrugs) which will be cleaved selectively by enzymatic or chemical environment present exclusively in the tumor cells which steer the location and rate of drug release from dendrimer-drug nano-conjugates. As majority of the chemotherapeutic agents are BCS class IV drugs, marked with extreme hydrophobicity,

further attempts can be undertaken to assess their loading and delivery efficiency to the cancer cells using this dendrimer system.

The developed nanocarriers could be further explored by incorporating combination therapeutics with molecularly targeted biologics and conventional small molecules. However, the toxicity of the constituents of hybrid nanosystems *vis a vis* the hybrid itself will have to be explored and established, if not ruled out. As has been aforementioned in this research, the targeting of drugs mediated through PAMAM is an area that must be further explored, and we have been trying to reach better selectivity by attaching various targeting ligands to achieve selectivity of dendrimers. However, the story of dendrimer from bench of chemist to formulation desk is still far from complete. Lot of vistas remains to be unfolded.

We anticipate that future research will be focused to achieve precision in terms of number of molecules of each type attached to the dendrimer molecule and a control over each step to reduce batch-to-batch variation which may lead clinical translation of developed dendrimer-based delivery systems in a cost-effective way.

Further research is necessary in developing in vivo models for actively targeted dendrimers for better understanding of the effectiveness of the chemotherapeutic system in the biological system. The assessment of pharmacokinetic and pharmacodynamic parameters of actively targeted dendrimer-based nano-systems to translate it into clinic is viable approach for efficient delivery of chemotherapeutics in cancer. Moreover, the developed dendrimer-based nanocarriers need to be explored for hepatotoxicity and nephrotoxicity to assess the safety.

Still dendrimer applications to drug delivery are in infancy and scientists are exploring different aspects of dendrimers as drug delivery vehicle.

Appendix

List of publications

From thesis work:

1. **Bhatt, H**., Ghosh, B. and Biswas, S., 2020. Cell-Penetrating Peptide and α-Tocopherol-Conjugated Poly (amidoamine) Dendrimers for Improved Delivery and Anticancer Activity of Loaded Paclitaxel. *ACS Applied Bio Materials*, 3(5), pp.3157-3169.
2. **Bhatt, H.**, Kiran Rompicharla, S.V., Ghosh, B., Torchilin, V. and Biswas, S., 2019. Transferrin/α-tocopherol modified poly (amidoamine) dendrimers for improved tumor targeting and anticancer activity of paclitaxel. *Nanomedicine*, 14(24), pp.3159-3176.
3. **Bhatt, H.**, Kiran Rompicharla, S.V., Ghosh, B. and Biswas, S., 2019. α-tocopherol succinate-anchored PEGylated Poly (amidoamine) dendrimer for the delivery of paclitaxel: assessment of in vitro and in vivo therapeutic efficacy. *Molecular pharmaceutics*, 16(4), pp.1541-1554.

Other publications

4. Sousa, Â., Faria, R., Albuquerque, T., **Bhatt, H**., Biswas, S., Queiroz, J.A. and Costa, D., 2020. Design of experiments to select triphenylphosphonium-polyplexes with suitable physicochemical properties for mitochondrial gene therapy. *Journal of Molecular Liquids*, p.112488.
5. Kumari, P., Paul, M., **Bhatt, H.**, Rompicharla, S.V.K., Sarkar, D., Ghosh, B. and Biswas, S., 2020. Chlorin e6 Conjugated Methoxy-Poly (Ethylene Glycol)-Poly (D, L-Lactide) Glutathione Sensitive Micelles for Photodynamic Therapy. *Pharmaceutical Research*, 37(2), pp.1-17.
6. Muddineti, O.S., Rompicharla, S.V.K., Kumari, P., **Bhatt, H.**, Ghosh, B. and Biswas, S., 2020. Lipid and poly (ethylene glycol)-conjugated bi-functionalized chlorine e6

micelles for NIR-light induced photodynamic therapy. *Photodiagnosis and Photodynamic Therapy*, 29, p.101633.

7. A muco-adhesive polymeric micellar structure and process for preparing the same: Swati Biswas, Balaram Ghosh, **Himanshu Bhatt**, Sanhita Roy: Patent authority: BITS-Pilani, Hyderabad Campus; **Indian Patent Application no. 201911034570** filed on 27th August, 2019.
8. Kumari, P., Rompicharla, S.V.K., **Bhatt, H.**, Ghosh, B. and Biswas, S., 2019. Development of chlorin e6-conjugated poly (ethylene glycol)-poly (d, l-lactide) nanoparticles for photodynamic therapy. *Nanomedicine*, 14(7), pp.819-834.
9. Rompicharla, S.V.K., Kumari, P., **Bhatt, H.**, Ghosh, B. and Biswas, S., 2019. Biotin functionalized PEGylated poly (amidoamine) dendrimer conjugate for active targeting of paclitaxel in cancer. *International journal of pharmaceutics*, 557, pp.329-341.
10. Muddineti, O.S., Rompicharla, S.V.K., Kumari, P., **Bhatt, H.**, Ghosh, B. and Biswas, S., 2019. Vitamin-E/lipid based PEGylated polymeric micellar doxorubicin to sensitize doxorubicin-resistant cells towards treatment. *Reactive and Functional Polymers*, 134, pp.49-57.
11. **Bhatt, H.**, Rompicharla, S.V., Komanduri, N., Aashma, S., Paradkar, S., Ghosh, B. and Biswas, S., 2018. Development of Curcumin-Loaded Solid Lipid Nanoparticles Utilizing Glyceryl Monostearate as Single Lipid Using QbD Approach: Characterization and Evaluation of Anticancer Activity Against Human Breast Cancer Cell Line. *Current drug delivery*, 15(9), pp.1271-1283.
12. Rompicharla, S.V.K., **Bhatt, H.**, Shah, A., Komanduri, N., Vijayasarathy, D., Ghosh, B. and Biswas, S., 2017. Formulation optimization, characterization, and evaluation

of in vitro cytotoxic potential of curcumin loaded solid lipid nanoparticles for improved anticancer activity. *Chemistry and physics of lipids*, 208, pp.10-18.

Papers presented in conferences

1. Transferrin receptor targeted Vitamin-E-conjugated dendrimers for the delivery of paclitaxel in cancer. 17th International Conference of Controlled Release Society: Indian Chapter 2019**,** Mumbai, India.
2. Vitamin-E-conjugated dendrimers for the Delivery of Paclitaxel in Cancer. 16th International Conference of Controlled Release Society: Indian Chapter 2018, Mumbai, India.

BHATT HIMANSHU NARENDRAKUMAR

Biography

Mr. Himanshu Bhatt has completed his Bachelor of Pharmacy from Poona College of Pharmacy, Bharati Vidyapeeth Deemed University, Pune, Maharashtra, India in 2010. He pursued his Master of Pharmacy in Pharmaceutics from Maliba Pharmacy College, Uka Tarsadia University, Gopal Vidhyanagar in 2013. Post his one and half year experiences at NIPER (Ahmedabad) as Junior Research Fellow, Mr. Himanshu joined Prof. Swati Biswas's lab at BITS Pilani Hyderabad Campus to pursue his doctoral research. Mr. Himanshu worked on tumor targeted dendrimers for the delivery of chemotherapeutics for cancer for his doctoral research. Moreover, Mr. Himanshu worked on an industrial project based on extended release depot formulations to treat bipolar disorder as research fellow. Furthermore, Mr. Himanshu has received senior research fellowship from CSIR to carry out the research work based on the development of polymeric micelles to treat multidrug resistance for the oral squamous cell carcinoma. He has published 10 peer-reviewed scientific publications in reputed international journals, one Indian Patent application and presented papers in various international conferences.

SWATI BISWAS

Biography

Prof. Swati Biswas is presently working as Associate Professor, in Department of Pharmacy, Birla Institute of Technology and Science, Pilani, Hyderabad Campus. She received her B. Pharm degree (1998) and M.Pharm (2000) from Jadavpur University, India. She was awarded her Ph.D. in Pharmaceutical Sciences in the year 2008 from Wayne State University, USA. After completion of doctoral studies, she pursued her postdoctoral studies in Northeastern State University, USA (2013). She has been involved in research for the last 17 years. She has to her credit more than 40 research publications, two US patents and two Indian Patents. She has authored 3 book chapters in “Dendrimers: Synthesis, Applications and Role in Nanotechnology”, “Drug Delivery Strategies for Poorly Water-Soluble Drugs” and “Handbook of Polymers for Pharmaceutical technologies, Volume 2: Processing and Applications”. She has successfully completed many sponsored projects and currently handling projects sponsored by DST, DBT, DST-LVPEI and DST-SERB-CRG. She has guided three Ph.D students and currently five students are pursuing their Ph.D. work under her supervision.

BALARAM GHOSH

Biography

Dr. Balaram Ghosh is presently working as an Assistant Professor, in the Department of Pharmacy, Birla Institute of Technology and Science, Pilani, Hyderabad Campus. He received his B. Pharm degree (1998) and M.Pharm (2000) from Jadavpur University, India. He was awarded his Ph.D. in Pharmaceutical Sciencesin the year 2009 from Wayne State University, Michigan, USA. After completion of doctoral studies, he pursued his postdoctoral studies at the Centre for Human Genetic Research (CHGR), Harvard Medical School, Harvard University, USA (2013). He has been involved in research for the last 15 years. He has published more than 54 research publications, three US patents and three Indian Patents. He has authored 4 book chapters. One of the research molecule (BG45) developed by him at Harvard Medical School has been commercialized with Sigma-Aldrich. He has successfully completed many sponsored projects and currently handling projects sponsored by SERB and CSIR, Government of India and Sun Pharma Advanced Research Company Ltd. (SPARC), India. Currently four students are pursuing their Ph.D. work under his guidance.